Structure - Property Relationships of Furanyl Thermosetting Polymer Materials

Derived from Biobased Feedstocks

A Thesis

Submitted to the Faculty

of

Drexel University

by

Fengshuo Hu

in partial fulfillment of the

requirements for the degree

of

Doctor of Philosophy

September 2016

Dedications

To my dear parents, family and friends for their invaluable support and inspiration.

Acknowledgments

First of all, I would like to express my sincere thanks to my research advisor, Professor Giuseppe R. Palmese, for his invaluable support and guidance during the course of my research. It has been a great honor and pleasant experience working under his supervision. From him, I learned how to independently evaluate and approach scientific problems, and more importantly, how to manage and conduct a successful professional career path. Without Professor Giuseppe R. Palmese, I would not be who I am now, and therefore, I will always be thankful for his valuable support and help.

Secondly, I would like to sincerely thank Professors Dr. Nicolas Alvarez, Dr. Kenneth Lau, Dr. Christopher Li, and Dr. John La Scala for being on my dissertation committee and for their invaluable discussion and guidance concerning my research study. I would like to offer special acknowledgement to Dr. Cameron Abrams, Dr. Yossef Elabd, Dr. Michael Walters, Dr. Yuesheng Ye, and the staff, Jennifer Bing, Andrea Falcone, Tracy McClure and Jerome Moses, in the Chemical and Biological Engineering department at Drexel University, for all their unforgettable help and input in my research study.

I also would like to express my immense gratitude to my dear parents and family for their continuous support at every stage of my life, especially during my PhD study at Drexel University. They are such an invaluable gift to me, and I am truly thankful and appreciative to have them in my life. Special thank goes to Ms. Danyang Wu who has

always been with me and encouraged me at this most critical stage in my life. I would not be able to succeed in this journey without each one of them.

I am also sincerely grateful to my colleagues and friends, in particular, Dr. An Du, Dr. Changwoon Jang, Gao Jian, Emre Kinaci, Dr. Sam Laurencin, Dr. Ian McAninch, Shan Mei, Xiangxi Meng, Mohammad Nozari, Dr. Amy Peterson, Purnomo Pratama, Sadella Santos, Dr. Majid Sharifi, John Vergara, Dr. Arianna Watters, Dr. Santosh Kumar Yadav, Dr. Joshua Sadler, Dr. James Throckmorton, Tim Wade and Dr. Jungho Yang, for their kind help and discussion in my research study. Special acknowledgement also goes to the Department of Chemistry at Drexel University for allowing me to use their NMR and MS facilities.

I sincerely acknowledge financial supports from the SERDP under Project WP-1758 and WP-2402, the U.S. Army Research Laboratory under the Army Materials Center of Excellence Program Contract W911NF-06-2-0013, and the Center for Sustainable Corrosion Protection (CSCP) Cooperative W911NF-13-2-0046. Support from the China Scholarship Council is also acknowledged. The views and conclusions contained in this document are those of the author and should not be interpreted as representing the official policies, either expressed or implied, of the Army Research Laboratory or the U.S. Government. The U.S. Government is authorized to reproduce and distribute reprints for Government purposes notwithstanding any copyright notation herein.

Table of Contents

List of Tables

Lists of Figures

Abstract

Structure - Property Relationships of Furanyl Thermosetting Polymer Materials Derived from Biobased Feedstocks

Fengshuo Hu

Thesis Advisor: Professor Giuseppe R. Palmese, Ph.D.

Biobased thermosetting polymers have drawn significant attention due to their potential positive economic and ecological impacts. New materials should mimic the rigid, phenylic structures of incumbent petroleum-based thermosetting monomers and possess superior thermal and mechanical properties. Furans and triglycerides derived from cellulose, hemicellulose and plant oils are promising candidates for preparing such thermosetting materials. In this work, furanyl diepoxies, diamines and di-vinyl esters were synthesized using biobased furanyl materials, and their thermal and mechanical properties were investigated using multiple techniques. The structure versus property relationship showed that, compared with the prepared phenylic analogues, biobased furanyl thermosetting materials possess improved glassy storage modulus (E'), advanced fracture toughness, superior high-temperature char yield and comparable glass transition temperature (T_g) properties. An additive molar function analysis of the furanyl building block to the physical properties, such as T_g and density, of thermosetting polymers was performed. The molar glass transition function value (Y_g) and molar volume increment value ($V_{a,i}$) of the furanyl building block were obtained. Biobased epoxidized soybean oil (ESO) was modified using different fatty acids at varying molar ratios, and these prepared materials dramatically improved the critical

strain energy release rate (G_{1c}) and the critical stress intensity factor (K_{1c}) values of commercial phenylic epoxy resins, without impairing their T_g and *E′* properties. Overall, it was demonstrated that biobased furans and triglycerides possess promising potential for use in preparing high-performance thermosetting materials, and the established methodologies in this work can be utilized to direct the preparation of thermosetting materials with thermal and mechanical properties desired for practical applications.

Chapter 1. Introduction: motivation, background and overview

1.1. Motivation

1.1.1. Thermosetting epoxy and vinyl ester reins

Thermosetting materials are an important class of polymer materials that have been extensively used for at least 50 years.[1] Highly crosslinked networks are formed in these thermosetting materials after curing, distinguishing them from thermoplastic materials.[2] This inherent crosslinking characteristic results in desirable properties, such as high durability, strength, elastic modulus, adhesion and thermal and chemical resistance. These properties make thermosetting materials good candidates for applications that require reliable performance, especially under harsh conditions such as high thermal or mechanical loads.

Epoxy and vinyl ester (VE) resins are two of the most important types of thermosetting materials. Epoxy resins contain highly reactive epoxide functional groups that can react with various functionalities, such as hydroxyl, amine, anhydride and carboxyl groups. The resulting materials possess versatile properties and are extensively used in adhesives, structural polymer composites, surface coatings and electrical insulation applications in the aviation and automobile manufacturing industries. Currently, more

than 80 % of the epoxy resins produced worldwide are obtained by reacting 2,2-bis(4'-hydroxyphenyl) propane (Bisphenol A) with epichlorohydrin to yield diglycidyl ether of bisphenol A (DGEBA) resins. The preparation reaction scheme of DGEBA resins is shown in Figure 1.1, and DGEBA resins with different molecular weights are further separated using distillation. The number of repeating bisphenol A moieties in DGEBA resins influences the processing and mechanical behavior of resulting networks, and these multiple aromatic phenyl rings in the chemical structures endow DGEBA resins with high thermal and mechanical properties.

Epoxy resins (difunctional or multifunctional) can be further modified using methacrylic and acrylic acids to prepare VE monomers that contain the carbon-carbon double bonds in place of the epoxy rings.[3] The simplest form of VE is the product of the reaction of one mole of DGEBA and 2 moles of methacrylic acid, which is schematically shown in Figure 1.2. Aromatic monofunctional styrene is often blended with these difunctional VE monomers as a reactive diluent with a concentration of 30 to 50 % by weight to reduce the resin viscosity, typically down to 0.2 – 2 Pa.s, and to improve crosslinking during cure.[4] Because of their high water and chemical resistance, good thermal and mechanical properties and low cost, VE resins are widely used in polymer composites in commercial and military applications.[5]

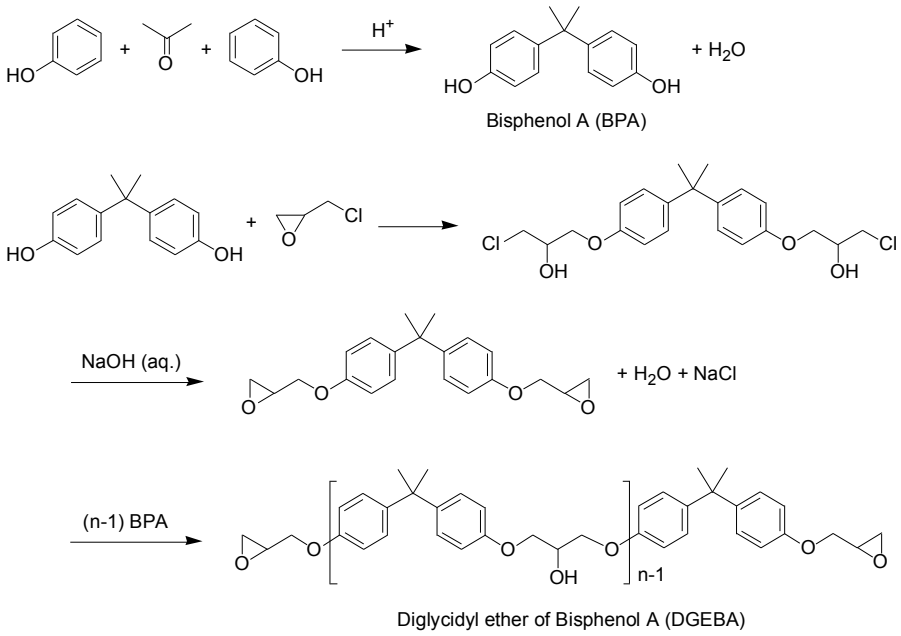

Figure 1.1. The reaction scheme for the preparation of DGEBA.

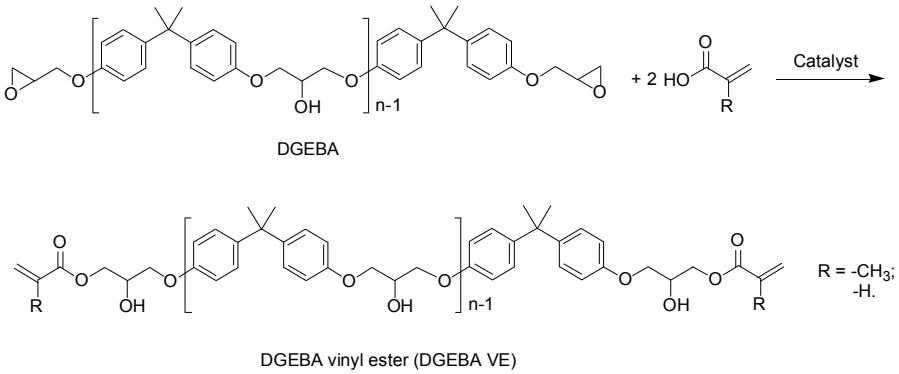

Figure 1.2. The reaction scheme of DGEBA with methacrylic acid for DGEBA VE preparation.

1.1.2. Properties and applications

Thermosetting epoxy and VE resins are used extensively in a wide range of applications due to their useful properties.[6] Table 1.1 summarizes their general properties and industrial application fields.[7] Several unique characteristics distinguish thermosetting epoxy resins from other thermosets: lower cure shrinkage, thus lower residual stress in cured products compared with unsaturated polyester and vinyl ester resins, wide temperature service range with a judicious selection of curing agents and crosslinking degree, and diverse availability of epoxy resins from low-viscosity liquids to tack-free solids. Because of these characteristics and resulting properties, epoxy resins are primarily used in the structural adhesives, surface coatings, electrical laminates, and high-strength engineering composites for automotive, marine construction and aerospace applications. Most composite applications employ conventional difunctional epoxy resins as their matrices, while high-performance composite applications, such as aerospace and military defence applications, often use multifunctional (functionality greater than two) epoxy resins. Epoxy resins are also extensively used in applications in the electronics industry, such as motor, generator, transformer and insulator applications, due to their good electrical insulation property.[8]

Table 1.1. Properties and application fields of thermosetting epoxy and vinyl ester resins.

Resins	Properties	Application fields
Epoxy	Low shrinkage, high temperature service capability, excellent corrosion and weather resistance, high strength and good electrical isolation properties	Structural adhesives, surface coatings, electrical laminates, engineering composites for automotive, marine constructions and aerospace applications
Vinyl ester	Excellent corrosion resistance, high flexibility, good adhesion with polar substrates	Corrosion and water resistant composites, electrical applications, corrosion resistant coatings, building constructions and marine constructions

Thermosetting VE resins have good processability and desirable mechanical properties as epoxy resins. Compared with a similar type of thermosetting resin - unsaturated polyester (UPE) resins, VE resins exhibit higher toughness due to fewer crosslinks and ether linkages in cured networks. Hydroxyl groups from the epoxy-acid reaction endow VE resins with better adhesion property with polar substrates through hydrogen bonding relative to UPE resins. VE resins also possess excellent corrosion resistance which results from the large chemical moiety between ester groups, low concentration of ester groups in cured networks and steric hindrance from the pendent methyl group in methacrylic acid. So, they are extensively used in corrosion-resistant applications, such as tanks, piping, ducts and vessels for dilute acids, solvents and fuels. VE resins are also water resistant, making them suitable for use in marine applications, such as sail and motor boats, fishing boats and naval vessels, and household applications, such as air conditioners and humidifiers. Fibre reinforced VE composites are also widely used for making components in electricity generating stations, such as transmission and distribution as well as electrical maintenance equipments, such as ladders and booms, in the electrical industry.[7]

1.1.3. Critical challenges: non-renewable feedstocks and brittleness

Although their properties are desirable, current thermosetting epoxy and VE resins face several critical challenges. One challenge is that these resins are produced using petroleum-based feedstocks which are non-renewable.[9] Due to economic and ecological

demands, a significant effort has been made by researchers to use renewable sources as potential sustainable substitutes for petroleum-based feedstocks in the design and preparation of thermosetting materials.[1, 10] New materials should mimic the rigid and phenylic structures of incumbent thermosetting epoxy and VE resins and possess comparable thermal and mechanical properties.[11] Numerous renewable sources, including plant oils,[12] cellulose,[13] hemicellulose,[1, 14] lignin,[13b, 15] starch[16] and chitin,[17] have been investigated as feedstocks for thermosetting materials. These renewable sources can be potentially degraded into useful chemicals possessing specific building blocks and further transformed into thermosetting monomers and polymers. Some examples of these building blocks include (i) fatty acids from triglycerides,[12] (ii) isosorbide from hemicellulose,[1, 14b, 14c, 18] (iii) phenolic derivatives from lignin,[15a] and (iv) furanyl structures from cellulose and hemicellulose.[13b, 19]

Triglyceride-based materials are comprised of aliphatic chains that do not inherently possess the strength and rigidity required for most thermosetting applications. Therefore, complex chemistries are needed to improve the properties of materials based on triglycerides.[20] Isosorbide is reputed to be nontoxic and rigid; however, isosorbide-derived epoxy resins, as well as the resulting polymer networks, suffer from relatively high hydrophilicity.[21] Even though phenolic derivatives from lignin are considered important thermosetting materials, due to their aromatic characteristics, their utilization is greatly limited by the challenge of breaking lignin down into useful chemicals.[22] Chemicals possessing biobased furanyl building blocks are considered promising

candidates for preparing thermosetting materials due to their aromatic characteristic and feasible availability.[23] Furanyl chemicals can be produced from existing biomass sources: cellulose, the most abundant compound in wood, can be chemically and bacterially degraded into hexose and converted into hydroxymethylfurfural (HMF), a potential precursor for thermosetting resins.[13b] Hemicellulose can be degraded into pentose and converted into furfuryl alcohol, making it also possible to be used as a renewable source.[1, 14c] Furfurylamine (FA)[24] and furfuryl glycidyl ether (FGE)[25] are commercial furanyl chemicals that could have applications in thermosetting resins. However, these monofunctional monomers do not provide the ability to crosslink and therefore are generally used as network modifiers, where furanyl rings become side groups of formed polymer networks. As discussed, high-performance thermosetting epoxy and VE materials are based on multifunctional epoxy and VE resins with aromatic ring structures that can directly build into cured polymer networks.[26] For example, highly crosslinked polymer structures with superior thermo-mechanical properties are formed when difunctional DGEBA with multiple aromatic rings on its main chain is cured using diamine curing agents, such as 4, 4′-methylene biscyclohexanamine (PACM) and diethyl toluene diamine (EPIKURE W).[27]

There have been limited reports of multifunctional furanyl thermosetting epoxy and VE resins. Cho et al. recently reported two difunctional furanyl epoxy monomers, BOF (a mono-furan di-epoxide, in Figure 2.1) and bFdE (a bis-furan di-epoxide, in Figure 2.1).[23a] The materials developed by Cho et al. were photo-cured cationically using IRGACURE

250 and triphenylsulfonium hexafluoroantimonate salt initiators, and the adhesive strengths of these materials were tested using a lap-shear configuration. Fundamental properties such as glass transition temperature (T_g) and tensile modulus were not reported. Moreover, a comparison was not made with petroleum-based phenyl analogues. It should also be noted that cationic cure of epoxy resins proceeds via a chain mechanism that results in vastly different network structures compared with step-growth epoxy-amine polymerization. The synthesis of BOF was also reported by Jeong et al.; however, BOF was only utilized as an intermediate for which thermo-mechanical properties were not investigated.[23b] It is crucial to fundamentally understand how the furanyl building block affects the thermo-mechanical properties of thermosetting epoxy and VE resins compared with the phenyl building block in order to better design furan-based thermosets with the goal of replacing petroleum-based systems. No direct comparisons of furanyl based epoxy and VE resins versus phenyl based analogues have been shown in literature. In this dissertation, we seek to understand the structure versus property relationships of furanyl based thermosetting epoxy and VE resins relative to those of phenyl based analogues.

There are numerous examples in the literature of biobased epoxy systems and their properties that provide general points of comparison. Table 1.2 summarizes these works in three categories: (1) lignin, (2) cellulose/hemicellulose and (3) plant oil. The table contains works where thermo-mechanical properties of the biobased epoxy systems were obtained and where comparisons were made to the standard DGEBA based

systems. Beginning with lignin derived structures as examples, Nouailhas et al. reported a catechin-based epoxy monomer with similar performance to DGEBA prepared with the same curing agent.[28] Aouf et al. reported a gallic acid derived epoxy resin that displayed a higher T_g compared with DGEBA when cured with isophorone diamine (IPD).[29] Ochi et al. synthesized a vanillin derived epoxy resin (BMPTU) with a similar structure to DGEBA that showed comparable T_g and storage modulus (E') to DGEBA when cured with 4,4'-diaminodiphenylmethane (DDM).[30] For cellulose/hemicellulose derived structures, Sachinvala et al. prepared a mixture of epoxy allyl sucroses (EAS) with variable epoxy groups per monomer.[31] This resin possessed a much lower T_g value relative to DGEBA when cured with diethylenetriamine (DETA). East et al. recently explored the preparation of an isosorbide-based epoxy resin.[32] Much lower T_gs compared to DGEBA when cured with an aliphatic triamine (Jeffamine T403) and DDM were reported. Łukaszczyk et al. reported a less pure isosorbide based epoxy resin with an epoxy number of 0.44 mol per 100 g, which was cured using triethylenetetramine (TETA) and IPD that possessed T_gs 70 °C lower than DGEBA.[21] Chrysanthos et al. recently synthesized two isosorbide-based epoxy resins, one containing the pure epoxy monomer ($DGEDAS_0$) and the other consisting of various oligomeric species ($DGEDAS_n$).[33] T_g values of the resulting thermosets prepared with IPD were consistently lower than analogous DGEBA systems. For the category of plant oil derived structures, Earls et al. reported the thermo-mechanical properties of several glycerides containing terminal/non-terminal epoxy groups on aliphatic chains with varying chain lengths.[34] The resulting thermosets cured with DDM possessed T_g values of 48-133 °C, much lower

than DGEBA-DDM system and with relatively lower flexural moduli. Lligadas et al. prepared two fatty acid derived epoxy resins, epoxidized 10-undecenoyl triglyceride (UDTGE) and epoxidized methyl 3,4,5-tris(10-undecenoyloxy)benzoate (UDBME), that possessed similar T_g values (~70 °C) when cured with DDM,[20b] both of which were significantly lower than DGEBA-DDM system (184 °C).[34]

Several factors affect the overall thermo-mechanical properties of thermosetting epoxy polymers. These include cure conditions, extent of reaction, purity, curing agent selection and building block type. The cure conditions, which determine the extent of reaction, are critical to the ultimate properties of epoxy thermosets. Identical thermosetting epoxy-amine systems cured to different degrees possess different thermo-mechanical properties. For example, DGEBA-IPD and DGEBA-DDM systems reported by different researchers in Table 1.2 show different T_gs. The use of different T_g measurement techniques are a possible reason for this observation. It should be noted that since most of the literature in Table 1.2 failed to provide the extent of reaction to indicate the full conversion between epoxy and amine functional groups, the reason for the observed difference is not clear. So, T_g data presented in the absence of cure conversion data can have significant uncertainties. The purity of biobased epoxy resins also has a significant impact on the overall performance. For example, the isosorbide based epoxy resin reported by Łukaszczyk et al.[21] was cured with IPD without purification, and a T_g of 73 °C was observed, whereas the monomer of isosorbide

Table 1.2. Thermo-mechanical properties of biobased epoxy resins in the literature.

Biobased Epoxy Resins	Curing Process	Properties	Comparison	Ref
		Lignin		
GEC[a]	Composition (1) 75wt%DGEBA/25wt%GEC, composition (2) 50wt%DGEBA/50wt%GEC and DGEBA were stoichiometrically cured with Epamine PC 19[b] at 60 °C for 24 h.	(1): ~55 °C[c], 2.46 GPa[d] (2): ~50 °C[c], 2.40 GPa[d]	DGEBA ~55 °C[c], 2.81 GPa[d]	Nouailhas et al.[28]
GEGA[e]	GEGA and DGEBA were stoichiometrically cured with IPD at 90 °C for 0.5 h and 200 °C for 2 h.	233 °C[f]	DGEBA 160 °C[f]	Aouf et al.[29]
BMPTU[g]	BMPTU was cured with DDM at 180 °C for 2 h and 200 °C for 4 h; DGEBA was cure with DDM at 80 °C for 2 h and 180 °C for 6 h.	167 °C[h]	DGEBA 174 °C[h]	Ochi et al.[30]; Koike et al.[35]
		Cellulose/Hemicellulose		
EAS3.7[i] EAS3.2[j] EAS1.6[k]	EAS3.7, EAS3.2 and EAS1.6 were stoichiometrically cured with DETA from 25 to 230 °C.[l]	EAS3.7: 72 °C[m] EAS3.2: 62 °C[m] EAS1.6: 16 °C[m]	DGEBA 134 °C[m]	Sachinvala et al.[31]

Isosorbide epoxy	Isosorbide epoxy was stoichiometrically cured with Jeffamine T403 at 100 °C for 4 h; with DDM at 80 °C for 2 h, 120 °C for 16h and 150 °C for 2 h.	T403: 48 °C[n] DDM: 89 °C[n]	DGEBA T403: 93 °C DDM: 174 °C	East et al.[32]; Fenouillot et al.[36]; Morgan et al.[37]; Ochi et al.[30]
IS-EPO[o]	IS-EPO and DGEBA were stoichiometrically cured with TETA at 25 °C for 24 h and 80 °C for 24 h; with IPD at the same curing condition.	TETA: 49 C[p], 5.5 GPa[q]; IPD: 73 °C[p], 14.6 GPa[q]	DGEBA TETA:116°C[p], 8.3 GPa[q]; IPD:141 °C[p], 10.4 GPa[q]	Łukaszczyk et al.[21]
DGEDAS$_0$[r] DGEDAS$_n$[s]	DGEDAS$_0$, DGEDAS$_n$ and DGEBA were stoichiometrically cured with IPD at 80 °C for 1 h and 180 °C for 2 h.	DGEDAS$_0$: 112 °C[t]; DGEDAS$_n$: 96 °C[t]	DGEBA 155 °C[t]	Chrysanthos et al.[33]
Plant oil				
Epoxidized triglyceride[u]	**1**,**2a**, **2b**, **2c**, **2d** and DGEBA were stoichiometrically cured with DDM. Cure temperature was increased by 25 °C per 2 h from initial temperature upon reaching final temperature with an additional 2 h: 120 to 200 °C for **1**; 120 to 180 °C for **2a** and **2c**; 90 to 180 °C for **2b**; 120 °C for **2d**. 120 to 180 °C for DGEBA.	**1**: 54 °C[v], 1.5 GPa[w]; **2a**: 56 °C[v], 1.1 GPa[w]; **2b**: 48 °C[v], 1.1 GPa[w]; **2c**: 68 °C[v], 1.9 GPa[w]; **2d**: 133 °C[v], 3.2 GPa[w]	DGEBA 184 °C[v], 2.4 GPa[w]	Earls et al.[34]

UDTGE[x]	UDTGE was stoichiometrically cured with DDM at 100 °C for 1.5 h and 140 °C for 1h.	UDTGE: 63 °C[z]	DGEBA	Lligadas et al.[20b]
UDBME[y]	UDBME was stoichiometrically cured with DDM at 90 °C for 1.5 h and 160 °C for 1 h.	UDBME: 74 °C[z]	174 °C	Ochi et al.[30]

[a]Glycidyl ether of catechin, 80% purity.
[b]A mixture of BPA-epichlorohydrin polymer, benzyl alcohol, 1,3-bis(aminomethyl)benzene and 3-aminomethyl-3,5,5-trimethylcyclohexylamine.
[c]T_g assigned as the temperature at the maximum of loss factor by DMA from 25 to 120 °C at 3 °C/min and a frequency of 5 Hz.
[d]Storage modulus at 30 °C.
[e]Glycidyl derivative of gallic acid.
[f]T_g assigned as the temperature at the maximum of tanδ curve by DMA from 30 to 300 °C at 3 °C/min, a frequency of 1 Hz and strain at 0.1%.
[g]3,9-bis[(3-methoxy-4-glycidyl)-phenyl]-2,4,8,l0-tetroxaspiro(5,5)undecane (epoxide equivalent: 282±5).
[h]T_g assigned as the temperature at the maximum of tanδ curve by an inverted, free-oscillation, torsion pendulum (RD-1100AD, Rhesca Co. Ltd.) from -160 to 250 °C at 0.7 °C/min in vacuo.
[i]Epoxy allyl sucroses (3.7 epoxy groups per sucrose).
[j]Epoxy allyl sucroses (3.2 epoxy groups per sucrose).
[k]Epoxy allyl sucroses (1.6 epoxy groups per sucrose).
[l]Cured by heating from 25 to 230 °C at 5 °C/min by DSC with 20–40 mg premixed epoxy–amine samples in open aluminum pans under dry nitrogen.
[m]T_g determined at the inflection point of the forward step curve by DSC from -140 to 200 °C at 10 °C/min.
[n]T_g measured by DSC.
[o]Isosorbide based epoxy resin, epoxy number: 0.44 mol/100 g.
[p]T_g measured by DSC from 0 to 250 °C at 10 °C/min.
[q]Flexural modulus measured on Zwick 100N5A with extensometer in accordance with the PN-EN ISO 178:2006 standard.
[r]The monomer of isosorbide diglycidyl ether, 100% purity (epoxide equivalent: 143).
[s]The oligomer of isosorbide diglycidyl ether (epoxide equivalent: 184).
[t]T_g assigned as the temperature at the maximum of tanδ curve by DMA from -100 to 200 °C at 3° C/min with a frequency of 1 Hz and strain at 0.5% under a nitrogen stream.
[u]Compound **1** was epoxidized linseed oil, compounds **2a**, **2b**, **2c** and **2d** were terminal-epoxidized trifunctional triglycerides with different chain lengths.
[v]T_g measured by DSC from -50 to 300 °C at 10 °C/min.

[w]Flexural modulus determined using ASTM method D-790.
[x]Epoxidized 10-undecenoyl triglyceride, 100% purity.
[y]Epoxidized methyl 3,4,5-tris(10-undecenoyloxy)benzoate, 100% purity.
[z]T_g assigned as the temperature at the maximum of loss-modulus curve by DMTA from -100 to 150 °C at 5 °C/min and a frequency of 1 Hz.

diglycidyl ether with a 100% purity prepared by Chrysanthos et al.[33] was cured with the same curing agent, and a much higher T_g (112 °C) was reported. The curing agent selected is another important factor affecting the properties of epoxy thermosets. Due to different structural rigidity and functionality of these amine curing agents, DGEBA cured with DDM gives the highest T_g (184 °C)[34] compared with other curing agents, such as IPD (155 °C),[33] DETA (134 °C)[31] and Jeffamine T403 (93 °C).[37] This makes it more difficult to compare the properties of biobased epoxy resins studied by different research groups.

Notwithstanding the above discussion concerning factors that influence thermo-mechanical properties of thermosets, lignin and cellulose derived building blocks endow thermosetting epoxy resins with higher thermo-mechanical properties compared with those from plant oils due to their aromatic characteristics. For example, when cured with DDM, BMPTU,[30, 35] isosorbide based epoxy[32, 36] and epoxidized linseed oil[34] exhibit T_gs of 167 °C, 89 °C and 54 °C, respectively. However, no direct property comparisons exist between thermosetting epoxy resins prepared using analogous phenyl and furanyl building blocks derived from lignin and cellulose, respectively. In order to appropriately assess the effects of biobased furanyl building block on the properties of thermosetting epoxy materials, difunctional furanyl epoxy resins, as well as their parallel phenyl analogues, should be synthesized and their properties should be compared with factors such as cure conditions, extent of reaction, purity and curing agent selection, being kept consistent.

Such direct property comparisons cannot be found between thermosetting vinyl ester resins prepared using biobased furanyl building blocks and their phenyl analogues either. A few examples of biobased vinyl ester systems and their properties exist in the literature. Table 1.3 summarizes these works in three categories: (1) aromatic structures from natural resources, (2) cycloaliphatic structures from natural resources, and (3) aliphatic structures from natural resources. The table contains the natural resources from which these biobased VE systems were prepared, and their thermal and mechanical properties. Beginning with the aromatic structures from natural resources as examples, Thielemans et al. investigated the solubility and compatibility of different lignins in various styrene-containing VE resins. Due to the incompatibility of polar lignins with nonpolar styrene, maleic anhydride (MA) was used to modify and incorporate lignins into VE resins through free radical polymerization and improve their effect on the matrix properties. This modification significantly improved the solubility of lignins in these VE resins and consequently enhanced the mechanical properties of cured resins.[38] Various aromatic compounds derived from lignin, such as lignin-based bio-oil,[15b] cardanol[39] and vanillin,[40] are also used extensively as biobased resources for preparing VE monomers and polymers. Stanzione III et al. prepared a methacrylated lignin-based bio-oil mimic (MBO) possessing a low viscosity of 30.3 cP at 25 °C. MBO consisted of methacrylated phenol, guaiacols and catechols, and was used without separations. When cured by itself through free radical polymerization, with a cure extent of 92.9 %, this VE resin showed thermo-mechanical and thermo-gravimetric properties, such as T_g of 115 °C, room temperature storage modulus of 3.2 GPa, initial decomposition

temperature of 306 °C and temperature of maximum decomposition rate at 418 °C, comparable with commercial petroleum-based VE thermosets.[15b] Jaillet et al. prepared a cardanol-based VE prepolymer by reacting a commercial cardanol diepoxy with methacrylic acid. Cardanol is derived from cashew nut shell liquid (CNSL), an important biobased starting material with abundant availability, low cost and unique structural features, including phenolic hydroxyl, aromatic ring and unsaturation(s) in the alkenyl side chain. By blending this cardanol-based VE prepolymer with different reactive diluents, cured cardanol-based VE resins exhibited good thermo-mechanical properties, such as T_gs of 86 °C (with 40 wt% of styrene) and 116 °C (with 40 wt% of isobornyl methacrylate), 60 - 70 °C lower compared with commercial DGEBA VE resin.[39c] Sultania et al. synthesized a cardanol-based epoxidized novolac VE resin through esterification of cardanol-based epoxidized novolac with methacrylic acid. This cardanol-based VE resin was thermally stable upon 260 °C - 285 °C when cured by blending with 0 – 50 wt% of styrene at 120 °C.[39d] Stanzione III et al. also prepared a vanillin-based VE resin (87 cP at 25 °C) containing 1 : 1 molar ratio of a monofunctional monomer (methacrylated vanillin) and a crosslinking agent (glycerol dimethacrylate) through a two-step one-pot methacrylation reaction of lignin-derived vanillin. When free radically polymerized, a potentially 100% biobased VE thermoset was produced possessing thermo-mechanical and thermo-gravimetric properties, such as T_g of 155 °C, room temperature storage modulus of 3.6 GPa and temperature of maximum decomposition rate of 426 °C, comparable with commercial petroleum-based VE thermosets in literature.[4, 40a] Zhang et al. modified vanillin and vanillyl alcohol into

methacrylated derivatives. Methacrylated vanillyl alcohol resin showed higher room temperature storage modulus, crosslinking density, T_g and thermal resistance than methacrylated vanillyl resin due to the higher vinyl functionalities in its chemical structure. Together with their low room temperature viscosity, these prepared biobased VE resins can be promising for use as reactive diluents in commercial VE resins.[40b] Aromatic structures derived from rosin, a class of hydrocarbon-rich biomass with abundance and low cost, are also used for preparing biobased VE monomers and polymers.[41] Rosin acids can be converted to vinyl, allyl ester and acrylic groups to radically polymerize. Relative to vinyl and allyl ester monomers, acrylic monomers showed great potential in the preparation of side-chain rosin-based polymers due to the increased reactivity of unsaturated carbon-carbon double bonds.[42] Lee et al. prepared several rosin-derived (meth)acrylic monomers and the cured copolymers showed T_gs ranging from 97 °C to 122 °C, depending on the length of the alkyl linkers.[41a] Zheng et al. prepared several gum rosin-derived (meth)acrylic polymers with T_gs ranging from 22 °C to 90 °C, depending on the length of spacers between side groups and backbone in their chemical structures.[41d] Do et al. synthesized a rosin-derived methacrylic monomer which was used as a tackifier in UV-crosslinkable polyacrylates to make pressure sensitive adhesives.[41e, 41f] For the cycloaliphatic structures from natural resources, Sadler et al. synthesized an isosorbide-methacrylate crosslinking VE resin (157 cP at 25 °C) through esterification of methacrylic anhydride (or methacryloyl chloride) with isosorbide, a non-toxic fused bi-heterocyclic compound with unique attributes derived from biobased carbohydrate feedstocks. When free-radically polymerized with a cure extent of 85%, the

formed polymer showed superior thermal and mechanical properties, such as flexural strength of 82 MPa, flexural modulus of 4.6 GPa, initial decomposition temperature of 305 °C and T_g of ~ 245 °C (tan δ peak), which is higher than any known commercial VE resins and many expensive epoxy resins.[43] Li et al. reported two VE resin monomers prepared using biobased dimer fatty acids (DA), DA-p-GMA and MA-m-DA-p-GMA, which were blended with different amounts of styrene and thermally cured. Form copolymers showed good thermo-mechanical and thermo-gravimetric properties, such as flexural strength of 29.1 MPa, tensile strength of 16.0 MPa, initial decomposition temperature above 390 °C and T_g ranging from 44 °C to 72 °C.[44] For the category of aliphatic structures from natural resources, plant oils[10] such as soybean oil,[45] linseed oil[46] and tung oil,[47] and fatty acids derived from plant oils[48] are also utilized extensively as biobased resources for preparing VE monomers and polymers. Khot et al. synthesized acrylated epoxidized soybean oil (AESO) using acrylic acid and biobased epoxidized soybean oil which is commercially available. Different amounts of styrene were blended with AESO to improve its processability and control the ultimate properties of AESO–styrene copolymers. Pure AESO polymer showed T_g of -10 °C, room temperature tensile modulus of ~440 MPa and tensile strength of ~6 MPa. While, AESO–styrene copolymer (40 wt% styrene) exhibited T_g of 44 °C, room temperature tensile modulus of 1.6 GPa and tensile strength of ~21 MPa, indicating the addition of styrene drastically improved the properties of AESO resin.[45b] Lu et al. synthesized several biobased VE resins, acrylated epoxidized linseed oil (AELO) and maleinized acrylated epoxidized linseed oil (MAELO), using linseed oil, the most molecularly unsaturated plant oil. Carbon-carbon

double bonds of linseed oil were epoxidized, acrylated and maleinized to prepare MAELO by adding more crosslink sites as well as acid functionality on the triglyceride molecules. With 33.3 wt% of styrene, cured polymers exhibited promising properties, such as storage moduli of 2.4 ± 0.1 GPa at 30 °C, T_gs higher than 100 °C and thermal stability upon 300 °C. These biobased VE resins could be promising alternatives for some petroleum-based resins in sheet-molding compound industry.[46] Yang et al. prepared two UV-curable VE monomers, acrylated diglycidyl ester of maleinized myrcene (ADMM) and acrylated tung oil polymerized glycidyl methacrylate (TOA-GMA), which were mixed at different weight fractions and cured under UV. With final cure extents up to 95%, pure ADMM polymer showed T_g of 77 °C, tensile strength of 49 MPa and initial decomposition temperature at 403 °C, whereas pure TOA-GMA polymer exhibited T_g of 35 °C, tensile strength of 4.8 MPa and initial decomposition temperature at 383 °C. With ADMM and TOA-GMA being rigid and tough materials, respectively, the cured copolymers reached a desired balanced performance with a 50–70 wt% of ADMM in mixed resin.[47] LaScala et al. used methacrylated lauric acid (MLA) comonomer as an alternative for styrene when formulating triglyceride-based crosslinker resins, including acrylated epoxidized soybean oil (AESO), maleinated AESO (MAESO), maleinated soybean oil monoglyceride (SOMG/MA) and maleinated castor oil monoglyceride (COMG/MA). Triglyceride-based crosslinker resins containing MLA exhibited lower polymer properties and higher viscosities than those containing styrene. Ternary blends of MLA, styrene and biobased resins were promising: SOMG/MA and COMG/MA containing 10 wt% of MLA and 25 wt% of styrene showed acceptable

viscosities of 600 cP at 25 °C, storage moduli of 1.22 GPa at 30 °C, and T_g of 100 °C, comparable with commercial petroleum-based VE resins. Thus, fatty acid-based VE materials can be utilized to reduce styrene usage, VOC emissions and health/environmental risks in VE polymers and composites.[48c]

In this dissertation, thermosetting epoxy resins, amine hardeners and VE resins with analogous furanyl and phenyl building blocks were synthesized. Their thermal, mechanical and thermal stability properties were investigated and compared. Cure kinetics studies of epoxy-amine step reaction and vinyl-ester free radical reaction of analogous furanyl and phenyl systems were conducted to evaluate the effects of furanyl and phenyl building blocks on the thermosetting cure behavior. The results suggest that the furanyl building block, relative to the phenyl analogue, exhibits distinguishing effects on the properties of thermosetting epoxy and VE resins. Structure versus property relationships associated with the use of furanyl versus phenyl building blocks was established and conclusions were drawn that support the competitiveness of biobased furanyl structures for use in high-performance thermosetting materials.

Another challenge for incumbent high-performance thermosetting materials is the inherent brittleness resulting from the formed highly crosslinked network structures, which significantly restricts their applications.[9, 49] Once cured, thermosetting materials generally exhibit poor resistance to fracture and typically reach failure before yielding with low energy absorption.[2] Thus, many research efforts have been made to develop

Table 1.3. Thermo-mechanical and thermo-gravimetric properties of biobased vinyl ester resins in the literature.

Biobased VE Resins	Natural resource	Properties	Ref
Aromatic structures from natural resources			
Lignin-MA[a]	Lignin	-	Thielemans et al.[38]
MBO[b]	Bio-oil from lignin	T_g: 115 °C E'_{RT}[c]: 3.2 GPa IDT[d]: 306 °C T_{max}[e]: 418 °C	Stanzione III et al.[15b]
CMAVE[f] BMAVE[g]	Cardanol from CNSL[h]	CMAVE/ST[i], T_g: 86 °C BMAVE/ST, T_g: 158 °C CMAVE/IBOMA[j], T_g: 116 °C BMAVE/IBOMA, T_g: 175 °C	Jaillet et al.[39c]
CNEVER[k]	Cardanol	CNEVER00ST, IDT: 260 °C CNEVER20ST[l], IDT: 285 °C CNEVER40ST, IDT: 265 °C CNEVER50ST, IDT: 270 °C	Sultania et al.[39d]
MVGDM[m]	Vanillin from lignin	MVGDM: T_g: 155 °C; E'_{RT}: 3.6 GPa; IDT: 244 °C; T_{max}: 426 °C	Stanzione III et al.[40a]
DGEBA VE828[n]		DGEBA VE828 with 45wt% ST: T_g: 145 °C; E′ at 35 °C: 2.7 GPa	La Scala et al.[4]
MV[o] MVA[p]	Vanillin and vanillyl alcohol	MV resin: Tg: 69 °C; E'_{RT}: 4.2 GPa; E′ at 80 °C: 0.7 GPa; T_{10}[q]: 280 °C MVA resin: T_g: 83 °C; E'_{RT}: 4.7 GPa E′ at 80 °C: 3.5 GPa; T_{10}: 341 °C	Zhang et al.[40b]
Rosin-derived (meth)acrylic monomers	Rosin	T_g: 97 °C - 122 °C	Lee et al.[41a]

PDAEA[r] PDABA[s] PDAEMA[t]	Gum rosin	PDAEA, T_g: 42 °C PDABA, T_g: 22 °C PDAEMA, T_g: 90 °C	Zheng et al.[41d]
Cycloaliphatic structures from natural resources			
IM[u]	Isosorbide	Flexural strength: 82 MPa Flexural modulus: 4.6 GPa IDT: 305 °C T_g: ~245 °C (tan δ peak)	Sadler et al.[43]
DA-p-GMA[v] MA-m-DA-p-GMA[w]	Dimer fatty acids (DA)	Flexural strength: 29.1 MPa Tensile strength: 16.0 MPa IDT: > 390 °C T_g: 44 °C - 72 °C	Li et al.[44]
Aliphatic structures from natural resources			
AESO[x] AESO-ST[y]	Epoxidized soybean oil	Pure AESO polymer: T_g: -10 °C RT tensile modulus: ~440 MPa Tensile strength: ~6 MPa AESO–ST copolymer (40 wt% ST) T_g: 44 °C RT tensile modulus: 1.6 GPa Tensile strength: ~21 MPa	Khot et al.[45b]
AELO[z] MAELO[aa]	Linseed oil	E′ (30 °C): 2.4 ± 0.1 GPa T_g: > 100 °C Thermal stability upon 300 °C	Lu et al.[46]
ADMM[ab] TOA-GMA[ac]	Myrcene and tung oil	Pure ADMM polymer: T_g: 77 °C; IDT: 403 °C Tensile strength: 49 MPa Pure TOA-GMA polymer: T_g: 35 °C; IDT: 383 °C Tensile strength: 4.8 MPa	Yang et al.[47]

MLA[ad] SOMG/MA[ae] COMG/MA[af]	Fatty acids from plant oils	(SOMG/MA)/10wt%MLA/25wt%ST: (COMG/MA)/10wt%MLA/25wt%ST: Viscosity (25 °C): 600 cP T_g: 100 °C; E′ (30 °C): 1.22 GPa	LaScala et al.[48c]

[a]Lignins modified using maleic anhydride (MA).
[b]Methacrylated Bio-Oil (MBO) comprised of methacrylated phenol, guaiacols and catechols.
[c]Room temperature storage modulus (E'_{RT}).
[d]Initial decomposition temperature (IDT).
[e]Temperature of maximum decomposition rate (T_{max}).
[f]Cardanol epoxy methacrylate vinyl ester (CMAVE).
[g]Bisphenol A epoxy methacrylate vinyl ester (BMAVE).
[h]Cashew Nut Shell Liquid (CNSL).
[i]Styrene (ST) at 40 wt%.
[j]isobornyl methacrylate (IBOMA) at 40 wt%.
[k]Cardanol-based epoxidized novolac vinyl ester resin (CNEVER).
[l]CNEVER20ST: CNEVER blended with 20wt% of ST.
[m]Methacrylated vanillin–glycerol dimethacrylate (MVGDM).
[n]Methacrylated DGEBA EPON 828 commercial epoxy resin (DGEBA VE828).
[o]Methacrylated vanillin (MV).
[p]Methacrylated vanillyl alcohol (MVA).
[q]Temperature of 10% degradation (T_{10}).
[r]Poly(dehydroabietic ethyl acrylate) (PDAEA).
[s]Poly(dehydroabietic butyl acrylate) (PDABA).
[t]Poly(dehydroabietic ethyl methacrylate) (PDAEMA).
[u]Isosorbide-methacrylate (IM).
[v]Dimer fatty acids polymerized glycidyl methacrylate (DA-p-GMA) resin.
[w]Maleic anhydride modified dimer fatty acids polymerized glycidyl methacrylate (MA-m-DA-p-GMA) resin.
[x]Acrylated epoxidized soybean oil (AESO) resin.
[y]Acrylated epoxidized soybean oil resin blended with styrene (AESO-ST).
[z]Acrylated epoxidized linseed oil (AELO).
[aa]Maleinized acrylated epoxidized linseed oil (MAELO).
[ab]Acrylated diglycidyl ester of maleinized myrcene (ADMM).
[ac]Acrylated tung oil polymerized glycidyl methacrylate (TOA-GMA).
[ad]Methacrylated lauric acid (MLA).
[ae]Maleinated soybean oil monoglyceride (SOMG/MA).
[af]Maleinated castor oil monoglyceride (COMG/MA).

methods of toughening thermosetting materials during the past decades.[50] Introducing secondary phase architectures into the cured network structures of thermosets by pre-mixing insoluble micro particles into polymer resins[51] or incorporating soluble reactive tougheners, which can be reaction-induced to phase separate in polymer matrices during cure,[52] is one of the major approaches. Secondary phase architectures formed in-situ can significantly enhance the fracture toughness properties of thermosetting materials through a high degree of matrix shear deformation during fracture.[53] Among the investigated tougheners prepared using renewable sources for thermosetting epoxy resins, plant oil is considered a promising candidate because its chemical structure possesses multiple types of functional groups that can be utilized and modified. Epoxidized soybean oil (ESO) can be readily prepared via the epoxidation of unsaturated soybean oil, which is one of the most abundant vegetable oils from plants.[54] ESO has been investigated to toughen epoxy resins since it contains triglyceride groups, secondary epoxy groups and aliphatic fatty esters with varying chain lengths on its chemical structure, which can react into and plasticize the cured matrices.[55] However, using ESO directly as a toughener, instead of forming phase separated rubbery particles, often leads to an unwanted plasticization effect and diminishes other properties, such as T_g and storage modulus (E').[56] Chemically modifying the structure, functionality and molecular weight (MW) of ESO, by endowing modified ESO with a capability to phase separate during cure, is necessary in order to limit this effect.[57] Chemicals, such as methacrylic, acrylic acids and fatty acids, have been used to modify ESO and toughen VE resins and composite materials.[52a, 58] A series of VE tougheners was prepared by

grafting methacrylic and fatty acids onto ESO, in which the MWs and functionalities of prepared tougheners can be controlled by adjusting the molar ratios of reactants. The ultimate phase separation sizes in the matrices, therefore, could be controlled. Because the ESO based tougheners are critically needed for epoxy resins, preparing such types of ESO based tougheners and evaluating their toughening effect on thermosetting epoxy resins is meaningful and necessary.

In this dissertation, a series of bio-rubber (BR) tougheners for thermosetting epoxy resins was prepared by grafting biobased fatty acids with different chain lengths onto ESO at varying molar ratios through an esterification reaction, providing these prepared BRs with diverse MWs, functionalities and compatibilities with epoxy resins. Biobased acids, including n-hexanoic acid,[59] n-octanoic acid,[60] n-decanoic acid,[61] n-lauric acid, n-myristic acid and n-palmitic acid, were used to make these BRs fully sustainable. The successful preparation of these BRs was verified using multiple characterization methods. Their overall effect on the commercial epoxy resins was evaluated by measuring the mechanical fracture toughness and thermal-mechanical properties of BR blended polymer samples. Secondary phase architectures with tunable rubbery particle sizes, depending on the BR type and weight fraction, were found to form in the cured networks of BR blended samples. Fracture toughness properties of these BR blended samples were dramatically improved compared with the control samples, which were BR-free. Thus, with other excellent advantages, such as low viscosity and competitive cost, these BRs are promising for use in commercial epoxy resins.

1.2. Background

1.2.1. Thermoset cure

Thermosetting polymers are materials that irreversibly cure through chemical reactions, heat or ultraviolet radiation, which results in linear or crosslinked network structures. The average molar mass increases and a polymer network structure starts to form along with the polymerization reaction. At a critical conversion of the reactive groups, called the gel point, the molar mass becomes infinite and a percolation path forms in the polymer network where the shear viscosity increases to infinite. In the post gelation stage, the polymerization reaction, which is restricted and becomes diffusion-controlled, continues and results in increases in both crosslinking density and elastic modulus of the polymer network. Vitrification, which occurs when the T_g of the thermoset network equals the cure temperature, is different from gelation and may or may not occur during the polymerization, depending on the cure temperature relative to the T_g of the fully cured network, $T_{g\infty}$. In order to achieve a complete conversion of the reactive groups and to obtain $T_{g\infty}$, the cure temperature should be at or above $T_{g\infty}$ to avoid vitrification.[62]

1.2.2. Epoxy-amine step-growth polymerization

Thermosetting epoxy polymers can be obtained by reacting epoxy monomers with various hardeners, such as amines, phenols, isocyanates, anhydrides and acids, among

which amines are one of the most common types.[63] The epoxy-amine reaction typically proceeds via a step-growth polymerization mechanism with a series of elementary reactions that form a new covalent bond between two functional groups. The number of functionalities per monomer and the molar ratio between monomers are two key factors that affect the resultant polymer network structures. In order to form a crosslinked structure, one co-monomer must possess functionality greater than two, while the other co-monomer must be bifunctional at least. The amine groups typically possess primary and secondary amino hydrogen atoms; therefore, the epoxy-amine reaction includes epoxy-primary amine reaction and epoxy-secondary amine reaction, as shown in Figure 1.3. In these two reactions, epoxy rings are opened by primary and secondary amine groups, and hydroxyl groups are generated as a result.

When the ratio between epoxy and amine functionalities is at stoichiometry or the amine functionality is in excess in the epoxy-amine mixture, no side reactions besides the epoxy-amine reactions occur. Since hydroxyl groups can catalyze epoxy-amine reactions by facilitating the nucleophilic attacks of primary and secondary amine groups, these epoxy-amine reactions are auto-catalyzed with the continuous formation of hydroxyl groups. Hydroxyl groups can also react with epoxy groups, known as the hydroxyl-epoxy etherification, demonstrated in Figure 1.4. When the epoxy functionality is in excess in the epoxy-amine mixture or the secondary amine group possesses a low reactivity, this hydroxyl-epoxy etherification reaction can compete with the epoxy-amine reactions.

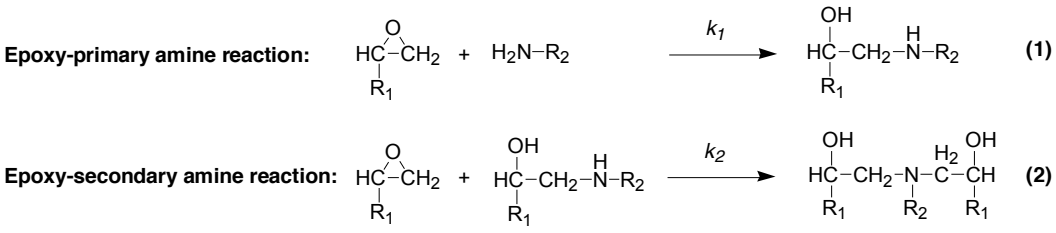

Figure 1.3. Epoxy-primary amine and epoxy-secondary amine reactions in which epoxy groups react with primary and secondary amine groups with k_1 and k_2 as the reactivity rates, respectively. Hydroxyl groups are formed in both reactions.

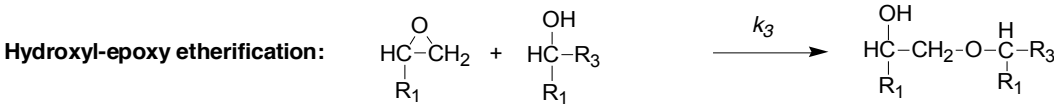

Figure 1.4. Hydroxyl-epoxy etherification reaction in which hydroxyl groups react and open the epoxy rings with k_3 as the reactivity rates.

1.2.3. Vinyl ester free-radical polymerization

VE resins are another important type of thermosetting polymer materials typically prepared through the addition reaction of epoxy resins and unsaturated mono-carboxylic acids, most commonly methacrylic and acrylic acids.[64] With terminal reactive carbon-carbon double bonds in their chemical structures, VE resins can form crosslinked polymer networks with or without the addition of another co-monomer. In many industrial applications, it is common to blend VE oligomers with a certain amount of low molecular weight co-monomers, such as styrene, methyl methacrylate and vinyl toluene, to serve as reactive diluents that reduce the room temperature viscosity to a typical processing range between 0.2 – 2 Pa.s.[4, 65] A viscosity of 0.5 Pa.s is often considered the maximum for most inexpensive liquid molding techniques.[66] VE resins are crosslinked through a free radical polymerization of their terminal (meth)acrylate groups with reactive diluents if added. This free radical polymerization mechanism consists of the following steps: initiation, propagation, termination and chain transfer to small molecules.

Free radicals that initiate the polymerization reaction are generated using several methods, such as thermal, redox process or photo-chemical decompositions of peroxides, hydroperoxides and (di)azo reagents, which are called the initiators. The decomposition of thermal initiators can be accelerated by applying heat or by promoters used to activate the decomposition reaction at a lower temperature. The determination of

initiator/promoter packages is often based on the type of vinyl ester resins, the process method and the requirement of target applications.[67]

The propagation step contains a series of radical addition reactions between the carbon-carbon double bonds of vinyl ester monomers and reactive diluents. These free radical functionalities remain reactive during the growth of polymer chains until two free radical sites combine to terminate or a radical transfer reaction occurs. The propagation step is chemically controlled and lasts less than one second from the time the chain is initiated to the time it is terminated.[68]

The propagating radicals can be terminated through radical combination or disproportionation. Termination by combination occurs when two free radicals combine to form a single covalent bond and connect two polymer chains together. Termination by disproportionation occurs when a β-hydrogen atom on a radical polymer chain transfers to another radical polymer chain and results in two separate non-radical polymer chains, one with a formed carbon-carbon double bond.

Chain transfer to small molecules can also take place during free radical polymerization, when a growing radical chain captures a weakly bonded hydrogen atom from a small molecule, resulting in a terminated polymer chain and a new reactive radical site on the small molecule. These small molecules can be the initiator, solvent, vinyl ester monomer or transfer agent which is used to control the formed polymer molecular weight distribution.[69]

1.2.4. Epoxy-amine cure kinetics

Various chemical reactions that occur during the cure of thermosetting materials drive the complex formation of polymer network morphologies and, in turn, determine the ultimate properties of these formed thermosets.[70] Therefore, in order to understand the cure process and adjust for the desired properties, it is essential to study the kinetics of the cure reactions of thermosetting epoxy and VE resins.[71]

As shown in Figure 1.3, in general, the cure of epoxy resins and amine hardeners can be described as a two-step reaction: in the first step, an epoxy group and a primary amine group react and form a secondary amine group and a hydroxyl group; in the second step, an epoxy group and a secondary epoxy group react and yield a tertiary amine group and another hydroxyl group.[72] The extent of epoxy-amine cure reaction can be determined using isothermal differential scanning calorimetry (DSC) by calculating the ratio between the heat generated under an isothermal condition and the total heat released by the reaction.[73] While very useful, this approach is significantly limited by its low accuracy at high conversions, insufficient capability of monitoring fast reactions and inability to determine independent conversions of epoxy and amine groups. Infrared spectroscopy (IR), contrary to DSC, not only provides better accuracy at high conversions of epoxy and amine groups, but also has the ability to independently determine epoxy and amine conversions by monitoring their corresponding IR absorption signals with very few errors. Compared to mid IR, near IR spectrum is more

advanced for use in monitoring the characteristic peaks of epoxy and amine groups during cure due to the observations of less overlapped bands.[74] Band intensities of epoxy and amine groups in this range are also lower compared to mid IR, so tested samples are more concentrated and result in data with improved accuracy. Two characteristic peaks, 4527 and 6060 cm^{-1}, correspond to epoxy groups in near IR, and the 4527 cm^{-1} peak is more commonly used in kinetics studies due to its sufficient separation from other peaks.[75] Two characteristic peaks, 4929 and 6507 cm^{-1}, are also intense and well distinguishable in near IR for amine groups. Both commonly used in kinetics studies, the 4929 cm^{-1} peak corresponds to the primary amine N-H bond, while the 6507 cm^{-1} peak relates to the combination of both primary and secondary amine N-H bonds.[76] The epoxy-amine cure process can be monitored by following the concentration evolutions of epoxy, primary amine and secondary amine groups using the height or area of their characteristic peaks in near IR spectra in which the Beer-Lambert law is satisfied.[77] For quantitative analysis, the concentration evolutions of epoxy and primary amine groups can be directly determined using the peaks at 4527 and 4929 cm^{-1}, respectively, and the degree of conversion of these two groups can be further calculated based on concentration changes. With known and measured epoxy and primary amine concentrations, mass balance is used to determine the concentration evolutions and conversion degrees of secondary and tertiary amine groups.

Bearing in mind the concentrations of all these involved groups, complex models can be used to fit the experimental data, and cure kinetics parameters for various steps in the

polymerization reaction can be calculated. Numerous kinetics models have been established and reported for epoxy-amine systems using model compounds. A catalytic effort of hydroxyl group to the epoxy-amine reaction was observed and explained using a third-order reaction mechanism.[78] Therefore, a model taking into account the catalytic effort of both initial and formed hydroxyl groups in epoxy-amine systems was proposed; this model has been widely used and further developed in many other epoxy-amine systems.[79] Commonly used kinetics mechanisms for the epoxy-amine reaction include two reaction pathways, the non-catalyzed and auto-catalyzed pathways. The auto-catalyzed pathway, with the presence of initial hydroxyl group in the epoxy-amine mixture, considers the mentioned formation of three-component complexes, which include hydroxyl, amine and epoxy groups.[80] Considering the reaction scheme, the epoxy [EP], primary amine [PA], secondary amine [SA], tertiary amine [TA] and hydroxyl [OH] concentrations, as a function of the reaction time are the concentrations of interest. Equation 1.1 and 1.2 describe the epoxy-amine reaction scheme via the auto-catalytic pathway, in which the k_1 and k_2 are the kinetic parameters of epoxy-primary amine and epoxy-secondary amine reactions in the auto-catalytic pathway, respectively. Kinetics equations for epoxy and primary amine conversions are listed in Equations 1.3 and 1.4.

[PA] and [EP] are measured using near IR. [SA], [TA] and [OH] are obtained from mass balance relations as shown in Equations 1.5 to 1.11. The initial epoxy concentration $[EP]_0$ is related to epoxy, secondary amine and tertiary amine instant concentrations shown in

Equation 1.5. The initial primary amine concentration $[PA]_0$ is related to the primary amine, secondary amine and tertiary amine instant concentrations shown in Equation 1.6. By rearranging Equations 1.5 and 1.6, [SA] and [TA] are expressed by Equations 1.7 and 1.8, respectively, and they can be calculated using the known and measured epoxy and primary amine concentrations.

$$[PA] + [EP] + [OH] \overset{k_1}{\rightarrow} [SA] + 2 * [OH] \tag{1.1}$$

$$[SA] + [EP] + [OH] \overset{k_2}{\rightarrow} [TA] + 2 * [OH] \tag{1.2}$$

$$\frac{d[EP]}{dt} = -k_1 * [PA] * [EP] * ([OH]_{auto} + [OH]_0) - k_2 * [EP] * [SA] * ([OH]_{auto} + [OH]_0) \tag{1.3}$$

$$\frac{d[PA]}{dt} = -k_1 * [PA] * [EP] * ([OH]_{auto} + [OH]_0) \tag{1.4}$$

$$[EP]_0 = [EP] + [SA] + 2 * [TA] \tag{1.5}$$

$$[PA]_0 = [PA] + [SA] + [TA] \tag{1.6}$$

$$[SA] = 2 * ([PA]_0 - [PA]) - ([EP]_0 - [EP]) \tag{1.7}$$

$$[TA] = ([EP]_0 - [EP]) - ([PA]_0 - [PA] \tag{1.8}$$

In Equation 1.9, [OH] is calculated as the sum of $[OH]_0$ and $[OH]_{auto}$, which are the initial hydroxyl concentration and instant hydroxyl concentration from the epoxy-amine reaction given in Equation 1.10. $[OH]_0$ is primarily determined by the reactants or impurities, such as moisture, in the epoxy-amine systems.

$$[OH] = [OH]_0 + [OH]_{auto} \tag{1.9}$$

$$[OH]_{auto} = [SA] + 2 * [TA] \tag{1.10}$$

The reactivity ratio between primary and secondary amine groups is defined as $R = k_2/k_1$. Since a primary amine group possesses two reactive hydrogen atoms, an equal reactivity of primary and secondary amine groups would yield R = 0.5. However, in most epoxy-amine systems, it is often experimentally observed and reported that a primary amine group shows a higher reactivity, which yields $R < 0.5$.[81] This is as expected because the addition of an epoxy segment to a primary amine group often increases the steric hindrance and decreases the nucleophilicity of nitrogen atom in the formed secondary amine group, both of which reduce its reactivity with another epoxy group. The R value can be used to interpret the formation of polymer network structures as well as the ultimate properties of formed thermosets. For instance, epoxy-amine systems with higher R values tend to possess more crosslinked yet brittle network structures, while

those with lower R values tend to form networks with more chain extensions, which are likely to be tougher.[76]

1.2.5. Vinyl ester cure kinetics

Cure kinetics of VE resins have been studied by many researchers using FT-IR via a copolymerization theory.[4, 40a, 82] Different from the DSC technique which can only generate cure information as a global nature, the FT-IR provides insights regarding the reaction rate and conversion degrees of each individual reactant during the cure process, which is crucial for understanding the network structure development and property performance of VE materials. A detailed investigation of the bulk copolymerization cure kinetics of VE resins was performed on a system of difunctional DGEBA based VE resins, which were blended with 28 – 60 wt% monofunctional styrene and cured at isothermal temperature ranging from 70 to 110 °C.[82a] Depletions of carbon-carbon double bonds in the VE and styrene (ST) monomers were independently monitored in mid IR spectra using the 945 cm^{-1} and 910 cm^{-1} peaks corresponding to the vinyl groups in VE and ST monomers, respectively. The 830 cm^{-1} and 700 cm^{-1} peaks were used as reference peaks to correct the effects associated with evaporation and dimensional changes in VE and ST, respectively. Normalized fractional conversions of VE and ST double bonds were calculated from the mid IR data using Equations 1.11 and 1.12, where α is the double band instant fractional conversion and ABS is the absorption intensity of involved peaks.

$$\alpha_{VE}(t) = 1 - \left(\frac{ABS(t)_{945\ cm^{-1}}}{ABS(t=0)_{945\ cm^{-1}}}\right) \Big/ \left(\frac{ABS(t)_{830\ cm^{-1}}}{ABS(t=0)_{830\ cm^{-1}}}\right) \quad (1.11)$$

$$\alpha_{ST}(t) = 1 - \left(\frac{ABS(t)_{910\ cm^{-1}}}{ABS(t=0)_{910\ cm^{-1}}}\right) \Big/ \left(\frac{ABS(t)_{700\ cm^{-1}}}{ABS(t=0)_{700\ cm^{-1}}}\right) \quad (1.12)$$

$$\frac{d\alpha_t}{t} = (k_1 + k_2 * \alpha_t^m) * (1 - \alpha_t)^{2-m} \quad (1.13)$$

$$\frac{d\alpha_t}{t} = k * \alpha_t^m * (\alpha_u - \alpha_t)^{2-m} \quad (1.14)$$

$$\alpha_t = \frac{\alpha_u * [k * t * \alpha_u * (1-m)]^{1/(1-m)}}{1 + [k * t * \alpha_u * (1-m)]^{1/(1-m)}} \quad (1.15)$$

Empirical autocatalytic kinetic models have been established to fit the experimental data. Equation 1.13 was developed to fit the isothermal cure kinetics of VE resins by Kamal and Sourour, in which k_1, k_2 and m are the reaction rate constants and reaction order, respectively.[83] Widely used by many researchers, Equation 1.14 is a simplified version of Equation 1.13 that neglects k_1 and includes α_u, a final fractional conversion, to provide more accuracy during fitting experimental data. Such empirical equations are developed for fitting the bulk copolymerization cure kinetics of vinyl ester resins, rather than illuminating the kinetics mechanism of the copolymerization reaction.[82a, 82c]

Equation 1.15 is the integrated solution of Equation 1.14 and works very well for fitting and analyzing double bond conversions of VE and ST monomers as a function of time from the mid IR cure kinetics data. Parameters obtained from the data-fitting process are the reaction rate constant, k, and the reaction order, m.[82c] It was found that the reaction rate of ST double bonds was initially lower than that of VE double bonds. With a higher final conversion degree, ST double bonds continued to react after the conversion of VE double bonds reached a plateau. The resin composition and cure temperature were found to significantly influence the reaction rates and conversation degrees of VE and ST double bonds. The reaction order remained relatively constant at 0.85 for both VE and ST monomers under all evaluated compositions and temperatures, though. The connectivity of formed network structures and its relation to material properties were not sufficiently discussed in this work.[82a] A later work investigated the relationship of cure kinetics, microstructure and mechanical properties for the VE-ST systems.[82b] Reactivity ratios of VE and ST double bonds were studied using mid IR and the conventional copolymer composition equation. The ratio of VE to ST double bonds incorporated into the network structure was highly dependent on the cure temperature, which led to significantly different mechanical properties of the VE-ST systems, including strength and fracture toughness. Phase separation was found to occur during cure, and microstructures with sizes affected by the cure temperature were formed in cured networks. This work clearly demonstrates that the cure temperature affected the copolymerization cure kinetics and, in turn, affected the material properties of VE-ST systems dramatically.[82b]

1.3. Overview

The objective of this dissertation is to use biobased building blocks to design and prepare thermosetting polymer materials that possess comparable thermal and mechanical properties to the petroleum-based systems. Two fundamental questions have been answered based on the current results: (1) How do biobased furanyl building blocks affect thermal and mechanical properties of thermosetting polymer materials relative to the phenyl analogue? and (2) How can plant oil triglycerides be used to improve the thermal and mechanical properties of commercial thermosetting materials? This dissertation presents the development of structure-property relationships for thermosetting materials possessing phenyl and biobased furanyl building blocks, and structure-property relationships for renewable triglyceride-based toughening agents for commercial epoxy resins.

There are eight chapters in this dissertation. Chapter 1 introduces the chemistries, properties and applications of thermosetting epoxy and VE materials. The two critical challenges associated with these materials, their non-renewable petroleum-based feedstocks and inherent brittleness, become the motivation and objective of this dissertation work. Chapter 2 begins with the preparation of two template epoxy resins that possess biobased furanyl and analogous phenyl building blocks. Furanyl and phenyl thermosetting polymer materials are prepared using these epoxy resins and commercial amine hardeners. Their thermal and mechanical properties are evaluated,

and a structure versus property relationship is drawn: the furanyl building block, compared with phenyl building block, endows thermosetting polymer materials with higher storage modulus, improved fracture toughness, better thermal stability and lower glass transition temperature properties. Chapter 3 introduces the epoxy-amine cure kinetics study of analogous furanyl and phenyl epoxy resins with previously used amine hardeners to investigate the relative effect of different building blocks on the cure behavior and structural network development of thermosetting polymer materials. The results suggest that hydrogen bonding on the furanyl ring potentially affects the reactivity and reactivity ratio of the epoxy-amine reactions, thus influencing the processing characteristics and the thermal and mechanical properties of furanyl epoxy systems relative to the phenyl analogues. Chapter 4 explores the preparation of furanyl di-amine hardeners and evaluates the effect of biobased furanyl building blocks on thermal and mechanical properties of thermosetting polymer materials from the amine hardener side. Chapter 5 presents the preparation of furanyl and phenyl VE resins and investigates the effect of furanyl building blocks on the properties of thermosetting VE polymer materials compared with the phenyl analogue. Chapter 6 presents an additive molar function analysis of the furanyl building block to the physical properties, such as T_g and density, of thermosetting polymers. The molar glass transition function value (Y_g) and molar volume increment value ($V_{a,i}$) of the furanyl building block for thermosetting polymer materials were calculated and obtained for the first time. Chapter 7 introduces the utilization of biobased sources for improving thermal and mechanical properties of commercial thermosetting materials. A series of biobased toughheners for epoxy resins is

prepared by grafting fatty acids onto epoxidized soybean oil, and their toughening effect is evaluated by measuring mechanical fracture toughness properties of thermosetting polymer materials containing these prepared tougheners. Secondary rubbery phases that improve the fracture toughness properties of the matrices through higher degrees of matrix shear deformation and energy dissipation are found to occur in the cured networks. Finally, Chapter 8 summarizes the key conclusions of this dissertation work and proposes a list of specific future work that can be the potential extension of this study.

Chapter 2. Synthesis and characterization of thermosetting furanyl based epoxy systems

2.1. Introduction

Thermosetting epoxy resins are extensively used for applications in the aerospace, automotive, insulation, electronics and sporting goods industries.[84] They possess excellent thermal and mechanical properties as a result of the formation of crosslinked polymer networks when cured.[1, 18, 85] Commercial epoxy resins are primarily produced from petroleum feedstocks. Recently, the non-renewability of fossil fuels and the demand of protecting health and environment have raised interest in preparing thermosets from biobased sources.[1, 9, 86] As introduced in Chapter 1, numerous biobased sources have been studied as feedstocks for thermosets, including plant oils,[12] cellulose,[13b] hemicellulose,[1, 14c] lignin,[15a] starch[16a] and chitin.[17a, 87] Due to their aromatic characteristics, biobased chemicals possessing furanyl building blocks are considered promising candidates to prepare thermosetting materials that have properties comparable to petroleum-based phenyl systems.[13b] In order to properly evaluate the effects of furanyl building block on thermo-mechanical properties of thermosets relative to the phenyl analogue, thermosetting resins with analogous structures in which only the building block is varied need to be prepared and compared.

In this chapter, two mimetic epoxy monomers, 2,5-bis[(2-oxiranylmethoxy)methyl]-furan (BOF) and 2,5-bis[(2-oxiranylmethoxy)methyl]-benzene (BOB), were prepared according to the literature and cured using standard amine hardeners, PACM and EPIKURE W. Thermal, mechanical and thermal stability properties of these analogous systems were evaluated with factors such as epoxy purity, cure condition and extent of reaction being kept consistent. A structure versus property relationship showed that furanyl based epoxy system possessed lower T_g, higher glassy modulus, improved fracture toughness and comparable thermal stability properties relative to the phenyl epoxy system. The furanyl ring has thus been demonstrated to be a viable building block for biobased high-performance epoxy resins, with promising potential for applications in other thermosetting polymer materials.

2.2. Experimental

2.2.1. Materials

All reagents and solvents used in this chapter, including tetrabutylammonium hydrogen sulfate (99+%), tetrabutylammonium bromide (98+%), epichlorohydrin (99%), ethyl acetate (99.8%), hexane (95%), sodium hydroxide (98%), tetrahydrofuran (THF, 99.9%), silica gel (60Å, 70-230mesh), furfuryl glycidyl ether (FGE, 96%), 1,4-benzenedimethanol

(99%), glacial acetic acid (99.7%), acetic anhydride (99+%), crystal violet indicator, perchloric acid (0.1 N solution in glacial acetic acid), methylene chloride (99.8%) and potassium acid phthalate (99.95%) were supplied by Sigma-Aldrich, USA; 1,4-bis(glycidyloxy)-benzene (DGEPP, 97+%) was supplied by Alfa Aesar, USA; 2,5-bis(hydroxymethyl)-furan (b-HMF, 98+%) was supplied by Pennakem, LLC, USA. EPON 828 composed of DGEBA and its low molecular weight oligomers, and EPIKURE W composed of isomers of diethyl toluene diamine were supplied by Miller-Stephenson chemical company, USA; PACM (99+%) was supplied by Air Products, USA. All chemicals were used as received.

Chemical structures of epoxy monomers and amine hardeners used in this chapter, as well as materials discussed in Chapter 1, are summarized in Figure 2.1. A and B are synthesized furanyl and phenyl based epoxy monomers; C, D and E are commercial epoxies used with or without A and B to prepare a number of thermosets cured by the amine hardeners F and G. H is the material discussed in Chapter 1.

2.2.2. Synthesis of 1, 4-bis[(2-oxiranylmethoxy)methyl]-benzene (BOB)

A 1000 mL three-necked round-bottom flask was equipped with a magnetic stirring bar, a constant-pressure dropping funnel, a thermometer and an inlet for dry nitrogen. Oxygen and moisture in the reactor was replaced with dry nitrogen.

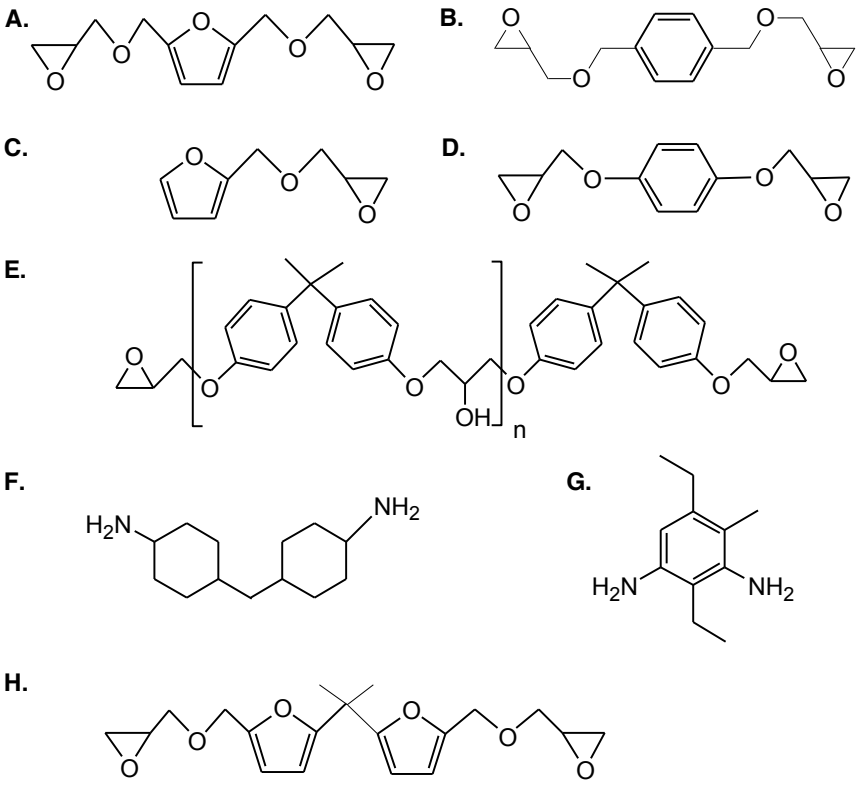

A. 2, 5-bis[(2-oxiranylmethoxy)methyl]-furan (**BOF**);
B. 1, 4-bis[(2-oxiranylmethoxy)methyl]-benzene (**BOB**);
C. Furfuryl glycidyl ether (**FGE**);
D. 1,4-bis(glycidyloxy)-benzene (**DGEPP**);
E. Diglycidyl ether of bisphenol A (**DGEBA**), EPON 828, n=0.13;
F. 4, 4′-methylene biscyclohexanamine (**PACM**);
G. Diethyl toluene diamine (**EPIKURE W**);
H. Bis-furan di-epoxide (**bFdE**).

Figure 2.1. Materials used in Chapter 2 and discussed in Chapter 1.

Tetrabutylammonium bromide was used as a catalyst.[88] 1, 4-benzenedimethanol (13.8 g, 0.1 mol), tetrabutylammonium bromide (TBAB, 3.22 g, 0.01 mol) and 40% w/w aqueous sodium hydroxide (250 ml) were vigorously stirred in the flask at 50 °C for 1 hour. Then, the flask was placed into an ice bath for half an hour before epichlorohydrin (73.6 g, 0.8 mol) was added dropwise using a constant-pressure dropping funnel over a period of 0.5 hours. The mixture was allowed to react for another 12 hours with vigorous stirring after the temperature reached room temperature (RT). The mixture was then poured into 125 ml ice/water and extracted three times with 50 ml diethyl ether. The combined organic phase was washed with deionized water to neutral pH, dried with anhydrous $MgSO_4$ and concentrated using vacuum. The residue was purified by reduced-pressure distillation to yield BOB as a colorless liquid. An overall yield of 90% was obtained (22.5 g) and the purity was 99% by ^1H NMR.

2.2.3. Synthesis of 2, 5-bis[(2-oxiranylmethoxy)methyl]-furan (BOF)

A 1000 mL four-necked round-bottom flask was equipped with a constant-pressure dropping funnel, a thermometer, a condenser, an inlet for dry nitrogen and a magnetic stirring bar. The air inside the system was replaced with nitrogen to eliminate oxygen and moisture. Tetrabutylammonium hydrogen sulfate was used as a catalyst.[89] With continuous stirring, epichlorohydrin (202.4 g, 2.2 mol) and tetrabutylammonium hydrogen sulfate (4.07 g, 0.012 mol) were charged into the flask at 65 °C. 2,5-bis(hydroxymethyl)-furan (b-HMF, 128.05 g, 1 mol) was added into the flask dropwise

after being melted (T_m = 68 °C). The reaction was allowed to proceed for 4 hours, then the mixture was cooled to 50 °C and 320 mL of sodium hydroxide aqueous solution (50% w/w) was added dropwise to complete the intramolecular ring-closing epoxidation reaction. After 2 hours, the mixture was extracted three times with 50 ml diethyl ether. The combined organic phase was washed with deionized water and dried with anhydrous $MgSO_4$. A rotary evaporator was used to remove the solvent, leaving a brown-red liquid residue. Silica gel chromatography with ethyl acetate/hexane (2 to 1 by volume) was used to purify the BOF as a yellow liquid. An overall yield of 60% was obtained (144 g) and the purity was 99% by ^{1}H NMR. More details regarding tips of preparing BOF and BOB epoxy monomers can be found in Appendix A.

2.2.4. Characterization of BOF and BOB

BOF and BOB were characterized by epoxy titration (ASTM D 1652-97), gel permeation chromatography (GPC), Fourier transform infrared spectroscopy (FTIR), ^{1}H NMR, ^{13}C NMR (nuclear magnetic resonance), rheometry and Mass Spectrometry (MS).

Epoxy titration was performed by following ASTM D1652-90, Procedure B,[90] to determine epoxy equivalent weight (EEW) of BOF and BOB. For example, a mixture was prepared with BOF (0.4 g), methylene chloride (10 mL), tetraethylammonium bromide solution (10 mL, 0.25 g/mL) and 8 drops of 0.1% solution of crystal violet indicator in glacial acetic acid. Titration was conducted using 0.1 N perchloric acid reagent. The

mixture displayed a sharp color change from blue to green and the volume of perchloric acid agent used was recorded. Multiple titrations were conducted.

GPC was used to measure the purity of BOF and BOB. A Waters 515 GPC with two 30 cm long, 7.5 mm diameter, 5 μm (poly)styrene-divinyl benzene columns (PLgel 5 μm MIXED-C column and PLgel 5 μm 50 Å column) in series. Columns were equilibrated and maintained at 45 °C with elution of THF at a rate of 1.0 mL/min. The column effluent was monitored using two detectors: a Waters 2487 dual absorbance detector operating at 280 and 254 nm, and a Waters 2410 refractive index detector at 25 °C. Samples (2 mg) were dissolved in THF (1 mL) and filtered before being injected into GPC. The total running time for each sample was 25 minutes.

Functional groups of BOF and BOB, such as furanyl, phenyl and epoxy, were identified using a Thermo Nicolet Nexus 870 Fourier transform infrared spectrometer (FTIR) in absorbance mode. Spectra were recorded with 32 scans at an 8 cm^{-1} resolution at RT with a deuterated tryglycine sulfate (DTGS) detector in 4000-8000 cm^{-1} range for near infrared spectra (N-IR) and 650-4000 cm^{-1} for mid-infrared spectra (M-IR).

Proton and carbon nuclear magnetic resonance (^{1}H NMR and ^{13}C NMR) measurements were used to confirm chemical structures of BOF and BOB. Both ^{1}H NMR and ^{13}C NMR were obtained using a Varian Unity Inova NMR (500 MHz) instrument with spectral window of ± 2000 Hz, 32 scans for ^{1}H NMR and 5000 scans for ^{13}C NMR at 293 K and 90° pulse width.

Monomer viscosity was measured using a TA AR2000 ex Rheometer with 40 mm flat plate configuration using a shear rate range from 0.01 to 1000 s^{-1}, with 10 measurements recorded per decade. Shear stress was measured every 2 s at each shear rate. Viscosity was reported as the average of three measurements at a shear rate of 1000 s^{-1}.

Mass Spectrometry (MS) was conducted by a Waters Micromass AutoSpec-Ultima triple sector high resolution mass spectrometer using chemical ionization with methane as the ionizing gas in positive ion mode.

2.2.5. Preparation of BOF and BOB polymer samples

PACM and EPIKURE W were used as curing agents. BOF polymer samples were prepared by varying the weight ratio of BOF to DGEBA and mixing with a stoichiometric quantity of a curing agent. To define polymer networks being discussed in this work, W_{epoxy} represents the weight fraction of BOF or BOB monomer blended with DGEBA before the addition of curing agents. For example, a sample of a 3:7 weight ratio of BOF to DGEBA was defined to be $W_{BOF} = 0.3$. Stoichiometric quantities of curing agent were calculated based on EEW = 188 for DGEBA, 120 for BOF, 125 for BOB, and amine hydrogen equivalent weight (AHEW) = 52.5 for PACM and 45 for EPIKURE W. BOF and BOB polymer samples were prepared with W_{BOB} and W_{BOF} varying from 0 to1.

BOF and BOB polymer samples were cast into rubber molds with dimensions of 10 × 40 × 2.0 mm and cured. The cure procedure, i.e. cure and post cure temperature and cure

time, was established based on TA Q2000 differential scanning calorimetry (DSC) and near-IR studies.[91] For example, BOF-PACM samples were cured at 60 °C and post-cured at 180 °C for 9 hours, respectively, to achieve fully cured polymers.[26] BOB polymer samples were prepared in a similar fashion. Polymer samples for dynamic mechanical analysis (DMA) measurement were sanded to uniform dimensions of 10 × 38 × 1.8 mm. Samples for fracture toughness measurement were prepared using rubber molds with dimensions of 140 × 14 × 6.0 mm and further processed into compact tension (CT) specimens with dimensions of 16 × 13 × 5.5 mm after curing. Samples for tensile measurements were prepared using rubber molds and tested following ASTM D 638-03.[92]

Full conversion of epoxy and amine groups in BOF and BOB polymer samples was verified using a Thermo Nicolet Nexus 870 N-IR spectrometer. Spectra of post-cured samples were recorded in a range of 4000-8000 cm^{-1}, with 8 cm^{-1} resolution and 32 scans operated in absorbance mode at RT.[91]

2.2.6. Polymer properties

Thermo-mechanical properties, i.e. glass transition temperature (T_g) and storage modulus (*E'*), of BOF and BOB polymer samples were measured using DMA on a TA Instruments 2980 in single cantilever geometry with a frequency of 1 Hz and an amplitude of 15 μm. Temperature ramp rate was at 2 °C/min from RT to a particular

temperature (generally approximately 60 °C higher than the sample T_g). Each sample was tested twice and the result of the second run was used to measure its E' and T_g which was assigned as the temperature corresponding to the peak of loss modulus curve. Fracture toughness properties, i.e. the critical stress intensity factor (K_{1c}) and critical strain energy release rate (G_{1c}) values, were obtained by testing seven specimens for each sample composition. An 8 mm long notch was cut into each specimen and a sharp pre-crack was made at the notch bottom using a fresh blade at -5 °C before testing with a 1.0 mm/min crosshead speed at RT. Stress-strain data was recorded, and K_{1c} and G_{1c} values were calculated following ASTM D 5045-99.[93] Tensile properties of BOF and BOB polymer samples were measured at RT using at least 5 dog-bone shaped specimens per composition following ASTM D 638-03. The thermal stability in ambient and inert environments was investigated using a TA instruments Q50 TGA with a 10 °C/min ramp rate from 25 to 800 °C in air and argon, respectively.

2.3. Results and Discussion

2.3.1. Preparation of BOF and BOB

BOF was synthesized via a two-step method. In the first step, an intermediate chlorohydrin ether was produced via etherification reaction between the oxirane ring of

epichlorohydrin and hydroxyl group of b-HMF with the presence of tetrabutylammonium hydrogen sulfate as a phase transfer catalysis. In the second step, the chlorohydrin ether experienced a ring-closing reaction to reform epoxy group due to a dehydrochlorination reaction under the help of alkali.

Pure BOF was obtained by the purification of crude product on a silica gel chromatography with an overall yield of 60%. Figure 2.2 presents the characteristic peaks of epichlorohydrin, and BOF before and after purification. Figure 2.2b is a magnification of 1a.

The characteristic peak of b-HMF is not displayed together in this figure because its solubility in THF is too low to be well monitored by the detectors. In Figure 2.2a, no peaks are present between 0 to 10 minute and 20 to 25 minute. In Figure 2.2b, crude BOF (black line) possesses four main peaks at 13.5 minute (4.2% by area), 14.5 minute (19.2% by area), 15.6 minute (62.7% by area) and 17.3 minute (6.6% by area), respectively. By comparing with epichlorohydrin curve (blue line) with only one peak at 17.3 minute, the component with the lowest molecular weight in crude BOF is identified as unreacted epichlorohydrin (epichlorohydrin was added at a mole ratio of 2.2 relative to b-HMF initially). Purified BOF (red line) possesses two peaks occurring at 15.0 minute (2.5% by area) and 15.6 minute (97.5% by area), respectively, meaning its purity is 97.5% by GPC. The dominant component (62.7% by area) in crude BOF is identified to be BOF, and its first and second peaks are identified as bi- and tri-monomer by calibration, respectively.

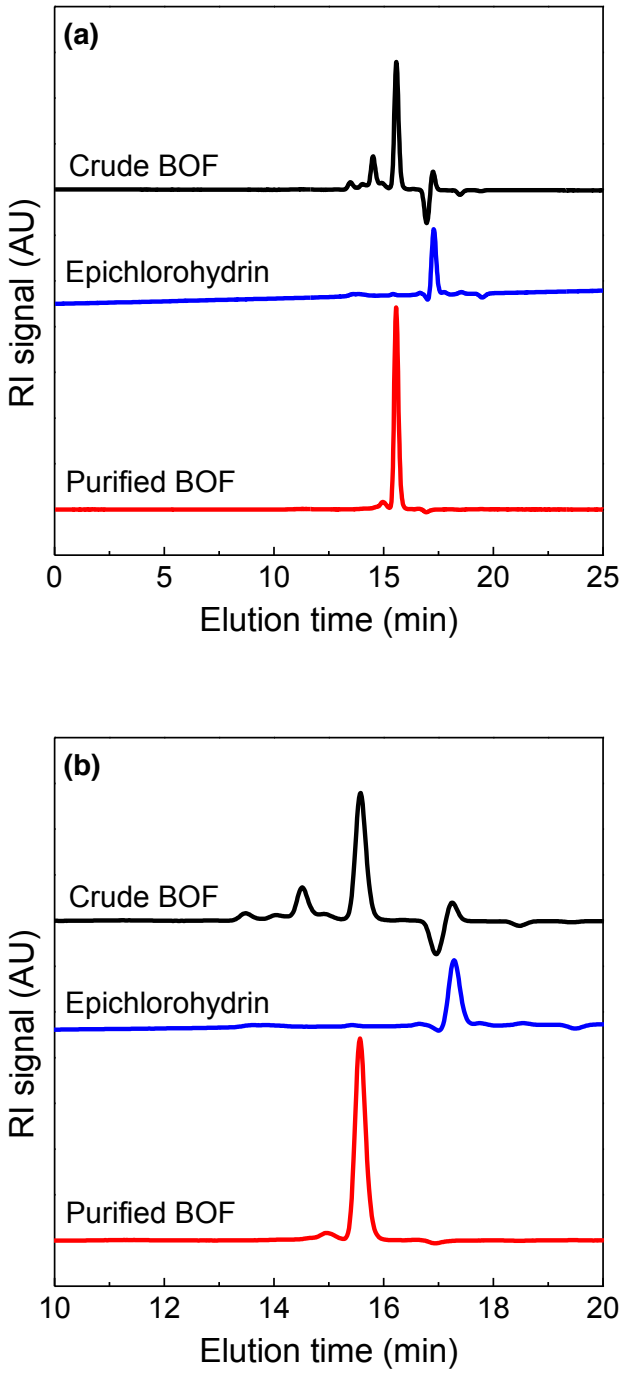

Figure 2.2. The GPC spectra of crude, purified BOF and epichlorohydrin.

Epoxy equivalent weight of purified BOF is measured to be 123 g/eq. by following ASTM D1652-90, Procedure B. This matches well with the theoretical value 120 g/eq. and its purity is measured to be 98% based on calculation of EEW.

^{1}H-NMR (500 MHz, $CDCl_3$) and ^{13}C-NMR (500 MHz, $CDCl_3$) were used to further confirm the chemical structure of BOF. In Figure 2.3, peaks at δ = 6.3 ppm are attributed to the protons on furanyl ring (designated as protons 1). Peaks at δ = 4.5 ppm (-OCH_2-furanyl ring, 2H) correspond to protons (2) on the glycidyl ether moiety to furanyl ring. Peaks at δ = 3.4-3.8 ppm indicate protons (3) of methylidyne adjacent to the oxirane ring. Peaks at δ = 3.15 ppm reflect methylidyne protons (4) on oxirane ring. While, those at δ = 2.6-2.8 ppm correspond to protons (5) of methylene on the oxirane ring. The integrated values of area under these peaks match well with the theoretical ratio of proton numbers at different positions of BOF and its purity was calculated as 99%. In Figure 2.4, peaks of ^{13}C-NMR spectrum of BOF are attributed as followed. 151.8 ppm and 110.2 ppm correspond with C1 and C2 on the furanyl ring. 70.7 ppm and 65.2 ppm indicate C3 and C4 bridging the furanyl ring and oxirane ring. 50.7 ppm and 44.3 ppm reflect C5 and C6 on the oxirane ring, respectively. Therefore, the purified product is verified to be BOF as expected.

Mass Spectrometry (MS) was employed to characterize purified BOF with CIMS (m/z (%)): 240.1 [M^+]. Calcd for $C_{12}H_{16}O_5$: 240.1. Found: 240.09. Viscosity of purified BOF was measured to be 0.05 Pa.s at RT.

Figure 2.5a and b present N-IR and M-IR spectra of purified BOF. In the N-IR spectrum, the oxirane ring is reflected by peaks at 6072 cm^{-1} (first overtone of terminal CH_2 stretching mode) and 4530 cm^{-1} (combination band of the second overtone of epoxy ring stretching with the fundamental C-H stretching).[94] In the M-IR spectrum, the oxirane ring is indicated by peaks at 927 cm^{-1} (stretching of C-O in oxirane group), 1254 and 854 cm^{-1} (stretching of C-O-C in oxirane group) and 3057 cm^{-1} (stretching of C–H in oxirane ring). In addition, the furanyl ring is reflected by peaks at 759 cm^{-1} (mono-substituted furan ring), 883 cm^{-1} (stretching of C-H in furan ring), 1078 cm^{-1} (stretching of C–O–C in furan ring), 1560 cm^{-1} (stretching of C=C in furan ring), 3125 and 3150 cm^{-1} (stretching of C-H in furan ring).[89] A broad peak is not present at 3200–3500 cm^{-1}, meaning no hydroxyl groups from water or chlorohydrin ether were present in the purified BOF.

BOB was synthesized with a one-step method condensation reaction between epichlorohydrin and 1, 4-benzenedimethanol. This one-step method works well because alkali, which is sodium hydroxide solution in this case, can catalyze both the etherification and the ring-closing reaction, meaning the etherification between epichlorohydrin and 1, 4-benzenedimethanol to form chlorohydrin ether and the ring-closing reaction of chlorohydrin ether to reform the oxirane ring share identical conditions.

BOB was purified by reduced-pressure distillation with an overall yield of 90%. Figure 2.6 shows the characteristic peaks of crude BOB, purified BOB and epichlorohydrin.

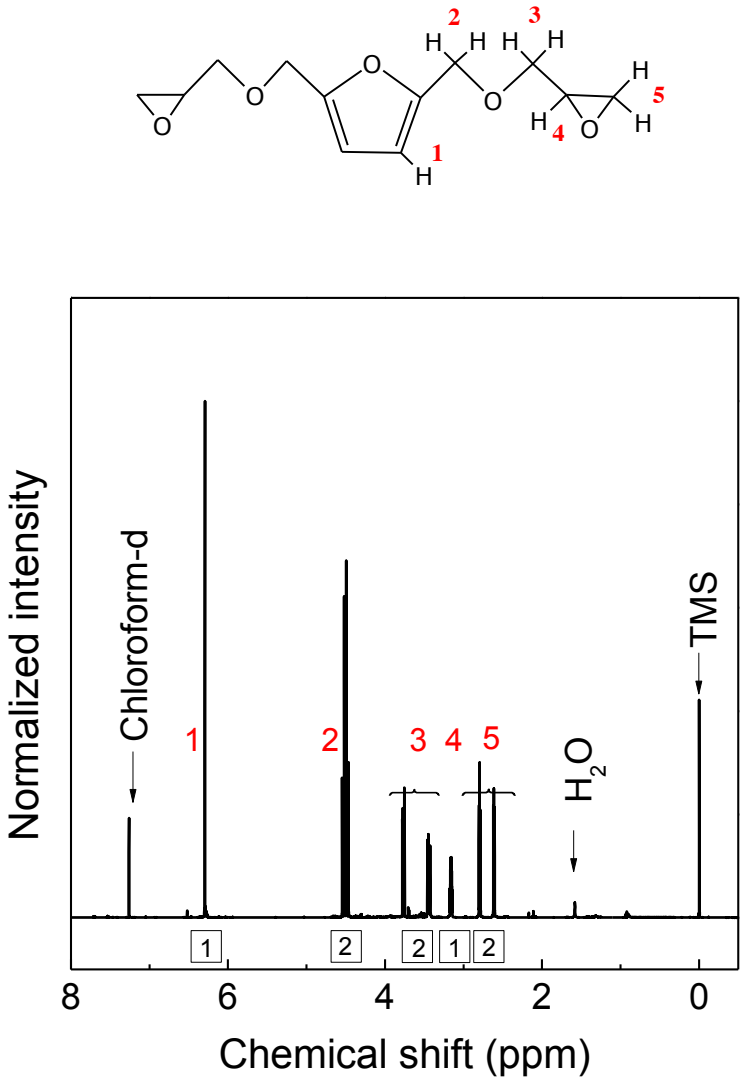

Figure 2.3. The ^{1}H-NMR spectrum of purified BOF.

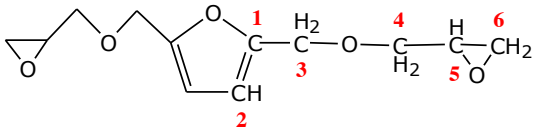

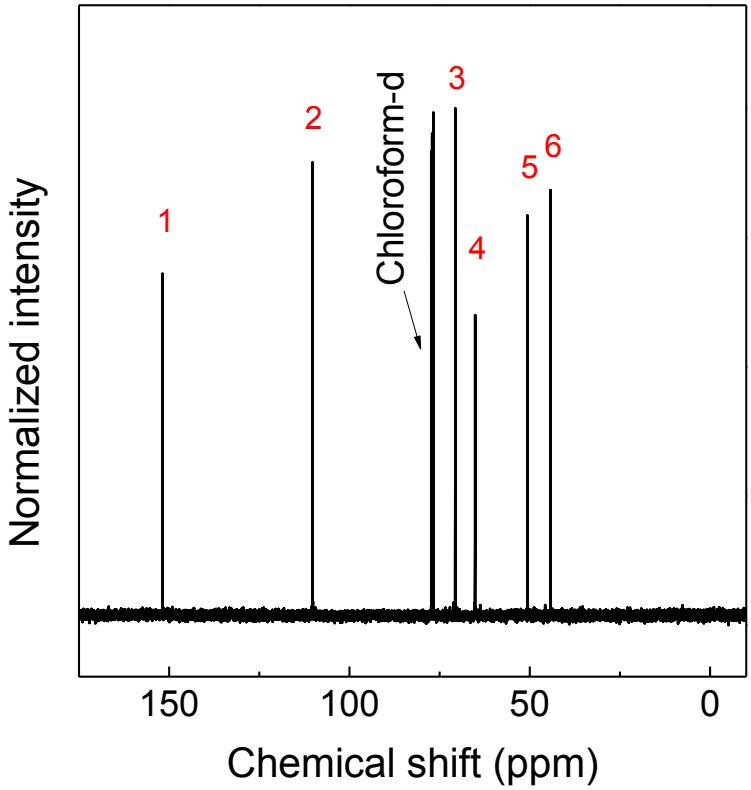

Figure 2.4. The ^{13}C-NMR spectrum of purified BOF.

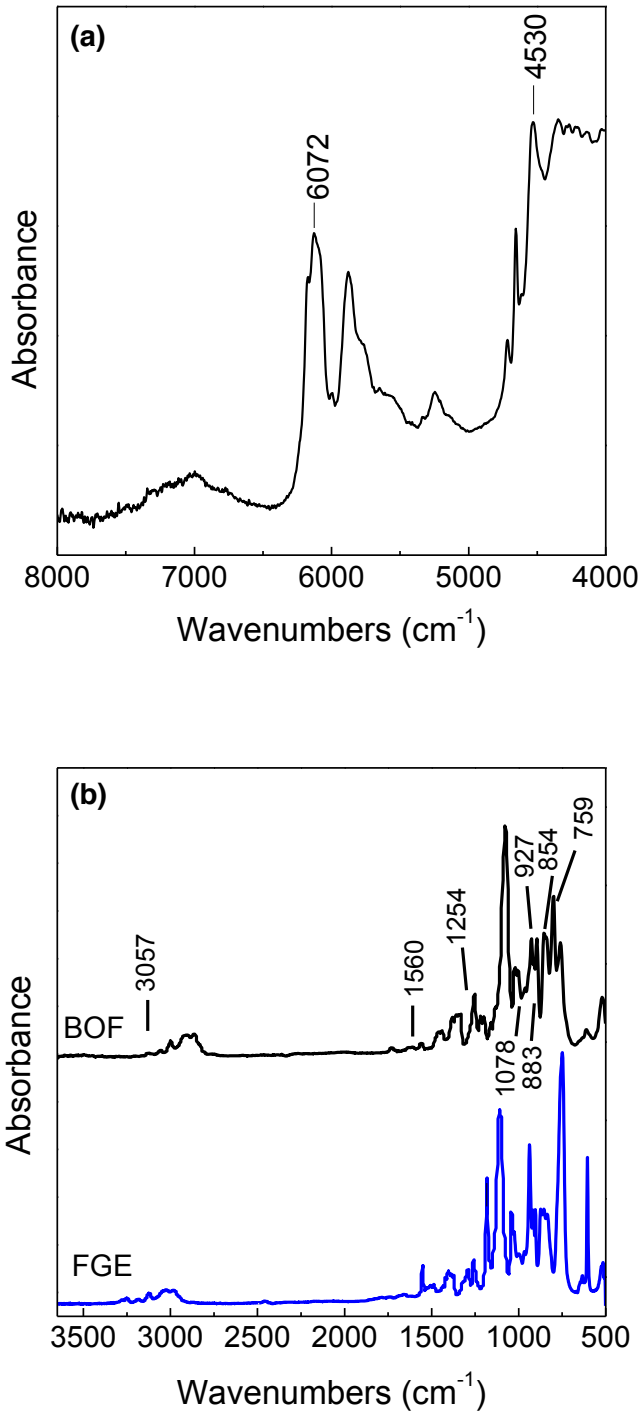

Figure 2.5. The N-IR spectrum (a) and M-IR spectrum (b) of purified BOF.

Figure 2.6b is a magnification of Figure 2.6a. In Figure 2.6a, no peaks are present between 0 to 10 minute and 20 to 25 minute. In Figure 2.6b, crude BOB (black line) exhibits two peaks at 15.5 minute (62.0% by area) and 17.3 minute (37.5% by area), respectively. By comparing with epichlorohydrin (blue line), the lower molecular weight component is identified as unreacted epichlorohydrin which is 300% in excess initially. Purified BOB (red line) presents only one peak at 15.5 minute after epichlorohydrin is removed. The dominant component (62.0% by area) in the crude BOB is identified to be BOB.

Epoxy equivalent weight of purified BOB is measured to be 126 g/eq. by following ASTM D1652-90, Procedure B. This matches well with the theoretical value 125 g/eq. and its purity is measured to be 99% based on calculation of EEW.

^{1}H-NMR and ^{13}C-NMR were employed to confirm the chemical structure of BOB. In Figure 2.7, peaks at δ = 7.3 ppm are attributed to the protons on phenyl ring (designated as protons 1). Peaks at δ = 4.6 ppm (-OCH_2-benzene ring, 2H) correspond to the protons (2) on the glycidyl ether moiety to phenyl ring. Peaks at δ = 3.5-3.8 ppm indicate protons (3) of the methylidyne adjacent to oxirane ring. Peaks at δ = 3.15 ppm reflect the methylidyne protons (4) on oxirane ring. Peaks at δ = 2.6-2.8 ppm correspond to protons (5) of the methylene on oxirane ring. The integrate values of area under these peaks match well with the theoretical ratio of proton numbers at different positions in the purified BOB and its purity was calculated as 99%. In Figure 2.8, the peaks in ^{13}C-NMR

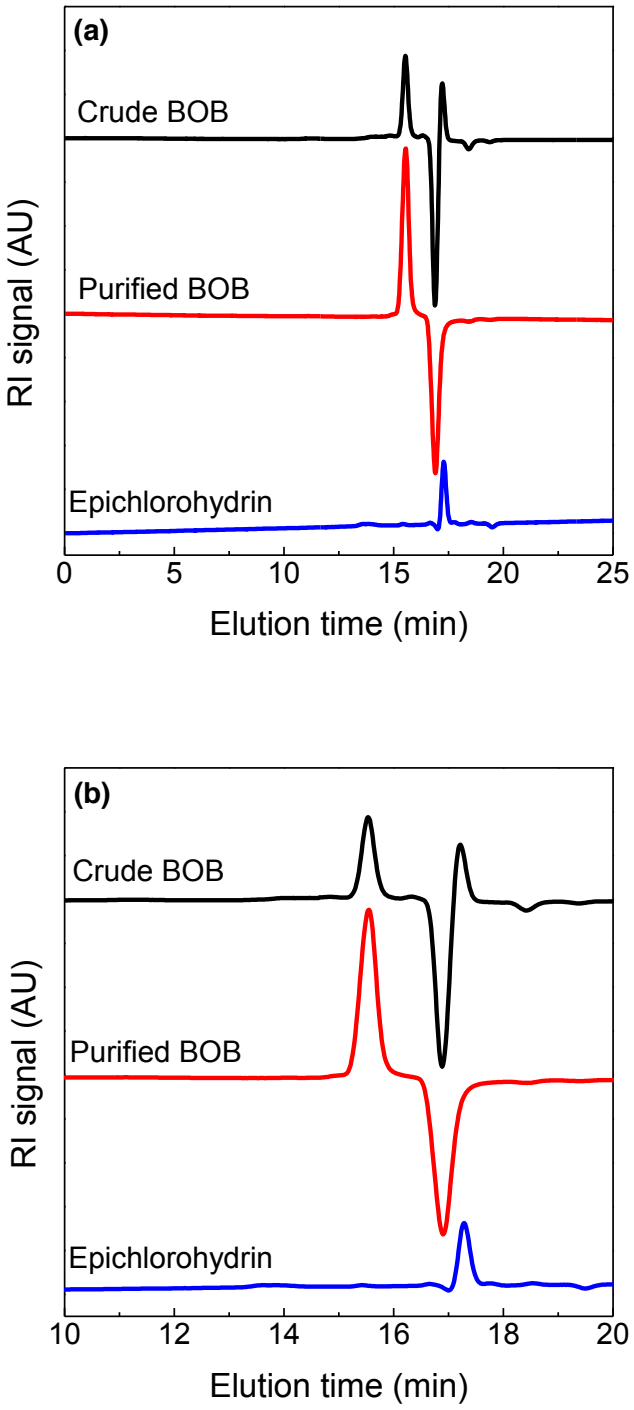

Figure 2.6. The GPC spectra of crude BOB, purified BOB and epichlorohydrin.

spectrum of BOB are attributed as followed. 137.5 ppm and 127.8 ppm correspond with C1 and C2 on the phenyl ring. 73.0 ppm and 70.8 ppm indicate C3 and C4 bridging the phenyl ring and oxirane ring. 50.8 ppm and 44.2 ppm reflect C5 and C6 on the oxirane ring, respectively. Therefore, the purified product is verified to be BOB as expected.

MS was employed to characterize the purified BOB with CIMS (m/z(%)): 250.1 [M^+]. Calcd for $C_{14}H_{18}O_4$: 250.1. Found: 250.15. Viscosity of the purified BOB was measured to be 0.05 Pa.s at RT.

Figure 2.9a and b show the N-IR and M-IR spectra of purified BOB. In the N-IR spectrum, the oxirane ring is reflected by peaks at 6067 cm^{-1} (first overtone of terminal CH_2 stretching mode) and 4524 cm^{-1} (combination band of the second overtone of the epoxy ring stretching with the fundamental C-H stretching).[94] In the M-IR spectrum, the oxirane ring is indicated by peaks at 900 cm^{-1} (stretching of C-O in the oxirane group), 1253 and 837 cm^{-1} (stretching of C-O-C in the oxirane group) and 3054 cm^{-1} (stretching of C–H in the oxirane ring). In addition, the phenyl ring is reflected by peaks at 1612 cm^{-1} (stretching of C=C in the phenyl ring), 1515 cm^{-1} (stretching of C-C in the phenyl ring) and 2860-2998 cm^{-1} (stretching of C-H of CH_2 and CH in the phenyl ring and aliphatic chain).[89] A broad peak is not present at 3200–3500 cm^{-1}, meaning no hydroxyl groups from water or chlorohydrin ether were present in the purified BOB.

Table 2.1 summarizes the yield, purity, viscosity and color of prepared BOF and BOB epoxy monomers.

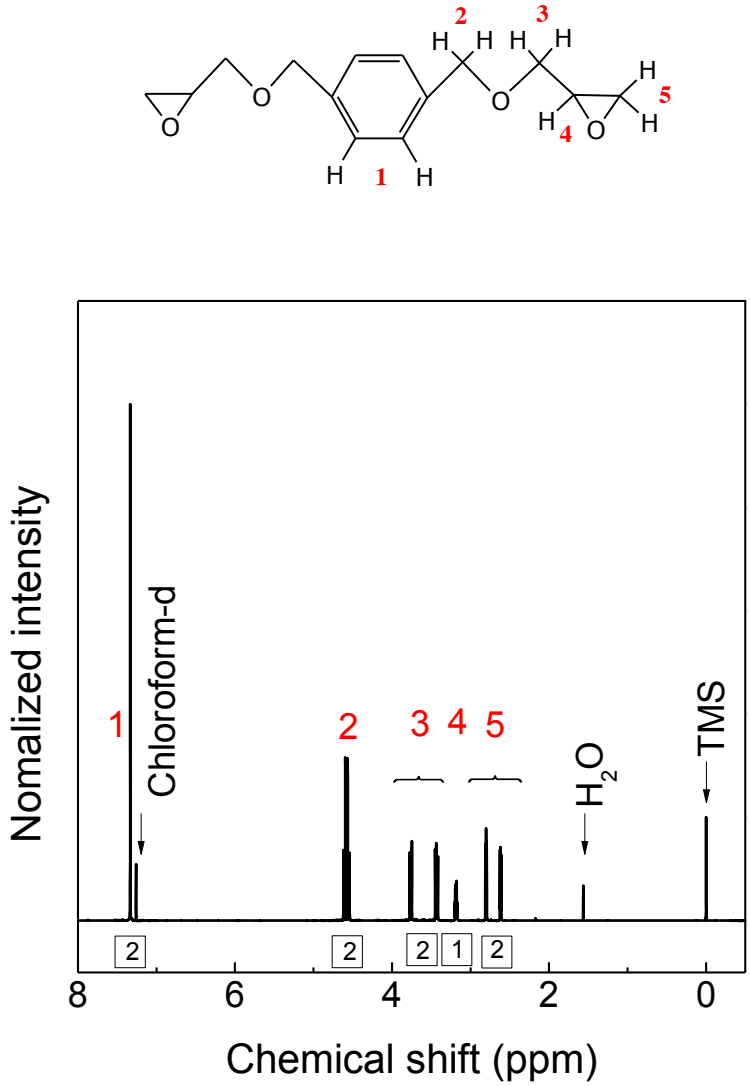

Figure 2.7. The ^{1}H-NMR spectrum of purified BOB.

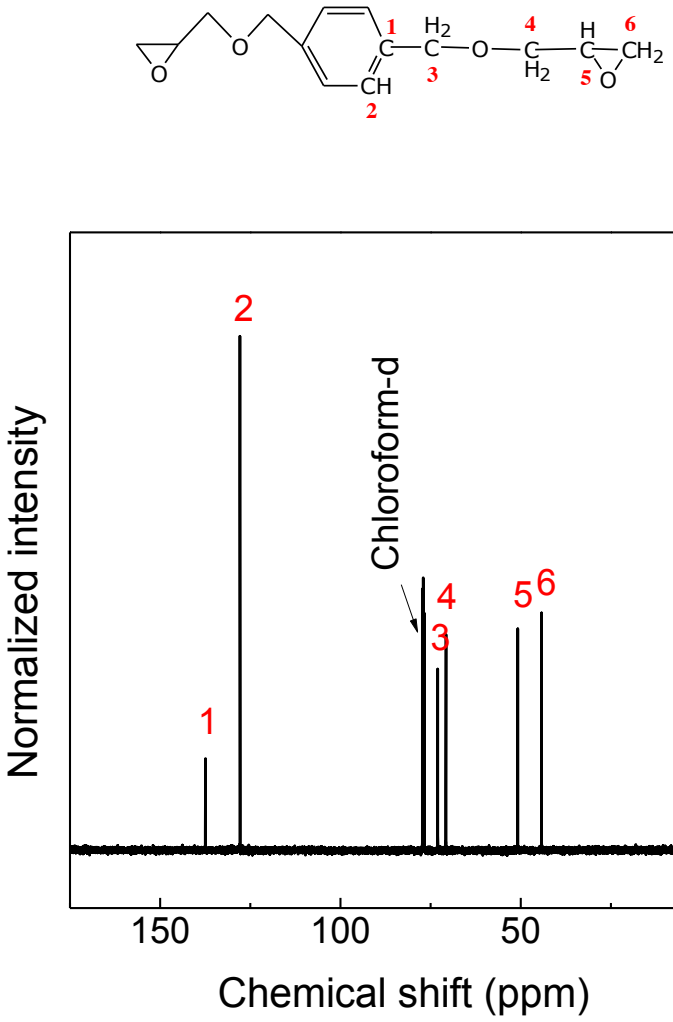

Figure 2.8. The ^{13}C-NMR spectrum of purified BOB.

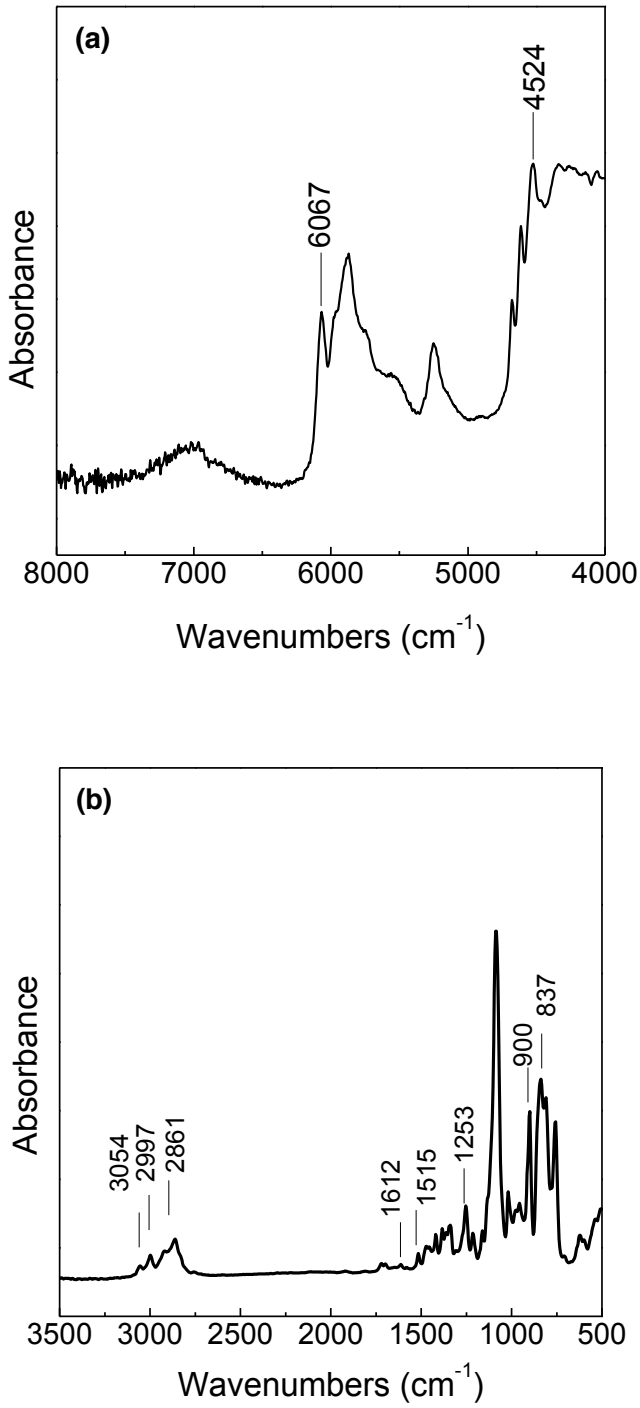

Figure 2.9. The N-IR and M-IR spectra of purified BOB.

Table 2.1. Yield, purity, viscosity and color of prepared BOF and BOB epoxy monomers

Monomer name	Yield (%)	Purity (%)	Viscosity at 30 °C (Pa.s)	Color
BOF	64	99	0.05	Light yellow
BOB	90	99	0.05	Colorless

2.3.2. BOF and BOB polymer samples cured with PACM and EPIKURE W

Full conversion of epoxy and amine groups in BOF and BOB polymer samples was confirmed using N-IR. For example, the N-IR spectra of a BOF-PACM polymer sample are shown in Figure 2.10, where black, red and blue curves represented the first scan at 60 °C, the last scan at 60 °C after 9 hours, and the last scan at 180 °C for another 9 hours, respectively. It is evident that at 60 °C the peak corresponding to epoxy groups (4530 cm^{-1}) decreased in conjunction with those corresponding to primary (4935 cm^{-1}) and primary/secondary (6500 cm^{-1}) amine groups at 60 °C, while the peak associated with hydroxyl groups (6990 cm^{-1}) formed by the epoxy ring opening reaction increased. After 9 hours at 60 °C, the presence of epoxy and secondary amines is evident while primary amine is not noticeable. This is consistent with known cure behavior of epoxies as primary amines are more reactive than secondary amines. Following post cure at 180 °C for 9 hours, epoxy, primary and secondary amine peaks are all no longer present, indicating that within the limits of infrared spectroscopy measurements, epoxy and amine groups are fully converted after the cure schedule is completed. These results are representative of all compositions evaluated.

DMA plots of BOF and BOB cured with PACM and EPIKURE W are shown in Figures 2.11 in which Figure 2.11a contains DMA plots of BOB and BOF cured with PACM and Figure 2.11b contains those for BOB and BOF cured with EPIKURE W. A sharp loss modulus peak is evident in all cases.

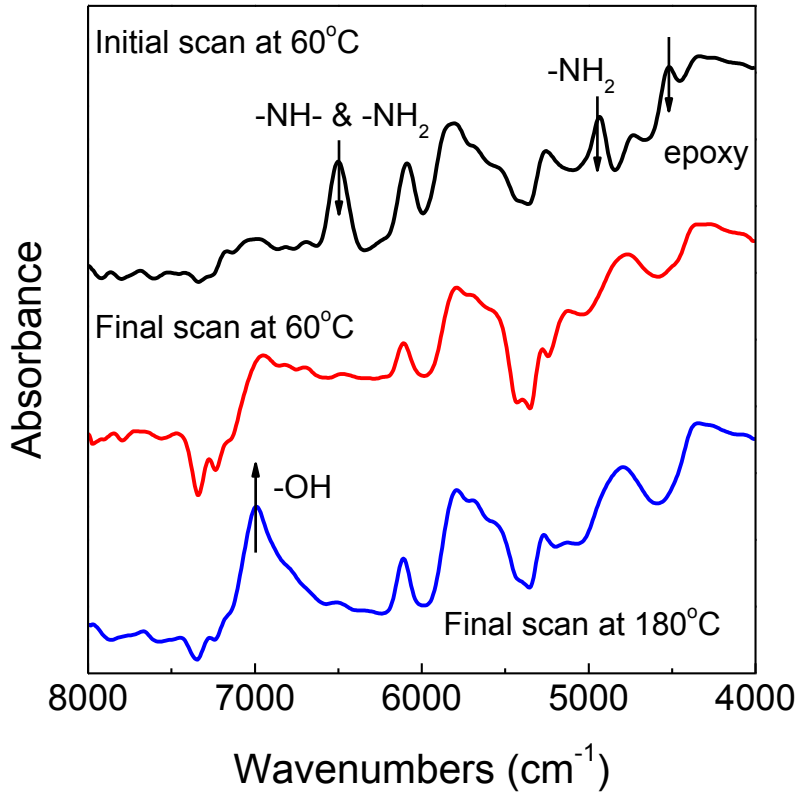

Figure 2.10. The N-IR spectra of a W_{BOF} = 1 sample cured and post-cured with PACM at 60 °C and 180 °C, respectively.

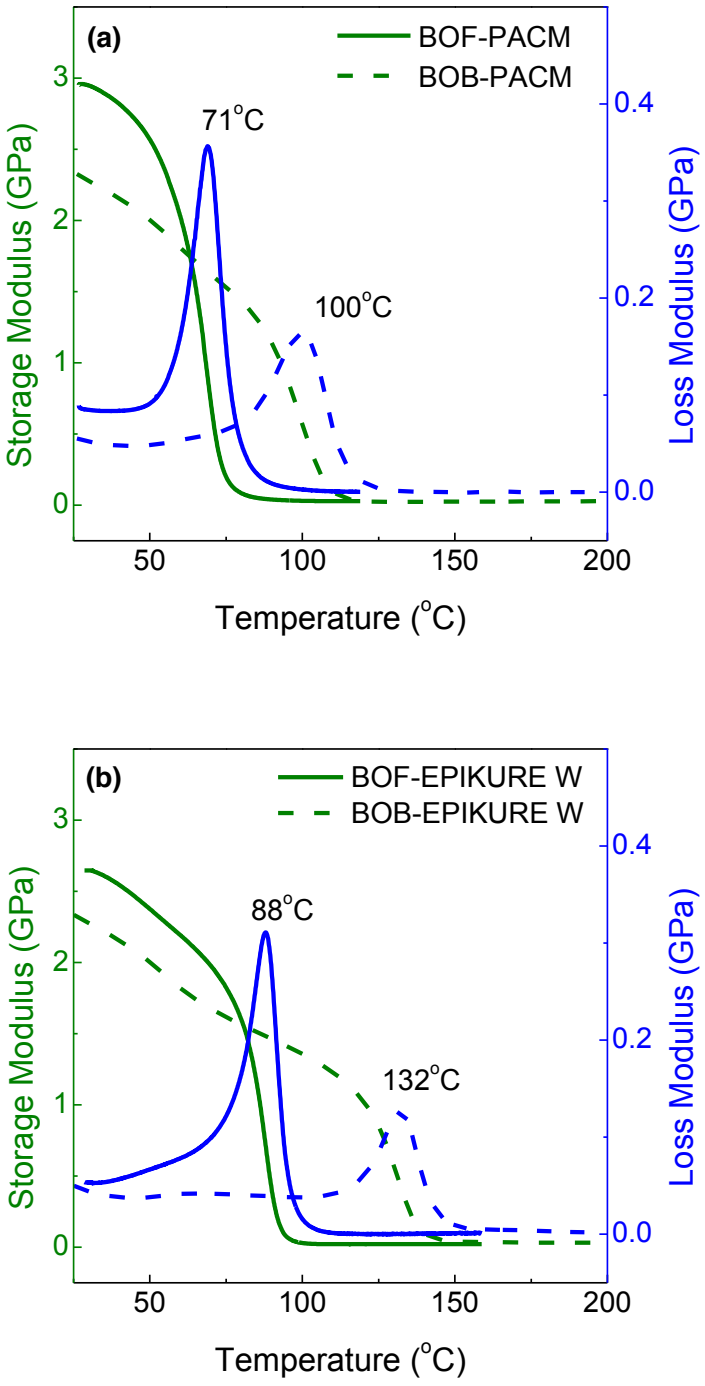

Figure 2.11. DMA thermograms of polymer samples of BOF and BOB cured with PACM and EPIKURE W, respectively.

On a basis of the peak position for samples cured with PACM, BOF has a T_g = 71 °C which is lower than the T_g of BOB at 100 °C. For samples cured with EPIKURE W, the T_g of BOF is 88 °C which is also lower than that of BOB at 132 °C. As expected, curing with the aromatic curing agent results in a higher T_g for both epoxy systems. However, for both the aromatic and cycloaliphatic curing agents BOF was found to have a lower T_g than the corresponding BOB epoxy system. The only difference in the chemical structures of these two epoxies is that BOF has a furanyl ring in place of the phenyl ring possessed by BOB. BOF polymer samples possess a higher storage modulus relative to the BOB samples all the way from room temperature through the glass transition for both PACM and EPIKURE W systems. The use of the furanyl building block increased the stiffness of cured polymer samples.

One of the potential reasons for the interesting thermo-mechanical behavior of BOF epoxies previously described is that hydrogen bonding occurs between the oxygen atoms of furan rings in BOF and the hydroxyl groups in the epoxy-amine polymer networks generated during epoxy cure. In order to test this hypothesis, M-IR was employed to evaluate hydrogen bonding, as described by others,[95] of BOF monomer and BOF polymer samples cured with PACM and EPIKURE W. The formation of hydrogen bonds can slightly influence bond lengths, energies and electron density distribution of involved chemical bonds, and these changes are normally around two or more orders of magnitude smaller compared with typical chemical changes. M-IR spectroscopy has the

capacity to detect the formation of hydrogen bond at a very sensitive level in this case. M-IR spectra of all three samples are plotted together in Figure 2.12, where the black curve represents BOF monomer, and red and blue curves correspond to BOF cured with PACM and EPIKURE W, respectively. As expected, a broad peak was present in the region of 3200-3500 cm^{-1}, representing the hydroxyl groups formed from the epoxy-amine reaction. There are no hydroxyl groups in BOF monomer. Meanwhile, the peak at 1078 cm^{-1} which corresponds to stretching of C–O–C on furan ring,[89] in BOF shifted to a lower frequency by 9 cm^{-1} after being cured with PACM and EPIKURE W. It has been suggested[95-96] that hydrogen bonding can shift the stretch vibration of corresponding functional groups to a lower frequency (red shift), and the value of this red shift is well correlated with the strength of hydrogen bond formed between involved functional groups. However, more evidence is needed to evaluate the significance of hydrogen bonding in affecting thermo-mechanical properties of BOF relative to BOB.

Another explanation for the observed phenomena of thermo-mechanical behavior associated with the furanyl building block is derived from the ring structural considerations. Even though the furanyl ring in BOF are asymmetric along the backbone of BOF molecules and rotations around the aromatic unit can theoretically hardly occur, the methylene linkages between furanyl and glycidyloxy groups may facilitate the rotations and allow large scale motion of the chains to occur at lower temperatures.

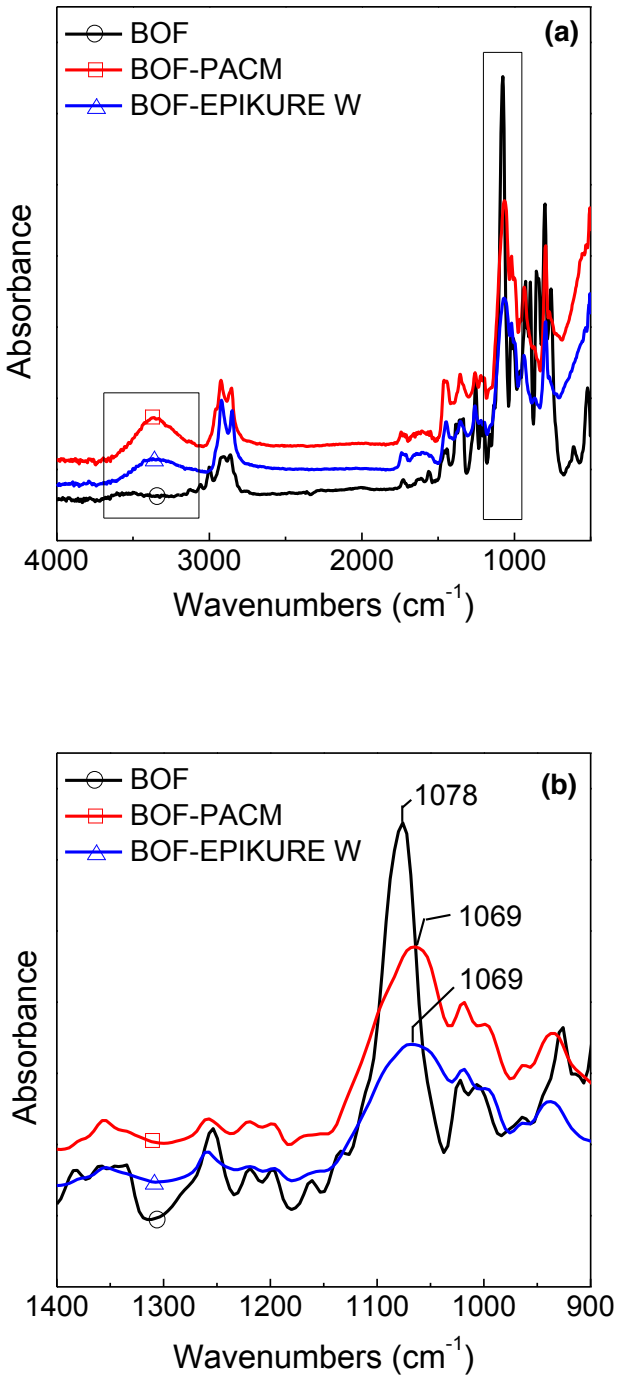

Figure 2.12. The M-IR spectra of BOF and BOF polymer samples cured with PACM and EPIKURE W, respectively. (b) is magnification of (a).

2.3.3. BOF and BOB polymer samples prepared by blending with DGEBA

In order to further explore the differences in properties associating with epoxy networks prepared using furanyl and phenyl building blocks, and to evaluate the viability of using furanyl based epoxies in conjunction with commercially available resins like DGEBA, polymer samples were prepared by blending with DGEBA at different concentrations. Four sets of polymers were prepared in which the weight fraction of epoxy monomers comprised of DGEBA was varied from 0% to 100% [0%, 30%, 50%, 70% and 100%]. These sets included: (1) BOF and DGEBA cured stoichiometrically with PACM; (2) BOB and DGEBA cured stoichiometrically with PACM; (3) BOF and DGEBA cured stoichiometrically with EPIKURE W and (4) BOB and DGEBA cured stoichiometrically with EPIKURE W. N-IR was used to ensure a complete conversion of epoxy and amine groups within the limits of the spectroscopic technique.

DMA thermograms of BOF and BOB polymer samples cured with PACM are shown in Figure 3.13 and Figure 3.14, respectively. DMA thermograms of BOF and BOB polymer samples cured with EPIKURE W are given in Figure 3.15 and Figure 3.16, respectively. When blending with DGEBA at different ratios, BOF polymer samples were found to consistently possess higher storage modulus and lower T_g compared with BOB polymer samples. Figures 2.13a and 2.14a show the storage modulus as a function of temperature of BOF-DGEBA-PACM and BOB-DGEBA-PACM samples, respectively. At RT, BOF

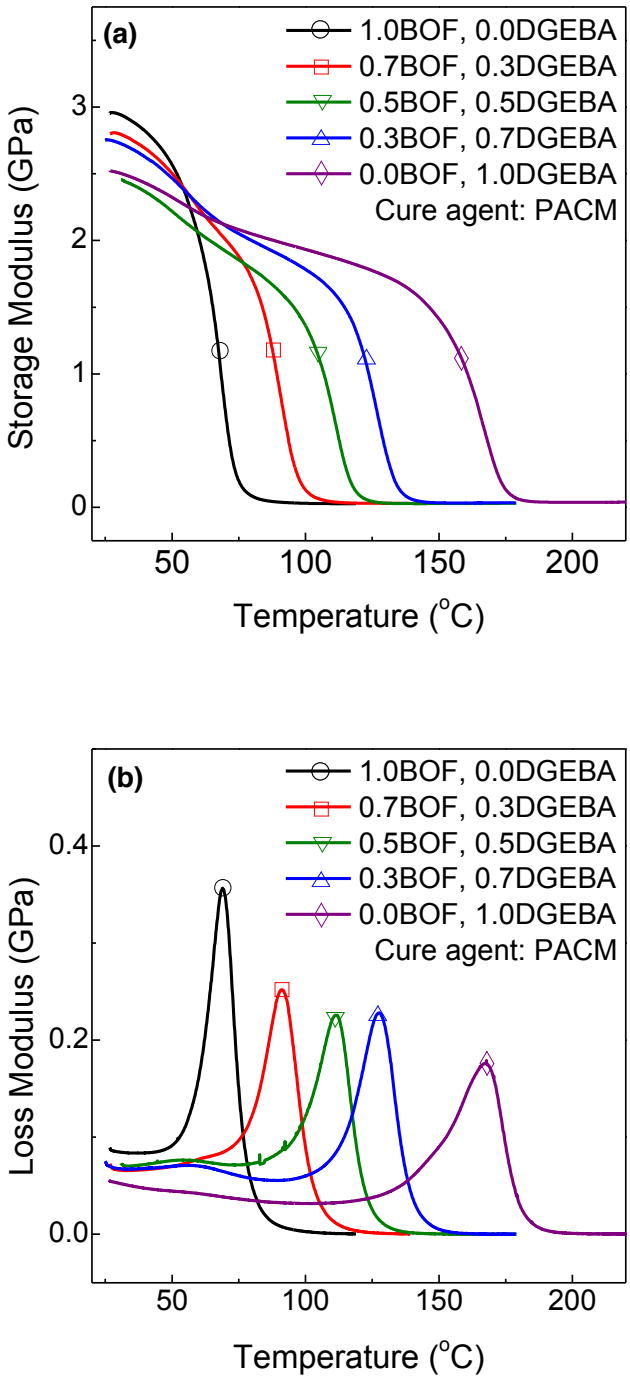

Figure 2.13. DMA thermograms of BOF polymer samples blending with DGEBA (EPON 828) at different ratios in the PACM system.

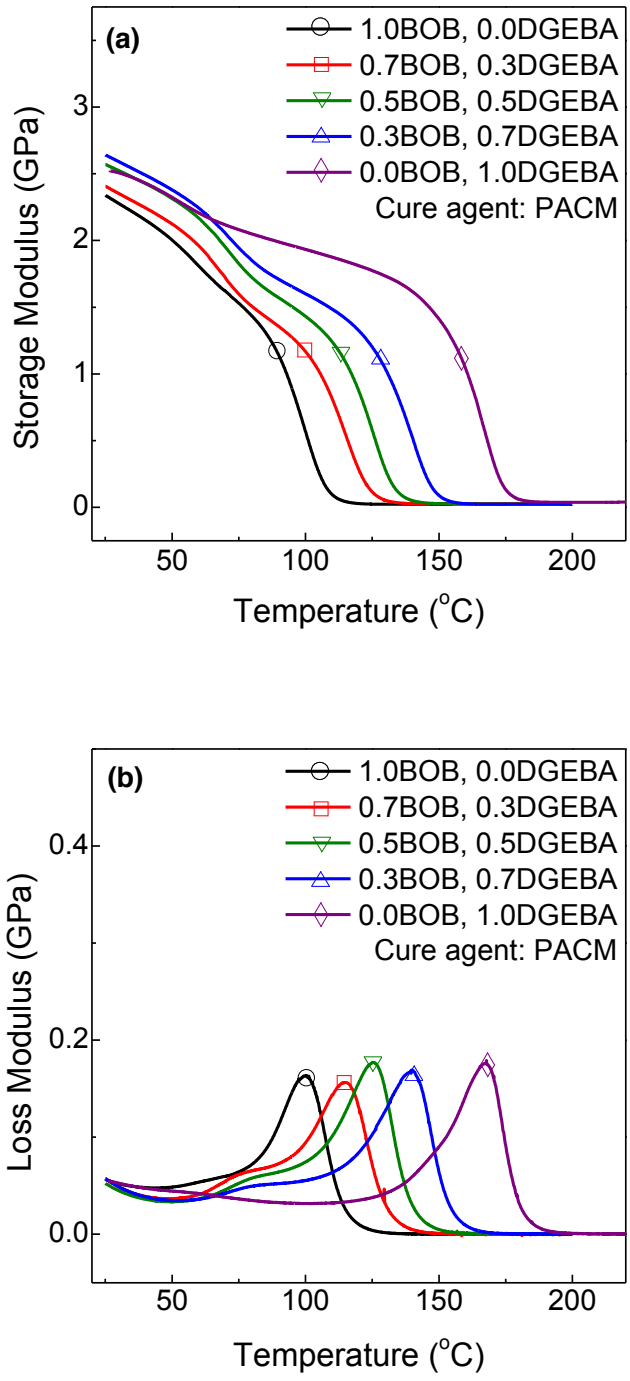

Figure 2.14. DMA thermograms of BOB polymer samples blending with DGEBA (EPON 828) at different ratios in the PACM system.

samples show increasing storage moduli along with BOF content. A similar trend is not observed for BOB containing samples. This result suggests that, for samples cured using PACM, the furanyl ring improves polymer glassy moduli even when blending with DGEBA which is not the cases when using BOB. Figure 2.13b and 2.14b show the loss modulus curves of BOF-DGEBA-PACM and BOB-DGEBA-PACM samples, respectively. All BOF and BOB samples display a single sharp loss modulus peak, suggesting that phase separation has not occurred in the cured polymer networks. The peak positions of loss modulus curves shift to higher temperatures with the increasing DGEBA content. Also, for BOF-DGEBA-PACM samples, the height of the loss modulus peak decreases with the increasing DGEBA content, and the area under the loss modulus-temperature curve in the vicinity of glass transition temperature decreases with the increasing DGEBA content. For BOB-DGEBA-PACM samples, the loss modulus peak height and the area under the loss modulus-temperature curve remains similar with the increasing DGEBA content. DMA thermograms of BOF and BOB polymer samples cured with EPIKURE W are shown in Figure 2.15 and 2.16, respectively. Figures 2.15a and 2.16a show the storage moduli as a function of temperature of BOF-DGEBA-EPIKURE W and BOB-DGEBA-EPIKURE W samples, respectively. At RT, the storage moduli of BOF-DGEBA-EPIKURE W samples did not clearly show the trend observed for the systems cured with PACM, since the addition of BOF produced moduli similar to those of pure BOF and DGEBA cured with EPIKURE W, respectively. The same behavior was observed for the set of BOB polymer samples. The loss modulus curves given in Figures 2.15b and 2.16b for BOF-DGEBA-EPIKURE W and BOB-DGEBA-EPIKURE W samples,

respectively, show that the systems cured with EPIKURE W behave very similarly to those cured with PACM. BOF and BOB samples display a single sharp loss modulus peak, suggesting that phase separation has not occurred. Loss modulus peak height decreases with the increasing DGEBA content and the peak positions of the loss modulus curves shift to higher temperatures with the increasing DGEBA content in BOF-DGEBA-EPIKURE W samples.

T_g values for these four sets of polymer samples were obtained using the peak positions of loss modulus curves in Figures 2.13b, 2.14b, 2.15b and 2.16b, and summarized in Table 2.2. All tested samples presented a single sharp T_g. A single composition-dependent glass transition is frequently considered as an indication of miscibility on an order of 20-40 nm.[97] We conclude that BOF and BOB are well miscible with DGEBA. As shown in Table 2.2, BOF always possesses a lower T_g than its phenyl analogue when cured with both aromatic and cycloaliphatic curing agents and also when blended with DGEBA. Based on previous discussions, this likely occurs because the methylene linkages between furanyl and glycidyloxy groups in BOF facilitate the rotations and allow large scale motion of the chains to occur at lower temperatures, even though furanyl rings in BOF are able to form hydrogen bonds and are not symmetrical, compared with phenyl rings in BOB. Polymer samples with EPIKURE W generally possessed higher T_gs than those with PACM in both BOF and BOB systems, because EPIKURE W with aromatic ring structures is more thermally rigid than PACM with

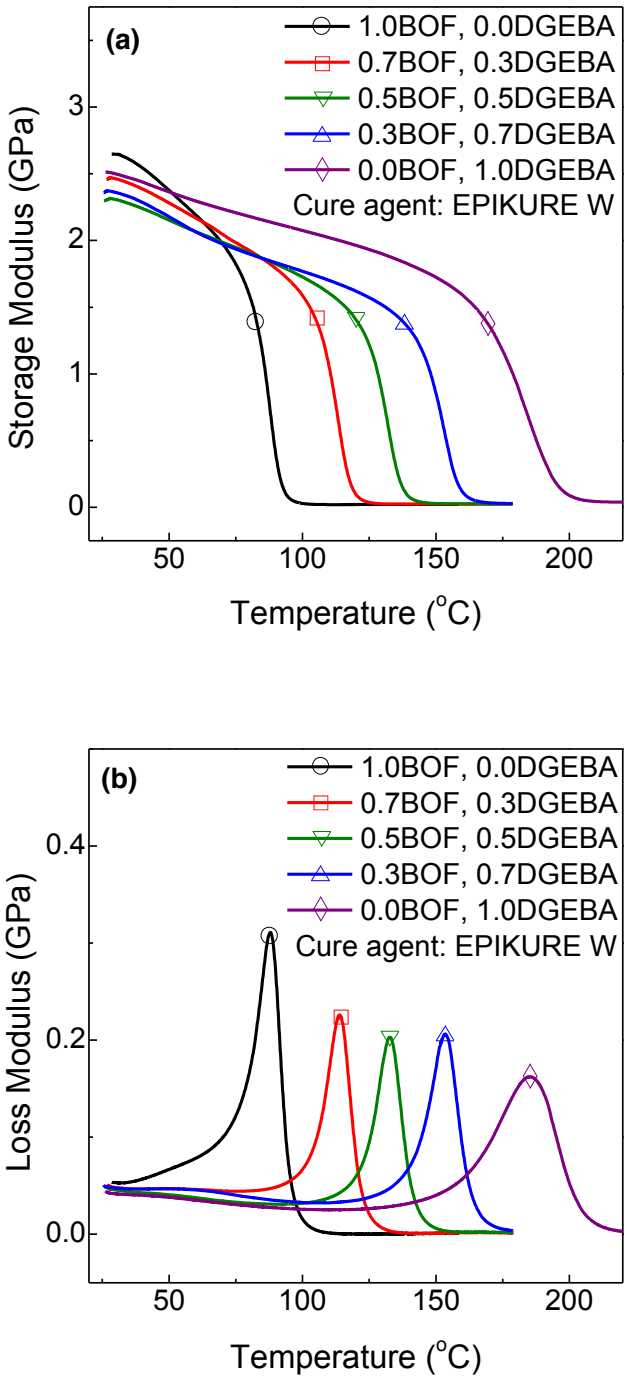

Figure 2.15. DMA thermograms of BOF polymer samples blending with DGEBA (EPON 828) at different ratios in the EPIKURE W system.

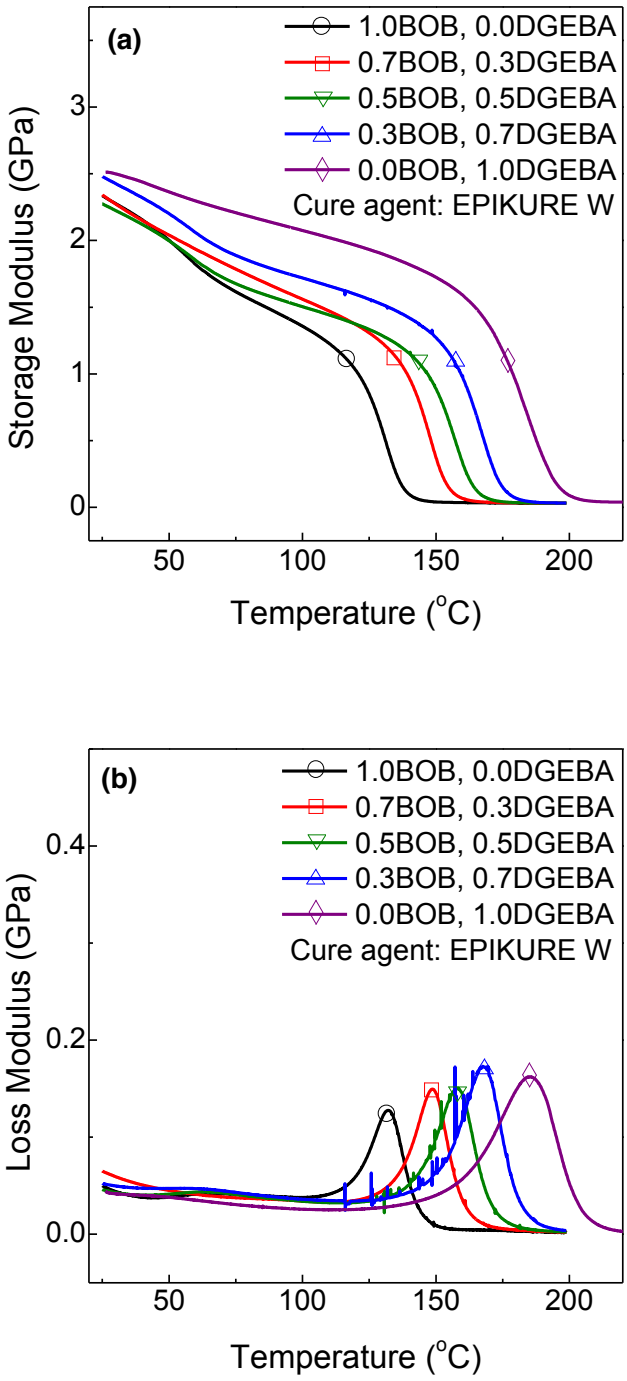

Figure 2.16. DMA thermograms of polymer samples of BOB blending with DGEBA (EPON 828) at different ratios in the EPIKURE W system.

Table 2.2. T_g data of DGEBA blended BOF and BOB polymer samples with PACM and EPIKURE W at stoichiometry, respectively

Weight ratio of epoxy monomers BOF(BOB):DGEBA	T_g(°C) by DMA[a]			
	PACM		EPIKURE W	
	BOF-DGEBA	BOB-DGEBA	BOF-DGEBA	BOB-DGEBA
100:0	71 (80)	100 (111)	88 (94)	132 (140)
70:30	96 (106)	115 (126)	114 (120)	148 (156)
50:50	111 (121)	125 (136)	133 (139)	158 (166)
30:70	131 (140)	140 (150)	153 (160)	168 (177)
0:100	167 (176)	167 (176)	185 (198)	185 (198)

[a]T_g assigned as the temperature at the peak position of loss modulus curve from DMA. Values in parentheses were T_gs assigned as the temperature at the maximum of tanδ curve from DMA.

cycloaliphatic ring structures.[6, 98] Furthermore, the difference of T_gs between BOF and BOB samples was found to decrease with the increasing DGEBA content.

T_g increased greatly with decreasing contents of BOF and BOB in PACM and EPIKURE W systems. The T_g differences between BOB-PACM (100 °C) and DGEBA-PACM (167 °C), as well as between BOB-EPIKURE W (132 °C) and DGEBA-EPIKURE W (185 °C) are 67 °C and 53 °C, respectively. By comparing chemical structures of BOF and BOB with DGEBA in Figure 2.1, an obvious difference is that DGEBA does not possess methylene groups between the phenyl and glycidyloxy groups that are found in both BOF and BOB. These additional methylene groups potentially decrease T_g of BOF and BOB samples since furanyl or phenyl segments attached to them are less constrained. In order to test this reasoning, DGEPP whose structure is given in Figure 2.1 was cured using EPIKURE W at stoichiometry. DGEPP differs structurally from BOB in that it lacks the methylene groups. DGEPP was mixed with EPIKURE W at 110 °C, which is the melting point of DGEPP, and poured into silicone molds. Cure was conducted at 140 °C for 9 hours and postcured at 240 °C for 3 hours. Its thermo-mechanical property is also measured using DMA with a temperature ramp rate of 2 °C/min from RT to 320 °C and the result is plotted in Figure 2.17 with that of DGEBA cured with EPIKURE W for comparison. A T_g of 193 °C was obtained for the DGEPP system which is slightly higher than that of DGEBA. More interesting is that the T_g of DGEPP-EPIKURE W is 61 °C higher than that of BOB-EPIKURE W. So we conclude that the additional methylene

linkages are responsible for the much lower T_g of BOF and BOB systems compared with DGEBA.

The Fox Equation (Equation 2.1) was employed to fit experimental T_g data reported in Table 2.2, and serves the purpose of describing T_g of the multicomponent networks as a function of relative epoxy monomer content.

$$\frac{1}{T_g} = \frac{w_1}{T_{g,1}} + \frac{w_2}{T_{g,2}} \tag{2.1}$$

In this equation w_1 and w_2 represent weight fractions of components 1 and 2, $T_{g,1}$ and $T_{g,2}$ are T_g values of polymer samples containing only components 1 and 2, respectively. For example, in the case of BOF-DGEBA-PACM system, component 1 is BOF-PACM and component 2 is DGEBA-PACM.

Figure 2.18 plots W_{BOF} or W_{BOB} versus the reciprocal of T_g for the four sets of polymer samples being discussed. Also plotted in Figure 2.18 are the best-fit lines corresponding to the Fox Equation for each set of data. All four sets of polymer samples show excellent agreement ($R^2 > 0.997$) with the Fox Equation. This further indicates that BOF and BOB both possess good miscibility with DGEBA implying the polymer networks are homogeneous.[99]

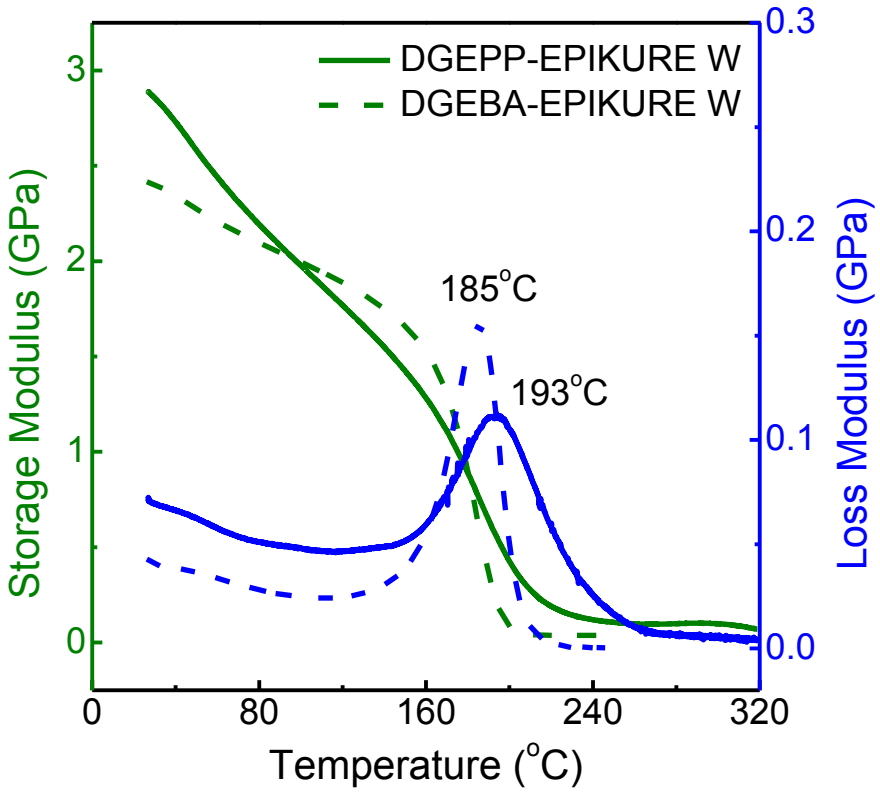

Figure 2.17. DMA thermograms of polymer samples of DGEPP and DGEBA (EPON 828) cured with EPIKURE W.

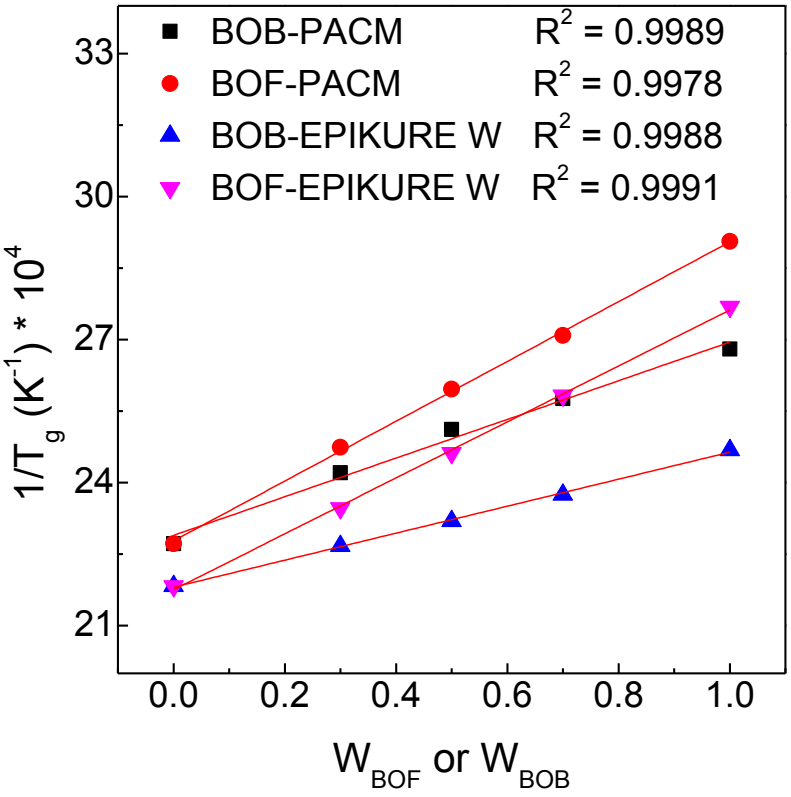

Figure 2.18. Relationship between $1/T_g$ and W_{BOF} or W_{BOB}.

2.3.4. Fracture toughness properties of BOF and BOB polymer samples

Sharp pre-cracks were initiated on all specimens at a low temperature in order to obtain reliable fracture toughness results.[100] Crack sharpness was confirmed visually prior to testing. Figure 2.19a and b plot G_{1c} and K_{1c} values, respectively, of BOF-DGEBA-PACM and BOB-DGEBA-PACM samples that were tested at 23 °C (RT). G_{1c} and K_{1c} values of BOB-PACM sample tested at 52 °C are also included in Figure 2.19a and b. When tested at RT, The BOF-PACM sample possesses G_{1c} and K_{1c} values of 1.31 KJ/m^2 and 2.00 MPa*m$^{1/2}$, respectively, which are both much higher compared with the BOB-PACM sample values of 0.52 KJ/m^2 and 1.22 MPa*m$^{1/2}$. When BOB-APCM sample was tested at 52 °C, to eliminate the influence of testing temperature relative to sample glass transition temperature relative to BOF-PACM sample, the G_{1c} and K_{1c} values increase slightly. However, BOB-PACM still possesses significantly lower fracture toughness compared with BOF-PACM. These results indicate that the furanyl building block improves the fracture toughness of thermosetting epoxy resins relative to its phenyl analogue, which could be due to the existence of hydrogen bonding associated with furanyl building blocks in the cured polymer networks. Dr. Ian McAninch was sincerely acknowledged for the valuable help in conducting mechanical property measurements of polymer samples in this part.

For samples containing DGEBA, BOF-DGEBA-PACM and BOB-DGEBA-PACM samples both show reduced G_{1c} and K_{1c} values with the increasing weight fractions of DGEBA.

DGEBA-PACM sample has G_{1c} and K_{1c} values of 0.14 KJ/m^2 and 0.61 MPa*m$^{1/2}$, respectively. This matches well with the data in literature where Watters et al. reported an EPON 828-PACM system with G_{1c} and K_{1c} values of 0.19 KJ/m^2 and 0.79 MPa*m$^{1/2}$.[101] DGEBA-PACM sample possesses inferior fracture toughness property compared with BOF-PACM and BOB-PACM samples because the chemical structure of DGEBA is more rigid than BOF and BOB due to the absence of methylene groups in its structure. Moreover, BOF-DGEBA-PACM samples show consistently higher G_{1c} and K_{1c} values compared with BOB-DGEBA-PACM samples.

2.3.5. Tensile properties of BOF and BOB polymer samples

Representative stress-strain curves of BOF-PACM, BOB-PACM and DGEBA-PACM samples are plotted in Figure 2.20 and the tensile test data is summarized in Table 2.3. As shown, BOF-PACM sample possesses the highest Young's modulus among these samples. The results are in general agreement with storage modulus values obtained using DMA which are summarized in Table 2.3. High Young's modulus of BOF-PACM sample is perhaps due to the existence of hydrogen bonding between the hydroxyl groups and oxygen atoms in furanyl rings, which are not present in BOB-PACM and DGEBA-PACM samples. Another observation is that BOF-PACM sample shows a strain softening behavior that is not seen in the other two samples. Strain softening is generally a result of localized shear deformation at the molecular scale, leading to stress reduction

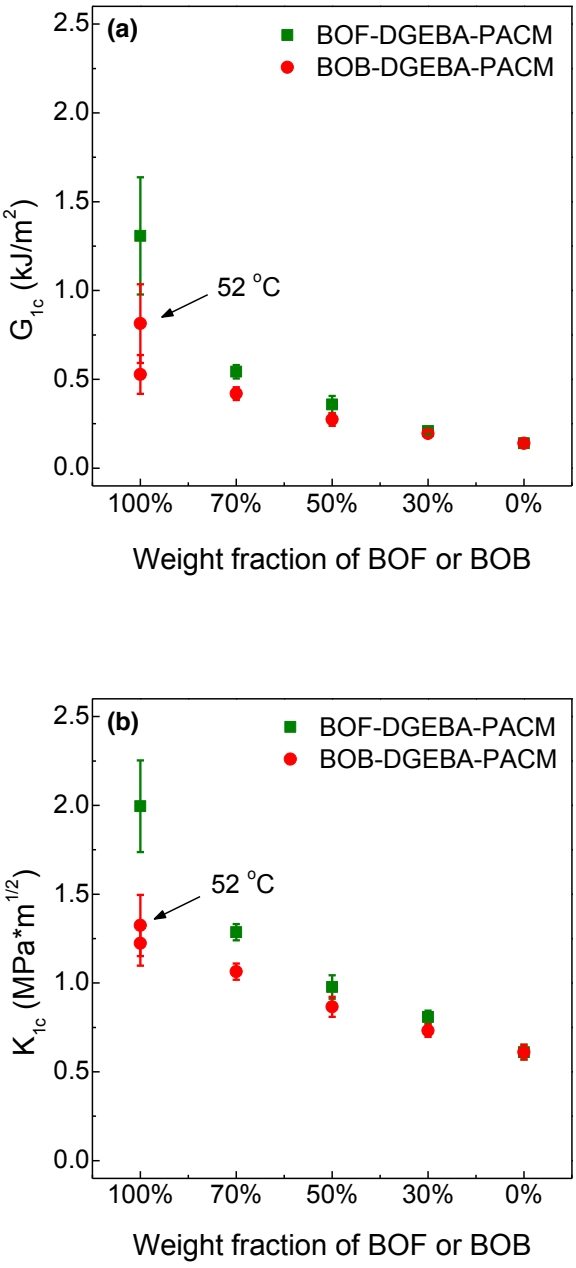

Figure 2.19. (a) G_{1c} and (b) K_{1c} values of BOF-DGEBA-PACM and BOB-DGEBA-PACM samples tested at 23 °C (RT) as a function of the weight fraction of BOF or BOB. The additional data points were G_{1c} and K_{1c} values of BOB-PACM sample tested at 52 °C to eliminate the influence of testing temperature relative to sample glass transition temperature.

without covalent bond-breaking.[102] For a glassy thermoset under tensile stress, this phenomenon can take place when T_g is close to the testing temperature. Since the T_g of BOF-PACM sample is around 71 °C, a 48 °C difference from the testing temperature could be enough to allow reorientation of molecules in the crosslinked network to dissipate the mechanical energy. High T_gs of BOB-PACM and DGEBA-PACM samples could considerably reduce this molecular scale shear deformation, eliminating the strain softening behavior. Dr. Majid Sharifi was sincerely acknowledged for his valuable help in conducting the mechanical measurements in this part.

Another explanation for the observed different stress-strain behaviors associated with the furanyl and phenyl building blocks is from the chemical structural consideration. BOF differs from BOB (as well as DGEBA) in two ways: the central ring structure and the non-collinear covalent bonds connecting to the furanyl ring in BOF molecule. Abrams group recently simulated and compared the thermo-mechanical properties including Young's moduli of BOF and DGEBA epoxy resins cured with two furanyl amine hardeners.[103] The simulated Young's moduli qualitatively agree with our experimental results which have been shown in Chapter 4. Their detailed analyses of the MD trajectories show that BOF polymer samples have higher glassy Young's moduli relative to DGEBA samples which are proposed to be due to the difference in 3-D structures of BOF and DGEBA molecules. All dihedrals in BOF possibly need to deform and store energy in response to the applied strain due to the non-collinear covalent bonds. However, except possibly re-arranging in the local packing, not all dihedrals in

DGEBA need to respond to the applied strain due to the collinearity of 1,4-phenylenes in DGEBA, which consequently results in lower Young's moduli. Even though it is DGEBA instead of BOB in the simulation, their computational results are supportive to our experimental stress-strain results of BOF-PACM and BOB-PACM samples due to the similar collinearity in BOB and DGEBA structures.

2.3.6. Thermal stability of BOF and BOB polymer samples

Figure 2.21 and Figure 2.22 plot TGA thermograms of BOF-DGEBA-PACM and BOB-DGEBA-PACM samples in air and argon, respectively. As shown in Figure 2.21a, BOF-PACM and DGEBA-PACM samples show $T_{-5wt\%}$ (temperature making 5% weight loss) at 268 °C and 325 °C in air, respectively, and $T_{-5wt\%}$ of BOF-DGEBA-PACM samples increases with the DGEBA content. In Figure 2.21b, BOB-PACM sample exhibits $T_{-5wt\%}$ around 325 °C and BOB-DGEBA-PACM samples all have similar thermal decomposition curves. These results indicate that phenyl based BOB and DGEBA samples behave similarly when heated, and decompose at higher temperatures compared with furanyl based BOF samples, suggesting phenyl structures are more thermally stable than furanyl structures in air condition. In inert argon environment, as shown in Figure 2.22a and b, BOF-PACM sample exhibits $T_{-5wt\%}$ around 270 °C which is still lower than those of BOB-PACM and DGEBA-PACM samples at 326 °C. $T_{-5wt\%}$ of BOF-DGEBA-PACM samples also increases with the DGEBA content and BOB-DGEBA-PACM samples show similar

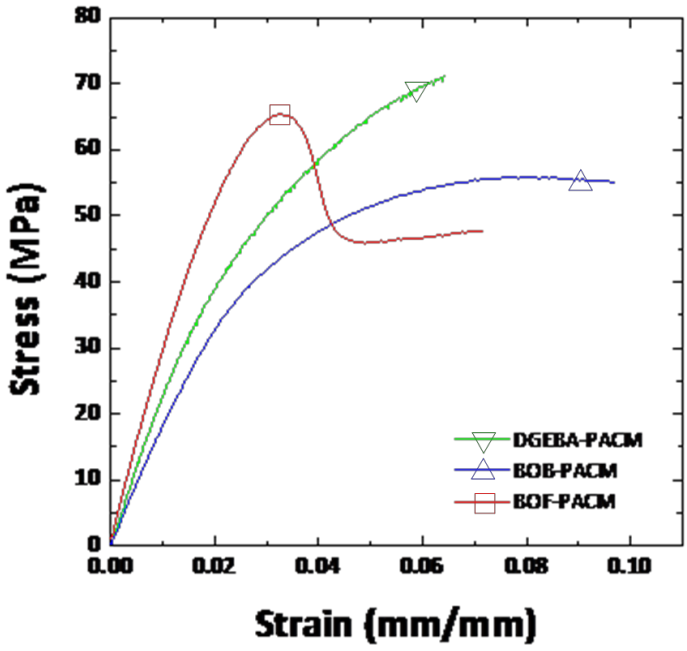

Figure 2.20. Representative stress-strain curves of BOF-PACM, BOB-PACM and DGEBA-PACM polymer samples.

Table 2.3. Storage modulus at RT and stress-strain results of BOF-PACM, BOB-PACM and DGEBA-PACM polymer samples.

Sample	Storage Modulus, E'_{RT} (GPa)	Young's Modulus, E (GPa)	Failure Strain, ε_r (%)	UTS, max σ (MPa)
BOF-PACM	2.97±0.15	2.8±0.1	6.6±2.6	65.2±1.1
BOB-PACM	2.34±0.12	1.8±0.1	10.4±3.5	54.4±1.7
DGEBA-PACM	2.53±0.13	2.3±0.1	7.2±1.7	71.3±5.1

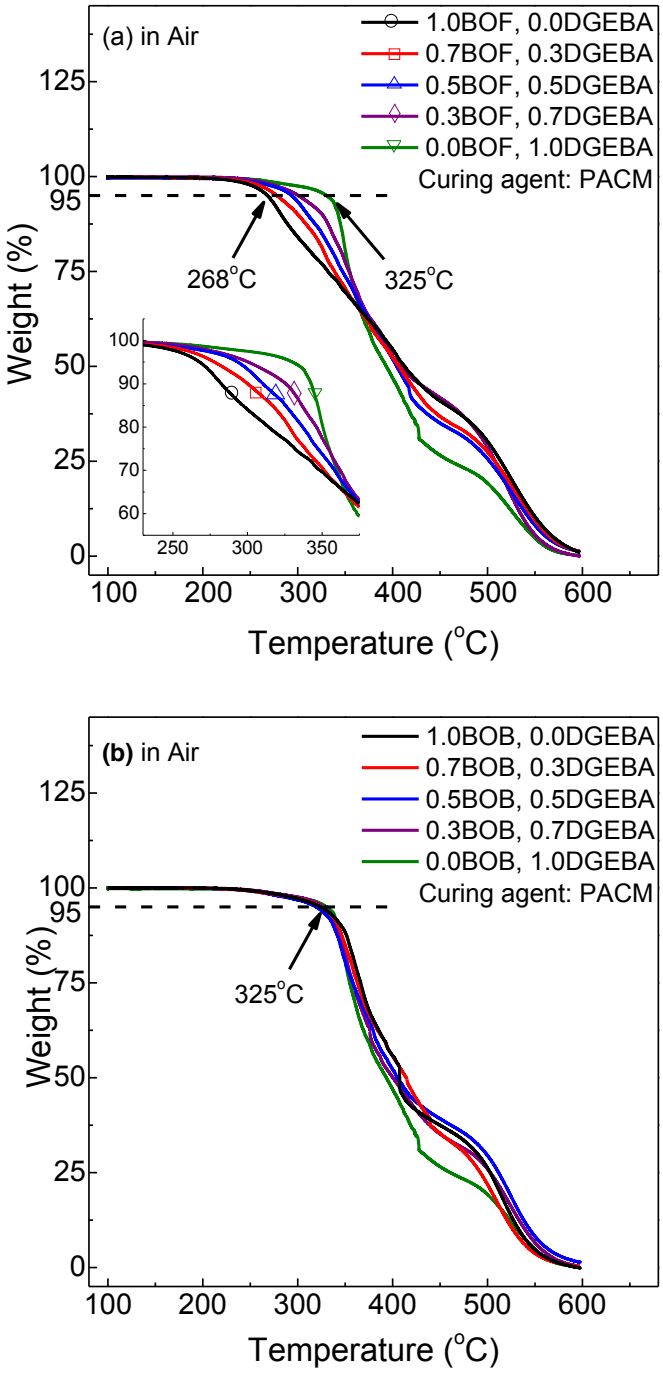

Figure 2.21. TGA thermograms of (a) BOF-DGEBA-PACM and (b) BOB-DGEBA-PACM samples in the air condition.

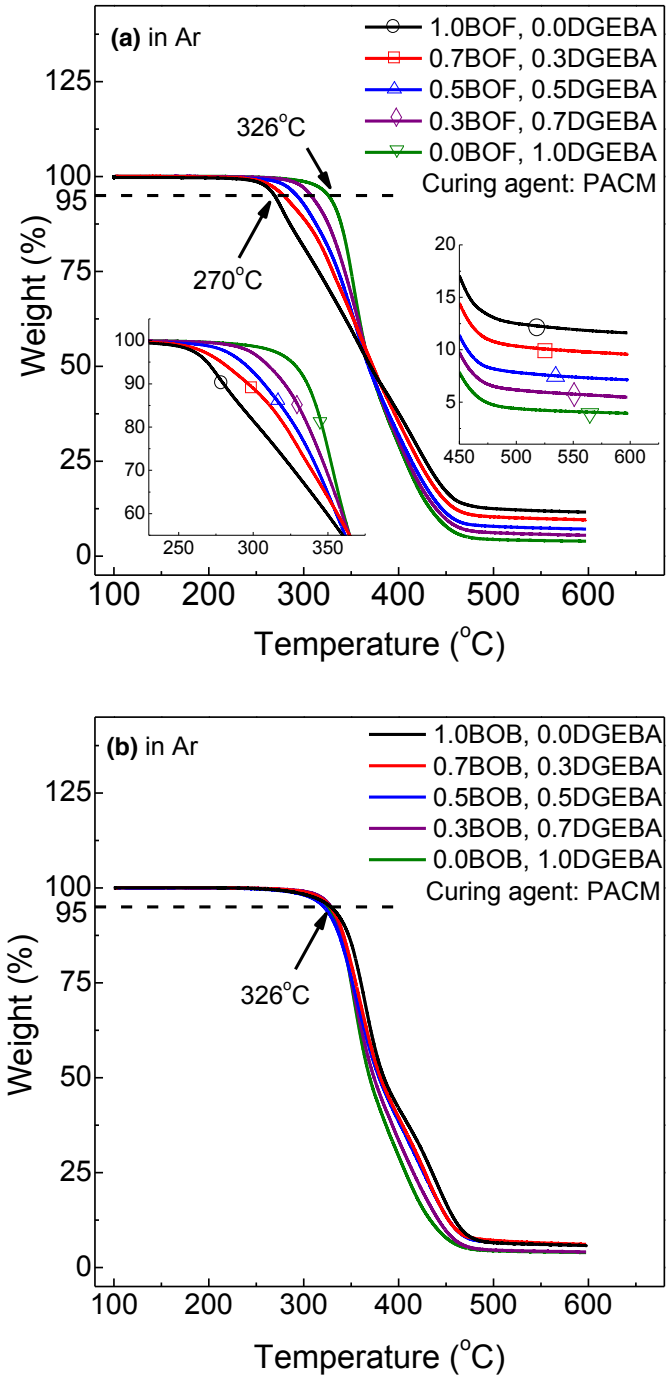

Figure 2.22. TGA thermograms of (a) BOF-DGEBA-PACM and (b) BOB-DGEBA-PACM samples in the argon condition.

Table 2.4. Char yields at 600 °C of BOF/DGEBA/PACM and BOB/DGEBA/PACM samples in both argon and air conditions.

Sample	Char yield at 600 °C (wt%)	
	Argon	Air
1.0BOF-0.0DGEBA-PACM	11.6	0.9
0.7BOF-0.3DGEBA-PACM	9.6	1.2
0.5BOF-0.5DGEBA-PACM	7.1	1.2
0.3BOF-0.7DGEBA-PACM	5.5	0.2
0.0BOF-1.0DGEBA-PACM	4.0	0.1
1.0BOB-0.0DGEBA-PACM	5.8	0.1
0.7BOB-0.3DGEBA-PACM	6.1	0.4
0.5BOB-0.5DGEBA-PACM	5.9	1.4
0.3BOB-0.7DGEBA-PACM	4.1	0.4

decomposition curves in argon. Differing greatly from the behavior observed in air, BOF-DGEBA-PACM samples possess higher char yields at 600 °C compared with BOB-DGEBA-PACM samples. Table 2.4 summarizes their char yields at 600 °C in both argon and air conditions. As shown in argon condition, these char yields increase with the increasing BOF content, suggesting that furanyl structures transform to more stable forms during heating in inert environment compared with phenyl structures. This result matches with our previous discovery that samples cured using furanyl amine hardeners also have high char yields at 800 °C in argon.[104] In air condition, char yields at 600 °C of both BOF-DGEBA-PACM and BOB-DGEBA-PACM samples are near or below 1 wt%. Moreover, as shown in Figure 2.21a and Figure 2.22a, BOF-DGEBA-PACM samples behave differently in air and argon conditions, suggesting different decomposition pathways in these two environments.

2.4. Conclusions

1, 4-bis[(2-oxiranylmethoxy)methyl]-furan (BOF) and its benzene analogue, 1, 4-bis[(2-oxiranylmethoxy)methyl]-benzene (BOB), were successfully synthesized. BOF and BOB are both liquids with low viscosity and good processability. After fully cured with standard PACM (cycloaliphatic) and EPIKURE W (aromatic) amine hardeners, BOF based thermosetting polymers were found to possess lower T_gs and higher storage moduli than BOB systems. Possible reasons could be that the methylene linkages

between furanyl and glycidyloxy groups in BOF facilitate the rotation of five-membered furanyl ring and that the hydrogen bonding possibly exists between the oxygen atoms in furanyl rings and the hydroxyl groups from epoxy-amine reaction. Furthermore, it was found that the additional methylene linkages between aromatic ring and glycidyloxy group in BOF and BOB lead to much lower T_g than thermosets made with phenolic glycidyl ethers like DGEBA and DGEPP that do not have them. BOF shows excellent miscibility with DGEBA resulting in the formation of homogenous networks that follow the Fox Equation with high fidelity. It is noteworthy that, when cured with PACM, BOF with furanyl building blocks showed superior fracture toughness properties compared with BOB with phenyl building blocks in the absence of the influence of testing temperature relative to sample glass transition temperature. In air and argon conditions, BOF-PACM sample thermally decomposed at a lower temperature compared with BOB-PACM and DGEBA-PACM samples. However, the BOF containing samples possess systematically higher char yields at 600 °C compared with their phenyl analogues tested in argon environment. These results suggest that the furanyl ring, which is available from many biomass sources, is a viable substitute for the incumbent petroleum-based thermosetting resins that use phenyl ring as a building block.

Chapter 3. Influence of furanyl building blocks on the cure kinetics of thermosetting epoxy-amine systems

3.1. Introduction

Thermosetting materials produced using renewable sources have received attention due to the economic and environmental concerns of petroleum sources which are primarily used to prepare incumbent thermosetting resins. So far, several types of biomass, including lignin,[105] cellulose,[13b] hemicellulose,[106] starch,[16a] chitin[17a] and triglycerides,[12b] have been investigated for preparing thermosetting materials. These renewable sources are abundant and robust, and the biobased thermosets derived from them are promising. Our previous research showed that furanyl epoxy resins possess comparable thermal and mechanical properties with their phenyl analogues. For example, using PACM as the amine hardener, BOF possesses an E'_{rt} of 2.97 GPa, 0.63 GPa higher relative to BOB, and a T_g of 71 °C, 29 °C lower than BOB. These findings are promising because furanyl chemicals, readily produced from several abundant biomasses, are considered promising candidates to substitute petroleum-based phenyl chemicals currently used for producing high-performance thermosetting materials. In order to further understand the influence of furanyl building block to the thermal and mechanical properties of thermosetting epoxy resins relative to its phenyl analogue, a cure kinetics investigation

on BOF-PACM, BOB-PACM and DGEBA-PACM systems was conducted to elucidate the influence of central building blocks on the cure behavior as well as on the network structure development which can determine the ultimate properties of these thermosetting materials.

3.2. Experimental

3.2.1. Materials

Epoxy resins and amine hardener used in this chapter are summarized in Figure 3.1. BOF and BOB were prepared in laboratory; DGEBA (n = 0.13) was supplied by Miller-Stephenson chemical company, USA. Their EEW values were determined by following ASTM epoxide titration technique, D 1652-97. The experimental results, 120.0 g/eq. for BOF, 125.0 g/eq. for BOB and 188.0 g/eq. for DGEBA, matched the theoretical values. Tetrafunctional amine hardener, PACM, with a 52.5 g/eq. AHEW value, was provided by Air Products, USA. Cure kinetics were investigated with reaction mixtures having stoichiometric quantities of epoxy and amine on the basis of the EEW and AHEW values.

3.2.2. Fourier transform infrared (FTIR) spectroscopy

Cure kinetics studies of BOF-PACM, BOB-PACM and DGEBA-PACM were conducted using FTIR spectroscopy in the near-infrared (N-IR, 4000-8000 cm^{-1}) at 60 °C. A Nexus 6700 FTIR spectrometer (Thermo-Nicolet Corp.) with a CaF_2 beam splitter and a DTGS KBr detector was used. Spectra were obtained at regular time intervals using 4 cm^{-1} resolution with 32 scans per spectrum. N-IR spectroscopy was used to monitor the concentrations of epoxy [EP] and primary amine [PA] in the resin mixture during reaction. Mass balance equations were employed to obtain the concentrations of secondary amines [SA] and tertiary amines [TA]. Epoxy peaks at 4529 cm^{-1} of DGEBA and 4527 cm^{-1} of BOF and BOB, respectively, were used to track the epoxy concentration. The primary amine peak at 4930 cm^{-1} of PACM was used for monitoring the primary amine concentration.

3.2.3. Experimental setup

Low hydroxyl silica glass tubes with 1.60 ± 0.05 mm inside diameter and 65 mm length were employed as sample holders.[102] Samples were prepared by mixing 1.000 gram of epoxy and the stoichiometric amount of PACM. The mixtures were then degassed and injected into a glass tube. To remove moisture, glass tubes were kept at 130 °C overnight before use. A temperature controlled aluminum sample holder shown schematically in Figure 3.2 was used for the N-IR experiments. This device allowed for control of

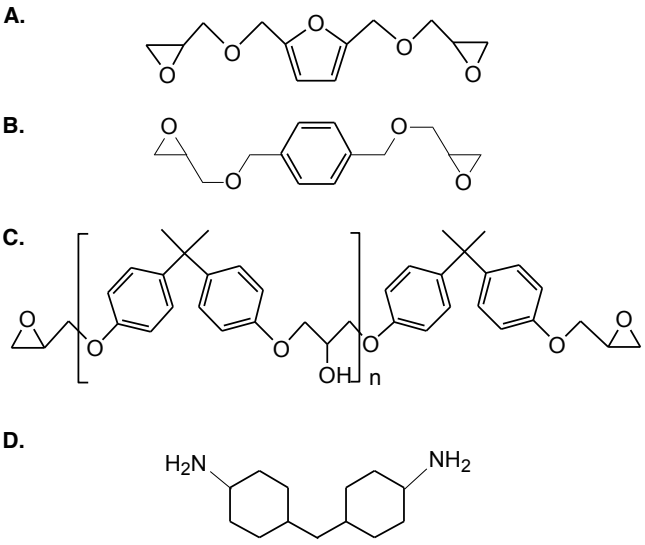

A. 2, 5-bis[(2-oxiranylmethoxy)methyl]-furan (**BOF**);
B. 1, 4-bis[(2-oxiranylmethoxy)methyl]-benzene (**BOB**);
C. Diglycidyl ether of bisphenol A (**DGEBA**, n = 0.13);
D. 4, 4′-methylene biscyclohexanamine (**PACM**).

Figure 3.1. Epoxy resins and amine hardener used in this chapter.

temperature within ± 0.5 °C of the 60 °C set point. A background scan was conducted before each experiment using the glass tube before filling.

3.2.4. Numerical procedure

The experimental concentrations of epoxy and primary amine were fitted to a two-parameter auto-catalytic model using a least-squares approach. A MATLAB code was generated and used for this purpose. The auto-catalytic rate equations were solved using MATLAB nonlinear ODE solver (ode45). Rate parameters for the set of numerical solutions that showed the least deviation from the experimental data points (epoxy and primary amine concentrations) were used as the rate constants for primary and secondary amine reactions.

3.3. Results and Discussion

The objective of this study was to evaluate cure behaviors of BOF-PACM, BOB-PACM and DGEBA-PACM in order to understand the influence of furanyl and phenyl building blocks on the cure reaction rates and network structure development. As introduced in Chapter 1, epoxy-amine cure reactions include epoxy-primary amine addition, epoxy-secondary amine addition, epoxy-hydroxyl etherification and epoxy-epoxy

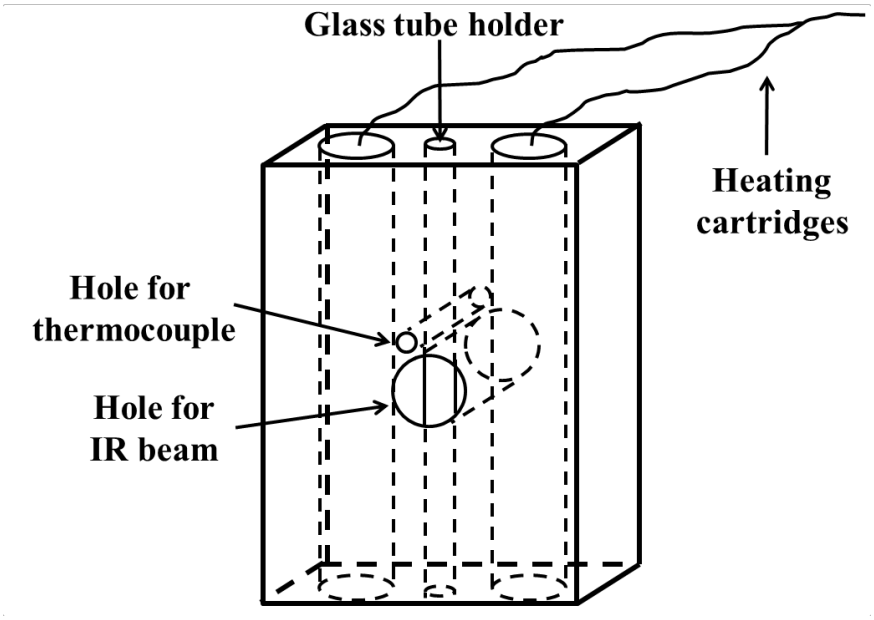

Figure 3.2. Sketch of the temperature controlled FTIR glass tube holder.

etherification. The occurrence and the extent of these reactions are affected by the cure temperature, formulation, and the presence of impurities and solvents. In this study only the epoxy-amine reactions were considered, as previous work showed that etherification was minimal for the investigated conditions.[81b] Hydroxyl groups present in the epoxy-amine system are known to catalyze the epoxy-amine addition reactions and need to be considered. Thus in our analysis we were interested in epoxy [EP], primary amine [PA], secondary amine [SA], tertiary amine [TA] and hydroxyl [OH] concentrations as a function of the reaction time.

Epoxy-amine reactions can proceed via an auto-catalytic pathway, given by Equations 3.1 and 3.2, or a non-catalytic pathway, Equations 3.3 and 3.4.

$$[PA] + [EP] + [OH] \overset{k_1}{\rightarrow} [SA] + 2 * [OH] \tag{3.1}$$

$$[SA] + [EP] + [OH] \overset{k_2}{\rightarrow} [TA] + 2 * [OH] \tag{3.2}$$

$$[PA] + [EP] \overset{k_1'}{\rightarrow} [SA] + [OH] \tag{3.3}$$

$$[SA] + [EP] \overset{k_2'}{\rightarrow} [TA] + [OH] \tag{3.4}$$

In these equations k'_1 and k'_2 were the kinetic parameters of epoxy-primary amine and epoxy-secondary amine addition reactions in the non-catalytic pathway, and k_1 and k_2 were those in the auto-catalytic pathway, respectively. The auto-catalytic pathway was selected due to the fact that DGEBA possessed a significant hydroxyl concentration, and BOF-PACM and BOB-PACM systems also possessed a comparable hydroxyl concentration as the DGEBA-PACM one because of the presence of small amounts of water despite drying.

As described in the experimental section, [EP] and [PA] were measured using N-IR. The concentrations [SA], [TA] and [OH] were obtained from mass balance relations as shown below. The initial epoxy concentration was related to epoxy, secondary amine and tertiary amine concentrations by Equation 3.5, and the initial primary amine concentration was related to primary amine, secondary amine and tertiary amine concentrations by Equation 3.6.

$$[EP]_0 = [EP] + [SA] + 2 * [TA] \tag{3.5}$$

$$[PA]_0 = [PA] + [SA] + [TA] \tag{3.6}$$

In these equations $[EP]_0$ and $[PA]_0$ are the concentrations (mol/L) of epoxy and primary amine in the system at t = 0, and [EP], [PA], [SA] and [TA] were corresponding concentrations at any time t. By re-arranging Equations 3.5 and 3.6, [SA] and [TA] concentrations, respectively, are expressed by Equations 3.7 and 3.8 below.

$$[SA] = 2 * ([PA]_0 - [PA]) - ([EP]_0 - [EP]) \quad (3.7)$$

$$[TA] = ([EP]_0 - [EP]) - ([PA]_0 - [PA]) \quad (3.8)$$

Using these equations, secondary and tertiary amine concentrations were calculated with the known and measured epoxy and primary amine concentrations.

Since the epoxy-amine reaction is catalyzed by the hydroxyl groups and as one hydroxyl group is formed for every epoxy-amine addition reaction, an expression is needed for the hydroxyl concentration as a function of conversion. The hydroxyl concentration [OH] is given by Equation 3.9.

$$[OH] = [OH]_{auto} + [OH]_0 \quad (3.9)$$

In this equation $[OH]_0$ and [OH] were the hydroxyl concentrations in the system at t = 0 and t, respectively. $[OH]_{auto}$ was the concentration of hydroxyl groups resulting from the epoxy-amine reaction at time t given by Equation 3.10.

$$[OH]_{auto} = [SA] + 2 * [TA] \tag{3.10}$$

$[OH]_0$ was predominately determined by the n value of DGEBA epoxy monomer in the DGEBA-PACM system, and by the initial hydroxyl concentration presumably from water in the BOF-PACM and BOB-PACM cases. In the DGEBA-PACM system, $[OH]_0$ was given by Equation 3.11, where $[OH]_0$ was proportional to $[EP]_0$ as indicated from the chemical structure of DGEBA.

$$[OH]_0 = \frac{0.13}{2} * [EP]_0 \tag{3.11}$$

In the BOF-PACM and BOB-PACM systems, $[OH]_0$ was calculated from the ratio between epoxy and hydroxyl peak heights in the N-IR spectrum taken at t = 0. As

previously mentioned, these initial hydroxyl concentrations were possibly due to the trace moisture in the systems.

Figure 3.3 shows the evolution of N-IR spectra of BOF-PACM, BOB-PACM and DGEBA-PACM systems as the reactions proceed at 60 °C for 3 hours. The spectra were normalized, and 10 representative spectra with an 18 minute interval between each are shown. Two epoxy peaks at 6075 and 4527 cm^{-1} for BOF, 6062 and 4527 cm^{-1} for BOB, 6063 and 4527 cm^{-1} for DGEBA can be used to track the epoxy concentration. However, the peak at 4527 cm^{-1} was preferred, since the one at the higher wavenumber typically overlapped with the aromatic peak in its neighborhood.[9] The primary amine peak at 4929 cm^{-1} was used to track the primary amine concentration. The extent of cure, α, based on the consumption of the epoxy groups, was obtained from the ratio of the corresponding peak heights at times $t = t$ and $t = 0$. As shown in Figure 3.3, in these three systems, the epoxy and primary amine peaks disappeared and the hydroxyl peak (7099 cm^{-1}) appeared as cure progressed. The peak at 6507 cm^{-1} represented the combination of both primary and secondary amines, and it also disappeared over time. According to the spectra, primary amines were fully consumed; however, the epoxy peak and the primary-secondary amine peak were decreasing, signifying that the epoxy-amine reactions were still proceeding after 3 hours at 60 °C. The reason for this was that the reactions became diffusion controlled as the systems reached vitrification, and this was particularly evident for the DGEBA-PACM system.

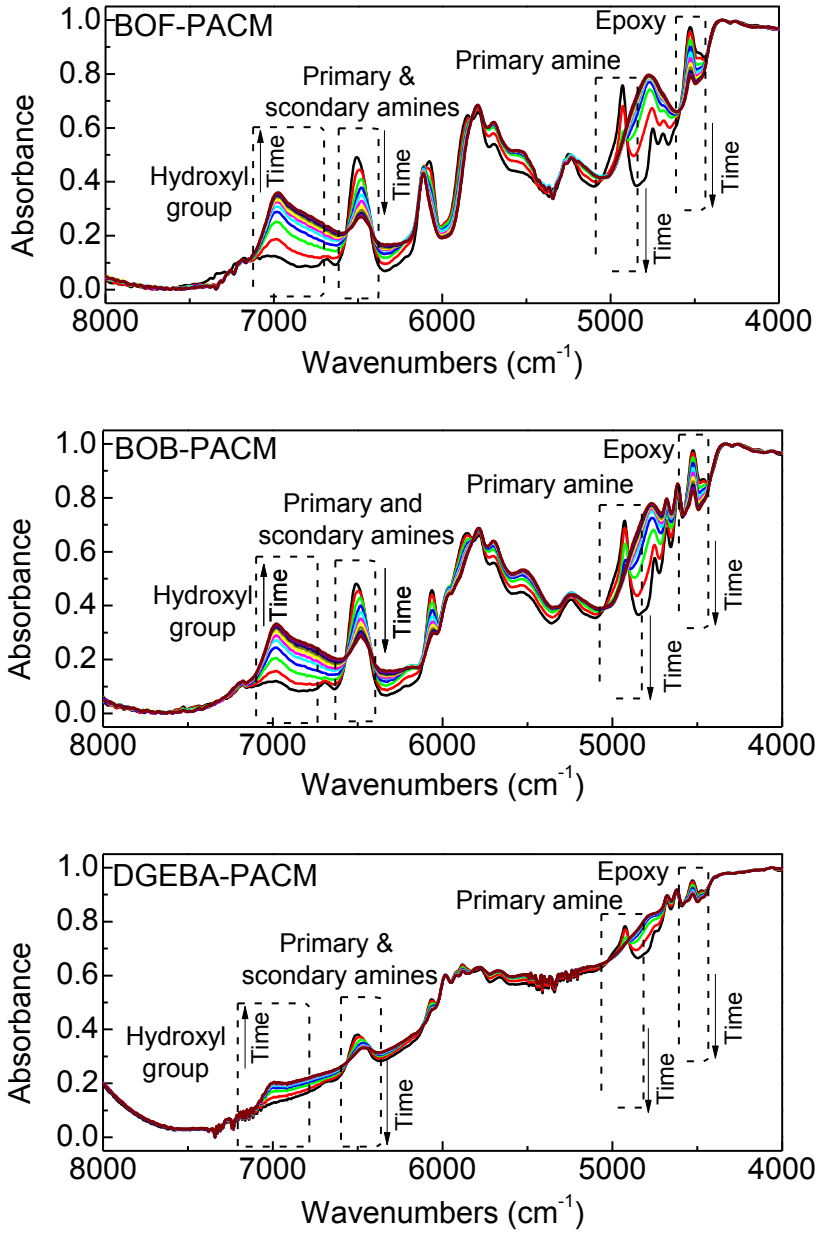

Figure 3.3. Selected spectra of BOF-PACM, BOB-PACM and DGEBA-PACM as the cure reactions occurred at 60 °C for 3 hours. The interval of the present spectra was 18 minutes. The epoxy peak was present at 4527 cm^{-1} and primary amine peak was present at 4929 cm^{-1}.The epoxy and amine peaks shrunk over time while the hydroxyl peak grew.

In cooperation with the N-IR data, the initial epoxy and primary amine concentrations, $[EP]_0$ and $[PA]_0$, were important for determining the rate constants. $[EP]_0$ and $[PA]_0$ were calculated using component weights, their densities at 60 °C and the assumption that no volumetric change occurred at mixing. Densities of the components were measured using a 25 mL glass volumetric flask at both room temperature and 60 °C, and the results are summarized in Table 3.1, together with the molecular weights, the EEW and AHEW values. These values were used to establish the formulations of the epoxy-amine systems and to calculate the initial conditions, i.e. $[EP]_0$ and $[PA]_0$, for the rate equations as summarized in Table 3.2.

The epoxy and primary amine concentrations obtained from N-IR experiments were used in conjunction with Equations 3.7 and 3.8 to calculate the secondary and tertiary amine concentrations and resulting time dependent concentration profiles. Figures 3.4, 3.5 and 3.6 show representative profiles for the BOF-PACM, BOB-PACM, and DGEBA-PACM systems, respectively. In all cases, the depletion of epoxy and primary amine, the formation and depletion of secondary amine and the formation of tertiary amines were observed.

Differential equations describing the time dependent reaction behaviors of the systems, based on Equations 3.1, 3.2, 3.7, 3.8, 3.9, and 3.10 and 3.11, are given by Equations 3.12 and 3.13 below.

Table 3.1. Molecular weights of the components, their densities at room temperature and 60°C, and the EEW and AHEW values.

Component	Molecular Weight (g/mol)	Density @ RT (g/ml)	Density @ 60 °C (g/ml)	EEW (g/eq.)	AHEW (g/eq.)
BOF	240.3	1.1858	1.1634	120.0	-
BOB	250.3	1.1501	1.1214	125.0	-
DGEBA	377.1	1.1604	1.1344	188.0	-
PACM	210.4	0.9590	0.9380	-	52.5

Table 3.2. Resin formulations of the epoxy-amine systems and the initial concentrations of epoxy and primary amine groups.

System	W_{epoxy} (g)	W_{amine} (g)	$[EP]_0$ (mol/L)	$[PA]_0$ (mol/L)
BOF-PACM	1.0000	0.4375	3.1384	1.5682
BOB-PACM	1.0000	0.4200	2.9826	1.4903
DGEBA-PACM	1.0000	0.2793	2.2488	1.1255

$$\frac{d[EP]}{dt} = -k_1 * [PA] * [EP] * ([OH]_{auto} + [OH]_0) - k_2 * [EP] * [SA] * ([OH]_{auto} + [OH]_0)$$

(3.12)

$$\frac{d[PA]}{dt} = -k_1 * [PA] * [EP] * ([OH]_{auto} + [OH]_0) \quad (3.13)$$

The above set of ordinary differential equations was used to fit the experimental concentrations such as those shown in Figures 3.4, 3.5 and 3.6 and to obtain the best fit of k_1 and k_2 values as described previously. These values are reported in Table 3.3. Three experiments were conducted for the BOB and BOF systems, and all results are provided in Table 3.3 with averages. In addition, Figures 3.4, 3.5 and 3.6 show the best-fit curves corresponding to the k_1 and k_2 values obtained for those sets of data. All reported kinetic parameters were obtained by solving the rate equations and minimizing the sum of square errors up to a certain stage of cure where the mixtures were still liquid, and the systems were in the "pre-gel" state. At higher concentrations above the gel point, a diffusion term would be needed to describe the cure behavior. Therefore, Figures 3.4, 3.5 and 3.6 only present the experimental data before gelation and demonstrate that the two-parameter model fits well with the experimental data during the initial stages of the cure.

One of the main purposes of this study was to measure the reactivity ratio, k_2/k_1. The epoxy-primary amine addition could potentially affect the reactivity of the secondary amine reaction, and this effect, often referred to as a substitution effect, can be measured by the reactivity ratio between the secondary amine reactivity rate to the primary amine, k_2/k_1. The substitution effect is critical since it can be used to provide insight into the structure of the developing network. A reactivity ratio of 0.5 indicates that both the primary and secondary amines react equally and form a completely random network. It should be noted that a primary amine has two reactive hydrogen atoms, and a secondary amine has one reactive hydrogen atom, thus an equal reactivity yields k_2/k_1 = 0.5. However, a ratio less than 0.5 shows that the reactivity of the secondary amine decreases due to the addition of an epoxy moiety to the primary amine group.[107] In this case, a linear chain is formed first, and crosslinks will appear later in the reaction.

Table 3.3 summarizes the epoxy-primary amine and epoxy-secondary amine addition kinetic parameters k_1 and k_2, respectively, for all three systems. With similar methods to the one used herein, Raman and Palmese reported reactivity ratios for a DGEBA-PACM system at 60 °C with k_1 = 0.00607±0.00041 $L^2/(mol^2\ min)$, k_2 = 0.00123±0.00014 $L^2/(mol^2\ min)$ and k_2/k_1 = 0.203, which match our results closely.[81b] Overall, BOF possessed the highest epoxy-primary amine reactivity and the lowest epoxy-secondary amine reactivity compared with BOB and DGEBA. This interesting observation suggests that furanyl and phenyl building blocks have different influences in the epoxy-primary

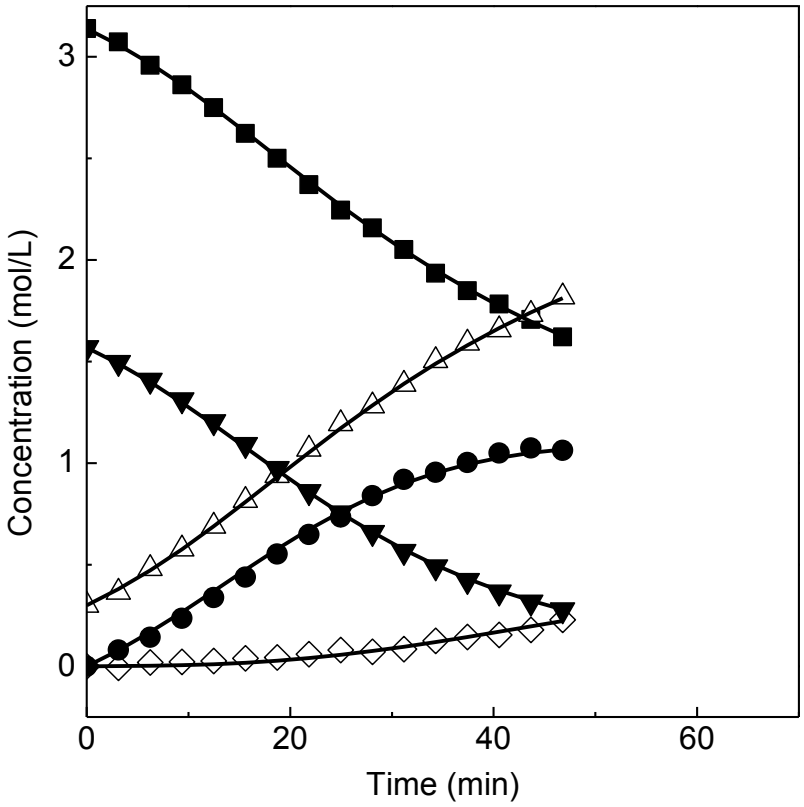

Figure 3.4. Experimental data (points) and the mode fits (lines) of the BOF-PACM system at 60 °C. ■, ▼, ●, ◊ and Δ represent the experimental concentrations of epoxy, primary, secondary, tertiary amines and hydroxyl groups, respectively.

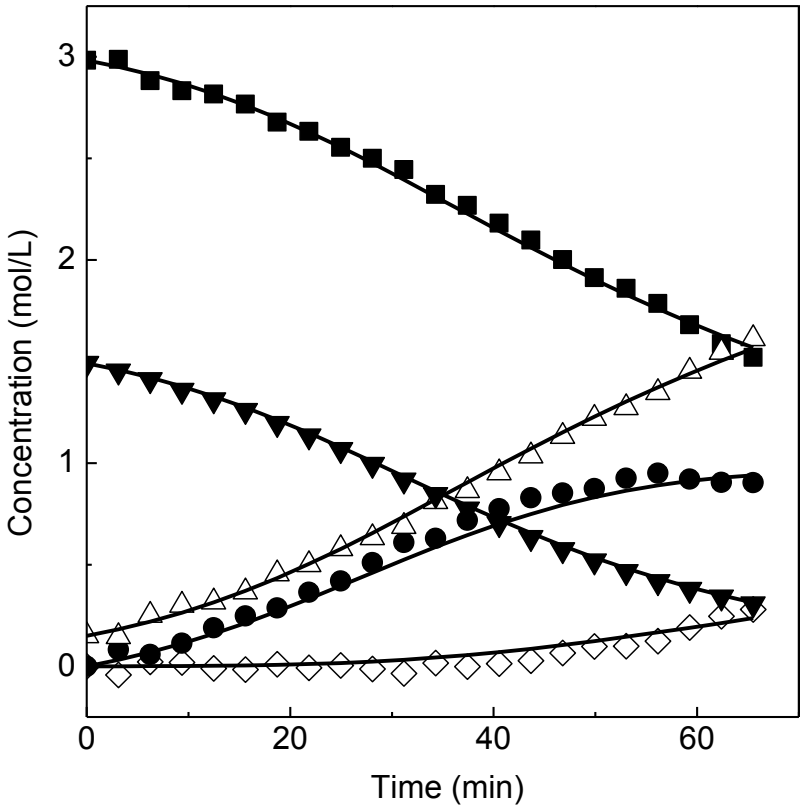

Figure 3.5. Experimental data (points) and the mode fits (lines) of the BOB-PACM system at 60 °C. ■, ▼, ●, ◊ and Δ represent the experimental concentrations of epoxy, primary, secondary, tertiary amines and hydroxyl groups, respectively.

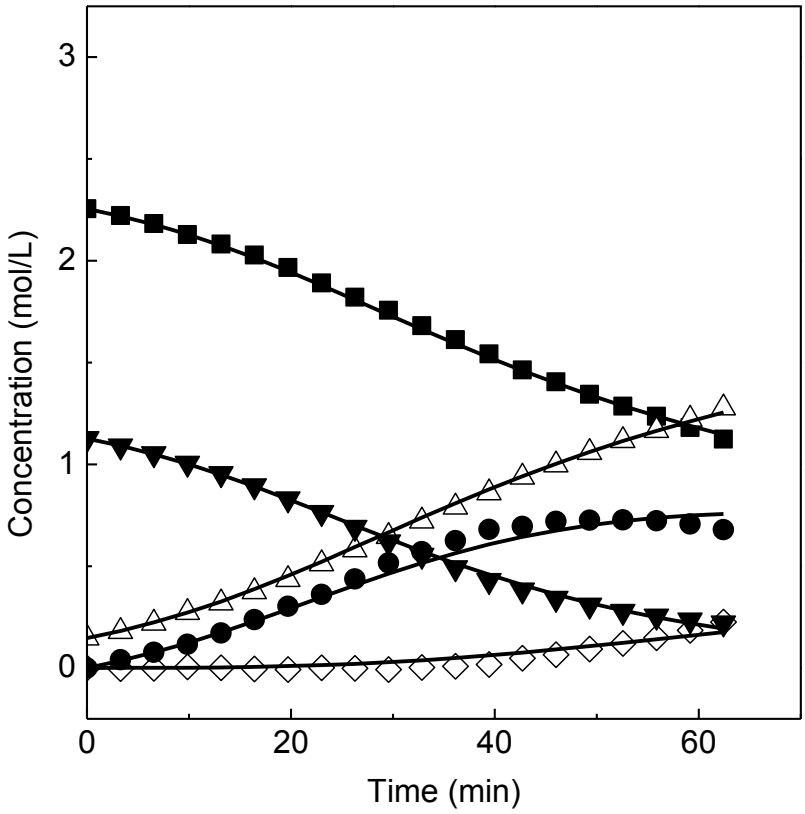

Figure 3.6. Experimental data (points) and the mode fits (lines) of the DGEBA-PACM system at 60 °C. ■, ▼, ●, ◊ and Δ represent the experimental concentrations of epoxy, primary, secondary, tertiary amines and hydroxyl groups, respectively.

Table 3.3. Summary of the kinetic parameters of auto-catalytic epoxy-primary amine addition (k_1) and epoxy-secondary amine addition (k_2) at 60 °C.

Epoxy-amine system	Entry	k_1 ($L^2/(mol^2\ min)$)	k_2 ($L^2/(mol^2\ min)$)	k_2/k_1
BOF-PACM	expt 1	0.0082	0.0014	0.171
	expt 2	0.0075	0.0009	0.120
	expt 3	0.0075	0.0009	0.120
	average	0.00773±0.00040	0.00107±0.00029	0.137
BOB-PACM	expt 1	0.0074	0.0017	0.230
	expt 2	0.0056	0.0015	0.268
	expt 3	0.0056	0.0016	0.286
	average	0.00620±0.00104	0.00160±0.00010	0.261
DGEBA-PACM	expt 1	0.0072	0.0014	0.189
	average	0.00723	0.00137	0.189

amine and epoxy-secondary amine reactions. Reasons for this could be the differences of (1) electron densities on the epoxy reactive groups and (2) intermolecular interactions on the amine reactive groups. For the first hypothesis, ^{1}H NMR results of BOF, BOB and DGEBA monomers showed minimal differences in epoxy peak positions (2.793 and 2.609 ppm for BOF, 2.797 and 2.621 ppm for BOB, and 2.894 and 2.743 ppm for DGEBA), and these indicated the electron density differences on the epoxy reactive groups were negligible. For the second hypothesis, the highly electronegative elements on the furanyl groups (oxygen atoms) would attract the electropositive elements (hydrogen atoms) on the amine hardener molecules, and the dipole-dipole interactions could activate the amine groups, facilitate the epoxy-primary amine reactions and result in an elevated k_1 value for BOF. However, as shown by the lowest k_2 value of BOF compared with BOB and DGEBA, this effect is significantly weakened in the epoxy-secondary amine reaction. This can be explained since hydroxyl groups, a more favorable hydrogen bonding donor compared with primary and secondary amines, are generated and associated with furanyl groups through a more stable hydrogen bonding. The combination of these effects would explain the observation that BOF has the smallest k_2/k_1 value in comparison to the other systems as well as the highest k_1 constant. A comparison between DGEBA-PACM and BOB-PACM showed that DGEBA possessed a larger k_1 value and a smaller k_2 value. ^{1}H NMR results indicated that epoxy peaks of DGEBA presented at relatively higher positions compared with BOB. This indicates DGEBA epoxy groups are more electron-deficient, i.e. more electrophilic and favored to react with primary amines - resulting in a larger k_1 value compared with that of BOB.

The structural difference between BOB and DGEBA which is responsible for this effect is the methylene linkage present in BOB between the phenyl group and oxygen atom. However, the secondary amine groups in the DGEBA-PACM network are perhaps more sterically hindered by the DGEBA than BOB, resulting in a smaller k_2 value.

3.4. Conclusions

The results of this investigation show clear differences in the reactivity of analogue diepoxy monomers prepared using furanyl (BOF) and phenyl building blocks (BOB). The overall reactivity of BOF was found to be significantly greater than that of BOB. More interestingly, the reactivity ratio k_2/k_1 of BOF with a standard amine curing agent was found to be about half that of BOB suggesting that the formation of the network structures in these two systems proceed very differently during cure. In particular, in the early stages, BOF systems should possess a network structure that is characterized by more chain extensions than that of analogue BOB thermosets. This behavior could lead to the differences in mechanical properties, such as strength and fracture toughness, of these furanyl and phenyl based systems as discussed in Chapter 2. Hydrogen bonding with the furanyl group in BOF during the course of the epoxy-amine reaction could explain the reactivity difference with BOB systems for which hydrogen bonding with the phenyl ring is not possible.

Chapter 4. Synthesis and characterization of fully furanyl based epoxy-amine systems

4.1. Introduction

Thermosetting materials are used extensively in numerous fields and for many applications as a result of their superior thermomechanical properties, excellent chemical resistance and outstanding processability.[11] Renewable thermosetting materials have received both academic and industrial attentions since they could potentially provide sustainable and eco-friendly alternatives to current petroleum-derived products. Biobased sources, such as vegetable oil, cellulose, hemicellulose, lignin, starch and chitin, have been investigated as raw materials for preparing thermosetting resins.[9, 55c] Epoxy resins possessing specific biobased building blocks, such as triglyceride, furanyl and phenol, have been reported.[108] In particular, furanyl epoxy resins exhibit promising thermal and mechanical properties when cured with amine hardeners.[11] Such furanyl building blocks are primarily derived from polysaccharides and sugars and can be used for preparing not only epoxy resins but also amine hardeners.[23c, 109] In the previous chapters, furanyl epoxy resins were synthesized and cured with PACM, resulting in lower T_g and higher E'_{rt} compared with a phenyl-based diepoxy analogue.[11]

Generally, between 20 to 50 wt.% of an epoxy-amine thermoset is comprised of an amine hardener that impacts the ultimate performance of the system.[110] Therefore, it is necessary to take amine hardeners into account when designing renewable alternatives to epoxy-amine systems. Aromatic amine hardeners are commonly used since they endow cured thermosets with superior thermo-mechanical properties; however, most of these hardeners, including 4,4'-methylenedianiline (MDA) and (EPIKURE W are non-renewable and toxic.[111] Cycloaliphatic diamines, such as PACM, that have reduced toxicity can be used to make high-performance resins, but they are also derived from non-renewable sources. Renewable furanyl derivatives are promising candidates for preparing epoxy-amine thermosets due to their aromaticity and eco-friendliness.[23c, 109] Several furanyl amine compounds have been reported in literature,[112] yet neither the synthesis of fully furanyl based epoxy-amine thermosets nor their thermo-mechanical properties have been reported to date. The work in this chapter was to prepare and evaluate epoxy-amine thermosets that are based fully on furanyl monomers. Thus, thermosetting systems were prepared using the furanyl epoxy monomer, BOF, which was evaluated in previous chapters using traditional curing agents,[11] and two furanyl amine hardeners, 5,5'-methylenedifurfurylamine (di-furanyl di-amine, DFDA) and 5,5'-ethylidenedifurfirylamine (CH_3-branched di-furanyl di-amine, CH_3-DFDA). Additional epoxy-amine systems were prepared using DGEBA and BOB with these two furanyl hardeners. The properties of these materials were compared to those of DGEBA and BOB cured with the standard hardener PACM.

4.2. Experimental

4.2.1. Materials

Chloroform (99%), tetrahydrofuran (THF, 99.9%), sodium hydroxide (98%), furfurylamine (99%), hydrochloric acid (37%), formaldehyde solution (37%), acetaldehyde (99%) were supplied by Sigma-Aldrich, USA; DGEBA (n = 0.13) and PACM (99%) were obtained from Miller-Stephenson chemicals and Air Products, USA, respectively. All chemicals were used as received. BOF (99%) was prepared in laboratory.[11] Structures of primary materials used in this chapter are summarized in Figure 4.1.

4.2.2. Preparation of DFDA and CH_3-DFDA

DFDA and CH_3-DFDA were prepared as previously reported in the literature.[112] For DFDA, furfurylamine (45 g, 464 mmol) and 6 M HCl solution (330 mL, 2 mol) were charged into a 2 L round-bottom flask, and 37 wt. % formaldehyde solution (18.4 mL, 232 mmol) was added dropwise at 25 °C. After 70 minutes, the reaction mixture was neutralized using 6 M NaOH solution (330 mL, 2 mol) and was then extracted with 200 mL chloroform several times. The combined organic layer was washed with 200 mL distilled water, dried with anhydrous $MgSO_4$ and vacuumed to yield a reddish-brown oily liquid. The liquid was distilled and further extracted with THF, and 10.0 g of

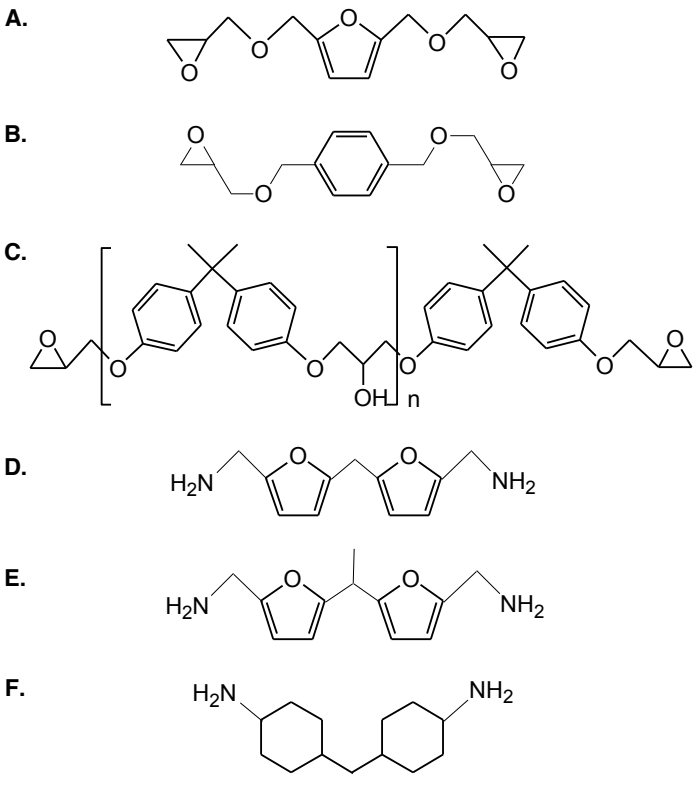

A. 2, 5-bis[(2-oxiranylmethoxy)methyl]-furan (**BOF**);
B. 1, 4-bis[(2-oxiranylmethoxy)methyl]-benzene (**BOB**);
C. Diglycidyl ether of bisphenol A (**DGEBA**, n = 0.13);
D. 5, 5'-methylenedifurfurylamine (**DFDA**);
E. 5, 5'-ethylidenedifurfurylamine (**CH_3-DFDA**);
F. 4, 4′-methylene biscyclohexanamine (**PACM**).

Figure 4.1. Primary materials used in this chapter.

5,5′-methylenedifurfurylamine (20.9% yield) was obtained. For CH_3-DFDA, furfurylamine (50 g, 516 mmol) and 6 M HCl solution (330 mL, 2 mol) were charged into a 2 L round-bottom flask. The mixture was cooled to 4 °C, and acetaldehyde (15.8 mL, 258 mmol) was quickly added. The reaction was kept at 40 °C for 50 minutes then cooled and neutralized using 6 M NaOH solution (330 mL, 2 mol). Extraction, distillation and purification of CH_3-DFDA were similarly carried out and 12.5 g 5,5'-ethylidenedifurfirylamine (21.4% yield) was achieved.

4.2.3. Characterization of DFDA and CH_3-DFDA

^{1}H NMR and FTIR were used for characterization. A ^{1}H NMR (500 MHz, Varian Unity Inova) unit was used to confirm the chemical structures of DFDA and CH_3-DFDA with a spectral window of ± 2000 Hz, 90° pulse width and 16 scans at 25 °C. A FTIR spectrometer (Thermo Nicolet Nexus) operating in transmission mode was used to collect spectra with a resolution of 8 cm^{-1}; 32 scans per spectrum were collected at 25 °C using a deuterated tryglycine sulfate (DTGS) detector.

4.2.4. Preparation of polymer samples using DFDA and CH_3-DFDA

Samples were prepared by curing DFDA, CH_3-DFDA and PACM with BOF, BOB or DGEBA at stoichiometry. The epoxy-amine combinations were mixed and cast into rubber molds with dimensions of 35.5 x 12.0 x 2.2 mm, and cured at 80 °C and post-

cured at 180 °C for 9 hours, respectively. Full conversion of epoxy and amine groups was verified using transmission FTIR in the 4000-8000 cm^{-1} range with 8 cm^{-1} resolution and 32 scans per spectra at 25 °C. DMA samples with dimensions of 35.4 x 11.9 x 2.1 mm were tested using a TA Q800 DMA in single cantilever geometry with 1 Hz frequency, 15 μm amplitude and 2 °C/min ramp rate from -150 to 200 °C. Each sample was tested twice, and the second scan was used to obtain its E′ and T_g from the loss modulus curve peak. A TA Q2000 DSC was used to measure T_gs for comparison to DMA results. Each sample was heated, cooled and reheated from 0 to 200 °C with 10 °C/min ramp rate, and its T_g was determined from the second heating scan. A TA Q50 TGA was used to investigate the thermal stability of samples in an argon environment by heating from 25 to 800 °C with a 10 °C/min ramp rate.

4.3. Results and Discussion

4.3.1. Characterization of DFDA and CH_3-DFDA

Figure 4.2 shows DFDA and CH_3-DFDA chemical structures and their ^{1}H NMR spectra. ^{1}H NMR spectra of DFDA and CH_3-DFDA were consistent with those previously reported in literature.[112] Five different groups of peaks were attributed to DFDA structure, and its purity was found to be >99%. Six different peaks were attributed to

CH_3-DFDA structure, and its purity was calculated to be 98%, with two sets of peaks attributed to impurities: the peaks at 1.25 ppm (1%) and the peak at 1.84 ppm from THF residue (1%), which could not be removed under vacuum overnight.

Table 4.1 summarizes the yield, purity and color of prepared DFDA and CH_3-DFDA amine hardeners.

4.3.2. Characterization of DFDA and CH_3-DFDA polymer samples

To obtain fully furanyl based thermosetting materials, DFDA and CH_3-DFDA were cured with BOF at stoichiometry. For comparison, DFDA and CH_3-DFDA were also cured with BOB and DGEBA at stoichiometry, respectively. The IR spectra of cured samples are plotted in Figure 4.3, including the spectrum of unreacted BOF-DFDA mixture for comparison. Within the limits of infrared spectroscopy measurements, no trace of primary and secondary amine peaks at 4940 and 6525 cm^{-1} or epoxy at 4530 cm^{-1} was observed in cured samples. The absence of these peaks shows complete reaction in the cured samples and further confirms the purity of materials since off-stoichiometric mixtures resulting from impurities would lead to unreacted epoxy and amine moieties.

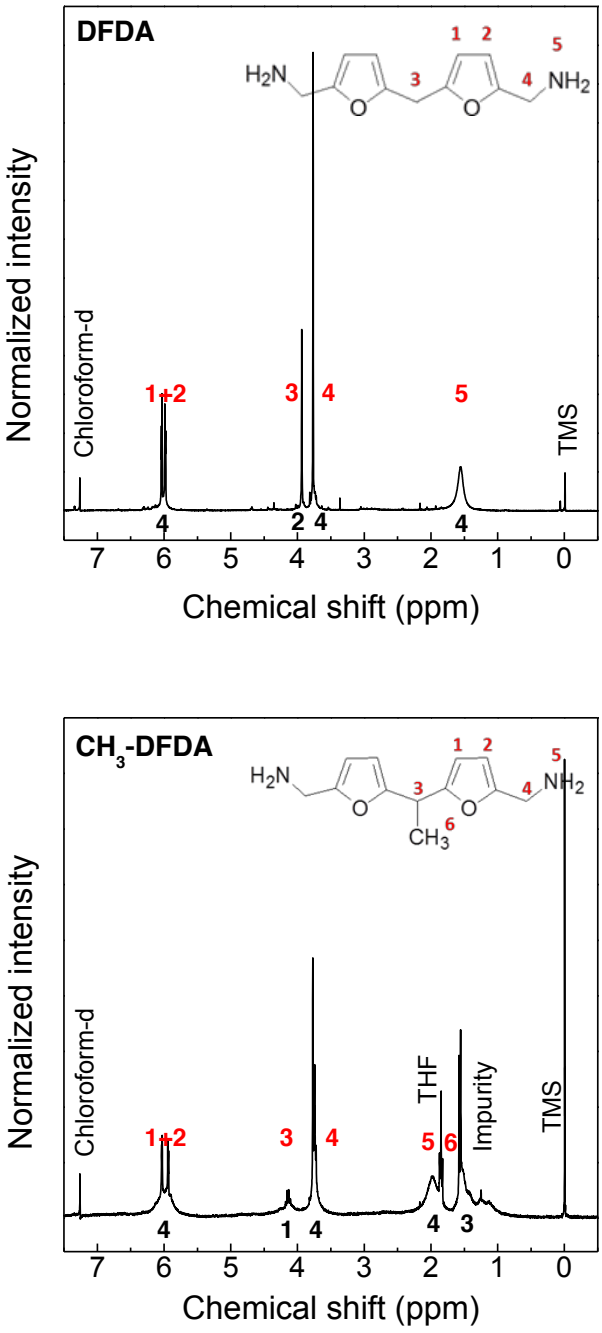

Figure 4.2. The ^{1}H NMR spectra of DFDA and CH_3-DFDA.

Table 4.1. Yield, purity and color of prepared DFDA and CH_3-DFDA amine hardeners

Hardener name	Yield (%)	Purity (%)	Color
DFDA	21	99	Brownish
CH_3-DFDA	22	98	Brownish

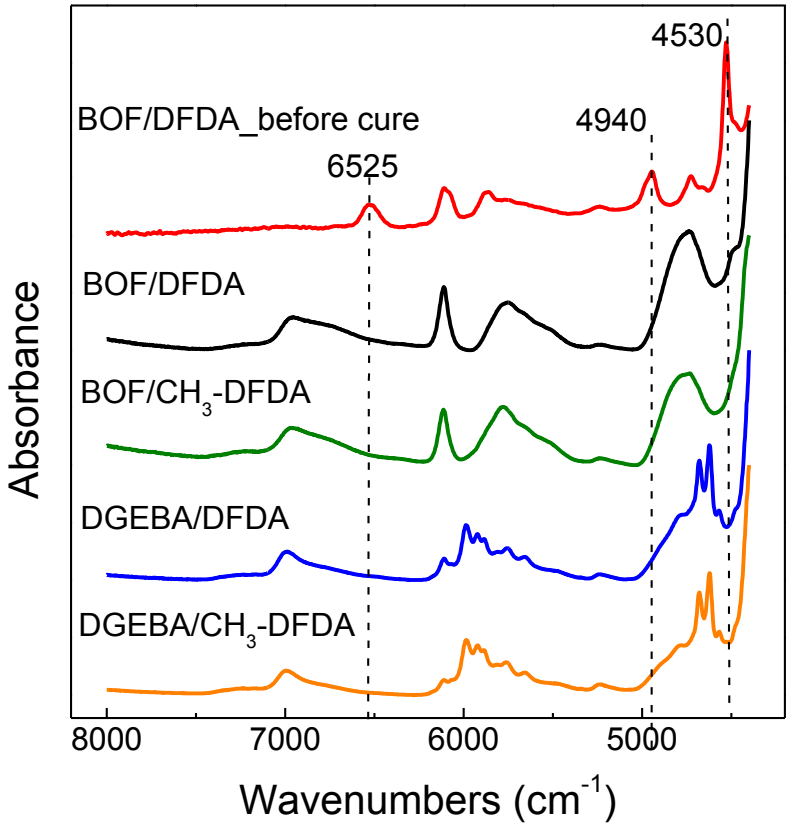

Figure 4.3. The N-IR spectra of cured samples of DFDA and CH_3-DFDA with BOF and DGEBA, as well as the BOF-DFDA sample before cure.

4.3.3. Thermo-mechanical Properties

Thermo-mechanical properties, such as T_g and E′, of fully furanyl based thermosetting samples were investigated using DMA and DSC. Thermograms of storage modulus, loss modulus and tan delta of cured BOF-DFDA and BOF-CH_3-DFDA samples are given in Figure 4.4a, b and c, respectively. In Figure 4.4a, storage modulus plots of BOF-DFDA and BOF-CH_3-DFDA show typical behavior of epoxy-amine thermosets progressing through the glass transition temperature. The transition is, however, much sharper for BOF-DFDA. In Figure 4.4b, BOF-DFDA shows a sharp loss modulus peak at 56 °C, whereas BOF-CH_3-DFDA displays a broader peak at the same temperature. These values were taken as their T_gs. In Figure 4.4c, BOF-CH_3-DFDA and BOF-DFDA display tan delta peaks at 69 °C and 62 °C, respectively, which indicates that the additional methyl group in CH_3-DFDA improves the sample T_g compared with DFDA. Similar behavior has been observed in bisphenol epoxy systems. For example, it has been reported that DGEBA-based networks possess higher T_gs than DGEBF counterparts.[113] The methyl group appears to restrict polymer chain mobility in the BOF-CH_3-DFDA system as well. The broader and lower peaks in the loss modulus and, in particular, the tan delta curves shown in Figures 4.4b and 4.4c support this. It should be noted that these broader peaks could also be due in part to the presence of minor impurities in CH_3-DFDA.

The BOF-PACM sample was prepared in a similar way, and the DMA thermograms are plotted in Figure 4.4. In Figure 4.4b, BOF-PACM possesses a T_g of 72 °C, 16 °C higher

than the T_gs of BOF-DFDA and BOF-CH_3-DFDA. This could be due to the presence of the methylene groups connecting the amine groups to the furanyl rings.[11] It should be noted that this effect is far less prevalent in BOF-diamine systems compared with the DGEPP-diamine system investigated earlier, in which case the T_g difference was 105 °C.[11] We suggest that this occurs because the concentration of flexible methylene linkages is reduced because the DFDA systems possess fewer methylene linkages per ring than BOF. BOF-DFDA and BOF-PACM have β-relaxations around -45 °C, but interestingly, that of BOF-CH_3-DFDA is significantly lower at -58 °C. This could be a result of the bis-E type structure relative to a bis-F structure of PACM and DFDA.

In Figure 4.4a, BOF-DFDA and BOF-CH_3-DFDA possess room temperature storage moduli around 3.5 GPa, while that of BOF-PACM is around 2.5 GPa. On the basis of our previous work and Abrams group work, this difference could be due to the hydrogen bonding associated with furanyl rings and the non-collinear covalent bonds linked with furanyl rings in the cured networks.[11, 103] Moreover, Figure 4.4d shows that BOF-PACM density is lower than BOF-DFDA and BOF-CH_3-DFDA. Glassy modulus is proportional to sample density, thus further explaining these modulus differences.[114] BOF-DFDA and BOF-CH_3-DFDA have similar densities and therefore similar moduli.

BOB was also used to cure with DFDA and CH_3-DFDA, and their DMA thermograms of storage modulus, loss modulus and tan delta curves are plotted in Figure 4.5a, b and c, respectively. In Figure 4.5a, storage modulus plots of BOB-DFDA and BOB-CH_3-DFDA

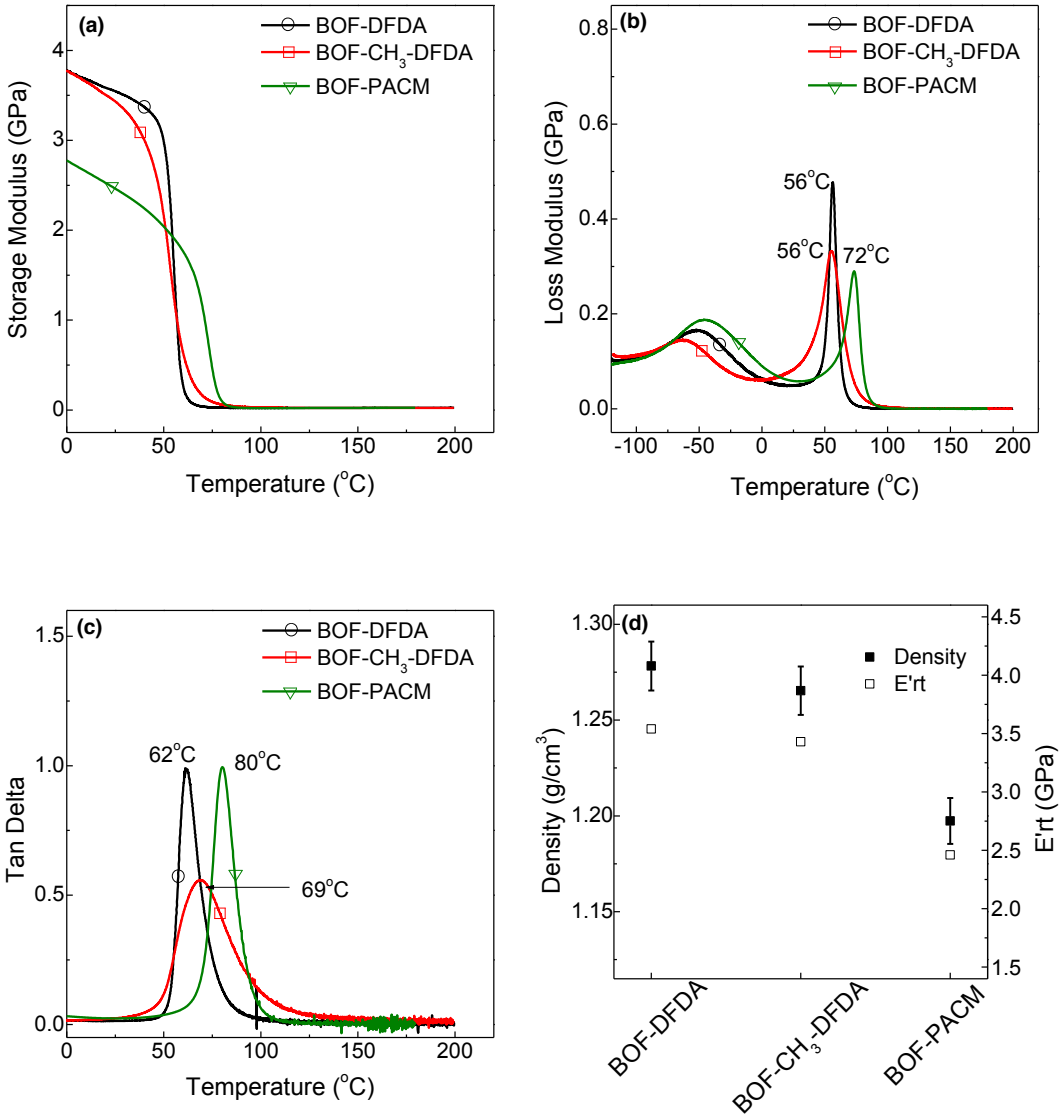

Figure 4.4. DMA thermograms and densities at RT of polymer samples of BOF cured with DFDA, CH_3-DFDA and PACM, respectively.

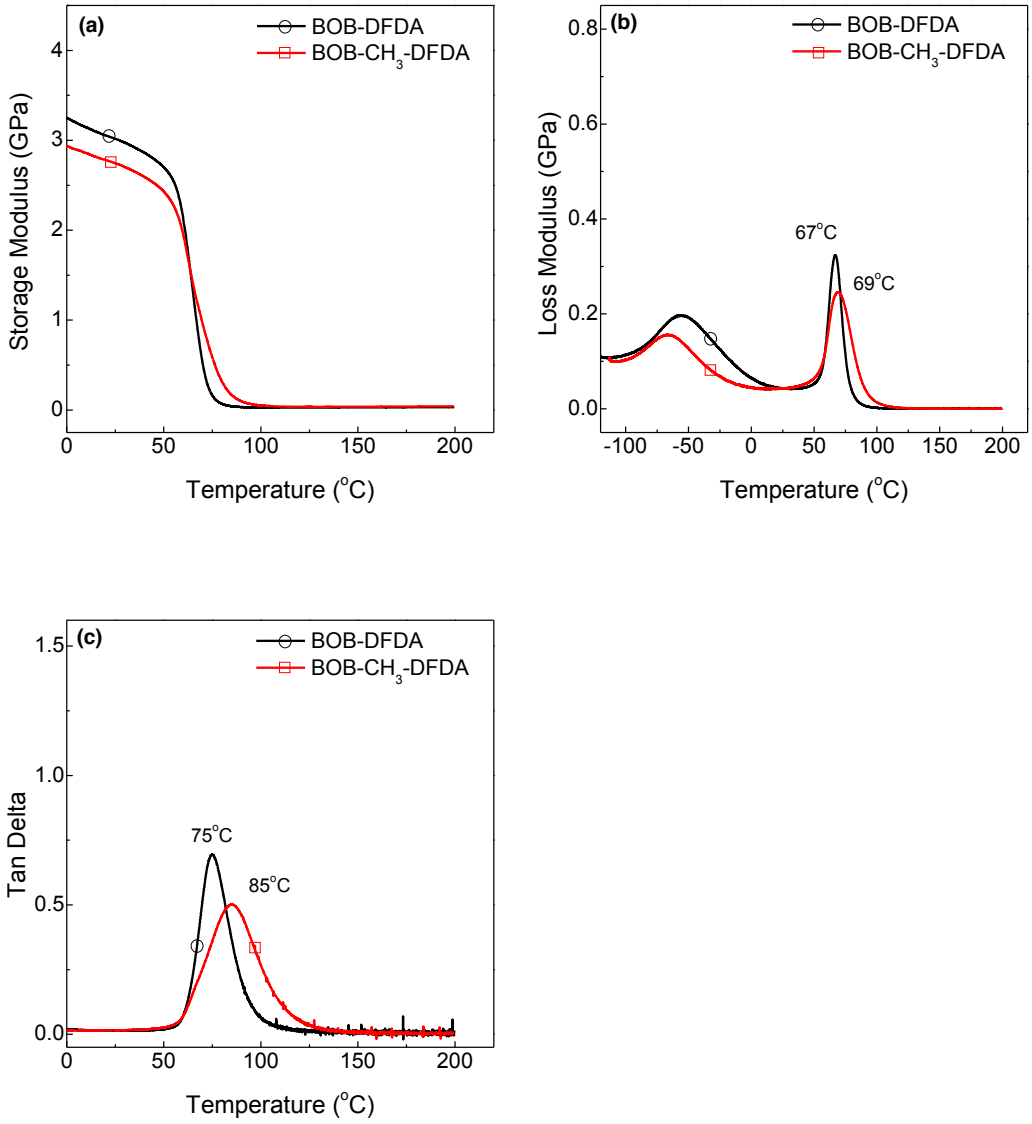

Figure 4.5. DMA thermograms of polymer samples of BOB cured with DFDA and CH_3-DFDA, respectively.

samples also present typical behavior of epoxy-amine thermosets progressing through the glass transition temperature. The transition is similarly much sharper for BOB-DFDA sample. BOB-DFDA and BOB-CH_3-DFDA possess room temperature storage moduli around 3.0 GPa and 2.7 GPa, respectively, which are lower than those of BOF-DFDA and BOF-CH_3-DFDA samples. This phenomenon could be used to confirm the existence of hydrogen bonding associated with the furanyl rings in BOF rather than BOB in cured networks. In Figure 4.5b, BOB-DFDA shows a sharp loss modulus peak at 67 °C, while BOF-CH_3-DFDA displays a broader peak at 69 °C, and these values were taken as their T_gs. It should be noted that, when cured with DFDA and CH_3-DFDA, BOB maintains higher T_gs than BOF by 11 °C and 13 °C. When cured with PACM and EPIKURE W, these T_g differences between BOB and BOF are 29 °C and 44 °C, respectively. This occurrence could be because that the increasing concentration of flexible methylene linkages in the chemical structures of amine hardeners eliminates the T_g enhancement of the phenyl building block relative to the furanyl building block. In Figure 4.5c, BOB-CH_3-DFDA and BOB-DFDA display tan delta peaks at 85 °C and 75 °C, respectively, also indicating the additional methyl group in CH_3-DFDA increases the sample T_g relative to DFDA.

To further evaluate the properties associated with DFDA and CH_3-DFDA, the viability of their use in conjunction with commercial epoxy resins, such as DGEBA, was explored. Polymer samples were prepared by curing DGEBA with DFDA, CH_3-DFDA and PACM. The DMA results are summarized in Figure 4.6. In Figure 4.6a, storage moduli of

DGEBA-DFDA and DGEBA-CH_3-DFDA drop into the rubbery region at a lower temperature compared with DGEBA-PACM, indicating that they possess lower T_gs. In Figure 4.6b, all samples show sharp loss modulus peaks, indicating their cured networks are homogeneous. As shown by loss modulus peak temperatures, DGEBA-DFDA and DGEBA-CH_3-DFDA exhibit T_gs of 121 °C and 128 °C, respectively. A higher T_g for DGEBA-CH_3-DFDA results from the additional methyl group in CH_3-DFDA structure. DGEBA-PACM displays a T_g of 168 °C, ≥40 °C higher than DGEBA-DFDA and DGEBA-CH_3-DFDA, which is due to the additional methylene linkage connecting the ring structure to the amines in DFDA and CH_3-DFDA structures. Figure 4.6c presents a similar trend of T_gs based on tan delta peaks. Meanwhile, DGEBA-CH_3-DFDA consistently displays broader and lower tan delta and loss modulus peaks compared with DGEBA-DFDA. This is also a result of the additional methyl group in CH_3-DFDA.

DSC measurements of these polymer samples were conducted and their second heating scans are plotted in Figure 4.7. Figure 4.7a summarizes the BOF samples cured with DFDA, CH_3-DFDA and PACM. As shown, BOF-DFDA and BOF-PACM exhibit sharp glass transitions, while that of BOF-CH_3-DFDA is less pronounced. This could be due to the additional methyl group in the CH_3-DFDA structure since this methyl group is located on the methenyl group connecting two furanyl rings, which appears to restrict polymer chain mobility during the glass transition stage when experiencing the transition from glassy stage to rubbery stage. This hypothesis is also supported by the broader and lower peaks in DMA loss modulus and tan delta curves of the BOF-CH_3-

DFDA sample in Figures 4.4b and c. T_gs of these cured samples were detected from their second heating scans of DSC traces and were found to be similar to those from DMA loss modulus measurements. Figure 4.7b summarizes DSC second heating scans of those DGEBA samples cured with DFDA, CH_3-DFDA and PACM. DGEBA-DFDA and DGEBA-PACM consistently exhibit sharp glass transitions, while the transition of DGEBA-CH_3-DFDA is relatively smooth due to the additional methyl group in CH_3-DFDA. T_gs of these samples were similarly detected from the DSC traces and they match with those from DMA loss modulus measurements.

It is worth noting that the T_g of DGEBA-PACM (168°C) was 96 °C higher than that of BOF-PACM (72 °C), which primarily resulted from the additional methylene groups connecting with furanyl rings in BOF epoxy.[11] However, T_gs of DGEBA-DFDA and DGEBA-CH_3-DFDA were only ~68 °C higher than those of BOF-DFDA and BOF-CH_3-DFDA, meaning this T_g difference was significantly reduced when DFDA and CH_3-DFDA were used. This further supports our hypothesis that reducing the content of methylene linkages increases T_g. BOF epoxy possesses two methylene linkage groups and one furanyl group, giving a ratio of two methylene groups per furanyl group, but DFDA and CH_3-DFDA possess a ratio of three methylene groups per two furanyl groups. So, it appears that each methylene spacer per ring reduces the T_g by 32-34 °C.

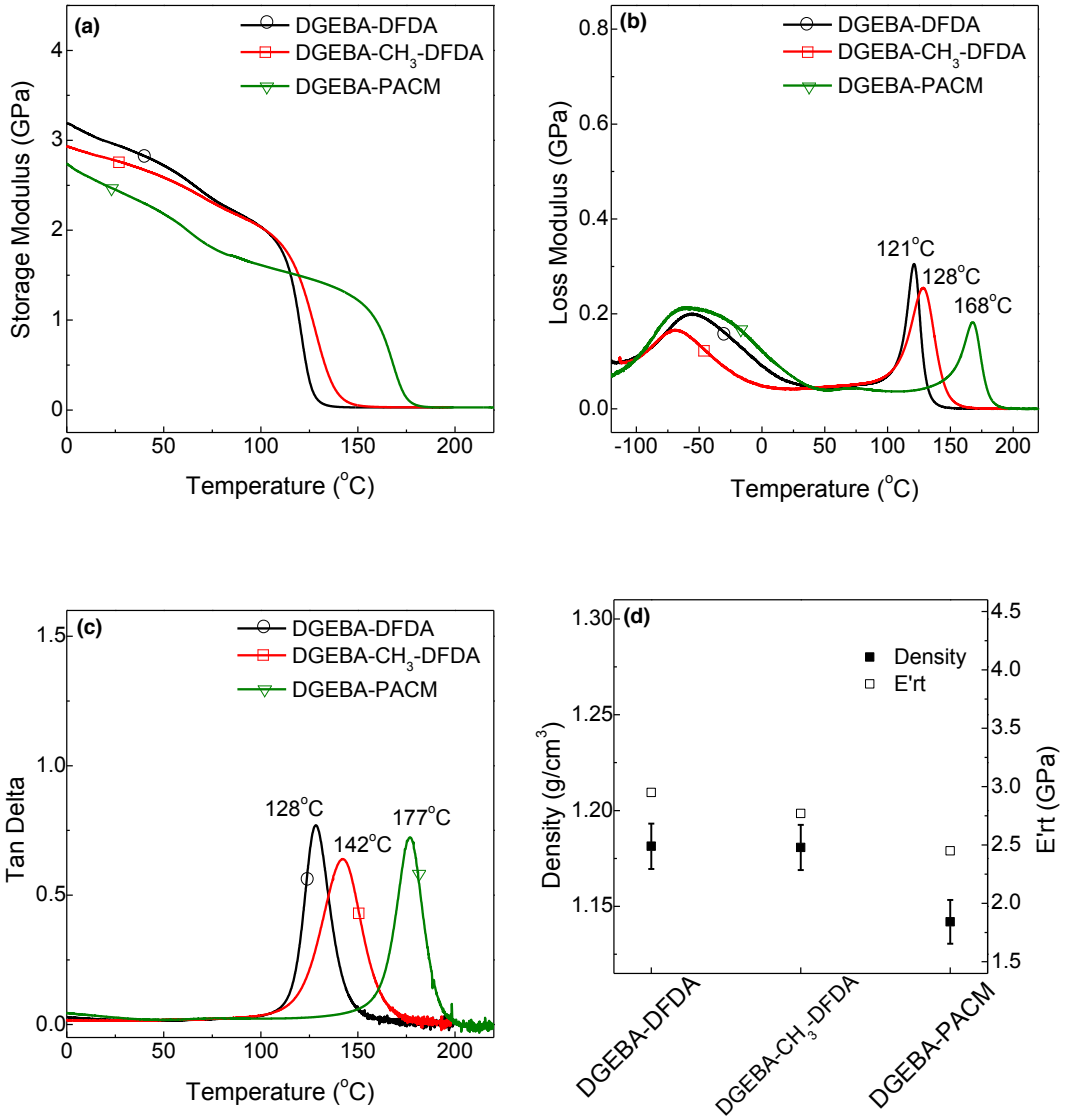

Figure 4.6. DMA thermograms and densities at RT of polymer samples of DGEBA cured with DFDA, CH_3-DFDA and PACM, respectively.

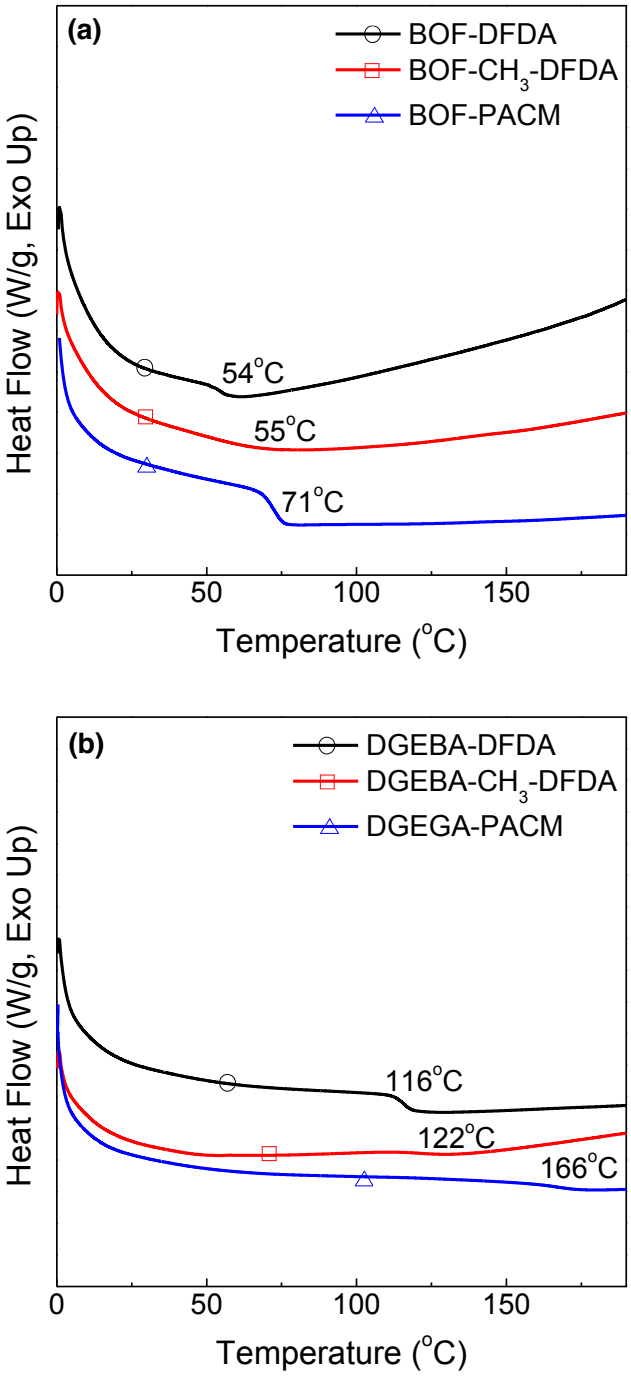

Figure 4.7. DSC traces of polymer samples of DFDA, CH_3-DFDA and PACM with BOF and DGEBA, respectively.

4.3.4. Thermal stability properties

TGA was used to investigate thermal properties of cured samples of DFDA, CH_3-DFDA and PACM with BOF and DGEBA in the argon atmosphere. TGA thermograms of cured samples are shown in Figures 4.8a and b, respectively. As shown in Figure 4.8a, the thermal decomposition temperatures corresponding to 5 wt.% loss are 272 °C for BOF-DFDA and BOF-CH_3-DFDA, and 303 °C for BOF-PACM. However, BOF-DFDA and BOF-CH_3-DFDA exhibit significantly lower degradation rates than that of BOF-PACM. For example, char yields at 500 °C are 51 wt.% and 46 wt.% for BOF-DFDA and BOF-CH_3-DFDA, respectively, but 7 wt.% for BOF-PACM. This indicates furanyl structures in amine hardeners transform to more stable forms during degradation compared with cycloaliphatic groups in PACM. Remarkably, at 750 °C, while BOF-PACM shows 6 wt.% char yield, an impressive 40 wt.% and 39 wt.% char yield was observed for BOF-DFDA and BOF-CH_3-DFDA samples, respectively. In Figure 4.8b, the thermal decomposition temperatures corresponding to 5 wt.% loss are 301 °C and 315 °C for DGEBA-DFDA and DGEBA-CH_3-DFDA, respectively, and 336 °C for DGEBA-PACM, which suggests the promising chemical stability of samples prepared with furanyl amine hardeners. Degradation rates of DGEBA-DFDA and DGEBA-CH_3-DFDA are consistently lower than that of DGEBA-PACM. BOF samples exhibit slightly lower decomposition temperatures but much lower degradation rates compared with DGEBA systems. This indicates that although furanyl monomers begin to decompose at lower temperatures, the furanyl structures are transformed to more stable forms during degradation relative

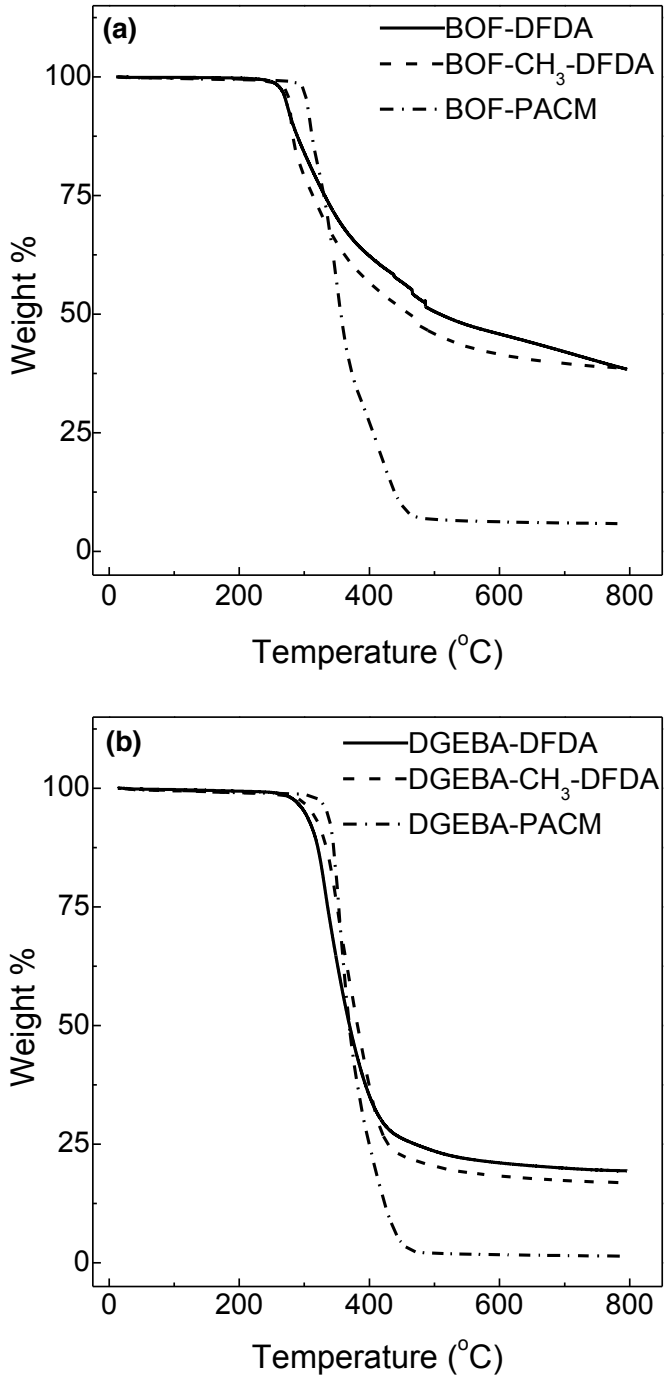

Figure 4.8. TGA thermograms of polymer samples of DFDA, CH_3-DFDA and PACM with BOF and DGEBA, respectively, in the argon environment.

to phenyl structures. The lower degradation temperatures in furanyl systems could be due to less chemically stable aliphatic bonds in the cured networks. High char yields associated with the furanyl monomers could prove advantageous for applications regarding high-temperature durability.

4.4. Conclusions

Fully furanyl based thermosetting polymers were prepared and their thermal and mechanical properties were investigated using different techniques. These biobased thermosets present high performance with promising T_gs above 50 °C, high room temperature storage moduli of 3.5 GPa and good thermal stability up to 272 °C (5 wt.% loss) in argon environment. Used as curing agents for DGEBA, DFDA and CH_3-DFDA show excellent performance with T_gs well above 120 °C. Therefore, renewable furanyl based thermosetting materials exhibit the potential to be utilized as alternatives for conventional thermosetting epoxy-amine resins, especially as coating and adhesive applications. More interestingly, this work enables quantification of the effect of methylene spacers between the aromatic ring and amine on T_g. The type E bis-furanyl diamine results in higher T_gs but broader glass transitions relative to the type F bis-furanyl diamine. In addition, furanyl based polymers have higher densities, resulting in higher glassy moduli relative to phenyl and cycloaliphatic epoxy-amine systems.

Chapter 5. Synthesis and characterization of thermosetting furanyl based vinyl ester resin systems

5.1. Introduction

In addition to thermosetting epoxy and amine materials, preparing vinyl ester (VE) resins using renewable resources as alternatives of petroleum feedstocks has also obtained significant attentions. The furanyl building block could also be a promising candidate for synthesizing thermosetting VE resins and a direct property comparison with the phenyl analogous VE resin is desirable. In this chapter, analogous furanyl and phenyl di-vinyl ester resin were synthesized through methacrylation of BOF and BOB epoxy monomers. With styrene (ST) as a reactive diluent at varying weight fractions (10, 20 and 30 wt%), VE polymer samples were thermally cured via free-radical polymerization. Thermo-mechanical properties of prepared polymer samples were measured using DMA and it was found that furanyl based VE samples possessed T_gs between 117 °C to 134 °C, which were lower than those of phenyl based VE samples at 119 °C to 146 °C. Cure kinetics studies of furanyl and phenyl VE resins were also conducted using M-IR, in which the furanyl building block showed different influences to the cure reactions relative to its phenyl analogue.

5.2. Experimental

5.2.1. Materials

Chemicals, including styrene (99%), methacrylate acid (99%), hydroquinone (99%), cobalt napthenate (CoNap) which is used as a catalyst to promote RT cure, were purchased from Sigma-Aldrich, USA; 1,4-bis(glycidyloxy)-benzene (DGEPP, 97+%) was purchased from Alfa Aesar, USA; AMC-2, a mixture of 50% trivalent organic chromium complexes and 50% phthalate esters, was purchased from Aerojet Chemicals, USA. Trigonox 239A, which contains 45% cumeme hydroperoxide, was purchased from Akzo Nobel Chemicals, USA. All chemicals were used as received. BOF and BOB were prepared in laboratory.

5.2.2. Preparation of VE resins

BOF VE, BOB VE and DGEPP VE resins were prepared through the methacrylation reaction of BOF, BOB and DGEPP epoxy monomers, respectively. For example, 12.0 g of BOF (50.1 mmol) and 7.5 g of methacrylic acid (110.2 mmol) were charged into a 20 mL vial containing a magnetic stirrer. 1.0 wt% of AMC-2 and 0.01 wt% of hydroquinone (based on the total weight of reactants) were added. The vial was sealed and reacted at 70 °C for 1 hour followed by 90 °C for another 3 hours. The color of the mixture changed

from light green to dark green and the reaction completion was determined using both GPC and ^{1}H-NMR with an epoxy conversion of 99+%.

5.2.3. Characterization of VE resins

Directly used without purification process, prepared VE resins were characterized using FTIR and ^{1}H-NMR. Functional groups, such as furanyl and phenyl rings, ester and carbon-carbon double bond, were identified using a Thermo Nicolet Nexus 870 FTIR and the spectra were recorded in the 650 - 4000 cm^{-1} range at RT. ^{1}H-NMR was used to characterize their chemical structures on a 500 Hz VARIAN VXR-Unity instrument.

5.2.4. Cure kinetics of VE resins

Cure kinetics of these VE resins was conducted using a Thermo Nicolet Nexus 870 FTIR spectrometer in the transmission mode. ST was blended with BOF VE, BOB VE and DGEPP VE resins at 0, 10, 20 and 30 wt%, respectively. 0.375 wt% CoNap and 1.5 wt% trigonox 239A (based on the total weight of mixtures) were added into VE resins. A small amount of well mixed resin mixtures was compressed between two NaCl transparent crystal plates (International Crystal Labs) with a 25 mm diameter. A Teflon spacer with a 0.025 mm thickness was used between these two plates to keep a constant sample thickness and to prevent the evaporation of styrene. The sandwich assembly was placed into a temperature controlled aluminum sample holder which allowed for

control of temperature within ± 0.5 °C of the set temperature point. 30 °C was used as the set point. A background scan was performed before each experiment using empty crystal plates. The conversion, α, was calculated by measuring the peak height of reactive groups relative to an internal standard which remained the same during the reaction.

5.2.5. Preparation of VE polymer samples

ST was blended with BOF VE, BOB VE and DGEPP VE resins at 0, 10, 20 and 30 wt%, respectively. 0.375 wt% CoNap and 1.5 wt% trigonox 239A (based on the total weight of mixtures) were added into VE resins. After mixing, the resin mixtures were poured into an aluminum mold with uniform dimensions of 10 × 40 × 2.0 mm and sealed to prevent evaporation of ST. Samples were allowed to cure at RT for 12 hours and then post cure at 200 °C for additional 2 hours, followed by being sanded to uniform dimensions of 10 × 39 × 1.9 mm for DMA measurements.

5.2.6. Polymer properties

Thermo-mechanical properties, such as T_g and E', of BOF VE, BOB VE and DGEPP VE polymer samples with different weight fractions of ST were measured using DMA on a TA Instruments 2980 in single cantilever geometry with a frequency of 1 Hz and an

amplitude of 15 μm. Temperature ramp rate was at 2 °C/min from – 160 °C to 200 °C. T_g was assigned as the temperature corresponding to the peak of loss modulus curve.

5.3. Results and Discussion

5.3.1. Characterization of VE resins

As shown in Figure 5.1, M-IR spectra of BOF VE indicated the peaks corresponding to epoxy groups, such as 3051 cm^{-1} (stretching of C–H in oxirane ring), 926 cm^{-1} (oxirane ring breathing), 860 and 1254 cm^{-1} (C–O–C), were all no long visible, meaning epoxy groups were fully reacted. In addition, furanyl rings, reflected by the peaks at 772 cm^{-1} (mono-substituted furanyl ring), 1081 cm^{-1} (furanyl ring breathing) and 1554 cm^{-1} (C=C in furanyl ring),[8] were still present in BOF VE. The broad absorption at 3200 - 3500 cm^{-1} associated with formed hydroxyl groups and the peak at 943 cm^{-1} corresponding to the attached methacrylate groups were also present in BOF VE.[82a] Therefore, it was clearly shown that epoxy groups of BOF reacted with methacrylic acid to form BOF VE.

^{1}H-NMR was used to confirm the chemical structure of BOF VE. As shown in Figure 5.2, peaks at δ = 6.3 ppm was attributed to the protons in furanyl ring (designated as protons 1), which can be used to indicate the furanyl ring structure. Peaks at δ = 4.5 ppm (-OCH_2-furanyl ring, 2H) corresponded to protons 2 connecting the glycidyl ether moiety to the

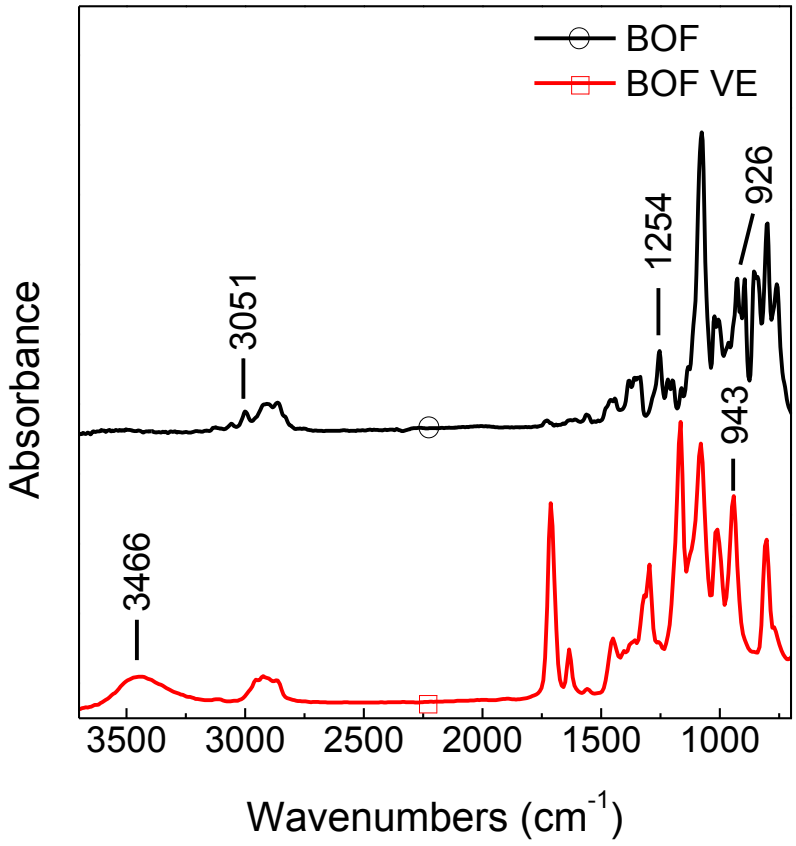

Figure 5.1 The M-IR spectra of prepared BOF VE monomer (red) and BOF monomer (black).

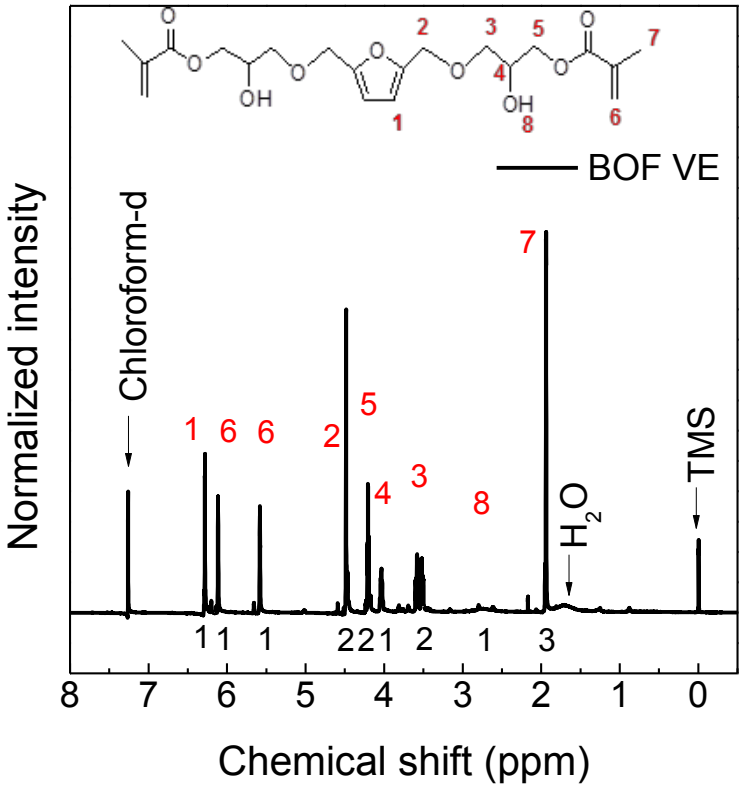

Figure 5.2. The ^{1}H-NMR spectrum of prepared BOF VE.

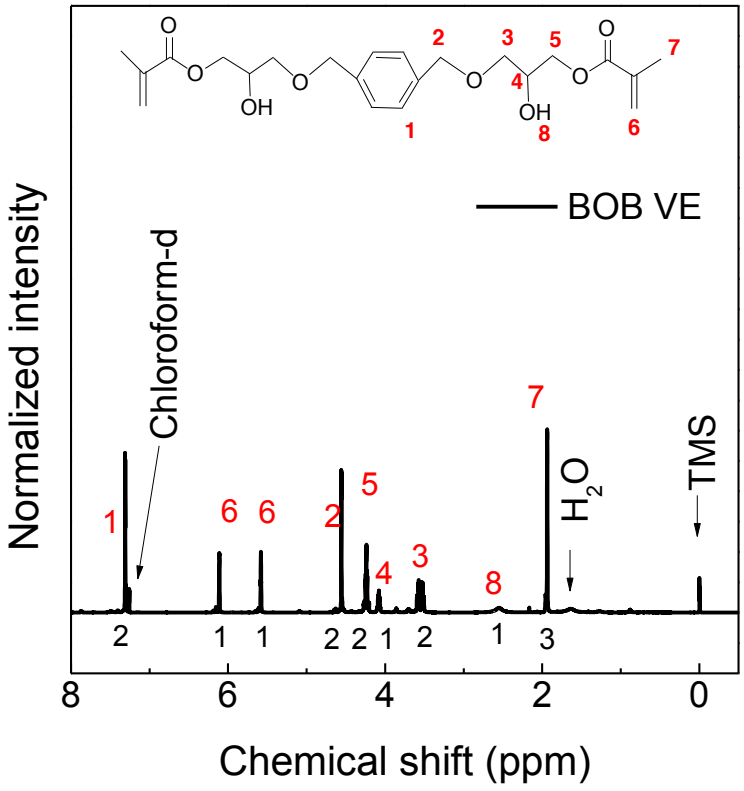

Figure 5.3. The ^{1}H-NMR spectrum of prepared BOB VE.

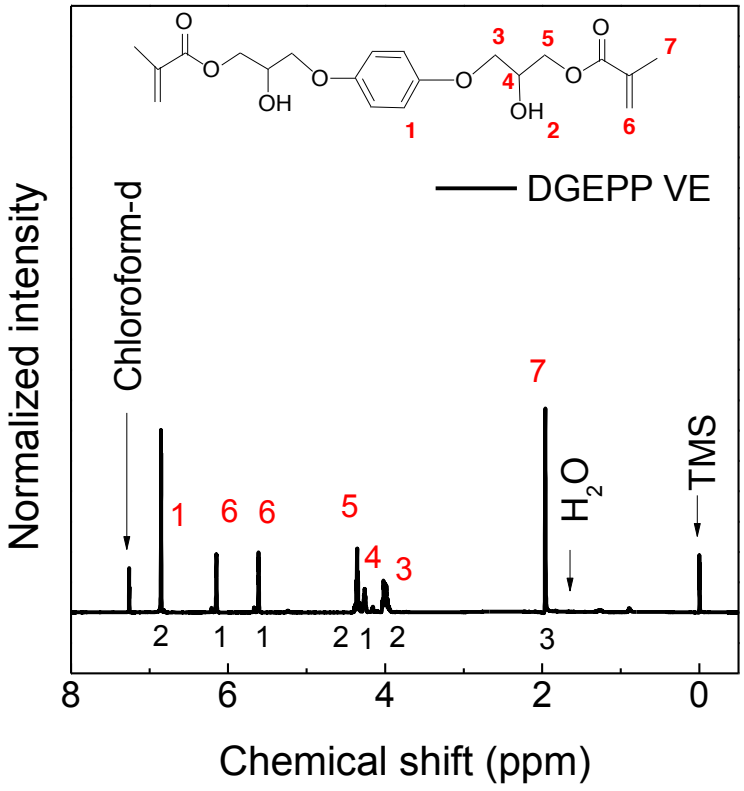

Figure 5.4. The ^{1}H-NMR spectrum of prepared DGEPP VE.

furanyl ring. Peaks at δ = 3.5 - 3.6 ppm indicated protons 3 of methylidyne. Peaks at δ = 4.05 ppm reflected proton 4 connecting the hydroxyl group. Peaks at δ = 4.2 ppm corresponded to the protons of methylene on position 5. Peaks at δ = 5.6 and 6.1 ppm corresponded to the protons 6 on the carbon atom of side C=C bond. Peaks at δ = 1.95 ppm reflected the protons 7 on the ending $–CH_3$ group. Integrated values of the area under these peaks matched with the ratio of proton numbers at different positions. Therefore, it was concluded that BOF VE was prepared as expected.

BOB VE and DGEPP VE were similarly prepared and characterized. Figure 5.3 and Figures 5.4 plot the ^{1}H-NMR spectra of prepared BOB VE and DGEPP VE monomers, respectively, with the peaks assigned and labeled according to their chemical structures. Table 5.1 summarizes the yield, purity, viscosity and color of prepared BOF VE, BOB VE and DGEPP VE monomers.

5.3.2. Polymer properties

DMA thermograms of cured polymer samples of BOF VE, BOB VE and DGEPP VE with 10, 20 and 30 wt% ST are plotted in Figure 5.5, Figure 5.6 and Figure 5.7, respectively. As shown in Figure 5.5a, BOF VE sample without ST possessed E'_{RT} at 3.95 GPa, and T_g around 134 °C from a broad loss modulus transition. This broad loss modulus curve was typical because of the unreacted double bonds trapped in VE networks in the absence of reactive diluents as observed in other VE systems.[66] BOF VE sample with 10 wt% ST

Table 5.1. Yield, purity, viscosity and color of prepared BOF VE, BOB VE and DGEPP VE monomers

Monomer name	Yield (%)	Purity (%)	Viscosity at 30 °C (Pa.s)	Color
BOF VE	100	>99	1.10	Light green
BOB VE	100	>99	1.10	Light green
DGEPP VE	100	>99	Solid	Light green

showed E'_{RT} at 3.52 GPa, and T_g around 118 °C from a narrower loss modulus curve. Generally, when ST was blended into BOF VE, cured polymer samples showed decreased E'_{RT} and lower T_g compared with BOF VE without ST. The reason for this behavior is that polystyrene possesses T_g around 100 °C,[115] lower than that of BOF VE. The addition of ST facilitated and improved the cure conversion of BOF VE which also resulted in the narrower loss modulus curves for BOF VE samples with ST. In Figure 5.6a, BOB VE without ST showed E'_{RT} at 3.77 GPa and T_g around 119 °C from a very broad loss modulus transition. The broad loss modulus curve was also due to the incomplete cure of BOB VE resin without blending reactive diluents. BOB VE sample with 10 wt% ST showed E'_{RT} at 3. 25 GPa, and a T_g around 146 °C from a narrower loss modulus transition. Clearly, the conversion of BOB VE was enhanced by adding ST since sample T_g was increased by 27 °C rather than decreasing and the loss modulus curve became narrower. Phenyl building block, relative to furanyl building block, should endow VE resins with higher T_gs based on the comparison of Figure 5.5b and 5.6b. BOB VE sample with 20 wt% ST presented E'_{RT} at 3.19 GPa, and T_g around 123 °C from an even narrower loss modulus transition, confirming the addition of ST enhanced the conversion of BOB VE and also decreased E'_{RT} and T_g of cured polymer samples. In Figure 5.7a, DGEPP VE without ST possessed E'_{RT} at 3.75 GPa, and a very broad loss modulus transition from 80 °C to 160 °C. Also due to the incomplete cure of VE resins with the absence of reactive diluents, this transition was broader than those of BOF VE and BOB VE because of the chemical structure differences, i.e. the absence of methylene groups in DGEPP VE as shown in Chapter 2, which made DGEPP VE less flexible.

DGEPP VE sample with 10 wt% showed E'_{RT} at 3.59 GPa and T_g around 146 °C from a less broader loss modulus curve. DGEPP VE sample with 20 wt% showed E'_{RT} at 3.35 GPa and T_g around 157 °C from an even narrower loss modulus curve. These results clearly showed that adding ST also improved the conversion of DGEPP VE and, due to its less flexibility, a higher concentration of ST was needed to do so in DGEPP VE system. Since polystyrene possesses a T_g of 100 °C, with weight fractions higher than 30 wt% of ST, a T_g reduction of cured DGEPP VE samples is believe to occur. In addition, DGEPP VE systems showed higher T_gs compared with BOF VE and BOB VE systems because of the lack of two methylene groups in DGEPP VE structure.

T_g, E'_{RT}, room temperature density, VE conversion and ST conversion of BOF VE, BOB VE and DGEPP VE post-cured polymer samples are summarized in Table 5.2. Density values of these samples were measured using a calibrated density gradient column at RT. As shown, BOF VE samples are denser than BOB VE samples as well as DGEPP samples, suggesting furanyl building block is denser relative to its phenyl analogue. DGEPP VE samples are also denser than BOB VE samples due to the lack of methylene linkages in the chemical structure. Density values of all BOF VE, BOB VE and DGEPP VE samples decrease with the increasing ST content due to the lower RT density of polystyrene which is 1.040 g/cm^3. The trend of density values of these VE samples matches with the trend of their E'_{RT} values. Although styrene conversion is more than 99% in all cases, the ultimate conversions of VE double bonds in BOF VE systems are systematically higher

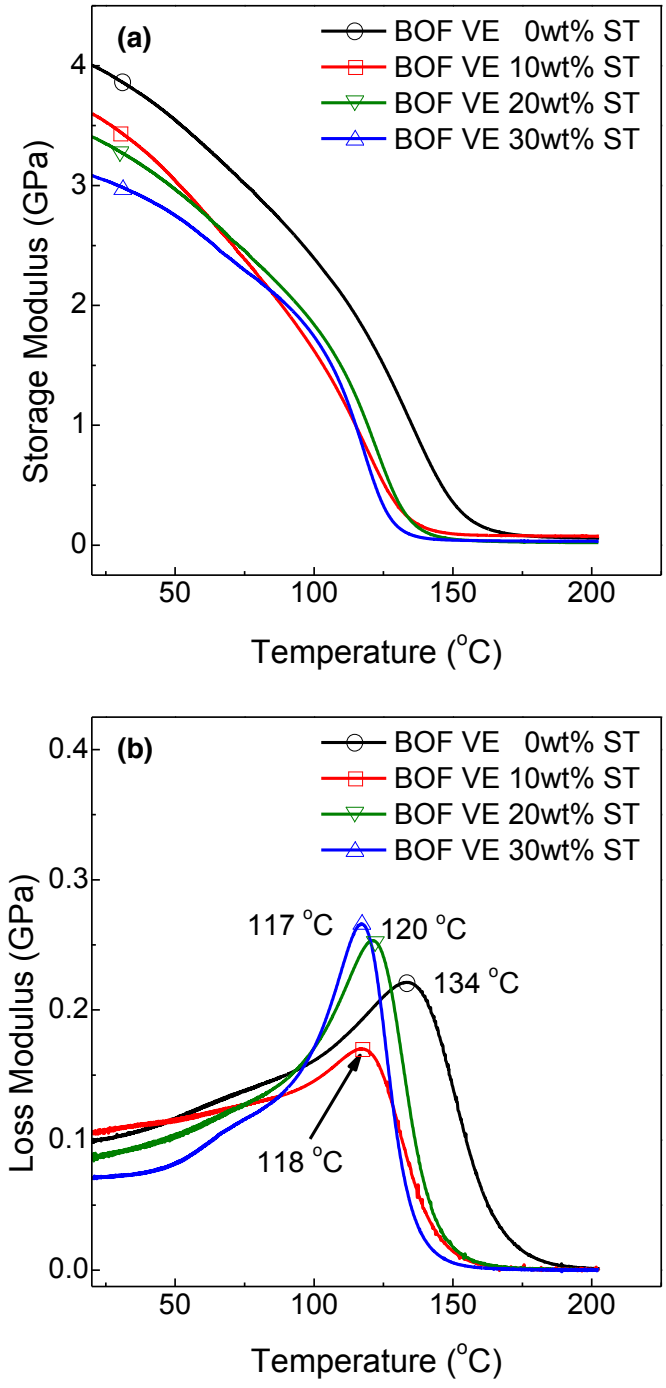

Figure 5.5. DMA thermograms of BOF VE polymer samples blended with styrene (ST) at 0, 10, 20 and 30 wt%.

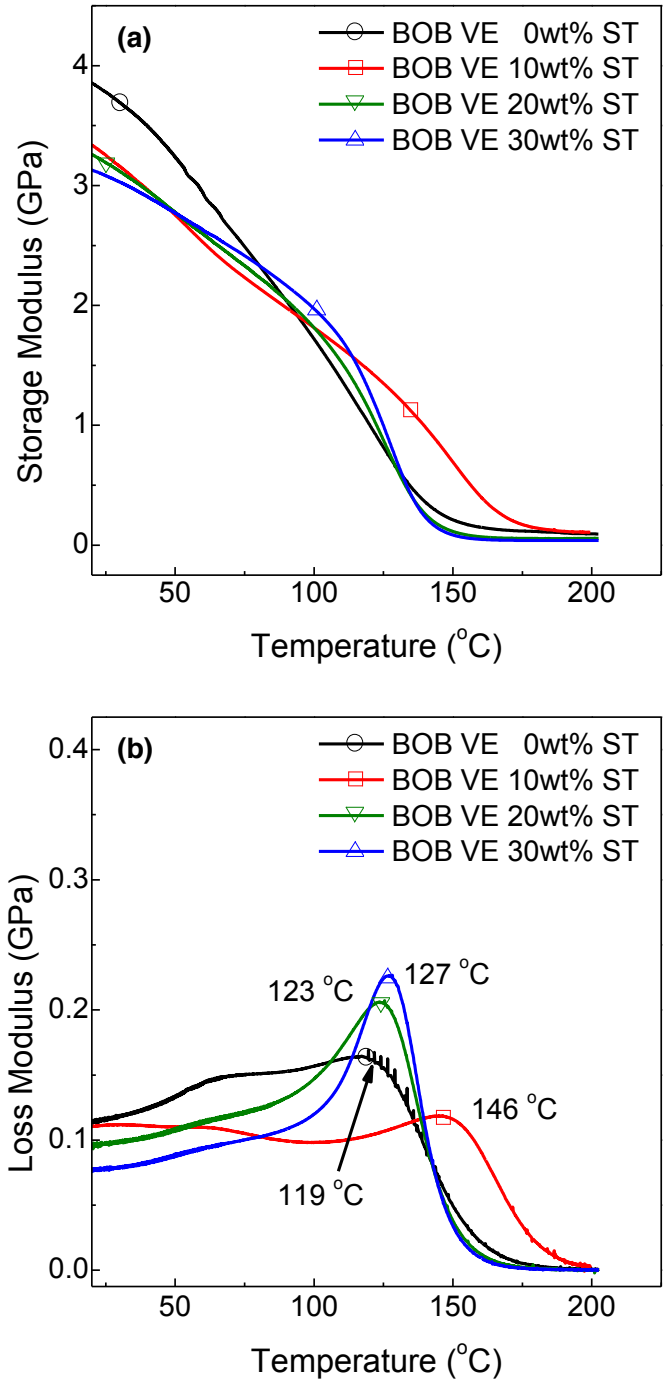

Figure 5.6. DMA thermograms of BOB VE polymer samples blended with styrene (ST) at 0, 10, 20 and 30 wt%.

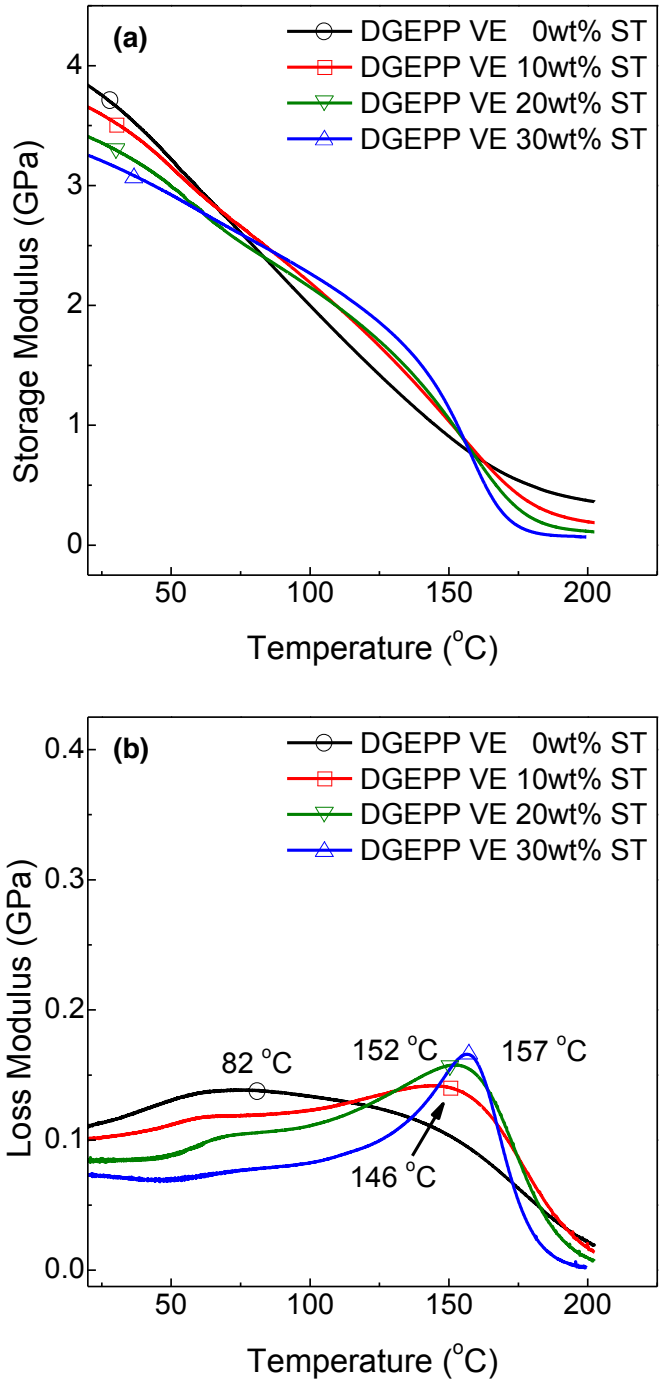

Figure 5.7. DMA thermograms of DGEPP VE polymer samples blended with styrene (ST) at 0, 10, 20 and 30 wt%.

relative to BOB VE systems with different ST weight fractions, indicating the furanyl building block can improve VE double bond conversion compared with its phenyl analogue. The ultimate conversion of VE double bonds in DGEPP VE systems is lower than BOB VE systems. The addition of ST shows less improvement on the ultimate conversions of VE double bonds in BOF VE system compared with BOB VE and DGEPP VE systems. This observation matches with the DMA T_g trends of these three VE systems that T_gs of BOF VE samples decrease with increasing ST contents from 0 to 30 wt%, while T_gs of both BOB VE and DGEPP VE samples initially increase when adding 10 wt% of ST but decrease when more ST is added. Generally, increasing ST content improves the ultimate conversion of VE double bonds while it has little effect on the ultimate conversion of ST double bonds. This is because styrene acts as a reactive diluent in thermosetting VE resins and facilitates the mobility of VE molecules to find available reactive site to crosslink after gelation occurs.[82a]

5.3.3. Cure kinetics of VE resins

A cure kinetics investigation of BOF VE and BOB VE with different weight fractions of ST was conducted at 30 °C. For VE-ST systems, the depletion in carbon-carbon double bonds of both VE and ST monomers indicated the cure reaction, i.e. polymerization. In M-IR spectra, the absorbance at 946 cm^{-1} and 948 cm^{-1} corresponded to the out-of-plane bending of =C-H bonds in vinyl groups of BOB VE and BOF VE, respectively. The absorbance at 914 cm^{-1} corresponded to the =C-H bonds in vinyl groups of ST.[116] These

Table 5.2. T_g, E'_{RT}, room temperature density, VE conversion and ST conversion of BOF VE, BOB VE and DGEPP VE polymer samples

Sample name	T_g (°C)	E'_{RT} (GPa)	Density @ RT (g/cm³)	VE conversion	ST conversion
BOF VE 0wt% ST	134	3.95	1.304±0.001	0.89	-
BOF VE 10wt% ST	118	3.52	1.274±0.001	0.89	0.99
BOF VE 20wt% ST	120	3.35	1.255±0.001	0.92	0.99
BOF VE 30wt% ST	117	3.04	1.222±0.001	0.91	0.99
BOB VE 0wt% ST	119	3.77	1.279±0.001	0.71	-
BOB VE 10wt% ST	146	3.25	1.251±0.001	0.77	0.99
BOB VE 20wt% ST	123	3.19	1.240±0.001	0.81	0.99
BOB VE 30wt% ST	127	3.08	1.206±0.001	0.81	0.99
DGEPP VE 0wt% ST	~120	3.75	1.298±0.001	0.54	-
DGEPP VE 10wt% ST	146	3.59	1.270±0.001	0.69	0.99
DGEPP VE 20wt% ST	152	3.35	1.243±0.001	0.74	0.99
DGEPP VE 30wt% ST	157	3.20	1.219±0.001	0.73	0.99

peaks were monitored independently during cure for reaction kinetics. Internal reference peaks were also used to eliminate the effects associated with component evaporations and dimensional changes. For BOB VE-ST systems, the peak at 815 cm^{-1} corresponding to the aromatic phenyl =C-H bonds in BOB VE and the peak at 703 cm^{-1} in ST were selected. For BOF VE-ST systems, the peak at 802 cm^{-1} corresponding to the aromatic furanyl =C-H bonds in BOF VE and the peak at 703 cm^{-1} in ST were used. Equations 5.1, 5.2 and 5.3 were used to normalize and calculate fractional conversions of BOB VE, BOF VE and ST from the M-IR experimental data, respectively.[4, 66] In these equations, α was the fractional conversion of carbon-carbon double bonds associated with each monomer at time *t*, and ABS was the peak absorption intensity at time *t*.

$$\alpha_{BOB\ VE}(t) = 1 - \left(\frac{ABS(t)_{946\ cm^{-1}}}{ABS(t=0)_{946\ cm^{-1}}}\right) \Big/ \left(\frac{ABS(t)_{815\ cm^{-1}}}{ABS(t=0)_{815\ cm^{-1}}}\right) \tag{5.1}$$

$$\alpha_{BOF\ VE}(t) = 1 - \left(\frac{ABS(t)_{948\ cm^{-1}}}{ABS(t=0)_{948\ cm^{-1}}}\right) \Big/ \left(\frac{ABS(t)_{802\ cm^{-1}}}{ABS(t=0)_{802\ cm^{-1}}}\right) \tag{5.2}$$

$$\alpha_{ST}(t) = 1 - \left(\frac{ABS(t)_{914\ cm^{-1}}}{ABS(t=0)_{914\ cm^{-1}}}\right) \Big/ \left(\frac{ABS(t)_{703\ cm^{-1}}}{ABS(t=0)_{703\ cm^{-1}}}\right) \tag{5.3}$$

Figure 5.8 shows the fractional conversions of carbon-carbon double bonds for BOF VE and ST monomers as a function of time in BOF VE-ST systems at 30 °C. The effect of ST weight fraction on BOF VE conversion is shown. As the ST weight fraction increased, fractional conversions of both VE and ST monomers were improved. Similar results were also observed in the BOB VE-ST systems as shown in Figure 5.9.

As introduced in Chapter 1, empirical models can be used to fit the cure behavior of thermosetting VE systems throughout polymerization reaction. Equations 1.14 and 1.15 were employed in this works to fit the fractional conversions of VE and ST monomers in the BOF VE-ST and BOB VE-ST systems and to obtain parameters, including reaction rate constant, k, and the reaction order, m. As a representative of all cases, Figure 5.10 shows the model fitting of experimental fractional conversions of BOF VE and ST monomers in BOF VE 30 wt% ST system at 30 °C using Equation 1.15. Model fitting of the other cases are given in Appendix B. These curves indicate that the model can fit the experimental data well. This was so for all other cases. Table 5.3 summarizes the obtained maximum fraction conversion, reaction rate constant and reaction order results for all investigated BOF VE-ST and BOB VE-ST systems at 30 °C. As shown, the reaction order, m, was shown to be between 0.54 to 0.87, with an average value of 0.74 for both VE and ST monomers for all resins compositions at 30 °C. Brill et al.[82a] and Lam et al.[117] reported the reaction order values of VE resins to be around 0.85 for isothermal cure at temperature ranging between 90 °C to 120 °C. This indicated that the employed empirical autocatalytic kinetic model was suitable to fit the BOF VE-ST and BOB VE-ST

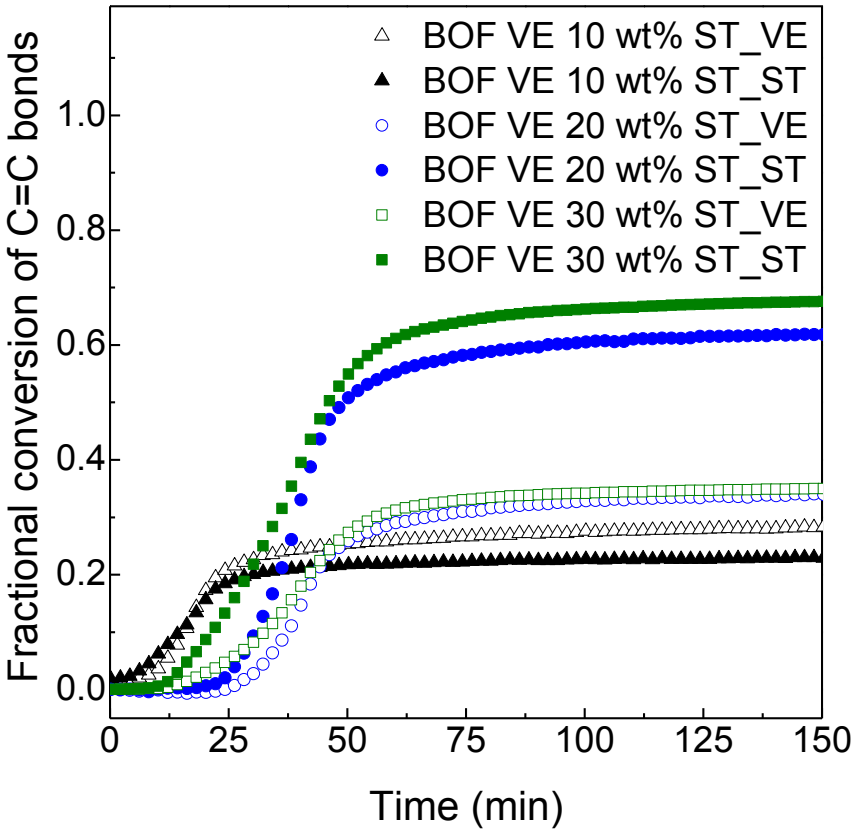

Figure 5.8. Fractional conversions of carbon-carbon double bonds for BOF VE and ST monomers as a function of time in BOF VE-ST systems at 30 °C.

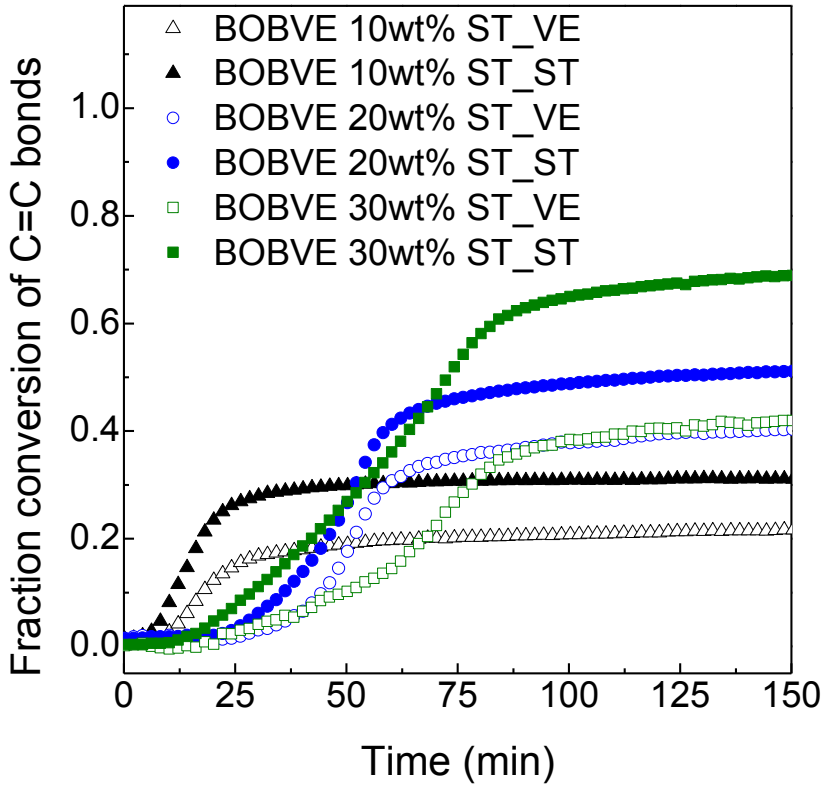

Figure 5.9. Fractional conversions of carbon-carbon double bonds for BOB VE and ST monomers as a function of time in BOB VE-ST systems at 30 °C.

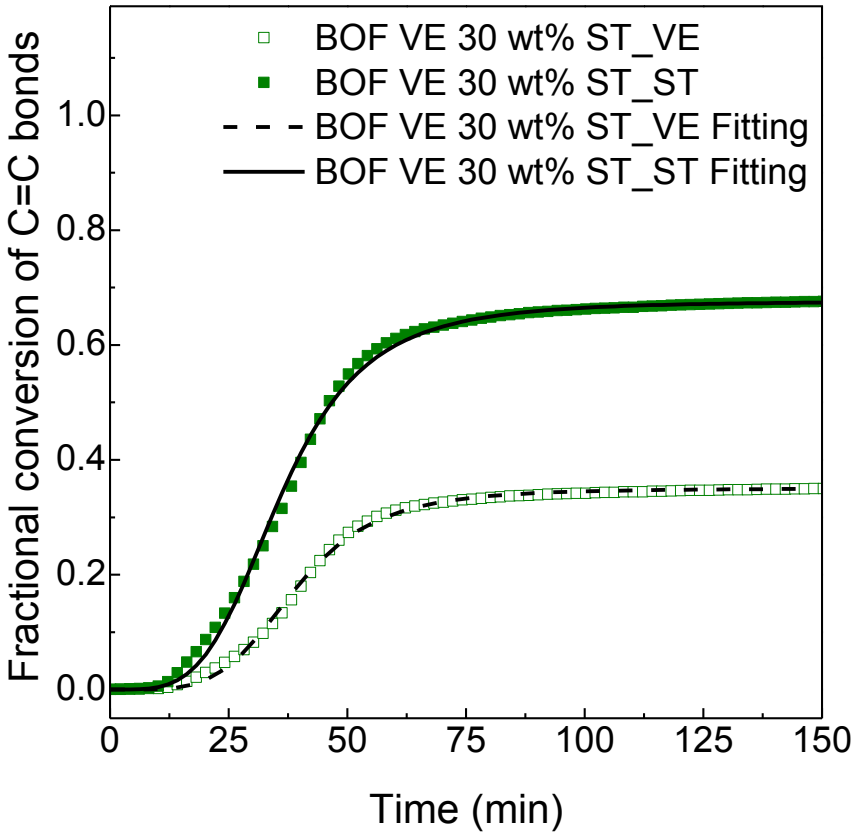

Figure 5.10. Model fitting of experimental fractional conversions of BOF VE and ST monomers in BOF VE 30 wt% ST system at 30 °C using Equation 1.15.

cure data and the obtained reaction rate constant values were reliable. In BOB VE-ST systems, when 10 wt% ST was added into BOB VE, vinyl groups in ST monomers showed a comparable reaction rate constant to that of BOB VE monomer. When more ST was added, the reaction rate constants of both BOB VE and ST monomers significantly decreased with ST weight fractions, and ST monomers started reacting more slowly compared with BOB VE monomers. This observation of lower reaction rates for ST monomers matched with the results reported in literature.[82a, 82c, 118] Similar trends were also found in the BOF VE-ST systems. It is expected that the network structures formed during the initial stage of cure could be affected by different reaction rates of vinyl groups of VE and ST monomers. In addition, the reaction rate constants of both BOF VE and ST monomers in BOF VE-ST systems were found to be consistently higher compared with those in BOB VE-ST systems, indicating that the furanyl building block, relative to its phenyl analogue, increases the reaction rates of both VE and ST monomers. It is also observed in Table 5.3 that the ultimate fractional conversions of both VE and ST double bonds in the BOF VE and BOB VE systems increase with increasing ST content at 30 °C. The increased VE double bond conversion is because the addition of ST facilitates the mobility of VE resins to crosslink with reactive sites and a higher fraction of VE is needed to react and incorporate into cured networks to reach a 30 °C vitrification temperature at higher ST concentrations. The increased ST double bond conversion is also due to the improved mobility of reactive species that more ST can be incorporated in cured networks at higher ST concentrations.[82c]

Table 5.3. Maximum fractional conversion and the parameters of autocatalytic kinetics model for the isothermal FTIR cure experiments of BOF VE-ST and BOB VE-ST systems at 30 °C

Systems	10 wt% ST			20 wt% ST			30 wt% ST		
	α_u	k	m	α_u	k	m	α_u	k	m
BOB VE-ST_VE	0.24	0.72	0.54	0.45	0.28	0.85	0.47	0.15	0.81
BOB VE-ST_ST	0.32	0.74	0.56	0.56	0.21	0.83	0.75	0.09	0.77
BOF VE-ST_VE	0.31	0.94	0.87	0.36	0.36	0.61	0.37	0.33	0.78
BOF VE-ST_ST	0.24	0.92	0.83	0.64	0.25	0.62	0.71	0.16	0.75

As discussed previously, VE resins cure via free radical bulk copolymerization of VE and ST monomers. The copolymerization behavior of these two co-monomers can significantly affect the ultimate network structures and their thermo-mechanical properties. For a VE-ST system, the propagation equations are listed as Equations 5.4 to 5.7, where the superscripts represent active species and k_{ij} indicates reaction rate constants. A main assumption is the reactivity of a growing chain solely depends on the terminal unit reactivity. Equation 5.8 was the employed copolymer composition equation, where $[M_1]$ and $[M_2]$ are the initial molar concentrations of carbon-carbon double bonds of ST and VE monomers, respectively. r_1 and r_2 are the reactivity ratios of vinyl groups of ST and VE monomers, respectively. An expression for $d[M_2]/d[M_1]$ is shown in Equation 5.9. Values of r_1 and r_2 can provide valuable information regarding the monomer compositions in formed copolymers. Fractional conversions of ST and VE monomers in both BOF VE-ST and BOB VE-ST systems from the M-IR study were used to obtain the r_1 and r_2 values. Equation 5.8 was used to plot r_2 as a function of r_1 for different $[M_1]$ to $[M_2]$ ratios, and the intersection of the lines gives the r_1 and r_2 values. Figure 5.11a and b show these plots for BOF VE-ST and BOB VE-ST systems for 30 °C cure, respectively.

As shown in Figure 5.11a and b, obtained r_1 and r_2 values were 0.60 and 0.12, respectively, in BOF VE-ST systems at 30 °C, and r_1 and r_2 values were 0.54 and 0.23 in BOB VE-ST systems. Based on these values and the definition of the reactivity ratios

$$ST^* + ST \xrightarrow{k_{11}} ST - ST^* \tag{5.4}$$

$$ST^* + VE \xrightarrow{k_{12}} ST - VE^* \tag{5.5}$$

$$VE^* + ST \xrightarrow{k_{21}} VE - ST^* \tag{5.6}$$

$$VE^* + VE \xrightarrow{k_{22}} VE - VE^* \tag{5.7}$$

$$r_2 = \frac{[M_1]}{[M_2]} * \left[\frac{d[M_2]}{d[M_1]} * \left(1 + \frac{r_1 * [M_1]}{[M_2]}\right) - 1\right];\ \ r_1 = \frac{k_{11}}{k_{12}};\ \ \ r_2 = \frac{k_{22}}{k_{21}} \tag{5.8}$$

$$\frac{d[M_2]}{d[M_1]} = \frac{d[M_{VE\ C=C}]}{d[M_{ST\ C=C}]} = \frac{[M_{VE\ C=C}]}{[M_{ST\ C=C}]} * \frac{d[\alpha_{VE\ C=C}]}{d[\alpha_{ST\ C=C}]} \tag{5.9}$$

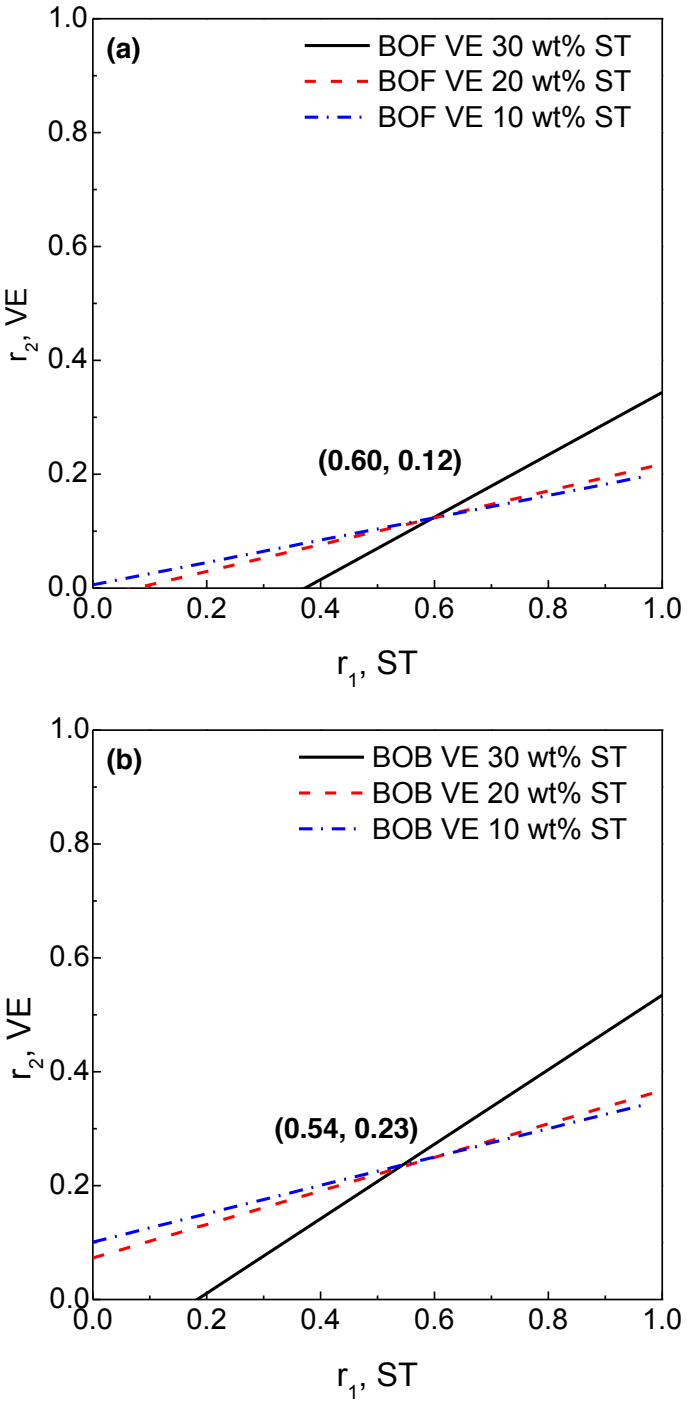

Figure 5.11. Plots of r_2 as a function of r_1 in (a) BOF VE-ST systems and (b) BOB VE-ST systems at 30 °C. Values of the line intercepts are also labeled inside the plots.

given in Equation 5.8, it may indicate that an active ST prefers to react with a VE rather than with another ST, and an active VE prefers to react with a ST rather than with another VE in both furanyl and phenyl VE systems during the initial stage of 30 °C cure. The furanyl building block didn't show a distinctly different influence on VE resins relative to its phenyl analogue in this case. Nevertheless, further investigations regarding the influence on VE resin structures are necessary. In particular, different cure temperatures should be conducted because temperature also has strong effects to the reactivity ratios of VE and ST monomers.

5.4. Conclusions

This chapter investigated the influence of furanyl building block on the thermo-mechanical properties of thermosetting vinyl ester resins. It was found that the furanyl based VE systems possess lower glass transition temperature compared with the phenyl analogues, similar to the observations in thermosetting epoxy resin systems. The T_g differences between furanyl and phenyl VE systems were smaller compared to those in the epoxy resin systems. Investigation of cure kinetics at 30 °C of these two parallel vinyl ester systems also indicated the different influences of furanyl building block relative to the phenyl analogue.

Chapter 6. Additive molar function analysis of furanyl building block to the physical properties of thermosetting polymers

6.1. Introduction

The ability to predict the key physical properties of polymer materials from their molecular structures prior to synthesis is of significant value in the design and preparation of polymer materials. With the recent rapid developments of technological applications, property performance requirements of polymer materials that used in these applications become more stringent. Therefore, the chemical structures of polymers that are suitable for advanced applications have also grown in complexity. As a result, the development of predictive computational abilities to evaluate candidates for specific applications has raised a wide interest.[119] Developing a simple general method based on the empirical and semi-empirical quantitative structure versus property relationships for predicting physical properties of polymers from the structures of their repeating units is highly desirable and applicable. Additive molar function or group contribution techniques are commonly used methods to predict polymer properties from their molecular structures and provide many useful simple correlations.[120] In this method, polymer properties are expressed as sums of additive contributions from distinct building blocks of the repeating units in their structures. In order to predict the property values of other polymers that are built using the same building blocks, this

method requires existing experimental data of polymer properties to develop a list of group contributions that are available for use.[121] The current dissertation work provides available data of many physical properties, including T_g, density and modulus, of furanyl based thermosetting polymer materials which can be used for developing group contribution parameters associated with the furanyl ring. In this chapter, an additive molar function analysis of the furanyl building block in relation to the physical properties, such as glass transition temperature, density and glassy storage modulus, of thermosetting polymers was conducted. The molar glass transition function value (Y_g) and molar volume increment value ($V_{a,i}$) of the furanyl building block for thermosetting epoxy-amine polymers were obtained. To our knowledge, such values do not exist in literature and will be very useful to allow us to estimate and predict physical properties of other furanyl based polymer materials besides thermosetting epoxy, amine and VE materials.

6.2. An additive molar function for the density calculation

Mass and packing are two most essential factors for determining the densities of materials. Mass of materials is clearly defined and measurable, while packing is not easy to be measured since it is highly dependent to many variables, such as the electronic structures of atoms, the bonding forces between atoms and the spatial structures of materials. The group contribution methods for molar volumes of materials at RT were

proposed by Traube at 1895 and Le Bas at 1915. Ever since then, a continuous effort has been performed by researchers on developing and advancing this concept for different types of materials. Being successful in predicting molar volumes of organic liquids at RT with satisfying accuracies, extensive systems of group contributions were developed for materials at solid states. Equation 6.1 is a simplified expression of group contributions for the molar volume per structural unit of glassy state polymer materials, and the recommended values for the group contributions (increments) to the various molar volumes at 298K are available in literature.[120] V_g (298K) is the sum of group contribution values to the molar volume at 298K for structural groups in the repeating unit of a glassy state polymer material and $V_{a,i}$ (298K) is the group contribution value to the molar volume at 298K for an individual structural group in a repeating unit.

$$V_g(298K) = \sum_i V_{a,i}(298K) \tag{6.1}$$

This method was applied to our thermosetting furanyl and phenyl epoxy-amine systems to validate its applicability. Figure 6.1 shows the repeating unit in the cured network structure of a BOB-PACM system, together with its groups, number of the groups and $V_{a,i}$ values for the group contribution to the molar volume at 298K. In Figure 6.1, $V_{a,i}$ (298K) for these structural groups are either obtained directly from literature or calculated based on the available values of groups with similar structures.[120]

(a) BOB-PACM system:

M: 355.47 g/mol
$\rho_{expt.}$: 1.178 g/cm^3

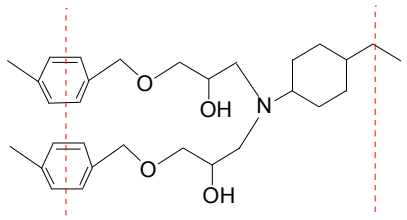

Group:	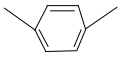	—CH_2—	—O—			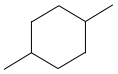
Number:	1	6.5	2	2	1	1
Va,i(298K) (cm^3/mol):	65.5	16.37	8.5	22.3	0	86

(b) BOB-EPIKURE W system:

M: 339.43 g/mol
$\rho_{expt.}$: 1.198 g/cm^3

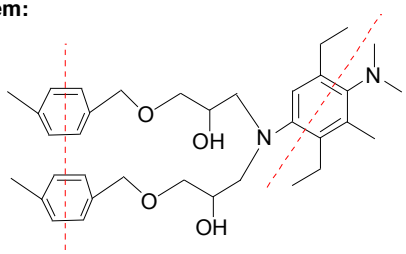

Group:	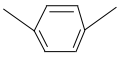	—CH_2—	—O—			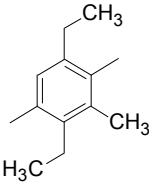
Number:	1	6	2	2	1	0.5
Va,i(298K) (cm^3/mol):	65.5	16.37	8.5	22.3	0	164

Figure 6.1. Repeating units in the cured network structures of (a) BOB-PACM system and (b) BOB-EPIKURE W system. Groups, numbers of groups and values for the group contributions to the molar volumes at 298K are also included.

With the molecular weight of structural repeating unit being 355.47 g/mol, its calculated density ρ_g(298K) based on this additive molar function is 1.112 g/cm^3, close to its experimental measured density $\rho_{exp.}$(298K), 1.178 g/cm^3. Detailed calculations can be found in Appendix C.

The same calculation was conducted for BOB-EPIKURE W system. Its repeating unit in the cured network structure, groups, number of the groups and values for the group contributions to the molar volumes at 298K are included in Figure 6.1. Va,i (298K) for most involved structural groups are available in literature except the EPIKURE W-like group. In this case, this structure is treated as a combination of two known structures, one 2,5-Tolyl group and two ethyl groups, and its Va,i (298K) is calculated as the sum of the known Va,i (298K) of these two groups. It should be noted that this calculated value could be slightly different from what it should be due to the simple "add-on" treatment. With the molecular weight of structural repeating unit being 339.43 g/mol, the calculated density ρ_g(298K) of BOB-EPIKURE W based on this additive molar function is 1.104 g/cm^3, slightly different from its experimental measured density $\rho_{expt.}$(298K) which is 1.198 g/cm^3. This deviation could be due to the inaccuracy of Va,i (298K) for the EPIKURE W-like group and a future improvement can be made if its accurate value is available.

With a general good agreement with the experimental density values, this additive molar function method for density calculation was applied to the polymer samples in

both furanyl and phenyl epoxy-amine systems, and our interest is to calculate the value for the furanyl group contribution to the molar volumes at 298K. The experimental RT density values of polymer samples were measured using a calibrated density gradient column and the results are summarized in Table 6.1. Storage moduli at the temperature relative to the T_gs of polymer samples in thermosetting furanyl and phenyl epoxy-amine systems were obtained from the DMA data in Chapter 2 and summarized in Table 6.2. The temperature at which these storage moduli were measured was consistently 46 °C lower than the sample T_g in order to eliminate the influence of differences between the testing and glass transition temperatures. Several interesting observations can be found in Table 6.1. As shown, at a given weight ratio of epoxy monomers, BOF based polymer samples always possessed higher density values compared with BOB based samples. The density values of polymer samples decreased with the increasing weight fractions of DGEBA in both furanyl and phenyl epoxy-amine systems. EPIKURE W cured polymer samples consistently showed higher density values compared with PACM cured samples. In Table 6.2, storage modulus values of BOF based polymer samples decreased with the increasing DGEBA content in both PACM and EPIKURE W cured systems, while BOB based samples did not show a similar trend. BOF based polymer samples always showed higher storage modulus values relative to BOB based samples at a given DGEBA content in both PACM and EPIKURE W cured systems, matching with their higher density values relative to the phenyl analogues. These observations are supportive for the existence of hydrogen bonding associated with furanyl rings and the

non-collinearity of covalent bonds connecting with furanyl rings which were discussed in Chapter 2.

In each curing agent category, two parallel polymer systems were paired together for conducting the additive molar function analysis. For example, relevant information of BOF-PACM and BOB-PACM samples is shown Figure 6.2. With the known molecular weight of the repeating unit and the measured density value, the overall values for the group contributions to the molar volumes at 298K for both samples can be calculated. Since the only difference between the repeating units of these two polymer samples was the central building blocks, the value for furanyl group contribution to the molar volumes at 298K can be obtained with the known value for the phenyl group. Based on the calculation listed in Appendix C, $V_{a,i}$ (298K) for the furanyl group contribution is obtained as 49.2 cm^3/mol in this sample pair. Other sample pairs were also studied and the results are summarized in Table 6.3. The obtained average value for furanyl group contribution to the molar volumes at 298K was 46.8 ± 2.4 cm^3/mol, quantitatively suggesting that the furanyl building block occupies much less space relative to the phenyl building block. Combining with the molecular weights of furanyl and phenyl rings which are 68 g/mol and 78 g/mol, respectively, the furanyl building block is found to be much denser compared with its phenyl analogue.

Table 6.1. Experimental RT density values of polymer samples in thermosetting furanyl and phenyl epoxy-amine systems.

Weight ratio of epoxy monomers BOF(BOB):DGEBA	Experimental RT density (g/cm^3)			
	PACM		EPIKURE W	
	BOF-DGEBA	BOB-DGEBA	BOF-DGEBA	BOB-DGEBA
100:0	1.210 ± 0.001	1.178 ± 0.001	1.239 ± 0.001	1.198 ± 0.001
70:30	1.195 ± 0.001	1.176 ± 0.001	1.221 ± 0.001	1.190 ± 0.001
50:50	1.185 ± 0.001	1.170 ± 0.001	1.207 ± 0.001	1.184 ± 0.001
30:70	1.174 ± 0.001	1.163 ± 0.001	1.194 ± 0.001	1.178 ± 0.001
0:100	1.150 ± 0.001	1.150 ± 0.001	1.170 ± 0.001	1.170 ± 0.001

Table 6.2. Storage moduli at the temperature relative to the T_gs of polymer samples in thermosetting furanyl and phenyl epoxy-amine systems.

Weight ratio of epoxy monomers BOF(BOB):DGEBA	Storage modulus (GPa) by DMA			
	PACM		EPIKURE W	
	BOF-DGEBA	BOB-DGEBA	BOF-DGEBA	BOB-DGEBA
100:0	2.95	1.93	2.51	1.50
70:30	2.50	1.52	2.07	1.54
50:50	1.99	1.74	1.85	1.43
30:70	1.95	1.66	1.82	1.58
0:100	1.81	1.81	1.80	1.80

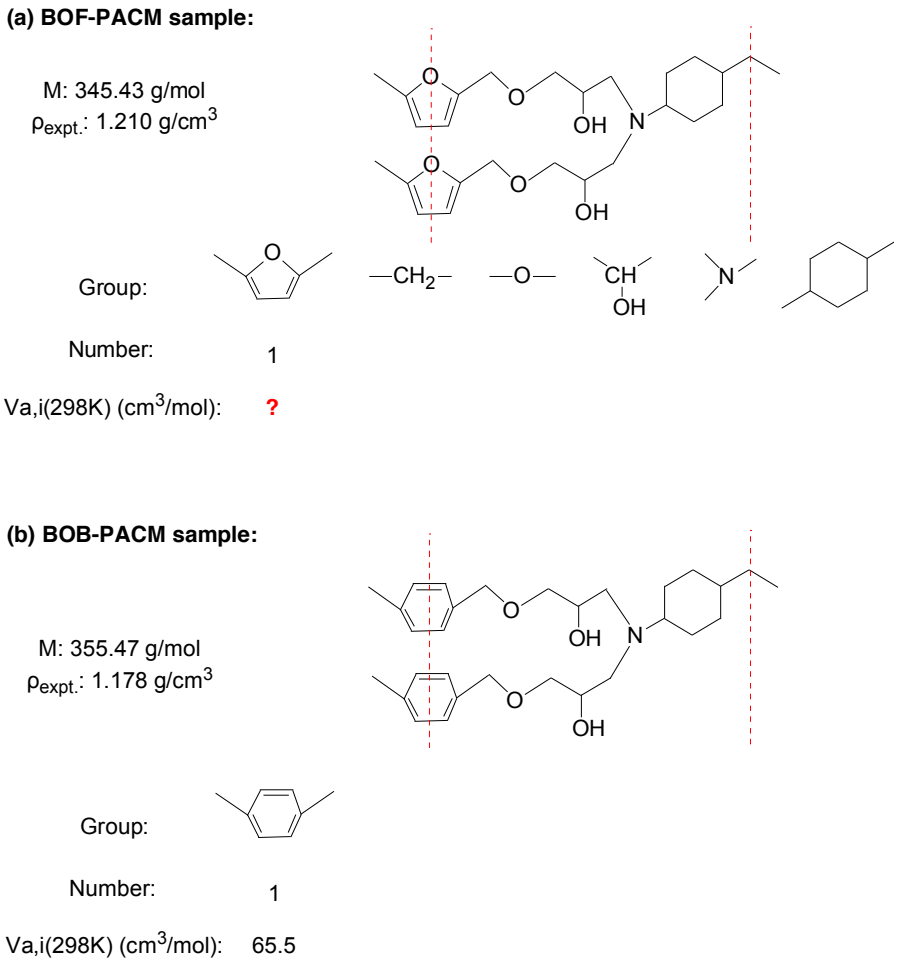

Figure 6.2. Relevant information of parallel (a) BOF-PACM and (b) BOB-PACM samples as a pair, including the repeating units in their cured network structures, the molecular weights and experimental density values.

Table 6.3. The obtained values for furanyl group contribution to the molar volumes at 298K based on the additive molar function analysis.

Parallel sample pairs		$V_{a,i\ furanyl}$ (298K) (cm^3/mol)
1.0BOF-0.0DGEBA-PACM	1.0BOB-0.0DGEBA-PACM	49.2
0.7BOF-0.3DGEBA-PACM	0.7BOB-0.3DGEBA-PACM	49.5
0.5BOF-0.5DGEBA-PACM	0.5BOB-0.5DGEBA-PACM	48.1
0.3BOF-0.7DGEBA-PACM	0.3BOB-0.7DGEBA-PACM	45.4
1.0BOF-0.0DGEBA-EPIKURE W	1.0BOB-0.0DGEBA-EPIKURE W	48.0
0.7BOF-0.3DGEBA-EPIKURE W	0.7BOB-0.3DGEBA-EPIKURE W	46.3
0.5BOF-0.5DGEBA-EPIKURE W	0.5BOB-0.5DGEBA-EPIKURE W	45.2
0.3BOF-0.7DGEBA-EPIKURE W	0.3BOB-0.7DGEBA-EPIKURE W	42.4
Average value		46.8 ± 2.4

6.3. An additive molar function for the T_g calculation

Van Krevelen and Hoftyzer proposed in their research work that the product T_g*M generally behaves as an additive function. It was named the Molar Glass Transition Function and expressed by Equations 6.2 and 6.3. Y_g represents the sum of group contribution values to the glass transition temperature for structural groups in the repeating unit of a glassy state polymer material, Y_{gi} is the group contribution value for an individual structural group in a repeating unit and M is the repeating unit molecular weight. These two equations have been used to the available experimental data on the T_gs of nearly 600 different polymer materials and the correlation rules for the group contributions to Y_g have been generated. It was found that the $Y_{g,i}$ values of the groups of interest are dependent on some neighboring groups present in the repeating unit of the system frameworks. The obtained group contributions and structural correlations are available in literature.[120]

$$Y_g = \sum_i Y_{gi} = T_g * M \tag{6.2}$$

$$T_g = \frac{Y_g}{M} = \frac{\sum_i Y_{gi}}{M} \tag{6.3}$$

This Molar Glass Transition Function method was applied to our thermosetting furanyl and phenyl epoxy-amine systems to validate its applicability. Figure 6.3 shows the repeating unit in the cured network structure of a BOB-PACM system, together with its groups, number of the groups and $Y_{g,i}$ values for the group contributions.

With the molecular weight of structural repeating unit being 355.47 g/mol, its calculated T_g based on this molar glass transition function is 60 °C, much lower compared with its experimental value, 100 °C. Detailed calculation can be found in Appendix C. As discussed above, the $Y_{g,i}$ values of the groups of interest are dependent on some neighboring groups present in the repeating unit of polymer materials, which could be the reason for this deviation.

The same calculation was conducted for BOB-EPIKURE W system. Its repeating unit in the cured network structure, groups, number of the groups and $Y_{g,i}$ values for the group contributions are included in Figure 6.3. With the molecular weight of structural repeating unit being 339.43 g/mol, its calculated T_g based on this molar glass transition function is 70 °C, also much lower compared to the experimental value, 132 °C, potentially due to the same reason. However, it should be noted that in this case the relative trend in T_g is predicted.

(a) BOB-PACM system:

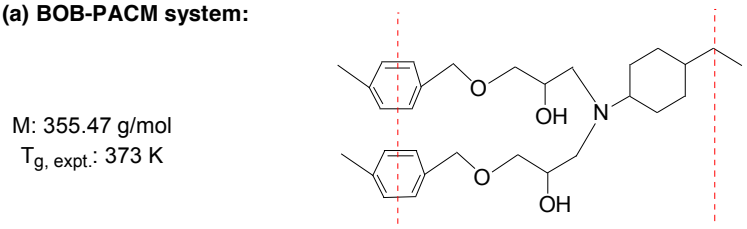

Group:		—CH_2—	—O—			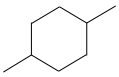
Number:	1	6.5	2	2	1	1
$Y_{g,i}$ (K Kg/mol):	29.5	4.3	4	13	0	27

(b) BOB-EPIKURE W system:

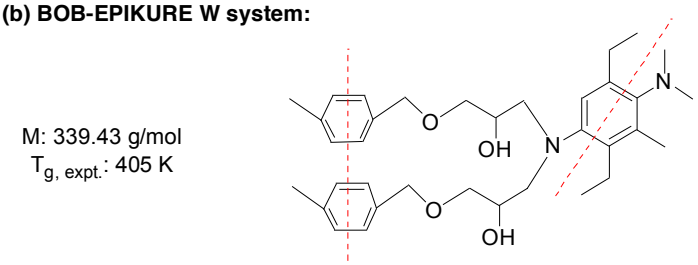

Group:	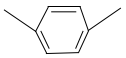	—CH_2—	—O—			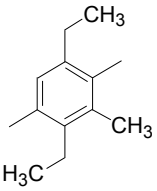
Number:	1	6	2	2	1	0.5
$Y_{g,i}$ (K Kg/mol):	29.5	4.3	4	13	0	54

Figure 6.3. Repeating units in the cured network structures of (a) BOB-PACM system and (b) BOB-EPIKURE W system. Groups, numbers of groups and $Y_{g,i}$ values for the group contributions are also included.

Even though there might be neighboring effect to the groups of interest in the repeating unit of cured networks, these effects could be eliminated if we only focus on the central furanyl and phenyl building blocks in the repeating units since the rests of the repeating units were identical in the analogous systems. Therefore, this molar glass transition function was still applied to the polymer samples in both furanyl and phenyl epoxy-amine systems, and our interest is to calculate the value for the furanyl group contribution to glass transition temperature. The experimental T_g values of polymer samples were reported in Chapter 2 and Chapter 4.

Using the same strategy used for the density analysis, two parallel polymer samples were paired. As an example, relevant information of BOF-PACM and BOB-PACM systems is shown Figure 6.4. With the known molecular weight of the repeating unit and the measured T_g value, the overall Y_g values for the group contributions for both samples can be calculated. Since the only difference between the repeating units of these two polymer samples was the central building blocks, the value for furanyl group contribution to glass transition temperature can be obtained with the known value for the phenyl group. Based on the calculation listed in Appendix C, $Y_{g,i}$ for the furanyl group contribution is obtained as 15.74 K·Kg/mol for this sample pair. Other sample pairs were studied and the results are summarized in Table 6.4. As shown, obtained $Y_{g,i}$ $_{furanyl}$ values in the PACM cured system were different from those in the EPIKURE W cured system, indicating that the neighboring effect influences the $Y_{g,i}$ value of the groups of interest. Overall, the obtained average value for furanyl group contribution to

(a) BOF-PACM sample:

M: 345.43 g/mol
$T_{g,expt.}$: 344 K

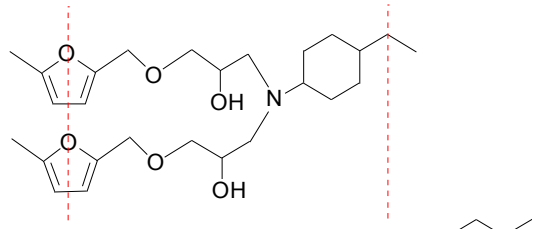

Group: 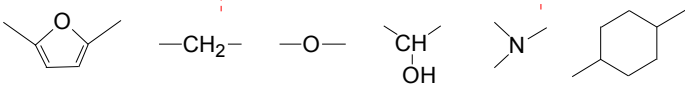

Number: 1

$Y_{g,i}$ (K Kg/mol): ?

(b) BOB-PACM sample:

M: 355.47 g/mol
$T_{g,\ expt.}$: 373 K

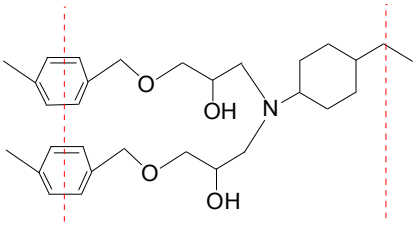

Group: 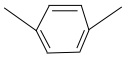

Number: 1

$Y_{g,i}$ (K Kg/mol): 29.5

Figure 6.4. Relevant information of parallel (a) BOF-PACM and (b) BOB-PACM samples as a pair, including the repeating units in their cured network structures, the molecular weights and experimental T_g values.

Table 6.4. The obtained values for furanyl group contribution to glass transition temperature based on the molar glass transition function analysis.

Parallel sample pairs		$Y_{g,i\ furanyl}$ (K·Kg/mol)
1.0BOF-0.0DGEBA-PACM	1.0BOB-0.0DGEBA-PACM	15.74
0.7BOF-0.3DGEBA-PACM	0.7BOB-0.3DGEBA-PACM	16.04
0.5BOF-0.5DGEBA-PACM	0.5BOB-0.5DGEBA-PACM	15.53
0.3BOF-0.7DGEBA-PACM	0.3BOB-0.7DGEBA-PACM	14.34
1.0BOF-0.0DGEBA-EPIKURE W	1.0BOB-0.0DGEBA-EPIKURE W	10.94
0.7BOF-0.3DGEBA-EPIKURE W	0.7BOB-0.3DGEBA-EPIKURE W	9.18
0.5BOF-0.5DGEBA-EPIKURE W	0.5BOB-0.5DGEBA-EPIKURE W	8.54
0.3BOF-0.7DGEBA-EPIKURE W	0.3BOB-0.7DGEBA-EPIKURE W	8.06
BOF-DFDA	BOB-DFDA	21.60
BOF-CH_3-DFDA	BOB-CH_3-DFDA	21.15
Average value[a]		12.3 ± 3.5

[a]this average value excluded the values associated with DFDA and CH_3-DFDA due to their different neighboring efforts in cured networks.

glass transition temperature was 12.3 ± 3.5 K·Kg/mol, suggesting that the furanyl building block provided lower T_g values when present in the repeating units of polymer materials compared with its phenyl analogue having $Y_{g,i\ phenyl}$ value of 29.5 K·Kg/mol. Interestingly, the $Y_{g,i\ furanyl}$ values obtained from the DFDA and CH_3-DFDA cured systems were significantly higher than those from PACM and EPIKURE W cured systems. Since $Y_{g,i\ furanyl}$ value was lower than $Y_{g,i\ phenyl}$ value, the results from the systems containing more furanyl contents, which were DFDA and CH_3-DFDA systems, should be even lower. Their surprisingly higher values indicated a strong neighbor effect may exist in the furanyl epoxy-furanyl amine systems, which did not occur in the phenyl based systems.

6.4. Conclusions

$V_{a,i}$ (298K) of furanyl building block is calculated as 46.8 ± 2.4 cm^3/mol, approximately 18.6 cm^3/mol lower than the literature value for phenyl building block (65.5 cm^3/mol). Y_g of furanyl building block is calculated as 12.3 ± 3.5 K·Kg/mol, about 17.2 K·Kg/mol lower than that of phenyl building block (29.5 K·Kg/mol). These values can be very useful in allowing us to estimate and predict physical properties of other furanyl based polymer materials besides thermosetting epoxy and amine materials.

Chapter 7. Preparation and characterization of biobased tougheners for commercial thermosetting epoxy resins

7.1. Introduction

Thermosetting epoxy resins are widely used in coating, adhesive, electric and composite industries in the current society.[1, 102, 122] Their versatile properties, including good thermal and chemical resistances, excellent adhesion, high electrical insulation and strength-to-weight ratio, are endowed by the formation of crosslinked networks after cure. However, when cured with multi-functional hardeners, such as amines and anhydrides, the formed highly crosslinked networks often result in an inherent brittleness which has significantly restricted their applications.[49, 123] Thus, many research approaches have been conducted to toughen thermosetting epoxy resins during the past decades.[50b-d, 124] Among all, introducing secondary phase architectures into cured networks by adding soluble reactive tougheners which can be reaction-induced to phase separate,[52b-d, 125] or insoluble micro particles into epoxy matrices,[51] has become one of the major approaches. McGarry and Willner reported a liquid carboxyl terminated butadiene-acrylonitrile (CTBN) copolymer to toughen DGEBA epoxy resins and resulted in a significant enhancement of toughness properties.[126] At the initial cure stage, these reactive tougheners are miscible with epoxy-hardener mixtures. As the cure reaction proceeds,

micro rubbery particles with these toughenners as nucleation cores start to precipitate out from cured networks due to the entropy effect, resulting in phase separation architectures after the gelation point. Covalently bonding to the matrices and uniformly dispersing in the networks, these formed secondary rubbery phases significantly enhance the fracture toughness properties through a high degree of matrix shear deformation and energy dissipation during fracture.[53]

Toughenners prepared using biobased materials have been investigated for epoxy resins, among which vegetable oil is considered a promising candidate since its chemical structure possesses multiple types of functional groups that can be used and modified. Epoxidized soybean oil (ESO) can be readily prepared through the epoxidation of unsaturated soybean oil, which is one of the most abundant vegetable oils from plants.[54] ESO has been investigated for toughening epoxy resins since it contains secondary epoxy groups, besides triglyceride groups and aliphatic fatty esters with varying chain lengths, on its chemical structure which can react into the epoxy matrices.[55] However, instead of forming rubbery particles and phase-separating, using ESO directly as a toughener often causes a negative plasticization effect to the epoxy matrices and hurt other properties, such as T_g and E'.[56] Modifications of its chemical structure, functionality and molecular weight (MW) are necessary to restrict this effect by endowing modified ESO with a capability to phase separate from the matrices during cure.[57] Chemicals, such as methacrylic, acrylic acids and fatty acids, have been used to modify ESO and toughen VE resins and composite materials.[58, 125, 127] A series of VE

tougheners were prepared by grafting methacrylic and fatty acids onto ESO with the MWs and functionalities of tougheners well tunable by adjusting the molar ratios of reactants. The ultimate phase separation sizes in the matrices can be controlled. It is meaningful and necessary to prepare such types of ESO based tougheners for thermosetting epoxy resins and evaluate their toughening effect.

In this chapter, a group of bio-rubber (BR) tougheners was prepared by grafting renewable fatty acids onto ESO at varying molar ratios to provide BRs with diverse MWs, functionalities and compatibilities with epoxy resins. Renewable acids, such as n-hexanoic acid,[59] n-octanoic acid,[60] n-decanoic acid,[61] lauric acid and myristic acid were used to make these BRs fully sustainable. The successful preparation of BRs was verified using multiple characterization methods. Their toughening effect on commercial thermosetting epoxy resins was investigated using aromatic DGEBA EPON 828 (n = 0.13) and EPIKURE W. Fracture toughness and thermo-mechanical properties of the control and BR toughened samples were evaluated. The fracture surface morphology was investigated using scanning electron microscope (SEM) and atomic force microscope (AFM). Secondary rubbery phases with tunable particle sizes depending on the BR type and its weight fraction were found to form in the cured networks of BR toughened samples. This phase separation was verified to be responsible for the improved fracture toughness property of BR toughened samples. With other excellent advantages, such as low viscosity and competitive cost, these BRs are demonstrated of promising use of toughening commercial thermosetting epoxy resins.

7.2. Experimental

7.2.1. Materials

n-hexanoic acid (99%), n-octanoic acid (99%), n-decanoic acid (99%), lauric acid (98+%), myristic acid (99%), 0.1 N perchloric acid reagent, hydroquinone (99%) and tetrahydrofuran (THF, 99%) were purchased from Sigma-Aldrich, US; ESO with the commercial name Drapex 6.8 was purchased from Galata Chemicals at Louisiana, US, and it has an average 4 epoxy groups per triglyceride; an esterification reaction catalyst with the commercial name AMC-2 was purchased from Aerojet Chemicals at California, US; EPIKURE W and DGEBA EPON 828 (n = 0.13) were purchased from Miller Stephenson Chemical Company, US. All materials were used as received.

7.2.2. Preparation of bio-rubber (BR) tougheners

BR tougheners were prepared by grafting fatty acids onto ESO with varying molar ratios of 1:1, 2:1, and 3:1 via an esterification reaction using AMC-2 as a catalyst. Used fatty acid and molar ratio were employed to name these prepared BRs. BR which was named HEX-2 was prepared using n-hexanoic acid at a molar ratio of 2 fatty acids to 1 ESO molecule. The preparation scheme of HEX-2 BR is shown schematically in Figure 7.1 as an example. 4.69 g n-hexanoic acid (40 mmol), 18.94 g ESO (20 mmol), 23.6 mg hydroquinone (0.1 wt.%) and 236.3 mg AMC-2 (1 wt.%) were added to a 500 mL three-

necked round-bottomed flask equipped with a thermometer, a stirring bar and a condenser. The vessel was sealed and the reaction was conducted at 70 °C for 1 hour followed by 90 °C for additional 3 hours. After cooling to RT, the obtained HEX-2 BR was an odorless liquid with a slightly green tinge. This was the case for all prepared BRs using different fatty acids and molar ratios investigated in this work.

7.2.3. Measurement of epoxy equivalent weight (EEW)

EEW values of ESO and prepared BRs were measured using the epoxy titration by following ASTM D 1652-97, procedure B.[90] For example, EEW of HEX-2 was measured by preparing a solution of 0.4 g HEX-2, 10 mL methylene chloride, 0.5 mL 0.1 wt% crystal violet indicator in glacial acetic acid and 10 mL 0.25 g/mL tetraethylammonium bromide in glacial acetic acid. 0.1 N perchloric acid reagent was used to titrate the solution until a sharp color change from blue to green was observed and the volume of consumed perchloric acid reagent was recorded. Three titrations were conducted and the average value was calculated for each EEW reported.

7.2.4. Characterization of BR tougheners

Multiple techniques, including GPC, FTIR, rheometry and epoxy titration, were used to characterize BRs. MW distribution of BRs was measured using a Waters GPC system with two 30 cm long, 7.5 mm diameter poly-styrene-divinyl benzene columns, PLgel 5

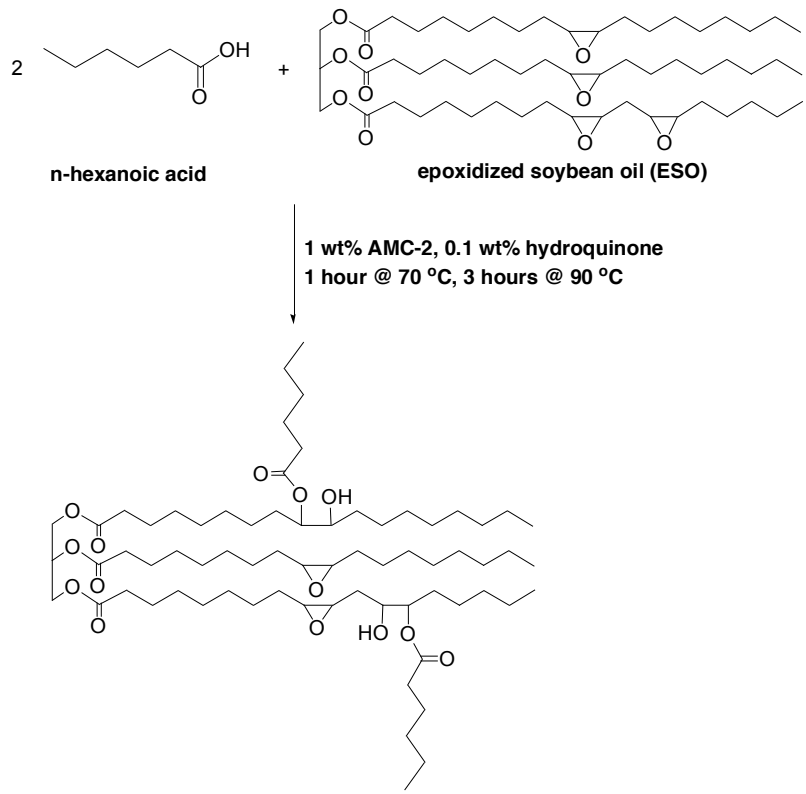

Figure 7.1. A representative preparation scheme of HEX-2 using n-hexanoic acid and ESO with a molar ratio of 2:1 between the two reactants; the structure of ESO is representative since ESO contains a distribution of fatty acids mostly with one or two epoxidized unsaturated sites such that the average epoxy content is 4 per molecule; additionally the product formed also results in a distribution of materials.

μm MIXED-C column and 5 μm 50 Å column, and a 2410 refractive index detector. 2 mg BR sample was dissolved in 1 mL THF and filtered before testing with THF as an eluent at a flow rate of 1.0 mL/min. Functional groups of BRs were investigated using a Thermo Nicolet Nexus 870 FTIR spectrometer in absorbance mode with an 8 cm-1 resolution, 32 scans per sample and a deuterated tryglycine sulfate detector in 650–4000 cm^{-1} at RT. Viscosities of BRs were measured on a TA AR2000ex rheometer using a 40 mm flat plate configuration at RT. Measurements were conducted with shear rate from 0.01 to 1000 s^{-1} and the shear stress was recorded every 2 seconds at each shear rate. An average of three measurements at the shear rate of 1000 s^{-1} was reported as the viscosity value of BR.

7.2.5. Preparation of BR toughened samples

BR toughened epoxy-amine samples were prepared by blending BR into epoxy resin at varying fractions (0, 10, 15 and 20 wt%) and adding a stoichiometric amount of EPIKURE W afterward. Polymer samples were named based on their compositions. For example, 15%HEX-3/85%828 represented a polymer sample comprised of EPIKURE W and an epoxy mixture containing 15 wt% of HEX-3 and 85 wt% of EPON 828. These components were mixed, degassed, poured into a rubber mold with dimensions of 140 × 14 × 6 mm. Polymer samples were cured at 140 °C for 9 hours followed by 200 °C for additional 3 hours, and then processed into a compact tension (CT) configuration for the fracture toughness testing. DMA specimens were similarly prepared using a rubber mold with dimensions of 40 × 10 × 5 mm, and then processed to dimensions of 38 × 9 × 4

mm. Polymer samples toughened using ESO and the control sample (without adding BRs or ESO) were prepared in a similar fashion for comparison.

7.2.6. Property measurements of polymer samples

The critical strain energy release rate (G_{1c}) and critical stress intensity factor (K_{1c}) values of polymer samples were measured using a servo-hydraulic INSTRON model 8872 apparatus following ASTM D5045-99, method E 399.[128] Five to seven CT specimens in each composition were prepared for testing. CT specimens were processed to dimensions of 16 × 13 × 5.5 mm and an 8 mm long notch was cut into each specimen using a diamond blade saw. A sharp pre-crack was made at the bottom of each notch using a fresh razor blade before testing. A constant crosshead speed of 1 mm/min was used with a termination criterion of 1 mm tensile extension at RT. Thermo-mechanical properties, i.e. T_g and E'_{RT}, of polymer samples were measured using a TA Q800 DMA in the single cantilever geometry. Two consecutive scans were conducted for each sample with an amplitude of 15 μm, a frequency of 1 Hz and a temperature ramp rate of 2 °C/min from -125 °C to 225 °C. The second run was used to measure T_g and E'_{RT} of the sample in which the T_g value was assigned as the loss modulus peak temperature.

7.2.7. Fracture surface morphology

Fracture surface morphology of tested CT specimens was evaluated to elucidate the phase separation, particle size and particle distribution using SEM and AFM. SEM imaging was conducted using a Zeiss Supra 50VP SEM equipped with an in-lens detector. A platinum layer 7-9 nm in thickness was sputter coated on the fracture surfaces before imaging. NIH image processing software (ImageJ) was used to analyze the surface morphology. Fracture surfaces were also investigated using a Bruker MultiMode AFM in PeakForce QNM mode. A RTESPA silicon cantilever with a nominal spring constant of 25.2 N/m and tip radius of 40.9 nm was used. The maximum applied force and scan rate were set at 50 nN and 0.5 Hz, respectively. AFM samples were fractured at RT and Bruker NanoScope Analysis software was used to perform AFM image processing.

7.3. Results and Discussion

7.3.1. Preparation of BR tougheners

Functional groups in the chemical structures of BRs were investigated using M-IR. Figure 7.2 plots M-IR spectra of ESO, HEX-1, HEX-2 and HEX-3 BRs. The peak between 800 and 850 cm^{-1} is attributed to the secondary epoxy group present in ESO.[129] As

expected, this peak decreases in the order of ESO, HEX-1, HEX-2 and HEX-3, as more fatty acids are grafted onto ESO via esterification of the epoxy groups. The peak around 3475 cm^{-1} corresponds to the formed hydroxyl group from the epoxy ring opening reaction.[129] As expected, this peak is the highest for HEX-3, and followed by HEX-2 and HEX-1, and not present in ESO. Similar phenomena are also observed for OCT, DEC, LAU, MYR BRs. These results are consistent with the expected chemistry used in the BR preparation and indicate the acids were successfully grafted onto ESO.

MW distributions of prepared BRs were studied qualitatively using GPC. Figure 7.3 plots the elution traces of ESO, HEX-1, HEX-2 and HEX-3 BRs whose characteristic elution peaks are shown at 13.41, 13.28, 13.14 and 13.06 min, respectively. "HEX" BRs also show broader elution peaks compared with ESO. These results indicate that MWs of BRs are higher than that of ESO and increase with the number of grafted acids.

Viscosity values of prepared BRs were measured. Results of ESO and HEX BRs are plotted in Figure 7.4 as an example. HEX-1, HEX-2 and HEX-3 possess viscosities of 0.87, 1.85, and 4.20 Pa.s at RT, respectively. The values are significantly lower than that of DGEBA EPON 828 resin reported at 10 - 16 Pa.s by suppliers. The addition of such BRs to a DGEBA epoxy formulation can significantly facilitate the processability of materials. Higher than that of ESO (0.38 Pa.s), the viscosity values of HEX BRs increase with the number of grafted acids, as a result of the increased MW and the intermolecular hydrogen bonding between polar ester groups and formed hydroxyl groups.

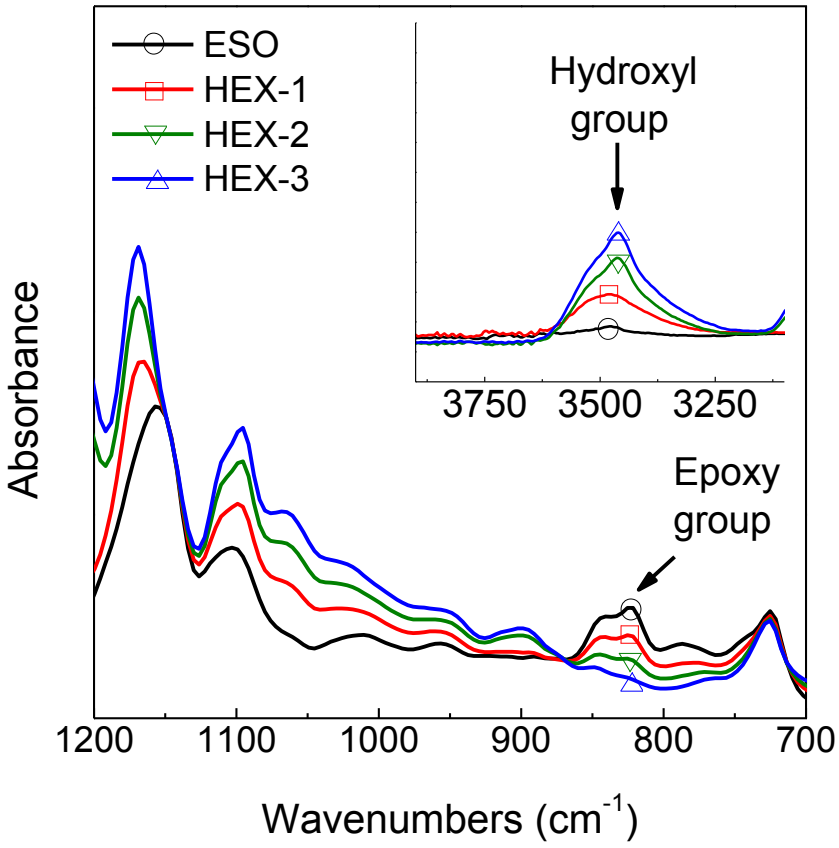

Figure 7.2. M-IR spectra of ESO, HEX-1, HEX-2 and HEX-3 BRs.

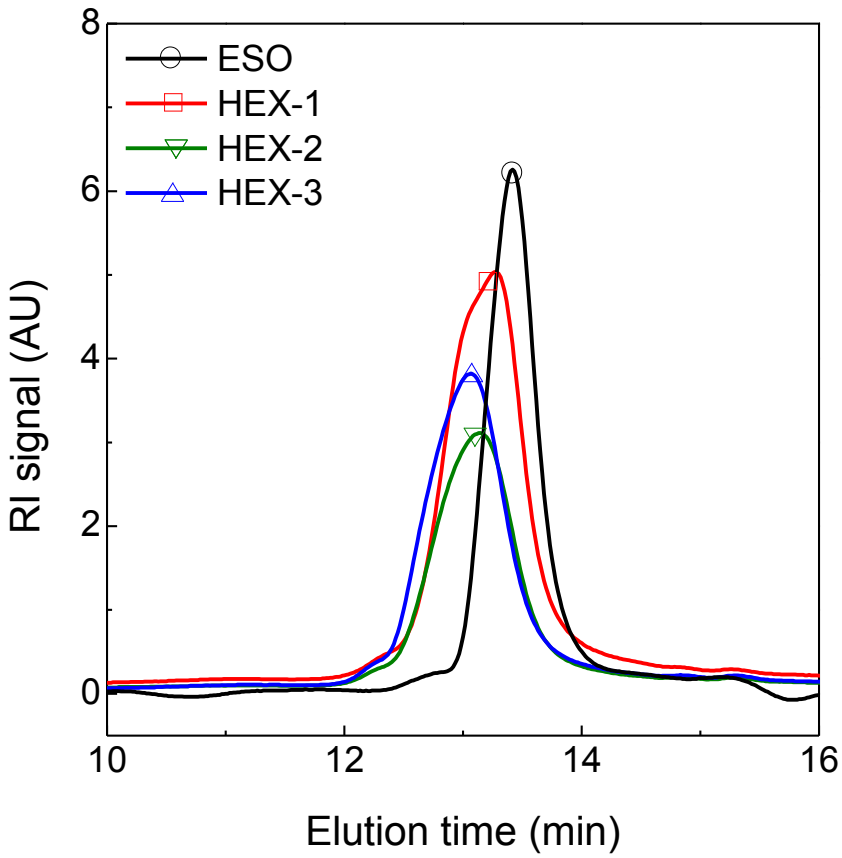

Figure 7.3. GPC spectra of ESO, HEX-1, HEX-2 and HEX-3 BRs.

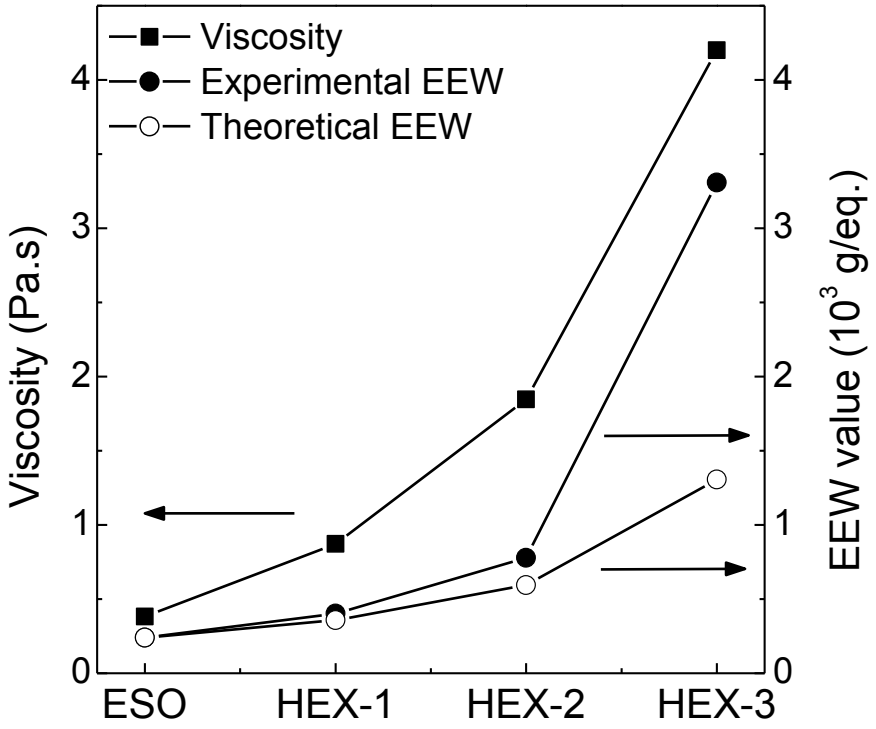

Figure 7.4. Viscosity, experimental and theoretical EEW values of ESO, HEX-1, HEX-2 and HEX-3 BRs.

Also plotted in Figure 7.4 are the measured and theoretical EEW values of HEX BRs. Higher than those of ESO, the experimental and theoretical EEW values of HEX BRs increase with the number of grafted acids since the grafting increases the MW but decreases the epoxy functionality of BRs. Interestingly, all HEX BRs have experimental EEW values higher than the theoretical values, and the deviation grows with the number of grafted acids. This behavior is due to the strong catalytic effect of AMC-2 which can also catalyzes the reaction between formed hydroxyl groups and remaining epoxy groups, leading to high experimental EEW values as well as MWs higher than expected.[48b, 130] The higher the concentration of hydroxyl groups, the greater the likelihood of this happening and the greater the observed differences between measured and theoretical EEW values.

The observations regarding the HEX series of BRs are paralleled by the BRs that were prepared with the other fatty acids investigated namely n-octanoic acid (OCT), n-decanoic acid (DEC), n-dodecanoic acid or lauric acid (LAU) and n-tetradecanoic acid or myristic acid (MYR). The GPC elution time, viscosity and EEW results are summarized in Table 7.1. For all systems the trends in BR properties as a function of the graft content mirror those discussed for the HEX series of BRs. An interesting observation is that, for any given grafting ratio, while the elution time decreases as the fatty acid MW increases which indicates the increased MWs of BRs, the viscosity values of BRs remain relatively constant. This suggests that the viscosity increase that should have resulted from the

Table 7.1. GPC elution time, viscosity, experimental and theoretical EEW values of prepared BRs.

BR	Elution Time[a] (min)			Viscosity[b] (Pa·s)			Experimental EEW[c] (g/eq.)			Theoretical EEW[d] (g/eq.)		
x =	1	2	3	1	2	3	1	2	3	1	2	3
HEX-x	13.28	13.14	13.06	0.87	1.85	4.20	402	779	3307	358	595	1305
OCT-x	13.25	13.09	12.97	0.90	1.94	3.79	421	846	3881	367	623	1390
DEC-x	13.11	13.02	12.90	0.79	1.67	3.45	419	871	4079	376	651	1474
LAU-x	13.08	12.96	12.82	0.90	1.88	3.71	430	896	4166	386	679	1558
MYR-x	13.09	12.91	12.77	0.89	1.91	3.61	434	925	4212	395	707	1642

[a]Data from the GPC tests. [b]Data from the rheometry tests at RT. [c]values determined by following ASTM D1652-97 procedure B. [d]values determined from the chemical structures of prepared BRs.

increased MW of BR is counteracted by the lower hydroxyl concentration that results from the higher MW of fatty acid used.

7.3.2. Preparation of BR toughened samples

Table 7.2 provides the EEW value of epoxy resin and the AHEW value of amine hardener that were used for preparing polymer samples. The components were mixed and degased, and in all cases resulted in stable homogeneous mixtures thus indicating BRs have a good miscibility with DGEBA EPON 828. The samples were cured under the same condition as described in the experimental section. Complete epoxy and amine conversions of cured polymer samples as measured using N-IR were attained.

7.3.3. Fracture surface morphology

A visual investigation indicates that samples toughened with different BRs and weight fractions exhibit different optical transparency characteristics. Fracture surface morphologies of BR toughened samples as well as the control and ESO toughened samples were investigated using SEM and AFM to determine the phase separation and associated degree. Table 7.3 summarizes the optical transparency and phase separation of all prepared polymer samples. As shown, the control sample, 15%ESO/85%828 sample, samples toughened with HEX series of BRs at 10 and 15 wt%, and 20%HEX-1/80%828 sample are transparent without phase separating. However,

Table 7.2. EEW and AHEW values of epoxy resin and amine hardener, respectively.

Epoxy and amine	EEW[a] (g/eq.)	EEW[b] (g/eq.)	AHEW[b] (g/eq.)
DGEBA EPON 828	188.0	185-192	-
EPIKURE W	-	-	45.0

[a]Experimental values determined by following ASTM D1652-97 procedure B. [b]values provided from suppliers.

20%HEX-2/80%828 sample which is found to phase separate with a small domain size in the cured network is interestingly being transparent. 20%HEX-3/80%828 sample is optically opaque and a higher degree of phase separation is found. This indicates, under the same cure condition, increasing the acid molar ratio of BRs prepared using the same fatty acid leads to phase separation, and it is due to the decreased epoxy functionality and increased MW of BRs. Compared with HEX series of BRs at 15 wt%, samples toughened with OCT, DEC and LAU series of BRs at 15 wt% (except 15%OCT-1/85%828 sample) are all opaque with phase separation occurring in cured networks. 15%OCT-1/85%828 sample, like 20%HEX-2/80%828 sample, also has phase separation but at a small degree and remaining transparent. This suggests that, under the same cure condition, increasing the fatty acid MW of BRs prepared at a given acid molar ratio also leads to phase separation because of the increased MW of BRs.

Figure 7.5 displays the fracture SEM images of selected polymer samples. As expected, 15%ESO/85%828 sample which is transparent shows a homogenous morphology. In contrast to 20%HEX-2/80%828 sample, 20%HEX-3/80%828 sample presents an enlarged phase separation in the cured network. Samples toughened with OCT-3 at 10, 15 and 20 wt% exhibit phase separation with increased particle sizes, indicating under the same cure condition, increasing BR concentration leads to larger phase separation degree. All SEM images were analyzed and the fracture surface morphology including area covered by particle and average particle diameter are summarized in Table 7.3. As shown, these

Table 7.3. Optical transparency, phase separation and fracture surface morphology of the control sample and samples toughened with BRs and ESO.

Sample	Optical transparency	Phase separation	%area covered by particle	Average diameter (nm)
Control (100%828)	Yes	No	-	-
15%ESO/85%828	Yes	No	-	-
10%HEX-1/90%828	Yes	No	-	-
10%HEX-2/90%828	Yes	No	-	-
10%HEX-3/90%828	Yes	No	-	-
15%HEX-1/85%828	Yes	No	-	-
15%HEX-2/85%828	Yes	No	-	-
15%HEX-3/85%828	Yes	No	-	-
20%HEX-1/80%828	Yes	No	-	-
20%HEX-2/80%828	Yes	Yes	2.0	88
20%HEX-3/80%828	No	Yes	20.9	1402
10%OCT-1/90%828	Yes	No	-	-
10%OCT-2/90%828	Yes	Yes	0.3	209
10%OCT-3/90%828	No	Yes	9.0	614
15%OCT-1/85%828	Yes	Yes	0.2	185
15%OCT-2/85%828	No	Yes	15.1	573
15%OCT-3/85%828	No	Yes	15.1	660
20%OCT-1/80%828	Yes	Yes	0.4	224
20%OCT-2/80%828	No	Yes	23.5	1348
20%OCT-3/80%828	No	Yes	22.1	1424
10%DEC-1/90%828	Yes	No	-	-
10%DEC-2/90%828	No	Yes	11.3	510
10%DEC-3/90%828	No	Yes	15.6	1171
15%DEC-1/85%828	No	Yes	0.7	241
15%DEC-2/85%828	No	Yes	22.5	982
15%DEC-3/85%828	No	Yes	19.6	1449
10%LAU-1/90%828	Yes	No	-	-
10%LAU-2/90%828	No	Yes	11.6	700
10%LAU-3/90%828	No	Yes	14.3	1212
15%LAU-1/85%828	No	Yes	8.2	943
15%LAU-2/85%828	No	Yes	20.0	1078
15%LAU-3/85%828	No	Yes	15.4	1394

"Yes" in "Optical transparency" indicates the sample is transparent by visual investigation, and "No" means opaque; "Yes" in "Phase separation" indicates phase separation occurs in the cured networks of polymer samples using SEM imaging, and "No" means no occurrence.

samples toughened with BRs possess a wide range of phase separation domain sizes. This suggests that, besides the BR weight fraction, BRs prepared using different MWs of fatty acids and different degrees of grafting can also affect the phase separation architectures in cured networks. Another important observation is that, same as the 20%HEX-2/80%828 and 15%OCT-1/85%828 samples, 10%OCT-2/90%828 and 20%OCT-1/80%828 samples possess phase separation with average particle diameter below 300 nm and remain optically transparent. As samples having average particle diameter greater than 300 nm are all opaque, it demonstrates that 300 nm is the phase separation criterion to sample optical transparency. However, since 15%DEC-1/85%828 sample with an average diameter of 241 nm is found to be opaque, it suggests that other factors, including the BR type and BR weight fraction, can also influence the transparency characteristics of phase-separated samples.

7.3.4. Thermo-mechanical properties of polymer samples

Thermo-mechanical properties, such as T_g and E'_{RT}, of BR toughened samples were evaluated using DMA. Figure 7.6a ad b plot DMA thermograms of the samples toughened with HEX and OCT BRs at 15 wt% as well as the control sample, respectively. As shown, samples toughened with HEX and OCT BRs at 15 wt% possess lower T_gs compared with the control sample, indicating these BRs all possess the plasticization effect to the epoxy-amine matrix. However, T_gs of the samples toughened with HEX BRs are even lower than those toughened with OCT BRs and this is due to a stronger

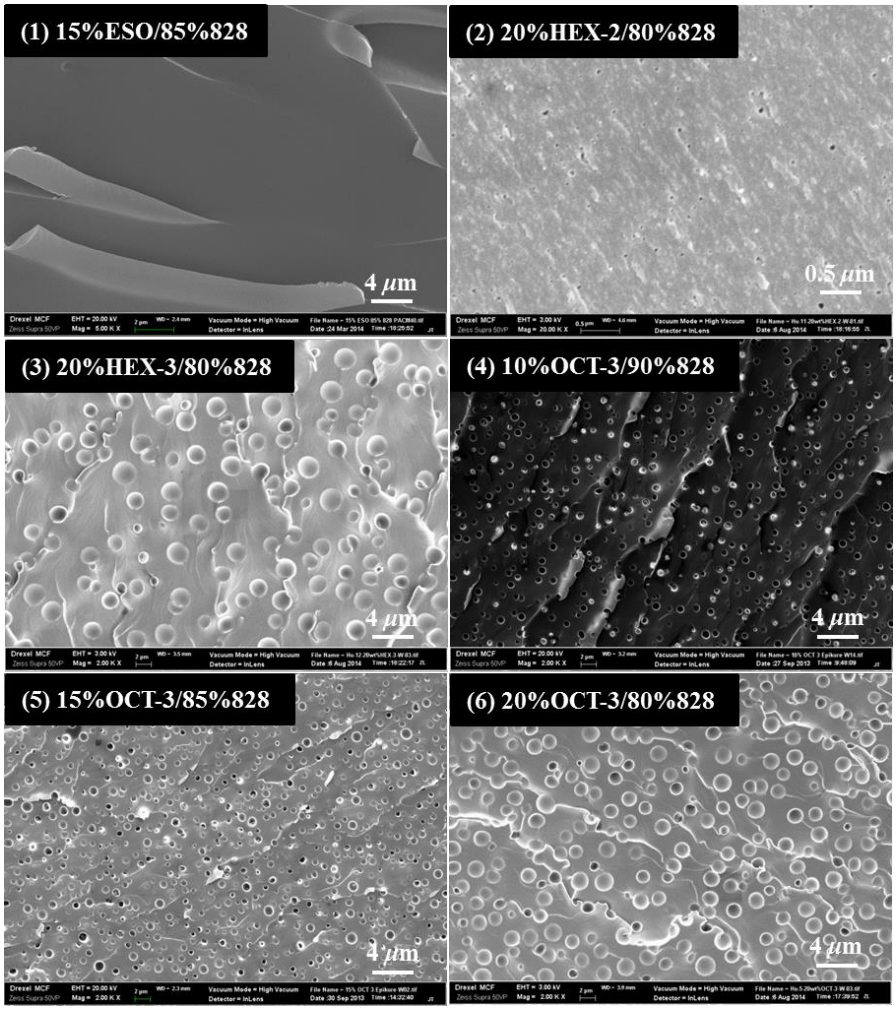

Figure 7.5. Fracture SEM images of selected samples toughened with BRs and ESO.

plasticization effect of HEX BRs with lower MWs. Meanwhile, samples toughened with these two series of BRs behavior similarly in a sense that HEX-3 toughened sample possesses the highest T_g and followed by HEX-2 and HEX-1 toughened samples because of the decreased epoxy functionalities and increased MWs of HEX-3 and OCT-3. On the other hand, samples toughened with HEX BRs at 15 wt% which possess homogenous networks based on SEM imaging show a very broad T_g transition including a secondary transition that starts around 50 °C. Instead, samples toughened with OCT BRs at 15 wt% possessing phase separation in cured network do not have this broad T_g transition as well as the secondary transition around 50 °C. Low-temperature curve in Figure 8.6a indicates the control sample possesses its β transition temperature (T_β) at - 67 °C, and HEX toughened samples which are non-phase separated present T_β around - 72 °C. In Figure 7.6b, OCT toughened samples which are phase-separated possess a broader loss modulus transition from - 65 °C to - 50 °C. This new transition starting around - 50 °C is assigned as the T_g of phase-separated OCT BRs. The higher T_β of OCT toughened samples around - 65 °C compared with HEX toughened samples is because OCT BRs are prepared using n-octanoic acid with a longer chain length (higher MW) and the β transition of localized side chain movements in the main chains of OCT toughened samples requires to occur at a higher temperature. OCT toughened samples possess lower E'_{RT} than HEX toughened samples and followed by the control sample due to the increased softness of BRs with the increasing MWs of grafted fatty acids.

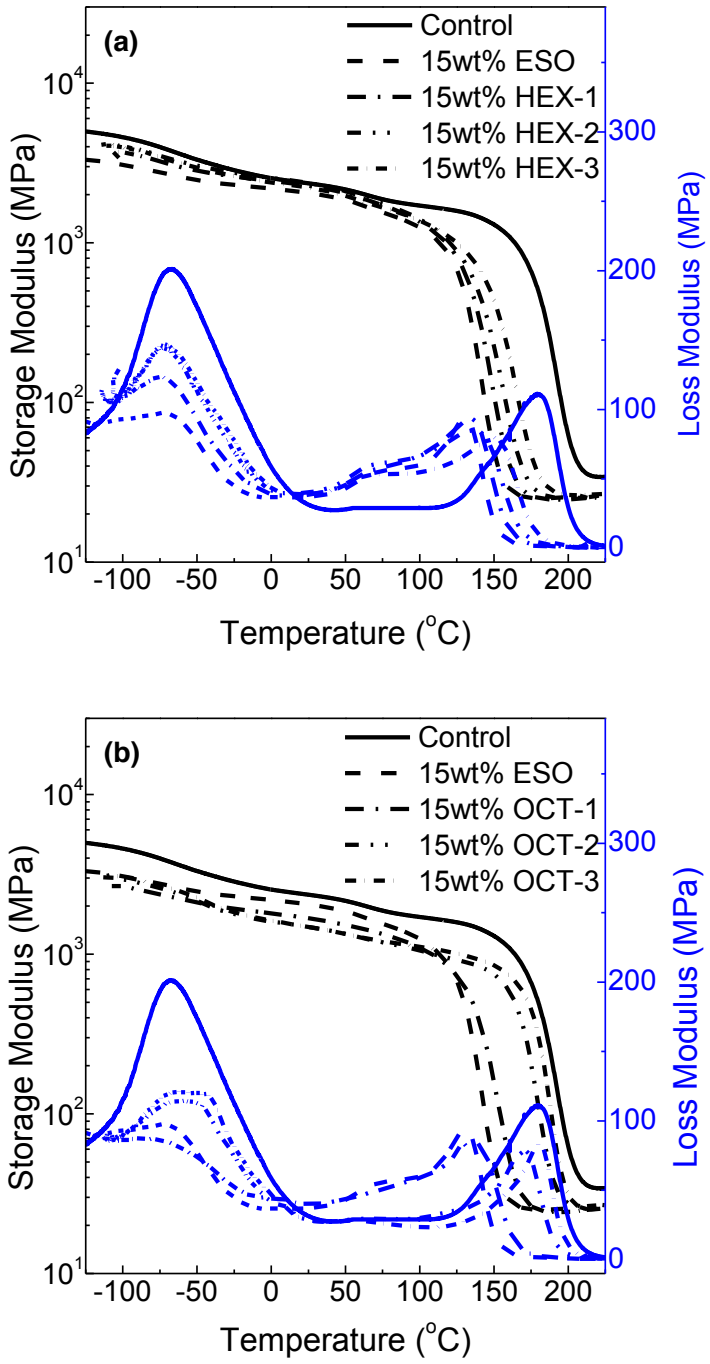

Figure 7.6. DMA thermograms of the control sample and samples toughened with ESO, HEX and OCT series of BRs at 15 wt%.

T_g and E'_{RT} of samples toughened with other BRs were also studies and results are summarized in Table 7.4. As shown, BRs toughened samples all present lower T_g and E'_{RT} values compared with the control sample and this is generally due to the plasticization effect of BRs to the epoxy matrix.[56] At a given BR weight fraction, OCT-3 toughened sample always possesses the highest T_gs (i.e. lowest T_g reduction from the control sample), followed by OCT-2 and OCT-1 toughened samples. This is because, with decreased epoxy functionality and increased MW resulted from the increasing acid molar ratio, OCT-3 is the most favorable to form phase separation in cured network and its plasticization effect is therefore restrained to result in a minimal T_g reduction. At a given acid molar ratio in the BR synthesis, BR prepared with the increasing acid MW tends to result in an increased T_g of BR toughened sample due to the restricted plasticization effect with increased BR MW. Meanwhile, E'_{RT} of BR toughened samples decreases with the increasing acid MW and molar ratio in the BR synthesis as well as BR weight fraction because of the intrinsically softness of BRs with the increasing BR MW.

7.3.5. Fracture toughness properties of polymer samples

BR toughening effect was studied by measuring fracture toughness properties of samples toughened with HEX and OCT series of BRs at 10, 15 and 20 wt%. A sharp pre-crack was made at the notch base of each CT specimen before testing since crack sharpness is critical for the accuracy of fracture toughness results for brittle

Table 7.4. T_g and E'_{RT} of the control sample and samples toughened with BRs at varying weight fractions.

Sample	T_g (°C)			E'_{RT} (GPa)		
Control (100%828)	185			2.52		
15%ESO/85%828	131			2.05		
x =	1	2	3	1	2	3
10%HEX-x/90%828	150	158	155	2.34	2.16	1.98
15%HEX-x/85%828	134	137	150	2.28	2.27	2.22
20%HEX-x/80%828	111	141	173	2.14	1.88	1.57
10%OCT-x/90%828	159	160	181	2.00	1.83	1.71
15%OCT-x/85%828	138	169	180	2.01	1.75	1.52
20%OCT-x/80%828	132	169	183	1.96	1.60	1.49
10%DEC-x/90%828	148	173	184	1.90	1.74	1.61
15%DEC-x/85%828	144	181	184	1.94	1.54	1.65

thermosets.[100] G_{1c} and K_{1c} values of the control and OCT BR toughened samples are plotted in Figure 7.7a and b, respectively. As shown in Figure 7.7a, low G_{1c} and K_{1c} values, 0.14 KJ/m^2 and 0.58 MPa.m$^{1/2}$, respectively, of the control sample indicate its intrinsic brittleness characteristics. Samples toughened with OCT BRs present enhanced G_{1c} values. At a given weight fraction, the different increases of G_{1c} values versus OCT BRs are primarily resulted from the epoxy reactivity and MW of BRs. OCT-1 BR with three residual epoxy groups tends to react into the epoxy matrix and plasticizes the cured network, resulting in a system with low T_g but high toughness. While OCT-3 BR with one residual epoxy group and the largest MW in OCT BR series tends to nucleate rubbery particles and form phase separated architectures, resulting in a system with low T_g reduction and improved fracture toughness through a higher degree of matrix shear deformation and energy dissipation from the cavitation and bifurcation of secondary rubbery phases. On the other hand, at 15 wt%, G_{1c} value of OCT-2 toughened sample is the highest among OCT BRs, but at 20 wt%, G_{1c} value of OCT-1 toughened sample is highest. This indicates BR weight fraction can also affect the toughening effect of OCT BRs, which is probably determined by a balance of several factors, including the matrix ductility with BR retention, formed particle size and interaction between particles and matrix.

G_{1c} and K_{1c} values of HEX BR toughened samples at varying weight fraction were also measured and all toughness results are summarized in Table 7.5. As shown, HEX BR toughened samples generally possess enhanced G_{1c} and K_{1c} values compared with the

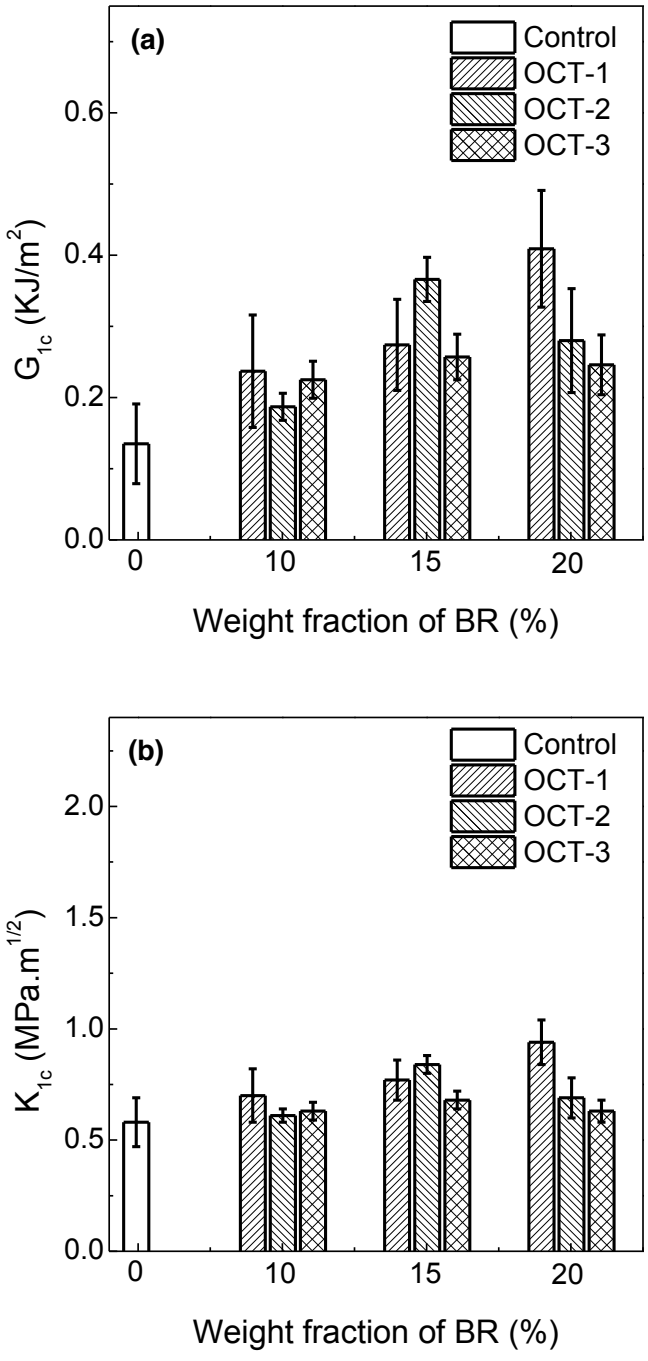

Figure 7.7. G_{1c} (a) and K_{1c} (b) values of the control sample and samples toughened with OCT series of BRs at different weight fractions.

control sample, except 10%HEX-1/90%828 and 10%HEX-3/90%828 samples possessing comparable facture toughness due to the low BR weight fraction. Sample toughened with ESO at 15 wt% presents a G_{1c} value of 224 J/m^2 due to its plasticization effect which results in the a 54 °C T_g reduction. Within a 20 °C T_g reduction calculated from Table 7.4, 20%HEX-3/80%828, 15%OCT-2/85%828, 20%OCT-2/80%828, 10%OCT-3/90%828, 15%OCT-3/85%828 and 20%OCT-3/80%828 samples possess higher G_{1c} values compared with 15%ESO/85%828 sample.

Fracture surface morphology of BR toughened samples was also investigated using AFM. Figure 7.8 displays three-dimension AFM images of selected phase-separated samples whose SEM images are in Figure 7.5. As shown, fracture surfaces of these samples are embedded with crater-like architectures and holes with different sizes, indicating that rubbery particles are formed in cured networks. When a phase-separated sample is fractured at RT, rubbery particles together with the matrix are also fractured. However, since these particles are much tougher and covalently bonded with the matrix, they are unevenly fractured and result in either crater-like architectures or holes. The crater-like architectures are fractured particles sticking on the surfaces and the holes are resulted from the rubbery particles being pulled out from the matrix in which particle residuals can be observed at the bottoms of the holes.[131]

Table 7.5. G_{1c} and K_{1c} values of the control sample and samples toughened with BRs at varying weight fractions.

Sample	G_{1c} (J/m²)			K_{1c} (MPa·m$^{1/2}$)		
Control (100%828)	135±56			0.58±0.11		
15%ESO/85%828	224±116			0.71±0.18		
x =	1	2	3	1	2	3
10%HEX-x/90%828	127±35	193±59	134±32	0.57±0.08	0.62±0.10	0.52±0.06
15%HEX-x/85%828	174±18	187±38	252±86	0.57±0.03	0.66±0.07	0.67±0.11
20%HEX-x/80%828	359±105	389±112	295±51	0.91±0.14	0.89±0.13	0.71±0.06
10%OCT-x/90%828	237±79	187±19	225±26	0.70±0.12	0.61±0.03	0.63±0.04
15%OCT-x/85%828	274±64	366±31	257±32	0.77±0.09	0.84±0.04	0.68±0.04
20%OCT-x/80%828	409±82	280±73	246±42	0.94±0.10	0.69±0.09	0.63±0.05

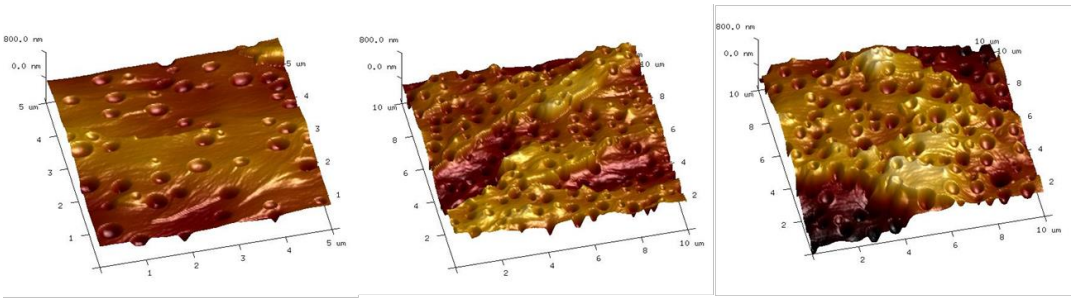

(a) 10%OCT-3/90%828 (b) 15%OCT-3/85%828 (c) 20%OCT-3/80%828

Figure 7.8. Three-dimension AFM images of fracture surfaces of selected samples toughened with OCT-3 BR.

7.4. Conclusions

A series of bio-rubber (BR) tougheners for thermosetting epoxy resins were prepared using epoxidized soybean oil (ESO) and renewable fatty acids with different chain lengths. These acids were grafted onto ESO at varying molar ratios in order to endow BRs with tunable molecular weights (MWs) and epoxy functionalities. BRs were successfully prepared and verified using Fourier transform infrared spectroscopy, gel permeation chromatography, rheometry and epoxy titration. BRs were blended with commercial epoxy resin, DGEBA EPON 828, at different weight fractions and stoichiometrically cured with an aromatic amine hardener, EPIKURE W, to prepare BRs toughened samples. BR toughening effect was investigated by measuring fracture toughness properties of the control and BR toughened samples. T_g and E' of prepared samples were measured using dynamic mechanical analysis. It was demonstrated that BRs with higher MWs and lower epoxy functionalities can dramatically enhance the sample fracture toughness properties without hurting T_g and E' properties. Overall, the thermo-mechanical properties of BR toughened samples were determined by the BR type and weight fraction. Scanning electron microscope and atomic force microscope were utilized to investigate fracture surface morphology of BR toughened samples and secondary phase separations are found to occur in some of BR toughened samples. Formed rubbery particles whose moduli were lower than the epoxy matrix possess varying particle sizes and 300 nm was found to be the particle diameter criterion for sample optical transparency.

Chapter 8. Conclusions and Future Work

8.1. Conclusions

Thermosetting polymer materials are extensively used in numerous industrial applications, such as polymer composites, surface coating, insulation materials and adhesives. These materials own excellent thermal, mechanical and adhesion properties due to the formed cross-linked structures when cure. Most commercial thermosetting materials in current industry are prepared using petroleum feedstocks. Due to the non-renewability of petroleum feedstocks and the demand of protecting health and environment, an increasing interest is raising in preparing thermosetting polymer materials using renewable sources. This dissertation work provides valuable research results regarding the influence of biobased furanyl building blocks, as alternatives to phenyl building blocks, on the cure kinetics and thermo-mechanical properties of thermosetting epoxy and vinyl ester materials. This study also provides a novel approach of using biobased materials, i.e. epoxidized soybean oils, to improve the thermo-mechanical properties of commercial thermosetting epoxy resins.

Accordingly, Chapter 2 introduced the preparation of a furanyl based epoxy resin and its phenyl analogue. After fully cured with amine hardeners, it was found that the furanyl based epoxy resin possesses lower glass transition temperature, higher storage

moduli and superior fracture toughness properties compared with its phenyl analogue. It was also found that furanyl based epoxy resin thermally decomposes at a lower temperature in inert argon environment, but it maintains a higher char yield at 600 °C. These results clearly indicate that biobased furanyl building blocks possess distinctively different influences, relative to the phenyl building blocks, on the thermal and mechanical properties of thermosetting epoxy materials. Furanyl based epoxy resins, therefore, are demonstrated as promising alternatives to the petroleum based thermosetting epoxy incumbents that possess phenyl building blocks.

In Chapter 3, cure kinetics study showed clear differences in the reactivity of these furanyl and phenyl based epoxy resins. The epoxy-primary amine reactivity of furanyl based epoxy resin was found to be significantly greater than that of its phenyl analogue. The reactivity ratio k_2/k_1 of furanyl based epoxy resin was about half that of phenyl analogue suggesting that the formation of network structures in these two systems proceed very differently during cure. Particularly, the furanyl based system should possess a network structure that is characterized by more chain extensions than that of phenyl based system. This result explains the differences in mechanical properties, such as strength and fracture toughness, of these furanyl and phenyl epoxy systems. Hydrogen bonding associated with furanyl groups in the furanyl based epoxy resin during the epoxy-amine reaction could explain the reactivity differences with the phenyl based system since hydrogen bonding with phenyl building block is not possible.

Chapter 4 explored the preparation of furanyl based amine hardeners and investigated the thermo-mechanical properties of fully furanyl based thermosetting polymers. These biobased thermosets present high performance with promising T_gs above 50 °C, high room temperature storage moduli of 3.5 GPa and good thermal stability up to 272 °C (5 wt.% loss) in inert argon environment. Used as amine hardeners for a commercial epoxy resin, DGEBA EPON 828, prepared furanyl based amine hardeners show excellent performance with T_gs well above 120 °C. Therefore, besides in the preparation of epoxy resins, biobased furanyl building blocks also exhibit promising potential for being used to prepare amine hardeners and fully biobased thermosetting polymers with high performance. Together with that in Chapter 2, the work in this chapter enables quantification of the effect of methylene spacers between the aromatic ring and terminal functional epoxy or amine groups on glass transition temperature property. In addition, the higher density values of furanyl based polymers match with their higher glassy storage moduli compared with the phenyl analogous systems.

Chapter 5 investigated the influence of furanyl building block on the thermo-mechanical properties of thermosetting vinyl ester resins. It was found that the furanyl based vinyl ester resin possesses lower glass transition temperature compared with its phenyl analogue, similar to the observations in thermosetting epoxy resin system. The T_g difference between furanyl and phenyl vinyl ester polymers was smaller compared with that in the epoxy resin system. Investigation of cure kinetics at 30 °C of these two

parallel vinyl ester systems indicated the different influences of furanyl building block relative to the phenyl analogue.

Based on the results in previous chapters, Chapter 6 summarized and discussed an additive molar function analysis of the furanyl building block to the physical properties, such as glass transition temperature, density and glassy storage modulus, of thermosetting polymer materials. The molar volume increment value ($V_{a,i}$) and molar glass transition function value (Y_g) of furanyl building block for thermosetting epoxy-amine polymers were obtained. $V_{a,i}$ (298K) of furanyl building block is calculated as 46.8±2.4 cm^3/mol, approximately 18.6 cm^3/mol lower than the recommended value for phenyl building block (65.5 cm^3/mol). Y_g of furanyl building block is calculated as 12.3±3.5 K·Kg/mol, about 17.2 K·Kg/mol lower than that of phenyl building block (29.5 K·Kg/mol). Not been reported in literature to our knowledge, these two values can be very useful in allowing us to estimate and predict physical properties of other furanyl based polymer materials besides thermosetting epoxy and amine materials.

Chapter 7 introduced a novel approach of using biobased materials, i.e. epoxidized soybean oil, to improve the thermo-mechanical properties of commercial thermosetting epoxy resins. Renewable fatty acids with different chain lengths were grafted onto epoxidized soybean oil at varying molar ratios to prepared biobased toughenners for commercial thermosetting epoxy resins. It was demonstrated that biobased toughenners with higher molecular weights and lower epoxy functionalities can dramatically

enhance fracture toughness properties through phase separation without hurting other properties, such as glass transition temperature and storage modulus. Overall, the thermo-mechanical properties of toughened polymer samples were determined by the toughener type and weight fraction. In addition, formed rubbery particles with moduli lower than epoxy matrix possessed varying particle sizes and 300 nm was found to be the particle diameter criterion for sample optical transparency.

It was demonstrated that biobased materials, such as aromatic furanyl building blocks and aliphatic plant oils, can be used as promising alternatives of non-renewable petroleum feedstocks for preparing thermosetting polymer materials with high performance. The results and methodologies in this dissertation can be directly utilized in both scientific and application aspects to direct the design and preparation of novel biobased thermosetting polymer materials.

8.2. Future work

Further investigations inspired by this dissertation work could include:

- Preparing 1, 3-bis[(2-oxiranylmethoxy)methyl]-benzene ("m"-BOB) epoxy monomer and investigating its thermo-mechanical properties to compare with BOF. One of the mentioned differences between BOF and BOB is the

non-collinearity of covalent bonds connecting with the central rings in these two epoxy monomers which is proposed to be responsible for their different thermal and mechanical properties. By experimentally comparing thermal and mechanical properties between "m"-BOB and BOF systems, significant understanding can be achieved to investigate this proposal from the experimental point of view.

- Investigating mechanical properties and higher-temperature cure kinetics of furanyl VE resins to further understand the influence of furanyl building block relative to its phenyl analogue in VE systems.

- Investigating the thermal chemistry of furanyl thermosetting polymers. Current results indicate that, in inert argon environment, furanyl thermosetting materials show very high char yields at high temperature above 600 °C which implies furans transform to more stable structures when heating. A clearer understanding of such transformation could be beneficial for preparing materials for high-temperature applications.

- Investigating the influence of furanyl building block on transport properties, such as mass diffusivity of particular molecules of interest, of thermosetting epoxy and amine materials relative to the phenyl analogues.

- Investigating ways to improve chemical reactions to produce studied furanyl materials with higher yields and industrially favourable processability.

List of References

1. Raquez, J. M.; Deleglise, M.; Lacrampe, M. F.; Krawczak, P., Thermosetting (bio)materials derived from renewable resources: A critical review. *Progress in Polymer Science* **2010,** *35* (4), 487-509.
2. Sharifi, M. Effect of Network Structure/Topology on Mechanical Properties of Crosslinked. Drexel University, 2015.
3. Holbery, J.; Houston, D., Natural-fiber-reinforced polymer composites in automotive applications. *Jom* **2006,** *58* (11), 80-86.
4. La Scala, J. J.; Sands, J. M.; Orlicki, J. A.; Robinette, E. J.; Palmese, G. R., Fatty acid-based monomers as styrene replacements for liquid molding resins. *Polymer* **2004,** *45* (22), 7729-7737.
5. Rogers, D., Lignin-Derived Thermosetting Vinyl Ester Resins for High Performance Applications. **2015**.
6. Pascault, J. P.; Sautereau, H.; Verdu, J.; Williams, R. J. J., *Thermosetting polymers*. CRC: 2002; Vol. 64.
7. Ratna, D., *Handbook of thermoset resins*. ISmithers Shawbury, UK: 2009.
8. Lee, H.; Neville, K., *Handbook of Epoxy Resins*. McGraw-Hill: New York, 1972.
9. Auvergne, R.; Caillol, S.; David, G.; Boutevin, B.; Pascault, J.-P., Biobased thermosetting epoxy: present and future. *Chemical Reviews* **2013,** *114* (2), 1082-1115.
10. Meier, M. A.; Metzger, J. O.; Schubert, U. S., Plant oil renewable resources as green alternatives in polymer science. *Chem Soc Rev* **2007,** *36* (11), 1788-1802.
11. Hu, F.; La Scala, J. J.; Sadler, J. M.; Palmese, G. R., Synthesis and Characterization of Thermosetting Furan-Based Epoxy Systems. *Macromolecules* **2014,** *47* (10), 3332-3342.
12. (a) Montero de Espinosa, L.; Meier, M. A., Plant oils: The perfect renewable resource for polymer science?! *European Polymer Journal* **2011,** *47* (5), 837-852; (b) Lacerda, T. M.; Gandini, A., Marriage of Furans and Vegetable Oils through Click Chemistry for the Preparation of Macromolecular Materials: A Succinct Review. *Journal of Renewable Materials* **2013**, 1-11.
13. (a) Thakur, V. K.; Thakur, M. K., Processing and characterization of natural cellulose fibers/thermoset polymer composites. *Carbohydrate polymers* **2014,** *109*, 102-117; (b) Wool, R.; Sun, X. S., *Bio-based polymers and composites*. Academic Press: 2011.
14. (a) Gay, D., *Composite materials: design and applications*. CRC press: 2014; (b) Belgacem, M. N.; Gandini, A., *Monomers, Polymers and Composites from Renewable*

Resources. 2011; p 220; (c) Belgacem, M. N.; Gandini, A., *Monomers, polymers and composites from renewable resources*. 1st ed.; Elsevier: Amsterdam: Boston, 2008; p 1.
15. (a) Guigo, N.; Mija, A.; Vincent, L.; Sbirrazzuoli, N., Eco-friendly composite resins based on renewable biomass resources: Polyfurfuryl alcohol/lignin thermosets. *European Polymer Journal* **2010,** *46* (5), 1016-1023; (b) Stanzione III, J. F.; Giangiulio, P. A.; Sadler, J. M.; La Scala, J. J.; Wool, R. P., Lignin-based bio-oil mimic as biobased resin for composite applications. *ACS Sustainable Chemistry & Engineering* **2013,** *1* (4), 419-426.
16. (a) Elchinger, P.-H.; Montplaisir, D.; Zerrouki, R., Starch–cellulose crosslinking—Towards a new material. *Carbohydrate Polymers* **2012,** *87* (2), 1886-1890; (b) Patil, N. V.; Netravali, A. N., Nonedible Starch Based "Green" Thermoset Resin Obtained via Esterification Using a Green Catalyst. *ACS Sustainable Chemistry & Engineering* **2016,** *4* (3), 1756-1764.
17. (a) Kasaai, M. R., A review of several reported procedures to determine the degree of N-acetylation for chitin and chitosan using infrared spectroscopy. *Carbohydrate Polymers* **2008,** *71* (4), 497-508; (b) Alhwaige, A. A.; Agag, T.; Ishida, H.; Qutubuddin, S., Biobased chitosan/polybenzoxazine cross-linked films: preparation in aqueous media and synergistic improvements in thermal and mechanical properties. *Biomacromolecules* **2013,** *14* (6), 1806-1815.
18. Hussain, F.; Hojjati, M.; Okamoto, M.; Gorga, R. E., Review article: Polymer-matrix nanocomposites, processing, manufacturing, and application: An overview. *J Compos Mater* **2006,** *40* (17), 1511-1575.
19. Wool, R. P.; Sun, X. S., *Bio-based Polymers and Composites*. 2011; p 7.
20. (a) Czub, P., Synthesis of high-molecular-weight epoxy resins from modified natural oils and Bisphenol A or BisphenolA-based epoxy resins. *Polymers for Advanced Technologies* **2009,** *20* (3), 194-208; (b) Lligadas, G.; Ronda, J. C.; Galià, M.; Cádiz, V., Development of novel phosphorus-containing epoxy resins from renewable resources. *Journal of Polymer Science Part A: Polymer Chemistry* **2006,** *44* (23), 6717-6727.
21. Łukaszczyk, J.; Janicki, B.; Kaczmarek, M., Synthesis and properties of isosorbide based epoxy resin. *European Polymer Journal* **2011,** *47* (8), 1601-1606.
22. (a) Holladay, J. E.; White, J. F.; Bozell, J. J.; Johnson, D. *Top Value-Added Chemicals from Biomass - Volume II—Results of Screening for Potential Candidates from Biorefinery Lignin*; U.S. Department of Energy, Technical Report Office of Scientific and Technical Information, NREL: Oak Ridge, TN, 2007; (b) Tuck, C. O.; Pérez, E.; Horváth, I. T.; Sheldon, R. A.; Poliakoff, M., Valorization of biomass: deriving more value from waste. *Science* **2012,** *337* (6095), 695-699.
23. (a) Cho, J. K.; Lee, J.-S.; Jeong, J.; Kim, B.; Kim, B.; Kim, S.; Shin, S.; Kim, H.-J.; Lee, S.-H., Synthesis of carbohydrate biomass-based furanic compounds

bearing epoxide end group (s) and evaluation of their feasibility as adhesives. *Journal of Adhesion Science and Technology* **2013,** *27* (18-19), 2127-2138; (b) Jeong, J.; Kim, B.; Shin, S.; Kim, B.; Lee, J.-S.; Lee, S.-H.; Cho, J. K., Synthesis and photo-polymerization of bio-based furanic compounds functionalized by 2-hydroxypropyl methacrylate group(s). *J Appl Polym Sci* **2013,** *127* (4), 2483-2489; (c) Gandini, A.; Belgacem, M. N., Furans in polymer chemistry. *Progress in Polymer Science* **1997,** *22* (6), 1203-1379.

24. (a) Peterson, A. M.; Jensen, R. E.; Palmese, G. R., Reversibly Cross-Linked Polymer Gels as Healing Agents for Epoxy− Amine Thermosets. *Acs Appl Mater Inter* **2009,** *1* (5), 992-995; (b) Peterson, A. M.; Palmese, G. R., Reaction Kinetics and Thermodynamic Aspects of Thermoreversibly Cross-Linked Polymer Networks. *Macromolecular Chemistry and Physics* **2013,** *214* (16), 1798-1805.

25. (a) Pratama, P. A.; Peterson, A. M.; Palmese, G. R., Diffusion and Reaction Phenomena in Solution-Based Healing of Polymer Coatings Using the Diels–Alder Reaction. *Macromolecular Chemistry and Physics* **2012,** *213* (2), 173-181; (b) Peterson, A. M.; Jensen, R. E.; Palmese, G. R., Kinetic Considerations for Strength Recovery at the Fiber–Matrix Interface Based on the Diels–Alder Reaction. *Acs Appl Mater Inter* **2013,** *5* (3), 815-821.

26. Palmese, G. R.; Mccullough, R. L., Effect of Epoxy Amine Stoichiometry on Cured Resin Material Properties. *J Appl Polym Sci* **1992,** *46* (10), 1863-1873.

27. (a) Knorr, D. B.; Jian, H. Y.; Richardson, A. D.; Hindenlang, M. D.; McAninch, I. M.; La Scala, J. J.; Lenhart, J. L., Glass transition dependence of ultrahigh strain rate response in amine cured epoxy resins. *Polymer* **2012,** *53* (25), 5917-5923; (b) Espinoza-Perez, J. D.; Nerenz, B. A.; Haagenson, D. M.; Chen, Z.; Ulven, C. A.; Wiesenborn, D. P., Comparison of curing agents for epoxidized vegetable oils applied to composites. *Polymer Composites* **2011,** *32* (11), 1806-1816; (c) Guo, Q., *Thermosets: Structure, properties and applications*. Elsevier: 2012; (d) Schäfer, A.; Seibold, S.; Walter, O.; Döring, M., Novel high Tg flame retardancy approach for epoxy resins. *Polymer Degradation and Stability* **2008,** *93* (2), 557-560.

28. Nouailhas, H.; Aouf, C.; Le Guerneve, C.; Caillol, S.; Boutevin, B.; Fulcrand, H., Synthesis and properties of biobased epoxy resins. part 1. Glycidylation of flavonoids by epichlorohydrin. *Journal of Polymer Science Part A: Polymer Chemistry* **2011,** *49* (10), 2261-2270.

29. Aouf, C.; Nouailhas, H.; Fache, M.; Caillol, S.; Boutevin, B.; Fulcrand, H., Multi-functionalization of gallic acid. Synthesis of a novel bio-based epoxy resin. *European Polymer Journal* **2013,** *49* (6), 1185-1195.

30. (a) Ochi, M.; Shimbo, M.; Saga, M.; Takashima, N., Mechanical and dielectric relaxations of epoxide resins containing spiro-ring structure. *Journal of Polymer Science Part B: Polymer Physics* **1986,** *24* (10), 2185-2195; (b) Ochi, M.; Shiba,

T.; Takeuchi, H.; Yoshizumi, M.; Shimbo, M., Effect of the introduction of methoxy branches on low-temperature relaxations and fracture toughness of epoxide resins. *Polymer* **1989,** *30* (6), 1079-1084.
31. Sachinvala, N. D.; Winsor, D. L.; Menescal, R. K.; Ganjian, I.; Niemczura, W. P.; Litt, M. H., Sucrose-based epoxy monomers and their reactions with diethylenetriamine. *Journal of Polymer Science Part A: Polymer Chemistry* **1998,** *36* (13), 2397-2413.
32. East, A.; Jaffe, M.; Zhang, Y.; Catalani, L. H. *Thermoset epoxy polymers from renewable resources*; Iowa Corn Promotion Board: 2009.
33. (a) Chrysanthos, M.; Galy, J.; Pascault, J.-P., Preparation and properties of bio-based epoxy networks derived from isosorbide diglycidyl ether. *Polymer* **2011,** *52* (16), 3611-3620; (b) Chrysanthos, M.; Galy, J.; Pascault, J. P., Influence of the Bio-Based Epoxy Prepolymer Structure on Network Properties. *Macromolecular Materials and Engineering* **2013,** *298* (11), 1209-1219.
34. Earls, J. D.; White, J. E.; López, L. C.; Lysenko, Z.; Dettloff, M. L.; Null, M. J., Amine-cured ω-epoxy fatty acid triglycerides: Fundamental structure–property relationships. *Polymer* **2007,** *48* (3), 712-719.
35. Koike, T., Progress in development of epoxy resin systems based on wood biomass in Japan. *Polymer Engineering & Science* **2012,** *52* (4), 701-717.
36. Fenouillot, F.; Rousseau, A.; Colomines, G.; Saint-Loup, R.; Pascault, J.-P., Polymers from renewable 1, 4: 3, 6-dianhydrohexitols (isosorbide, isomannide and isoidide): A review. *Progress in Polymer Science* **2010,** *35* (5), 578-622.
37. Morgan, R. J.; Kong, F.-M.; Walkup, C. M., Structure-property relations of polyethertriamine-cured bisphenol-A-diglycidyl ether epoxies. *Polymer* **1984,** *25* (3), 375-386.
38. Thielemans, W.; Can, E.; Morye, S.; Wool, R., Novel applications of lignin in composite materials. *J Appl Polym Sci* **2002,** *83* (2), 323-331.
39. (a) Voirin, C.; Caillol, S.; Sadavarte, N. V.; Tawade, B. V.; Boutevin, B.; Wadgaonkar, P. P., Functionalization of cardanol: towards biobased polymers and additives. *Polymer Chemistry* **2014,** *5* (9), 3142-3162; (b) Li, S.; Yang, X.; Huang, K.; Li, M.; Xia, J., Design, preparation and properties of novel renewable UV-curable copolymers based on cardanol and dimer fatty acids. *Progress in Organic Coatings* **2014,** *77* (2), 388-394; (c) Jaillet, F.; Nouailhas, H.; Auvergne, R.; Ratsimihety, A.; Boutevin, B.; Caillol, S., Synthesis and characterization of novel vinylester prepolymers from cardanol. *Eur J Lipid Sci Tech* **2014,** *116* (7), 928-939; (d) Sultania, M.; Rai, J.; Srivastava, D., Studies on the synthesis and curing of epoxidized novolac vinyl ester resin from renewable resource material. *European Polymer Journal* **2010,** *46* (10), 2019-2032.

40. (a) Stanzione III, J. F.; Sadler, J. M.; La Scala, J. J.; Reno, K. H.; Wool, R. P., Vanillin-based resin for use in composite applications. *Green Chemistry* **2012,** *14* (8), 2346-2352; (b) Zhang, C.; Madbouly, S. A.; Kessler, M. R., Renewable polymers prepared from vanillin and its derivatives. *Macromolecular Chemistry and Physics* **2015,** *216* (17), 1816-1822.
41. (a) Lee, J. S.; Hong, S. I., Synthesis of acrylic rosin derivatives and application as negative photoresist. *European Polymer Journal* **2002,** *38* (2), 387-392; (b) Wilbon, P. A.; Zheng, Y.; Yao, K.; Tang, C., Renewable rosin acid-degradable caprolactone block copolymers by atom transfer radical polymerization and ring-opening polymerization. *Macromolecules* **2010,** *43* (21), 8747-8754; (c) Wang, J. F.; Lin, M. T.; Wang, C. P.; Chu, F. X., Study on the synthesis, characterization, and kinetic of bulk polymerization of disproportionated rosin (β-acryloxyl ethyl) ester. *J Appl Polym Sci* **2009,** *113* (6), 3757-3765; (d) Zheng, Y.; Yao, K.; Lee, J.; Chandler, D.; Wang, J.; Wang, C.; Chu, F.; Tang, C., Well-defined renewable polymers derived from gum rosin. *Macromolecules* **2010,** *43* (14), 5922-5924; (e) Do, H.-S.; Park, J.-H.; Kim, H.-J., UV-curing behavior and adhesion performance of polymeric photoinitiators blended with hydrogenated rosin epoxy methacrylate for UV-crosslinkable acrylic pressure sensitive adhesives. *European Polymer Journal* **2008,** *44* (11), 3871-3882; (f) Do, H. S.; Park, J. H.; Kim, H. J., Synthesis and characteristics of photoactive-hydrogenated rosin epoxy methacrylate for pressure sensitive adhesives. *J Appl Polym Sci* **2009,** *111* (3), 1172-1176.
42. Wilbon, P. A.; Chu, F.; Tang, C., Progress in renewable polymers from natural terpenes, terpenoids, and rosin. *Macromolecular rapid communications* **2013,** *34* (1), 8-37.
43. Sadler, J. M.; Nguyen, A.-P. T.; Toulan, F. R.; Szabo, J. P.; Palmese, G. R.; Scheck, C.; Lutgen, S.; La Scala, J. J., Isosorbide-methacrylate as a bio-based low viscosity resin for high performance thermosetting applications. *Journal of Materials Chemistry A* **2013,** *1* (40), 12579-12586.
44. Li, S.; Xia, J.; Li, M.; Huang, K., New vinyl ester bio-copolymers derived from dimer fatty acids: preparation, characterization and properties. *Journal of the American Oil Chemists' Society* **2013,** *90* (5), 695-706.
45. (a) Grishchuk, S.; Karger-Kocsis, J., Hybrid thermosets from vinyl ester resin and acrylated epoxidized soybean oil (AESO). *Express Polymer Letters* **2011,** *5* (1), 2-11; (b) Khot, S. N.; Lascala, J. J.; Can, E.; Morye, S. S.; Williams, G. I.; Palmese, G. R.; Kusefoglu, S. H.; Wool, R. P., Development and application of triglyceride-based polymers and composites. *J Appl Polym Sci* **2001,** *82* (3), 703-723; (c) Fu, L.; Yang, L.; Dai, C.; Zhao, C.; Ma, L., Thermal and mechanical properties of acrylated expoxidized-soybean oil-based thermosets. *J Appl Polym*

Sci **2010,** *117* (4), 2220-2225; (d) La Scala, J.; Wool, R. P., Property analysis of triglyceride-based thermosets. *Polymer* **2005,** *46* (1), 61-69.
46. Lu, J.; Wool, R. P., Novel thermosetting resins for SMC applications from linseed oil: synthesis, characterization, and properties. *J Appl Polym Sci* **2006,** *99* (5), 2481-2488.
47. Yang, X.; Li, S.; Xia, J.; Song, J.; Huang, K.; Li, M., Novel renewable resource-based UV-curable copolymers derived from myrcene and tung oil: Preparation, characterization and properties. *Industrial Crops and Products* **2015,** *63*, 17-25.
48. (a) Glodek, T. E.; Boyd, S. E.; McAninch, I. M.; LaScala, J. J., Properties and performance of fire resistant eco-composites using polyhedral oligomeric silsesquioxane (POSS) fire retardants. *Composites science and technology* **2008,** *68* (14), 2994-3001; (b) Campanella, A.; La Scala, J. J.; Wool, R. P., The use of acrylated fatty acid methyl esters as styrene replacements in triglyceride-based thermosetting polymers. *Polymer Engineering & Science* **2009,** *49* (12), 2384-2392; (c) Campanella, A.; Scala, J. J. L.; Wool, R., Fatty acid-based comonomers as styrene replacements in soybean and castor oil-based thermosetting polymers. *J Appl Polym Sci* **2011,** *119* (2), 1000-1010.
49. (a) Sharifi, M.; Jang, C.; Abrams, C. F.; Palmese, G. R., Epoxy Polymer Networks with Improved Thermal and Mechanical Properties via Controlled Dispersion of Reactive Toughening Agents. *Macromolecules* **2015,** *48* (20), 7495-7502; (b) Bagheri, R.; Marouf, B.; Pearson, R., Rubber-toughened epoxies: a critical review. *Journal of Macromolecular Science®, Part C: Polymer Reviews* **2009,** *49* (3), 201-225.
50. (a) Zhou, H. S.; Song, X. X.; Xu, S. A., Mechanical and thermal properties of novel rubber-toughened epoxy blend prepared by in situ pre-crosslinking. *Journal of Applied Polymer Science* **2014,** *131* (22); (b) Wu, S.; Guo, Q.; Kraska, M.; Stuhn, B.; Mai, Y.-W., Toughening epoxy thermosets with block ionomers: the role of phase domain size. *Macromolecules* **2013,** *46* (20), 8190-8202; (c) Jin, Q.; Misasi, J. M.; Wiggins, J. S.; Morgan, S. E., Simultaneous reinforcement and toughness improvement in an aromatic epoxy network with an aliphatic hyperbranched epoxy modifier. *Polymer* **2015,** *73*, 174-182; (d) Declet-Perez, C.; Francis, L. F.; Bates, F. S., Deformation Processes in Block Copolymer Toughened Epoxies. *Macromolecules* **2015**.
51. (a) Liu, S.; Fan, X.; He, C., Improving the Fracture Toughness of Epoxy with Nanosilica-Rubber Core-Shell Nanoparticles. *Composites Science and Technology* **2016**; (b) Quan, D.; Ivankovic, A., Effect of core–shell rubber (CSR) nano-particles on mechanical properties and fracture toughness of an epoxy polymer. *Polymer* **2015,** *66*, 16-28; (c) Zhang, J.; Deng, S.; Wang, Y.; Ye, L., Role of

rigid nanoparticles and CTBN rubber in the toughening of epoxies with different cross-linking densities. *Composites Part A: Applied Science and Manufacturing* **2016,** *80*, 82-94; (d) Guan, L. Z.; Gong, L. X.; Tang, L. C.; Wu, L. B.; Jiang, J. X.; Lai, G. Q., Mechanical properties and fracture behaviors of epoxy composites with phase-separation formed liquid rubber and preformed powered rubber nanoparticles: A Comparative study. *Polymer Composites* **2014**; (e) Tang, L.-C.; Wan, Y.-J.; Yan, D.; Pei, Y.-B.; Zhao, L.; Li, Y.-B.; Wu, L.-B.; Jiang, J.-X.; Lai, G.-Q., The effect of graphene dispersion on the mechanical properties of graphene/epoxy composites. *Carbon* **2013,** *60*, 16-27.

52. (a) Palmese, G. R.; LaScala, J. J.; Sands, J. M.; Geng, X., Toughening cross-linked thermosets. Google Patents: 2014; (b) Palmese, G. R.; Yadav, S. K.; Hu, F., Toughening of Anhydride Cured Thermosetting Epoxy Polymers Using Grafted Triglycerides. US Patent 20,160,075,872: 2016; (c) Rico, M.; López, J.; Montero, B.; Bellas, R., Phase separation and morphology development in a thermoplastic-modified toughened epoxy. *European Polymer Journal* **2012,** *48* (10), 1660-1673; (d) Mathew, V. S.; George, S. C.; Parameswaranpillai, J.; Thomas, S., Epoxidized natural rubber/epoxy blends: Phase morphology and thermomechanical properties. *J Appl Polym Sci* **2014,** *131* (4).

53. (a) Yee, A. F.; Pearson, R. A., Toughening mechanisms in elastomer-modified epoxies. *J Mater Sci* **1986,** *21* (7), 2462-2474; (b) Bascom, W.; Ting, R.; Moulton, R.; Riew, C.; Siebert, A., The fracture of an epoxy polymer containing elastomeric modifiers. *J Mater Sci* **1981,** *16* (10), 2657-2664.

54. (a) Liu, Z.; Erhan, S. Z.; Akin, D. E.; Barton, F. E., "Green" composites from renewable resources: preparation of epoxidized soybean oil and flax fiber composites. *Journal of agricultural and food chemistry* **2006,** *54* (6), 2134-2137; (b) Wang, R.; Schuman, T. P., Vegetable oil-derived epoxy monomers and polymer blends: a comparative study with review. *eXPRESS Polymer Letters* **2013,** *7* (3), 272-292.

55. (a) Sahoo, S. K.; Mohanty, S.; Nayak, S. K., Synthesis and characterization of bio-based epoxy blends from renewable resource based epoxidized soybean oil as reactive diluent. *Chinese Journal of Polymer Science* **2015,** *33* (1), 137-152; (b) Ratna, D.; Banthia, A. K., Epoxidized soybean oil toughened epoxy adhesive. *Journal of Adhesion Science and Technology* **2000,** *14* (1), 15-25; (c) Tan, S.; Chow, W., Biobased epoxidized vegetable oils and its greener epoxy blends: A review. *Polymer-Plastics Technology and Engineering* **2010,** *49* (15), 1581-1590; (d) Tan, S. G.; Ahmad, Z.; Chow, W. S., Interpenetrating polymer network structured thermosets prepared from epoxidized soybean oil/diglycidyl ether of bisphenol A. *Polymer International* **2014,** *63* (2), 273-279.

56. Ratna, D.; Banthia, A. K., Rubber toughened epoxy. *Macromolecular research* **2004,** *12* (1), 11-21.
57. Sharma, V.; Kundu, P., Addition polymers from natural oils—a review. *Progress in Polymer Science* **2006,** *31* (11), 983-1008.
58. Khot, S. N.; Lascala, J. J.; Can, E.; Morye, S. S.; Williams, G. I.; Palmese, G. R.; Kusefoglu, S. H.; Wool, R. P., Development and application of triglyceride-based polymers and composites. *J Appl Polym Sci* **2001,** *82* (3), 703-723.
59. Chokhawala, H. A high yield route for the production of compounds from renewable sources. 2015.
60. Biermann, U.; Bornscheuer, U.; Meier, M. A.; Metzger, J. O.; Schäfer, H. J., Oils and fats as renewable raw materials in chemistry. *Angewandte Chemie International Edition* **2011,** *50* (17), 3854-3871.
61. Knothe, G., Biodiesel and renewable diesel: a comparison. *Progress in Energy and Combustion Science* **2010,** *36* (3), 364-373.
62. (a) Prime, R. B.; Turi, E. A., Thermal characterization of polymeric materials. *Turi, EA, Ed* **1981,** *1380*; (b) Wisanrakkit, G.; Gillham, J.; Enns, J., The glass transition temperature (Tg) as a parameter for monitoring the cure of an amine/epoxy system at constant heating rates. *J Appl Polym Sci* **1990,** *41* (7-8), 1895-1912.
63. Pascault, J.-P.; Williams, R. J., *Epoxy polymers*. John Wiley & Sons: 2009.
64. Bruins, P. F., *Unsaturated polyester technology*. CRC Press: 1976.
65. Li III, H., Synthesis, characterization and properties of vinyl ester matrix resins. **1998**.
66. La Scala, J. J.; Orlicki, J. A.; Winston, C.; Robinette, E. J.; Sands, J. M.; Palmese, G. R., The use of bimodal blends of vinyl ester monomers to improve resin processing and toughen polymer properties. *Polymer* **2005,** *46* (9), 2908-2921.
67. Mishra, M.; Yagci, Y., *Handbook of radical vinyl polymerization*. CRC Press: 1998; Vol. 73.
68. Monyatsi, O., Free Radical Polymerization studies of vinyl ester monomers using Pulsed-Lased Polymerization with Size Exclusion Chromatography (PLP-SEC). **2015**.
69. Young, R. J.; Lovell, P. A., *Introduction to polymers*. CRC press: 2011.
70. Moroni, A.; Mijovic, J.; Pearce, E. M.; Foun, C. C., Cure kinetics of epoxy resins and aromatic diamines. *J Appl Polym Sci* **1986,** *32* (2), 3761-3773.
71. Zhao, L.; Hu, X., A variable reaction order model for prediction of curing kinetics of thermosetting polymers. *Polymer* **2007,** *48* (20), 6125-6133.
72. González, M. G.; Baselga, J.; Cabanelas, J. C., *Applications of FTIR on epoxy resins-identification, monitoring the curing process, phase separation and water uptake*. INTECH Open Access Publisher: 2012.

73. Zvetkov, V., Comparative DSC kinetics of the reaction of DGEBA with aromatic diamines.: I. Non-isothermal kinetic study of the reaction of DGEBA with m-phenylene diamine. *Polymer* **2001,** *42* (16), 6687-6697.
74. Mijovic, J.; Andjelic, S., A study of reaction kinetics by near-infrared spectroscopy. 1. Comprehensive analysis of a model epoxy/amine system. *Macromolecules* **1995,** *28* (8), 2787-2796.
75. Xu, L.; Schlup, J. R., Etherification versus amine addition during epoxy resin/amine cure: An in situ study using near-infrared spectroscopy. *J Appl Polym Sci* **1998,** *67* (5), 895-901.
76. Fengshuo, H.; Majid, S.; Giuseppe, P., Influence of Furanyl Building Blocks on the Cure Kinetics of a Renewable Epoxy-Amine System. In *Green Polymer Chemistry: Biobased Materials and Biocatalysis*, American Chemical Society: 2015; Vol. 1192, pp 387-399.
77. Mijovic, J.; Andjelic, S.; Yee, C. W.; Bellucci, F.; Nicolais, L., A study of reaction kinetics by near-infrared spectroscopy. 2. Comparison with dielectric spectroscopy of model and multifunctional epoxy/amine systems. *Macromolecules* **1995,** *28* (8), 2797-2806.
78. Smith, I. T., The mechanism of the crosslinking of epoxide resins by amines. *Polymer* **1961,** *2*, 95-108.
79. (a) Horie, K.; Hiura, H.; Sawada, M.; Mita, I.; Kambe, H., Calorimetric investigation of polymerization reactions. III. Curing reaction of epoxides with amines. *Journal of Polymer Science Part A-1: Polymer Chemistry* **1970,** *8* (6), 1357-1372; (b) Simon, S. L.; Mckenna, G. B.; Sindt, O., Modeling the evolution of the dynamic mechanical properties of a commercial epoxy during cure after gelation. *J Appl Polym Sci* **2000,** *76* (4), 495-508.
80. Ehlers, J.-E.; Rondan, N. G.; Huynh, L. K.; Pham, H.; Marks, M.; Truong, T. N., Theoretical study on mechanisms of the epoxy-amine curing reaction. *Macromolecules* **2007,** *40* (12), 4370-4377.
81. (a) Varley, R. J.; Liu, W.; Simon, G. P., Investigation of the reaction mechanism of different epoxy resins using a phosphorus-based hardener. *J Appl Polym Sci* **2006,** *99* (6), 3288-3299; (b) Raman, V. I.; Palmese, G. R., Influence of tetrahydrofuran on epoxy-amine polymerization. *Macromolecules* **2005,** *38* (16), 6923-6930.
82. (a) Brill, R. P.; Palmese, G. R., An investigation of vinyl-ester - Styrene bulk copolymerization cure kinetics using Fourier transform infrared spectroscopy. *J Appl Polym Sci* **2000,** *76* (10), 1572-1582; (b) Ziaee, S.; Palmese, G. R., Effects of temperature on cure kinetics and mechanical properties of vinyl-ester resins. *J Polym Sci Pol Phys* **1999,** *37* (7), 725-744; (c) Dua, S.; McCullough, R.; Palmese, G., Copolymerization kinetics of styrene/vinyl-ester systms: Low

temperature reactions. *Polymer composites* **1999,** *20* (3), 379-391; (d) Liu, C.; Li, T.; Zhang, J.; Chen, S.; Xu, Z.; Zhang, A.; Zhang, D., Preparation and properties of phosphorous–nitrogen containing UV-curable polymeric coatings based on thiol–ene click reaction. *Progress in Organic Coatings* **2016,** *90*, 21-27; (e) Scott, T. F.; Cook, W. D.; Forsythe, J. S., Kinetics and network structure of thermally cured vinyl ester resins. *European Polymer Journal* **2002,** *38* (4), 705-716; (f) Sadler, J.; McAninch, I. M.; Toulan, F. R.; Levine, F.; La Scala, J. J. *Resin Characterization*; DTIC Document: 2015.

83. Kamal, M.; Sourour, S., Kinetics and thermal characterization of thermoset cure. *Polymer Engineering & Science* **1973,** *13* (1), 59-64.

84. McCrum, N. G.; Buckley, C. P.; Bucknall, C. B., *Principles of polymer engineering*. Oxford University Press.: New York, 1997.

85. (a) Painter, P. C.; Coleman, M. M., *Fundamentals of polymer science: an introductory text*. Technomic Pub. Co.: Lancaster, Pa., 1997; (b) Ellis, B., *Chemistry and Technology of Epoxy Resins*. Blackie: New York, 1992; (c) May, C. A., *Epoxy Resins: Chemistry and Technology*. 2nd ed.; Marcel Dekker: New York, 1988; (d) Zheng, S.; Pascault, J.; Williams, R., Epoxy polymers: new materials and innovations. *Pascault, JP, Williams, RJJ, Eds* **2010**.

86. Meier, M. A. R.; Metzger, J. O.; Schubert, U. S., Plant oil renewable resources as green alternatives in polymer science. *Chem Soc Rev* **2007,** *36* (11), 1788-1802.

87. Ravi Kumar, M. N., A review of chitin and chitosan applications. *Reactive and functional polymers* **2000,** *46* (1), 1-27.

88. (a) Tsujigami, T.; Sugai, T.; Ohta, H., Microbial asymmetric reduction of alpha-hydroxyketones in the anti-Prelog selectivity. *Tetrahedron-Asymmetr* **2001,** *12* (18), 2543-2549; (b) Sun, F. L.; Xu, G.; Wu, H. P.; Yang, L. R., Efficient lipase-catalyzed kinetic resolution of 4-arylmethoxy-3-hydroxybutanenitriles: application to an expedient synthesis of a statin intermediate. *Tetrahedron-Asymmetr* **2006,** *17* (20), 2907-2913.

89. Tian, Q.; Rong, M. Z.; Zhang, M. Q.; Yuan, Y. C., Synthesis and characterization of epoxy with improved thermal remendability based on Diels-Alder reaction. *Polymer International* **2010,** *59* (10), 1339-1345.

90. ASTM D1652-97, Standard Test Methods for Epoxy Content of Epoxy Resins. ASTM International: West Conshohocken, PA, 1997; p 3.

91. McAninch, I. M.; Palmese, G. R.; Lenhart, J. L.; La Scala, J. J., Characterization of epoxies cured with bimodal blends of polyetheramines. *J Appl Polym Sci* **2013,** *130* (3), 1621-1631.

92. ASTM D638-03, Standard Test Method for Tensile Properties of Plastics. In *Annual Book of ASTM Standards. Part*, ASTM International: West Conshohocken, PA, 1998.
93. ASTM D5045-99, Standard Test Methods for Plane-Strain Fracture Toughness and Strain Energy Release Rate of Plastic Materials. ASTM International: West Conshohocken, PA, 1999.
94. (a) Mijovic, J.; Andjelic, S., A Study of Reaction-Kinetics by near-Infrared Spectroscopy .1. Comprehensive Analysis of a Model Epoxy/Amine System. *Macromolecules* **1995,** *28* (8), 2787-2796; (b) George, G. A.; Coleclarke, P.; Stjohn, N.; Friend, G., Real-Time Monitoring of the Cure Reaction of a Tgddm/Dds Epoxy-Resin Using Fiber Optic Ft-Ir. *J Appl Polym Sci* **1991,** *42* (3), 643-657.
95. (a) He, Y.; Zhu, B.; Inoue, Y., Hydrogen bonds in polymer blends. *Progress in Polymer Science* **2004,** *29* (10), 1021-1051; (b) Su, Y.-C.; Kuo, S.-W.; Yei, D.-R.; Xu, H.; Chang, F.-C., Thermal properties and hydrogen bonding in polymer blend of polybenzoxazine/poly(*N*-vinyl-2-pyrrolidone). *Polymer* **2003,** *44* (8), 2187-2191.
96. (a) He, Y.; Asakawa, N.; Inoue, Y., Studies on poly (ε-caprolactone)/thiodiphenol blends: The specific interaction and the thermal and dynamic mechanical properties. *Journal of Polymer Science Part B: Polymer Physics* **2000,** *38* (14), 1848-1859; (b) Liu, Y.; Goh, S.; Lee, S.; Huan, C., Miscibility and Interactions in Blends and Complexes of Poly (N-acryloyl-N'-methylpiperazine) with Poly (p-vinylphenol). *Macromolecules* **1999,** *32* (6), 1967-1971; (c) Chen, N.; Hong, L., Surface phase morphology and composition of the casting films of PVDF–PVP blend. *Polymer* **2002,** *43* (4), 1429-1436; (d) Iriondo, P.; Iruin, J.; Fernandez-Berridi, M., Thermal and infra-red spectroscopic investigations of a miscible blend composed of poly (vinyl phenol) and poly (hydroxybutyrate). *Polymer* **1995,** *36* (16), 3235-3237.
97. Duan, Y.; Pearce, E. M.; Kwei, T.; Hu, X.; Rafailovich, M.; Sokolov, J.; Zhou, K.; Schwarz, S., Surface enrichment in polymer blends involving hydrogen bonding. *Macromolecules* **2001,** *34* (19), 6761-6767.
98. Bellenger, V.; Verdu, J.; Morel, E., Effect of Structure on Glass-Transition Temperature of Amine Cross-Linked Epoxies. *J Polym Sci Pol Phys* **1987,** *25* (6), 1219-1234.
99. (a) Peterson, A. M.; Jensen, R. E.; Palmese, G. R., Room-Temperature Healing of a Thermosetting Polymer Using the Diels-Alder Reaction. *Acs Appl Mater Inter* **2010,** *2* (4), 1141-1149; (b) Sheng, X.; Kessler, M.; Lee, J., The influence of cross-linking agents on ring-opening metathesis polymerized thermosets. *Journal of thermal analysis and calorimetry* **2007,** *89* (2), 459-464.

100. Ma, J.; Qi, Q.; Bayley, J.; Du, X.-S.; Mo, M.-S.; Zhang, L.-Q., Development of SENB toughness measurement for thermoset resins. *Polymer testing* **2007,** *26* (4), 445-450.
101. Watters, A. L., Synthesis and Characterization of a Well-Dispersed Nanostructured Polymer System. **2014**.
102. Sharifi, M.; Jang, C.; Abrams, C.; Palmese, G., Toughened epoxy polymers via rearrangement of network topology. *Journal of Materials Chemistry A* **2014,** *2* (38), 16071-16082.
103. Yang, J. S. A. J., C. W.; Abrams, C. F., Relationships Between Molecular Structure and Thermomechanical Properties of Bio-Based Thermosetting Polymers. *Submitted to J. Polym. Sci., Part B: Polym. Phys.* **2016**.
104. Hu, F.; Yadav, S. K.; La Scala, J. J.; Sadler, J. M.; Palmese, G. R., Preparation and Characterization of Fully Furan-Based Renewable Thermosetting Epoxy-Amine Systems. *Macromolecular Chemistry and Physics* **2015,** *216* (13), 1441-1446.
105. Fache, M.; Auvergne, R.; Boutevin, B.; Caillol, S., New vanillin-derived diepoxy monomers for the synthesis of biobased thermosets. *European Polymer Journal* **2014**.
106. Belgacem, M. N.; Gandini, A., *Monomers, polymers and composites from renewable resources*. Elsevier: 2011.
107. Mijovic, J.; Fishbain, A.; Wijaya, J., Mechanistic modeling of epoxy-amine kinetics. 1. Model compound study. *Macromolecules* **1992,** *25* (2), 979-985.
108. Gandini, A., Polymers from renewable resources: a challenge for the future of macromolecular materials. *Macromolecules* **2008,** *41* (24), 9491-9504.
109. Gandini, A.; Coelho, D.; Gomes, M.; Reis, B.; Silvestre, A., Materials from renewable resources based on furan monomers and furan chemistry: work in progress. *J Mater Chem* **2009,** *19* (45), 8656-8664.
110. Chang, R.; Qin, J.; Gao, J., Fully biobased epoxy from isosorbide diglycidyl ether cured by biobased curing agents with enhanced properties. *Journal of Polymer Research* **2014,** *21* (7), 1-7.
111. (a) Siraki, A. G.; Chan, T. S.; Galati, G.; Teng, S.; O'Brien, P. J., N-oxidation of aromatic amines by intracellular oxidases. *Drug Metabolism Reviews* **2002,** *34* (3), 549-564; (b) Ding, C.; Matharu, A. S., Recent developments on biobased curing agents: a review of their preparation and use. *ACS Sustainable Chemistry & Engineering* **2014,** *2* (10), 2217-2236.
112. Holfinger, M. S.; Conner, A. H.; Holm, D. R.; Hill Jr, C. G., Synthesis of difurfuryl diamines by the acidic condensation of furfurylamine with aldehydes and their mechanism of formation. *The Journal of Organic Chemistry* **1995,** *60* (6), 1595-1598.

113. Bellenger, V.; Verdu, J.; Morel, E., Effect of structure on glass transition temperature of amine crosslinked epoxies. *Journal of Polymer Science Part B: Polymer Physics* **1987,** *25* (6), 1219-1234.
114. Javni, I.; Zhang, W.; Petrović, Z. S., Effect of different isocyanates on the properties of soy-based polyurethanes. *J Appl Polym Sci* **2003,** *88* (13), 2912-2916.
115. Mark, J. E., *Polymer data handbook*. Oxford university press: 2009.
116. Bellamy, L., *The infra-red spectra of complex molecules*. Springer Science & Business Media: 2013.
117. Lam, P.; Plaumann, H.; Tran, T., An improved kinetic model for the autocatalytic curing of styrene-based thermoset resins. *J Appl Polym Sci* **1990,** *41* (11-12), 3043-3057.
118. Ziaee, S.; Palmese, G. R., Effects of temperature on cure kinetics and mechanical properties of vinyl–ester resins. *Journal of Polymer Science Part B: Polymer Physics* **1999,** *37* (7), 725-744.
119. Bicerano, J., Prediction of the properties of polymers from their structures. *Journal of Macromolecular Science, Part C: Polymer Reviews* **1996,** *36* (1), 161-196.
120. Van Krevelen, D. W.; Te Nijenhuis, K., *Properties of polymers: their correlation with chemical structure; their numerical estimation and prediction from additive group contributions*. Elsevier: 2009.
121. Hopfinger, A.; Koehler, M.; Pearlstein, R.; Tripathy, S., Molecular modeling of polymers. IV. Estimation of glass transition temperatures. *Journal of Polymer Science Part B: Polymer Physics* **1988,** *26* (10), 2007-2028.
122. Thomas, S.; Sinturel, C.; Thomas, R., *Micro and Nanostructured Epoxy/Rubber Blends*. John Wiley & Sons: 2014.
123. Auvergne, R. m.; Caillol, S.; David, G.; Boutevin, B.; Pascault, J.-P., Biobased thermosetting epoxy: present and future. *Chemical reviews* **2013,** *114* (2), 1082-1115.
124. (a) Zhou, H. S.; Song, X. X.; Xu, S. A., Mechanical and thermal properties of novel rubber-toughened epoxy blend prepared by in situ pre-crosslinking. *J Appl Polym Sci* **2014,** *131* (22); (b) Chen, J.; Kinloch, A.; Sprenger, S.; Taylor, A., The mechanical properties and toughening mechanisms of an epoxy polymer modified with polysiloxane-based core-shell particles. *Polymer* **2013,** *54* (16), 4276-4289; (c) Li, X.; Kang, H.-l.; Shen, J.-x.; Nishi, T.; Ito, K., Miscibility, intramolecular specific interactions and mechanical properties of a DGEBA based epoxy resin toughened with a sliding graft copolymer. *Chinese Journal of Polymer Science* **2015,** *33* (3), 433-443; (d) Liu, W.; Zhou, R.; Goh, H. L. S.; Huang, S.; Lu, X., From Waste to Functional Additive: Toughening Epoxy Resin with Lignin. *Acs Appl Mater Inter* **2014,** *6* (8), 5810-5817; (e) Buonocore, G. G.; Schiavo, L.; Attianese, I.; Borriello, A., Hyperbranched polymers as modifiers of epoxy adhesives.

Composites Part B: Engineering **2013,** *53*, 187-192; (f) Dhevi, D. M.; Jaisankar, S.; Pathak, M., Effect of new hyperbranched polyester of varying generations on toughening of epoxy resin through interpenetrating polymer networks using urethane linkages. *European Polymer Journal* **2013,** *49* (11), 3561-3572; (g) Mohan, P., A Critical Review: The Modification, Properties, and Applications of Epoxy Resins. *Polymer-Plastics Technology and Engineering* **2013,** *52* (2), 107-125.
125. Palmese, G. R.; LaScala, J. J.; Sands, J. M.; Geng, X. Toughening cross-linked thermosets. 2014.
126. McGarry, F. J.; Willner, A. M., *Toughening of an epoxy resin by an elastomeric second phase*. MIT Department of Civil Engineering, Materials Research Laboratory: 1968.
127. Yang, X.; Li, S.; Xia, J.; Song, J.; Huang, K.; Li, M., Renewable Myrcene-based UV-curable Monomer and its Copolymers with Acrylated Epoxidized Soybean Oil: Design, Preparation, and Characterization. *BioResources* **2015,** *10* (2), 2130-2142.
128. ASTM D5045-99, Standard Test Methods for Plane-Strain Fracture Toughness and Strain Energy Release Rate of Plastic Materials. In *Annual Book of ASTM Standards. Part*, ASTM International: West Conshohocken, PA, 1999; Vol. 8.
129. Lin, B.; Yang, L.; Dai, H.; Yi, A., Kinetic studies on oxirane cleavage of epoxidized soybean oil by methanol and characterization of polyols. *Journal of the American Oil Chemists' Society* **2008,** *85* (2), 113-117.
130. Esen, H.; Küsefoğlu, S.; Wool, R., Photolytic and free-radical polymerization of monomethyl maleate esters of epoxidized plant oil triglycerides. *J Appl Polym Sci* **2007,** *103* (1), 626-633.
131. VanLandingham, M.; McKnight, S.; Palmese, G.; Elings, J.; Huang, X.; Bogetti, T.; Eduljee, R.; Gillespie Jr, J., Nanoscale indentation of polymer systems using the atomic force microscope. *The Journal of adhesion* **1997,** *64* (1-4), 31-59.

Appendix A. Initial attempts at preparing BOF and BOB epoxy monomers

Catalyst, reaction temperature and sodium hydroxide solution concentration are critical for the preparation of BOF and BOB. The reported reaction conditions are the optimization after several initial attempts. It should be noted that when preparing BOF, one should pay extra attention to control the reaction temperature below 50 °C when adding the high-concentration sodium hydroxide solution slowly into the reactor. No more than 2 hours shall the second step of the reaction be allowed; otherwise the overall yield of BOF will be lower than as expected. The post-treatment of BOF-contained mixture should be conducted right after the reaction is finished since BOF monomer, i.e. the furanyl ring, is not inert in the alkaline environment. One can add epichlorohydrin in excess when preparing BOF which will certainly improve the yield of BOF, but this action leads to extra labor during the post-treatment and epichlorohydrin recycling steps. During the purification step, one can use the flash chromatography instead of the regular column chromatography which can significantly shorten the purification time. BOF can be directly used without purification, similarly with the DGEBA case, and the resulting properties can be desirable based on the application requirement. As discussed in Chapters 1 and 2, the reason of purifying BOF is to investigate the influence of furanyl ring by eliminating undesirable factors such as impurities.

Appendix B. Model fitting of experimental fractional conversions of VE and ST double bonds in BOF VE-ST and BOB VE-ST systems at 30 °C

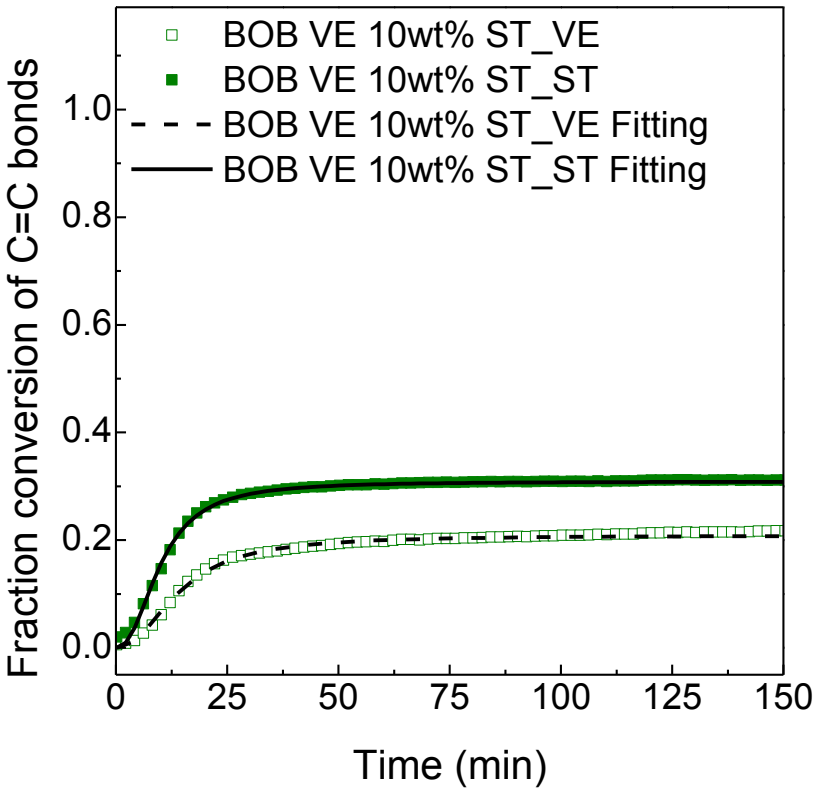

Figure B.1. Model fitting of experimental fractional conversions of BOB VE and ST monomers in BOB VE 10 wt% ST system at 30 °C using Equation 1.15.

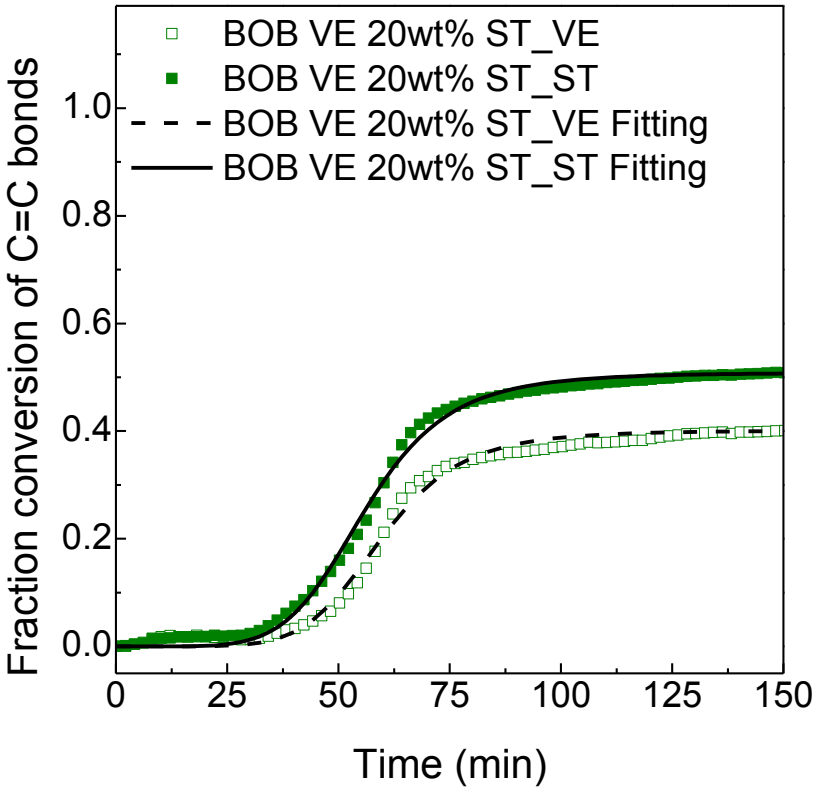

Figure B.2. Model fitting of experimental fractional conversions of BOB VE and ST monomers in BOB VE 20 wt% ST system at 30 °C using Equation 1.15.

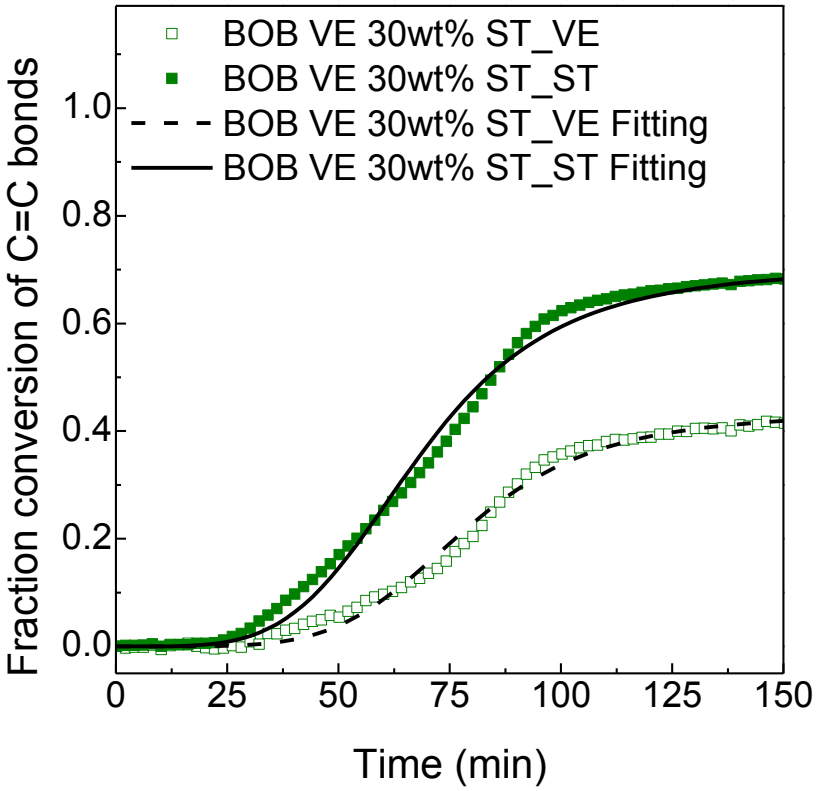

Figure B.3. Model fitting of experimental fractional conversions of BOB VE and ST monomers in BOB VE 30 wt% ST system at 30 °C using Equation 1.15.

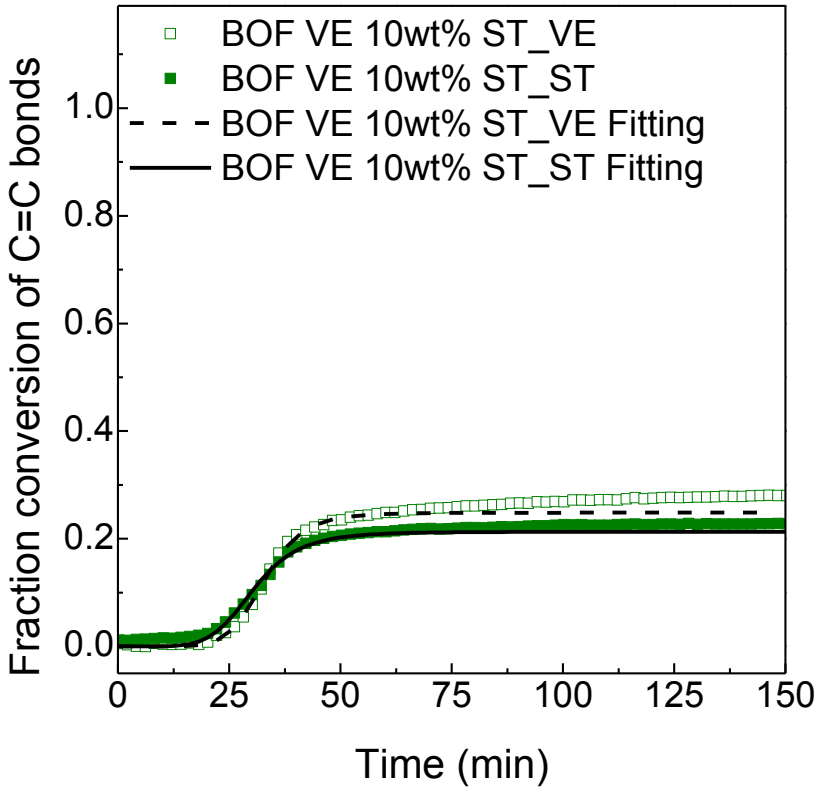

Figure B.4. Model fitting of experimental fractional conversions of BOF VE and ST monomers in BOF VE 10 wt% ST system at 30 °C using Equation 1.15.

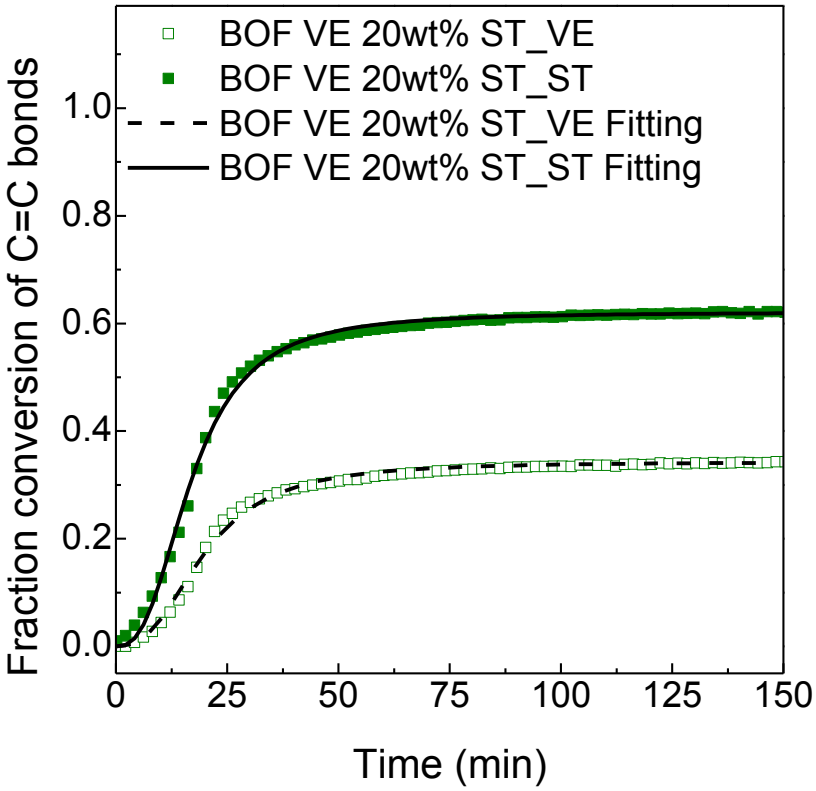

Figure B.5. Model fitting of experimental fractional conversions of BOF VE and ST monomers in BOF VE 20 wt% ST system at 30 °C using Equation 1.15.

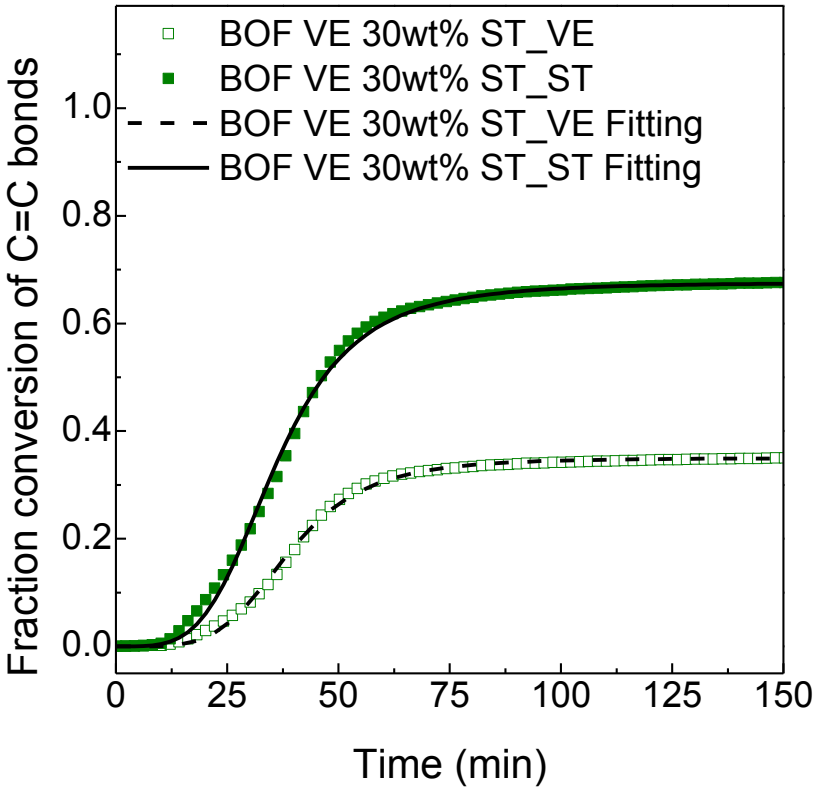

Figure B.6. Model fitting of experimental fractional conversions of BOF VE and ST monomers in BOF VE 30 wt% ST system at 30 °C using Equation 1.15.

Appendix C. Calculations in Chapter 6

Calculation of ρg(298K) for BOB-PACM system:

$V_{g,BOB-PACM}(298K) = \sum_i V_{a,i}\,(298K) = 1 * 65.5 + 6.5 * 16.37 + 2 * 8.5 + 2 * 22.3 + 1 * 0 + 1 * 86 = 319.56\ cm^3/mol$

$\rho_{g,BOB-PACM}(298K) = \frac{M_{BOB-PACM}}{V_{g,BOB-PACM}(298K)} = \frac{355.47\ g/mol}{319.56\ cm^3/mol} = 1.112\ g/cm^3$

Calculation of ρg(298K) for BOB-EPIKURE W system:

$V_{g,BOB-EPIKURE\,W}(298K) = \sum_i V_{a,i}\,(298K) = 1 * 65.5 + 6 * 16.37 + 2 * 8.5 + 2 * 22.3 + 1 * 0 + 0.5 * 164 = 307.32\ cm^3/mol$

$\rho_{g,BOB-EPIKURE\,W}(298K) = \frac{M_{BOB-EPIKURE\,W}}{V_{g,BOB-EPIKURE\,W}(298K)} = \frac{339.43\ g/mol}{307.32\ cm^3/mol} = 1.104\ g/cm^3$

Calculation of $V_{a,i\ furanyl}$ (298K) from BOF-PACM and BOB-PACM sample pair:

$$V_{g,BOF-PACM}(298K) = \frac{M_{BOF-PACM}}{\rho_{exp.\ BOF-PACM}} = \frac{345.43\ g.mol}{1.210\ g/cm^3} = 285.50\ cm^3/mol$$

$$V_{g,BOB-PACM}(298K) = \frac{M_{BOB-PACM}}{\rho_{exp.\ BOB-PACM}} = \frac{355.47\ g.mol}{1.178\ g/cm^3} = 301.76\ cm^3/mol$$

$$V_{g,BOB-PACM}(298K) - V_{g,BOF-PACM}(298K) = V_{a,i\ phenyl}(298K) - V_{a,i\ furanyl}(298K) =$$

$$301.76 - 285.50 = 16.3\ cm^3/mol$$

$$V_{a,i\ furanyl}(298K) = V_{a,i\ phenyl}(298K) - 16.3 = 65.5 - 16.3 = 49.2\ cm^3/mol$$

Calculation of T_g for BOB-PACM system:

$$Y_{g,BOB-PACM} = \sum_i Y_{g,i} = 1 * 29.5 + 6.5 * 4.3 + 2 * 4 + 2 * 13 + 1 * 0 + 1 * 27 =$$
$$118.45\ K\ Kg/mol$$

$$T_{g,BOB-PACM} = \frac{Y_{g,BOB-PACM}}{M_{BOB-PACM}} = \frac{118.45\ K\ Kg/mol}{355.47\ g/mol} = 333\ K = 60\ ℃$$

Calculation of T_g for BOB-EPIKURE W system:

$$Y_{g,BOB-EPIKURE\ W} = \sum_i Y_{g,i} = 1 * 29.5 + 6 * 4.3 + 2 * 4 + 2 * 13 + 1 * 0 + 0.5 * 54 =$$
$$116.30\ K\ Kg/mol$$

$$T_{g,BOB-EPIKURE\ W} = \frac{Y_{g,BOB-EPIKURE\ W}}{M_{BOB-EPIKURE\ W}} = \frac{116.30\ K\ Kg/mol}{339.43\ g/mol} = 343\ K = 70\ ℃$$

Calculation of $Y_{g,i\ furanyl}$ from BOF-PACM and BOB-PACM sample pair:

$$Y_{g,BOF-PACM} = T_{g,BOF-PACM} * M_{BOF-PACM} = \frac{344K*345.43\frac{g}{mol}}{1000} = 118.83\ K\ Kg/mol$$

$$Y_{g,BOB-PACM} = T_{g,BOB-PACM} * M_{BOB-PACM} = \frac{373K*355.47\frac{g}{mol}}{1000} = 132.59\ K\ Kg/mol$$

$$Y_{g,BOB-PACM} - Y_{g,BOF-PACM} = Y_{g,i\ phenyl} - Y_{g,i\ furanyl} = 132.59 - 118.83 = 13.76\ K\ Kg/mol$$

$$Y_{g,i\ furanyl} = Y_{g,i\ phenyl} - 13.76 = 29.5 - 13.76 = 15.74\ K\ Kg/mol$$

Vita

Fengshuo Hu was born in Fuxin, Liaoning, China on September 29, 1986. He graduated from Dalian University of Technology in Dalian, China in 2009 with a B.Sc. degree in Applied Chemistry. After receiving his B.Sc. degree, he continued pursuing M.S. degree in Applied Chemistry at Dalian University of Technology and worked as Research Assistant in China State Key Laboratory of Fine Chemicals at Dalian for two years. In 2011, he was admitted into the graduate Chemical Engineering program at Drexel University where he pursued his doctoral research on investigating the structure versus property relationship of thermosetting polymer materials derived from biobased feedstocks under the supervision of Prof. Giuseppe Palmese. Fengshuo Hu's research work on biobased thermosetting polymers has generated several outstanding research awards recognized by professional organizations, such as TRFA, SAMPE, TAFDV, ACS and College of Engineering at Drexel University. A number of high-impacted publications and patents have also been achieved from this dissertation work, including one ACS book chapter, two peer-reviewed journal articles, two patent applications, several conference proceedings and at least three additional publications forthcoming. Fengshuo also had a five-month research intern experience with Huntsman Corporation at the Woodlands, TX, in 2015 where he conducted an industrial product R&D project. Fengshuo has given numerous oral and poster presentations in several professional conferences, and he is currently a member of the ACS, AIChE and SAMPE.